

**STRUCTURAL, CORROSION INHIBITION, CHELATION,
BIOLOGICAL AND *IN SILICO* STUDIES OF SCHIFF BASES**

Submitted to
University of Calicut
in partial fulfillment of the requirements
for the award of the Degree of

**Doctor of Philosophy
in
Chemistry**

By

RAGI K

Under the guidance of

Dr. Joby Thomas K



**RESEARCH AND POSTGRADUATE DEPARTMENT OF CHEMISTRY
ST. THOMAS' COLLEGE (AUTONOMOUS)
(UNIVERSITY OF CALICUT)
THRISSUR, KERALA – 680001
DECEMBER - 2020**



**RESEARCH AND POSTGRADUATE DEPARTMENT OF CHEMISTRY
ST. THOMAS' COLLEGE
THRISSUR, KERALA-680001**

(Nationally reaccredited at 'A' level by NAAC & affiliated to University of Calicut)

Dr. JOBY THOMAS K M.Sc.,M.Phil.,MBA,Ph.D

24-06-2021

CERTIFICATE

I hereby certify that, this is the revised version of the thesis entitled "Structural, corrosion inhibition, chelation, biological and in silico studies of Schiff bases" submitted by Ms. RAGI. K under my guidance after incorporating the necessary corrections/suggestions made by the adjudicators. Also certify that the contents in the thesis and the soft copy are one and the same.

Dr. Joby Thomas. K
(Supervising Teacher)



RESEARCH AND POSTGRADUATE DEPARTMENT OF CHEMISTRY
ST. THOMAS' COLLEGE
THRISSUR, KERALA-680001

(Nationally reaccredited at 'A' level by NAAC & affiliated to University of Calicut)

Dr. JOBY THOMAS K M.Sc.,M.Phil.,MBA,Ph.D

Associate Professor & HOD

04-12-2020

CERTIFICATE

*This is to certify that the thesis entitled “**Structural, corrosion inhibition, chelation, biological and in silico studies of Schiff bases**” is an authentic record of research work carried out by **Ms. RAGI. K** under my supervision in partial fulfillment of the requirements for the degree of **Doctor of Philosophy, in Chemistry of University of Calicut** and further that no part thereof has been presented before for any other degree.*

Dr. Joby Thomas. K
(Supervising Teacher)

DECLARATION

I hereby declare that the thesis entitled, “**Structural, corrosion inhibition, chelation, biological and *in silico* studies of Schiff bases**”, submitted to the University of Calicut in partial fulfillment of the requirements for the award of the Degree of Doctor of Philosophy in Chemistry is a bonafide research work done by me under the supervision and guidance of Dr. Joby Thomas. K, Associate Professor & Head, Department of Chemistry, St. Thomas’ College (Autonomous), Thrissur, Kerala.

I further declare that this thesis has not previously formed the basis of any degree, diploma or any other similar title.

04-12-2020



RAGI K

ACKNOWLEDGEMENT

First of all I thank God Almighty, for His showers of blessing throughout my research to complete the work successfully. I would also like to express my deep and sincere gratitude to my Research Supervisor and my Mentor Dr. Joby Thomas K for giving me the opportunity to do research and providing invaluable guidance throughout this research. I would always cherish this experience in the rest of my life and it was a great privilege and honour to work and study under his guidance.

I am extremely grateful to my parents for their love, prayers and caring for educating and preparing me for my future. I am very much thankful to my Husband Rohith who is always by my side when times I needed him most and helped me a lot to fulfil my ambition. Also I express my thanks to my Son Gautham, Mother in law and Father in law for their tolerance and support.

The support rendered by the St. Thomas College Team – Dr. Joy K, L, Principal, Dr. Jenson P. O and Dr. Ignatius Antony, Former Principal, all the faculty members of the Chemistry Department, Lab Assistants and Office Staffs has been really high. They served as a light house in my journey towards the completion of this voyage.

I would like to express my sincere gratitude to the support and help rendered by my seniors Dr. Vinod P. Raphael, Dr. Shaju K, S, Dr. Nimmy Kuriakose and Dr. Aby Paul. Special thanks to Dr. Vinod P. Raphael for his constant guidance and support which helped me a lot during the entire research period.

The support and help rendered by my research colleagues Sini, Reeja, Binsi, Vidhya, Ramesh, Dinoop, Anju, Martin, Savitha, Swathy, Rohini, Drishya, Siji, Aji, Nithya, Neera, Sr. Jisha, Sr. Cinu, Raji and Memcy helped me a lot in completing this thesis, they sincerely worked as a unit. Really it was an honour to work with them.

The help given by the Biotechnology lab of St. Joseph College, Irinjalakuda was really appreciable. I would like to express my sincere thanks to Najil George and Kavya for the successful completion of the antimicrobial studies. The advice given by

Dr. Deepu Mathew and Dr. Ravi Shankar, Bioinformatics centre (DIC), Kerala Agricultural University helped me a lot in doing the Docking studies. I also acknowledge Dr. Pradeep Kumar K, Sree Vyasa NSS College for his patience and comments in checking and editing grammatical errors.

I am grateful to Council of Scientific & Industrial Research (CSIR) for providing financial assistance for the research work,

I hereby acknowledge the help rendered by the STIC-CUSAT and Mr. Vishnu of IISER Trivandrum in analysing the compounds, which were really worthwhile to mention. I also thank the staff of CHMK Library of Calicut University for helping me frame a smooth bibliography.

Last but not the least, I sincerely thank the hard work of Mr. M. I. Pauly of Educare, Thrissur who did the DTP work for this project.

I have no valuable words to express my thanks, but my heart is still full of the favours received from every person.

RAGI K

To
My Family

PREFACE

Schiff bases are versatile molecules and have received much attention in many fields of research. They are compounds with a functional group that contains a carbon-nitrogen double bond with the nitrogen atom connected to an aryl or alkyl group. Because of the relative ease of preparation, synthetic flexibility, and the special property of C=N group, Schiff bases are generally excellent chelating agents. Presence of lone pair of electrons in the sp^2 hybridised orbital of nitrogen atom of the azomethine group explains the very good chelating ability of Schiff bases, especially when combined with one or more donor atoms close to the azomethine group. Schiff base ligand is able to coordinate many different metals, and to stabilize them in various oxidation states. They are important compounds because of their wide range of biological activities.

Literature survey revealed that coordination compounds, especially Schiff base complexes, possess significant inhibitory activity towards the growth of different types of microbes. Researchers in this area are on active analysis to explore potent antibacterial drugs, which may find the current need of fighting against diseases caused by microbial infection. Schiff bases are also reported to have corrosion inhibitory power for different metals and alloys in acidic media. Heteroatoms present in these molecules are of key importance and responsible for the corrosion inhibition in acidic media on the metal surface. In the present course of investigation synthesis, characterization, corrosion inhibition efficiency, chelating ability, *in vitro* antibacterial activity and *in silico* analysis of Schiff bases were discussed. For convenience and better understanding, the entire work has been presented in this thesis as three parts.

In the first part of the thesis, five Schiff bases namely, 2,2'-(5,5-dimethylcyclohexane-1,3-diylidene)bis(azanylylidene)diphenol (DMCHDP), N,N'-(5,5-dimethylcyclohexane-1,3-diylidene)dianiline (DMCHDA), 2,2'-(5,5-dimethylcyclohexane-1,3-

diylidene)bis(hydrazinecarboxamide) (DMCHHC), 2-((2hydroxybenzylidene)amino) phenol (2HBAP), 2-(cyclohexylideneamino)phenol (2CHAP) were synthesized. Their structural characterization was done by elemental analysis, fourier transform infrared (FTIR) spectroscopy, ultraviolet-visible (UV-visible) spectroscopy, nuclear magnetic resonance (NMR) spectroscopy (^1H and ^{13}C), mass spectroscopy and cyclic voltammetry (CV). The corrosion inhibition efficiency of these compounds on mild steel in 1.0 M HCl and 0.5 M H_2SO_4 were monitored by using weight loss studies and electrochemical studies such as electrochemical impedance spectroscopy, potentiodynamic polarization studies and electrochemical noise measurements. In order to illustrate the mechanism of inhibition, adsorption and surface morphological studies were performed. Temperature dependent gravimetric analysis and quantum chemical studies were also evaluated. This part is divided into five chapters.

The first chapter deals with introduction to corrosion and Schiff bases as inhibitors, economic impact of corrosion, classification and factors affecting corrosion, methods to prevent corrosion, importance of Schiff bases, and a thorough review of published work on Schiff bases as corrosion inhibitors. This chapter is concluded by giving the scope and aims of the present investigations. Chapter 2 includes the methods and reagents used for preparing Schiff bases, techniques used for their characterization and to monitor corrosion inhibition efficiency are included in this chapter. The synthesis and characterization of the Schiff bases DMCHDP, DMCHDA, DMCHHC, 2HBAP and 2CHAP are discussed in detail in chapter 3. Chapter 4 describes corrosion inhibition efficiency analysis of these five Schiff bases on mild steel in 1.0 M HCl. The quantum chemical studies were also included in this chapter. The corrosion inhibition studies of the synthesized Schiff bases on mild steel in 0.5 M H_2SO_4 was discussed in chapter 5. A brief summary of the corrosion inhibition studies of the Schiff bases are followed thereafter along with relevant references.

The second part of the thesis deals with synthesis and characterization of three heterocyclic Schiff bases 3-(1-(2-phenylhydrazono)ethyl)pyridine (3PHEP), 2-(1-(pyridine-3-yl)ethylidene)hydrazine carbothioamide (2PEHCT) and 3-((thiophen-2-ylmethylene)amino)benzoic acid (3TMAB). Characterization was done by physicochemical analysis such as elemental analysis and spectral studies. FTIR, UV-Vis, NMR (^1H and ^{13}C) and Mass spectroscopic techniques were utilized to derive the structures. The chelating ability of these Schiff bases were investigated by synthesizing inner transition metal complexes of La(III), Nd(III) and Sm(III). These metal chelates were characterized by means of elemental (CHN & metal%) analysis, FTIR, UV, magnetic moment and molar conductance measurements. This part is divided into three chapters.

Chapter 6 includes introduction to coordination chemistry, rare earth metals in coordination chemistry and thorough literature survey on Schiff bases complexes, rare earth metal complexes of Schiff bases including heterocyclic Schiff bases and the scope and aims of the present investigations. The methods used for the preparation of Schiff bases, complexes and the characterization techniques employed are well documented in chapter 7. The details of synthesis and characterization of the three heterocyclic Schiff bases 3PHEP, 2PEHCT, 3TMAB and their La(III), Nd(III) and Sm(III) complexes are presented in chapter 8 which is sub divided into three sections.

Section I deals with synthesis and characterization of the Schiff base ligand 3-(1-(2-phenylhydrazono)ethyl)pyridine (3PHEP) and its inner transition metal complexes. Synthesis and characterization of the Schiff base ligand 2-(1-(pyridine-3-yl)ethylidene)hydrazine carbothioamide (2PEHCT) and its inner transition metal complexes are discussed in section II. Section III includes synthesis and characterization of the Schiff base ligand 3-((thiophen-2-ylmethylene)amino)benzoic acid (3TMAB) and its inner transition metal

complexes. All the results are briefly summarized at the end of this part followed by references.

Analysis on antibacterial activity of the Schiff bases and their metal chelates along with the *in silico* molecular docking studies against the target proteins in pathogenic bacteria are discussed in detail in third part. This part comprises of three chapters.

Chapter 9 deals with introduction to bacteria, classification and factors affecting bacteria, *in vitro* antibacterial and *in silico* molecular docking studies. A thorough review on published work on Schiff bases and their metal chelates as antibacterial agents and molecular docking studies with proteins as target are included in this chapter followed by scope and aims of the present investigations. Method employed for screening antibacterial activity by *in vitro* analysis, Lipinski rule, softwares used and steps involved in molecular docking studies and the target proteins present in *Staphylococcus aureus* and *Escherichia coli* are well documented in chapter 10.

Chapter 11 includes the results of *in vitro* antibacterial activity analysis of the ten Schiff bases, 2,2'-(5,5-dimethylcyclohexane-1,3-diylidene)bis(azanylylidene)diphenol (DMCHDP), N,N'-(5,5-dimethylcyclohexane-1,3-diylidene)dianiline (DMCHDA), 2,2'-(5,5-dimethylcyclohexane-1,3-diylidene)bis(hydrazinecarboxamide) (DMCHHC), 2-((2-hydroxybenzylidene) amino) phenol (2HBAP), 2-(cyclohexylideneamino)phenol (2CHAP), 3-(1-(2-phenylhydrazono)ethyl)pyridine (3PHEP), 2-(1-(pyridine-3-yl)ethylidene)hydrazine carboxamide (2PEHC), 2-(1-(pyridine-3-yl)ethylidene)hydrazine carbothioamide (2PEHCT), 3-((thiophen-2-ylmethylene)amino)benzoic acid (3TMAB) and 2-(1-(2-phenylhydrazono)ethyl)pyridine (2PHEP) against two pathogenic bacteria *Staphylococcus aureus* and *Escherichia coli*. The details of the *in silico* studies carried out to understand the mechanism by which the Schiff base compounds inhibit the growth of bacteria are also included. Sortase-A (PDB ID: 1T2P), DNA gyrase (PDB ID: 3U2D), dihydrofolate reductase (DHFR) (PDB

ID: 2W9S), clumping factor A (ClfA) (PDB ID: 1N67), dehydrosqualene synthase (CrtM) (PDB ID: 2ZCO), undecaprenyl diphosphate synthase (UPPS) (PDB ID: 4H8E) are the target proteins of *Staphylococcus aureus* and β -ketoacyl-acyl carrier protein synthase III (ecKAS III) (PDB ID: 1HNJ), peptide deformylase (PDF) (PDB ID: 1G2A), L-glutamine: D-fructose-6-phosphate amido-transferase (PDB ID: 2VF5), murB (PDB ID: 2MBR), heptosyltransferase WaaC (PDB ID: 2GT1), Mur D (PDB ID: 2X5O) and biotin carboxylase (BC) (PDB ID: 2W6O) are the target proteins of *Escherichia coli* selected for conducting molecular docking studies.

This is followed by the details of investigations on the antibacterial activity of the three heterocyclic Schiff bases 3-(1-(2-phenylhydrazono)ethyl)pyridine (3PHEP), 2-(1-(pyridine-3-yl)ethylidene)hydrazine carbothioamide (2PEHCT) and 3-((thiophen-2-ylmethylene)amino)benzoic acid (3TMAB) and their La(III), Nd(III) and Sm(III) complexes against three gram-positive bacteria (*Staphylococcus aureus*, *Enterococcus faecalis*, *Enterococcus casseliflavus*) and three gram-negative bacteria (*Escherichia coli*, *Pseudomonas aeruginosa* and *Enterobacter hormaechei*). Also the antibacterial activities of the Schiff bases and complexes are compared with the standard drug ampicillin. A brief summary of these investigations are also reported at the end of this part which is followed by bibliography.

ABBREVIATIONS

DMCHDP	2,2'-(5,5-dimethylcyclohexane-1,3-diylidene)bis(azanylylidene)diphenol
DMCHDA	N,N'-(5,5-dimethylcyclohexane-1,3-diylidene)dianiline
DMCHHC	2,2'-(5,5-dimethylcyclohexane-1,3-diylidene)bis(hydrazinecarboxamide)
2HBAP	2-((2hydroxybenzylidene)amino) phenol
2CHAP	2-(cyclohexylideneamino)phenol
3PHEP	3-(1-(2-phenylhydrazono)ethyl)pyridine
2PEHCT	2-(1-(pyridine-3-yl)ethylidene)hydrazine carbothioamide
3TMAB	3-((thiophen-2-ylmethylene)amino)benzoic acid
2PEHC	2-(1-(pyridine-3-yl)ethylidene)hydrazine carboxamide
2PHEP	2-(1-(2-phenylhydrazono)ethyl)pyridine
DM	5,5-dimethyl-1,3-cyclohexanedione
2AP	2-aminophenol
AN	Aniline
SZ	Semicarbazide
SAY	Salicylaldehyde
CH	Cyclohexanone
MS	Mild steel
DMSO	Dimethyl sulphoxide
EIS	Electrochemical impedance spectroscopy
FTIR	Fourier-transform infrared
UV-Vis	Ultraviolet-visible
NMR	Nuclear magnetic resonance
SCE	Saturated calomel electrode
OCP	Open circuit potential
CPE	Constant phase element
ECN	Electrochemical noise
PSD	Power spectral density
FFT	Fast Fourier transform

MEM	Maximum entropy method
DFT	Density functional theory
CV	Cyclic voltammetry
SEM	Scanning electron microscopy
HOMO	Highest occupied molecular orbital
LUMO	Lowest unoccupied molecular orbital
HSAB	Hard and soft acid and base
EDTA	Ethylenediaminetetraacetic acid
Ln	Lanthanide ion in a complex
L	Ligand moiety in the complex
BM	Bohr magneton
PDB ID	Protein data bank identification
MHA	Mueller-Hinton agar
DHFR	Dihydrofolate reductase
ClfA	Clumping factor A
UPPS	Undecaprenyl diphosphate synthase
PDF	Peptide deformylase
BC	Biotin carboxylase

ABSTRACT

Schiff bases are most widely used organic compounds that coordinate to metal ions via azomethine nitrogen and have a wide variety of applications in many fields including analytical, biological, and inorganic chemistry. They are also excellent corrosion inhibitors in acid media. The lone pair of electrons on N and S atoms, and the planarity of the molecule are useful for its adsorption to the metal surface. In the present study Schiff bases were synthesized, characterized and their chelating ability was proved by forming complex with inner transition metal complexes of La(III), Nd(III) and Sm(III). The antimicrobial activity, molecular docking study and corrosion inhibition efficiency of the Schiff bases were also evaluated. The entire work is presented in this thesis as three parts.

In the first part five Schiff base compounds were synthesized and their characterization was done by various physicochemical methods. The corrosion inhibition efficiency of these Schiff bases on mild steel in 1.0 M HCl and 0.5 M H₂SO₄ was also evaluated. The corrosion monitoring techniques employed for the study includes weight loss studies, electrochemical impedance spectroscopy (EIS), potentiodynamic polarization studies and electrochemical noise measurements. Adsorption and surface morphological studies were carried out to determine the mechanism of adsorption. Temperature studies was done at temperatures 301 K, 313 K, 323 K and 333 K to find out the parameters of corrosion of mild steel. Quantum chemical studies were also carried out.

In part two three heterocyclic Schiff bases were synthesized and characterized using elemental analysis and spectral studies such as FTIR, UV-Vis, NMR (¹H and ¹³C) and Mass spectroscopy. The chelating ability of these Schiff bases were proved by synthesizing inner transition metal complexes of La(III), Nd(III) and Sm(III). Elemental (CHN) analysis, FTIR, UV-Vis, magnetic moment, estimation of metal and molar conductance studies were

employed for the characterization of the complexes. 1:1 stoichiometry exists between metal and ligand and octahedral geometry is assigned to all complexes.

In the third part antibacterial activity of the ten Schiff bases were done against *Staphylococcus aureus* and *Escherichia coli*. Disc diffusion method is employed for the antibacterial screening. All the compounds have appreciable growth inhibitory power on comparing with the activity of the standard drug ampicillin. As a preliminary test Lipinski rule of five is evaluated to check the drug ability of the molecule. In order to identify the mechanism by which the Schiff bases inhibit the growth of bacteria molecular docking studies were also carried out using AutoDock 4.2. For carrying out the docking studies six target proteins of *Staphylococcus aureus* and seven target proteins of *Escherichia coli* were selected. The antibacterial activity of the three heterocyclic Schiff bases and their La(III), Nd(III) and Sm(III) complexes were also evaluated against six pathogenic bacteria's such as *Staphylococcus aureus*, *Enterococcus faecalis*, *Enterococcus casseliflavus*, *Escherichia coli*, *Pseudomonas aeruginosa* and *Enterobacter hormaechei* by means of disc diffusion method.

LIST OF CONTENTS

PART I		
CORROSION INHIBITION STUDIES		
CHAPTER 1	INTRODUCTION AND REVIEW	1
	Economic impact of corrosion	2
	Classification of corrosion	3
	Factors affecting corrosion	4
	Methods to prevent corrosion	5
	Schiff bases	8
	Importance of Schiff bases	10
	Schiff bases as corrosion inhibitors in acid media- A review	12
	Schiff bases of salicylaldehyde and cyclic ketones as corrosion inhibitors in acid media- A review	16
	Schiff bases of 2-aminophenol as corrosion inhibitors in acid media- A review	19
	Schiff bases of aniline as corrosion inhibitors in acid media- A review	20
	Schiff bases of semicarbazide and thiosemicarbazide as corrosion inhibitors in acid media- A review	22
	Scope and aims of present investigations	25
CHAPTER 2	MATERIALS AND METHODS	27
CHAPTER 3	SYNTHESIS AND CHARACTERIZATION OF SCHIFF BASES	41
	Synthesis and characterization of 2,2'-(5,5-dimethylcyclohexane -1,3-diylidene)bis(azanylylidene)diphenol	41
	Synthesis and characterization of N,N'-(5,5-dimethylcyclohexane -1,3-diylidene)dianiline	44
	Synthesis and characterization of 2,2'-(5,5-dimethylcyclohexane-1,3-diylidene)bis(hydrazinecarboxamide)	46
	Synthesis and characterization of 2-((2-hydroxybenzylidene)amino)phenol	49
	Synthesis and characterization of 2-(cyclohexylideneamino)phenol	51
CHAPTER 4	CORROSION INHIBITION STUDIES OF SCHIFF BASES IN 1.0 M HCL MEDIUM	54
	Weight loss studies	54
	Comparison between $\eta_w\%$ of Schiff bases with its parent compounds	57
	Adsorption studies	58
	Temperature studies	60
	Electrochemical impedance spectroscopy	64
	Potentiodynamic polarization studies	68
	Electrochemical noise measurements	72
	Surface morphological studies	75
	Quantum chemical investigations	77
CHAPTER 5	CORROSION INHIBITION STUDIES OF SCHIFF BASES IN 0.5 M H₂SO₄ MEDIUM	80
	Weight loss studies	80
	Comparison between $\eta_w\%$ of Schiff bases with its parent	82

	compounds	
	Adsorption studies	83
	Temperature studies	85
	Electrochemical impedance spectroscopy	89
	Potentiodynamic polarization studies	92
	Electrochemical noise measurements	98
	Surface morphological studies	101
	SUMMARY	103
	REFERENCES	106
PART II		
CHELATION STUDIES		
CHAPTER 6	INTRODUCTION AND REVIEW	115
	Schiff base complexes - A review	116
	Rare earth metals in coordination chemistry	121
	Rare earth metal complexes of Schiff bases- A review	122
	Rare earth metal complexes of heterocyclic Schiff bases- A review	125
	Scope and aims of present investigations	128
CHAPTER 7	MATERIALS AND METHODS	129
CHAPTER 8	STUDIES ON INNER TRANSITION METAL COMPLEXES OF HETEROCYCLIC SCHIFF BASES	132
Section I	La(III), Nd(III) and Sm(III) complexes of 3-(1-(2-phenyl hydrazono)ethyl)pyridine	133
	Synthesis and characterization of 3PHEP and its inner transition metal complexes	133
Section II	La(III), Nd(III) and Sm(III) complexes of 2-(1-(pyridine-3-yl) ethylidene)hydrazine carbothioamide	138
	Synthesis and characterization of 2PEHCT and its inner transition metal	138
Section III	La(III), Nd(III) and Sm(III) complexes of 3-((thiophen-2-yl methylene)amino)benzoic acid	143
	Synthesis and characterization of 3TMAB and its inner transition metal complexes	143
	SUMMARY	148
	REFERENCES	150
PART III		
BIOLOGICAL STUDIES		
CHAPTER 9	INTRODUCTION AND REVIEW	155
	Gram-positive bacteria	155
	Gram-negative bacteria	157
	Gram's method	159
	Factors affecting the growth of bacteria	160
	Antibacterial agents	162
	Molecular docking	163
	Schiff bases and its metal complexes as antibacterial agents – A review	165
	Molecular docking studies with proteins as targets – A review	171
	Scope and aims of present investigations	173
CHAPTER 10	MATERIALS AND METHODS	175

CHAPTER 11	IN VITRO ANTIBACTERIAL AND IN SILICO MOLECULAR DOCKING STUDIES ON SCHIFF BASES AND THEIR INNER TRANSITION METAL COMPLEXES	193
	<i>In vitro</i> antibacterial studies of the Schiff bases	194
	<i>In silico</i> molecular docking studies	195
	Docking studies of Schiff base compounds with targets in <i>Staphylococcus aureus</i>	196
	Docking studies of DMCHDP with dihydrofolate reductase (DHFR)	199
	Docking studies of DMCHDA with dihydrofolate reductase (DHFR)	200
	Docking studies of DMCHHC with clumping factor A (ClfA)	201
	Docking studies of 2HBAP with dehydrosqualene synthase (CrtM)	201
	Docking studies of 2CHAP and 3PHEP with undecaprenyl diphosphate synthase (UPPS)	202
	Docking studies of 2PEHC with clumping factor A (ClfA) (PDB ID: 1N67)	202
	Docking studies of 2PEHCT with dihydrofolate reductase (DHFR)	202
	Docking studies of 3TMAB with clumping factor A (ClfA)	203
	Docking studies of 2PHEP with dihydrofolate reductase (DHFR)	203
	Docking studies of Schiff base compounds with targets in <i>Escherichia coli</i>	204
	Docking studies of DMCHDP with biotin carboxylase (BC)	214
	Docking studies of DMCHDA with murB	217
	Docking studies of DMCHHC with biotin carboxylase (BC)	217
	Docking studies of 2HBAP with L-glutamine: D-fructose-6-phosphate amido-transferase	217
	Docking studies of 2CHAP and 3PHEP with murB	218
	Docking studies of 2PEHC with peptide deformylase (PDF)	218
	Docking studies of 2PEHCT with peptide deformylase (PDF)	219
	Docking studies of 3TMAB and 2PHEP with murB	219
	<i>In vitro</i> antibacterial studies of the heterocyclic Schiff bases and their inner transition metal complexes	230
	Schiff base 3PHEP and its inner transition metal complexes	231
	Schiff base 2PEHCT and its inner transition metal complexes	231
	Schiff base 3TMBA and its inner transition metal complexes	233
	SUMMARY	234
	REFERENCES	237
LIST OF PUBLICATIONS AND CONFERENCE PAPERS		244

LIST OF TABLES

TABLE No.	TITLE	PAGE No.
PART I		
CORROSION INHIBITION STUDIES		
4.1	Rate of corrosion of MS in mmy^{-1} with and without Schiff bases DMCHDP, DMCHDA, DMCHHC, 2HBAP and 2CHAP in 1.0 M HCl	55
4.2	Corrosion inhibition efficiency ($\eta_w\%$) of Schiff bases DMCHDP, DMCHDA, DMCHHC, 2HBAP and 2CHAP on MS in 1.0 M HCl	55
4.3	Corrosion inhibition efficiency ($\eta_w\%$) of Schiff bases and their parent compounds on MS in 1.0 M HCl	57
4.4	Correlation coefficients of the Schiff bases derived from various adsorption isotherms	59
4.5	Thermodynamic parameters for the adsorption of DMCHDP, DMCHDA, DMCHHC, 2HBAP and 2CHAP on MS in 1.0 M HCl	59
4.6	Thermodynamic parameters of corrosion of MS with and without Schiff bases in 1.0 M HCl	63
4.7	Impedance data of MS coupons with and without Schiff bases in 1.0 M HCl	67
4.8	Polarization data of MS coupons with and without Schiff bases in 1.0 M HCl	71
4.9	Quantum chemical parameters of the Schiff base molecules calculated using DFT method	77
5.1	Rate of corrosion of MS in mmy^{-1} with and without Schiff bases DMCHDP, DMCHDA, DMCHHC, 2HBAP and 2CHAP in 0.5 M H_2SO_4	81
5.2	Corrosion inhibition efficiency ($\eta_w\%$) of Schiff bases DMCHDP, DMCHDA, DMCHHC, 2HBAP and 2CHAP on MS specimen in 0.5 M H_2SO_4	81
5.3	Corrosion inhibition efficiency of Schiff bases and their parent compounds on MS in 0.5 M H_2SO_4	83
5.4	Correlation coefficients of the Schiff bases derived from various isotherms	84
5.5	Thermodynamic parameters for the adsorption of DMCHDP, DMCHDA, DMCHHC, 2HBAP and 2CHAP on MS in 0.5 M H_2SO_4	84
5.6	Thermodynamic parameters of corrosion of MS with and without Schiff bases in 0.5 M H_2SO_4	88
5.7	Impedance data of MS coupons with and without Schiff bases in 0.5 M H_2SO_4	91
5.8	Polarization data of MS coupons with and without Schiff bases in 0.5 M H_2SO_4	95

PART II CHELATION STUDIES		
8.1	Microanalytical, magnetic and conductance data of 3PHEP and its inner transition metal complexes	136
8.2	Characteristic infrared absorption frequencies (cm^{-1}) of 3PHEP and its inner transition metal complexes	137
8.3	Microanalytical, magnetic and conductance data of 2PEHCT and its inner transition metal complexes	140
8.4	Characteristic infrared absorption frequencies (cm^{-1}) of 2PEHCT and its inner transition metal complexes	141
8.5	Microanalytical, magnetic and conductance data of 3TMAB and its inner transition metal complexes	145
8.6	Characteristic infrared absorption frequencies (cm^{-1}) of 3TMAB and its inner transition metal complexes	146
PART III BIOLOGICAL STUDIES		
9.1	Classification of bacteria based on the temperature range required for the growth	161
9.2	Classification of antibiotics with examples and their mechanism of action	163
11.1	Antibacterial activity of the Schiff base compounds	194
11.2	Lipinski rule of five	196
11.3	Binding energy and number of interactions of Schiff bases, DMCHDP, DMCHDA, DMCHHC, 2HBAP and 2CHAP docked with target proteins in <i>S.aureus</i>	197
11.4	Binding energy and number of interactions of Schiff bases, 3PHEP, 2PEHC, 2PEHCT, 3TMAB and 2PHEP docked with target proteins in <i>S.aureus</i>	198
11.5	Coordinate values of active sites in target proteins of <i>S.aureus</i>	199
11.6	Interactions of Schiff bases, DMCHDP, DMCHDA, DMCHHC, 2HBAP and 2CHAP with amino acid residues present in the binding pockets of various target proteins of <i>S.aureus</i>	205
11.7	Interactions of Schiff bases, 3PHEP, 2PEHC, 2PEHCT, 3TMAB and 2PHEP with amino acid residues present in the binding pockets of various target proteins of <i>S.aureus</i>	206
11.8	Binding energy and number of interactions of Schiff bases, DMCHDP, DMCHDA, DMCHHC, 2HBAP and 2CHAP docked with target proteins in <i>E.coli</i>	215
11.9	Binding energy and number of interactions of Schiff bases, 3PHEP, 2PEHC, 2PEHCT, 3TMAB and 2PHEP docked with target proteins in <i>E.coli</i>	216
11.10	Coordinate values of active sites in target proteins of <i>E. coli</i>	217
11.11	Interactions of Schiff bases (DMCHDP, DMCHDA, DMCHHC, 2HBAP and 2CHAP) with amino acid residues present in the binding pockets of various target proteins of <i>E.coli</i>	221
11.12	Interactions of Schiff bases, 3PHEP, 2PEHC, 2PEHCT, 3TMAB and 2PHEP with amino acid residues present in the binding pockets of various target proteins of <i>E.coli</i>	222
11.13	Diameter of zone of inhibition (mm) at different concentration	232

	(μgdisc^{-1}) of the Schiff bases and their inner transition metal complexes	
--	---	--

LIST OF FIGURES

FIGURE No.	TITLE	PAGE No.
PART I		
CORROSION INHIBITION STUDIES		
1.1	Mechanism of rusting	2
1.2	Structure of DAMMT	12
1.3	Structure of Salpr	16
1.4	Structure of Salen	18
1.5	Structure of MTMP	18
1.6	Structure of 2-PTA	22
1.7	Structure of 4-CCMA	22
1.8	Structure of 3APSC	23
1.9	Structure of a) CPFASC b) NPFASC	24
2.1	Electrical circuit for impedance measurement	33
2.2	Nyquist plot	35
2.3	Bode plot	35
2.4	Tafel plot	37
2.5	Linear polarization plot	37
2.6	a) Current noise Vs time plot b) pitting index curve c) PSD plot	39
3.1	Structures of DMCHDP and its tautomer	43
3.2	Cyclic voltammogram of DMCHDP a) at a scan rate of 0.10 V/s b) at scan rates 0.02-0.10 V/s	44
3.3	Redox mechanism occurring at azomethine moiety of DMCHDP	44
3.4	Structures of DMCHDA and its tautomer	46
3.5	Cyclic voltammogram of DMCHDA at a scan rate of 0.10 V/s	47
3.6	Structure of DMCHHC	48
3.7	Cyclic voltammogram of DMCHHC at a scan rate of 0.10 V/s	49
3.8	Structure of 2HBAP	50
3.9	Cyclic voltammogram of 2HBAP at a scan rate of 0.10 V/s	51
3.10	Structure of 2CHAP	52
3.11	Cyclic voltammogram of 2CHAP at a scan rate of 0.10 V/s	53
4.1	Comparison of corrosion rate of mild steel at different concentrations of the Schiff bases DMCHDP, DMCHDA, DMCHHC, 2HBAP and 2CHAP in 1.0 M HCl	56
4.2	Comparison of corrosion inhibition efficiency ($\eta_w\%$) of the Schiff bases DMCHDP, DMCHDA, DMCHHC, 2HBAP and 2CHAP on MS in 1.0 M HCl	56
4.3	Comparison of corrosion inhibition efficiency ($\eta_w\%$) of Schiff bases and their parent compounds on MS in 1.0 M HCl	58
4.4	Langmuir adsorption isotherm of a) DMCHDP b) DMCHDA and c) DMCHHC and Frumkin adsorption isotherm of d) 2HBAP and e) 2CHAP on MS in 1.0 M HCl at 28 ^o C	60
4.5	Plot of a) log K vs 1000/T b) log K/T vs 1000/T with and without DMCHDP on MS in 1.0 M HCl	61
4.6	Plot of a) log K vs 1000/T b) log K/T vs 1000/T with and without	61

	DMCHDA on MS in 1.0 M HCl	
4.7	Plot of a) log K vs 1000/T b) log K/T vs 1000/T with and without DMCHHC on MS in 1.0 M HCl	62
4.8	Plot of a) log K vs 1000/T b) log K/T vs 1000/T with and without 2HBAP on MS in 1.0 M HCl	62
4.9	Plot of a) log K vs 1000/T b) log K/T vs 1000/T with and without 2CHAP on MS in 1.0 M HCl	62
4.10	a) Nyquist and b) Bode plots of MS coupons with and without DMCHDP in 1.0 M HCl	64
4.11	a) Nyquist and b) Bode plots of MS coupons with and without DMCHDA in 1.0 M HCl	65
4.12	a) Nyquist and b) Bode plots of MS coupons with and without DMCHHC in 1.0 M HCl	65
4.13	a) Nyquist and b) Bode plots of MS coupons with and without 2HBAP in 1.0 M HCl	65
4.14	a) Nyquist and b) Bode plots of MS coupons with and without 2CHAP in 1.0 M HCl	66
4.15	The equivalent circuit used to fit the Nyquist plots	68
4.16	Comparison of corrosion inhibition efficiency ($\eta_{EIS}\%$) of the Schiff bases on MS in 1.0 M HCl	68
4.17	a) Tafel and b) linear polarization plots of MS coupons with and without DMCHDP in 1.0 M HCl	69
4.18	a) Tafel and b) linear polarization plots of MS coupons with and without DMCHDA in 1.0 M HCl	69
4.19	a) Tafel and b) linear polarization plots of MS coupons with and without DMCHHC in 1.0 M HCl	70
4.20	a) Tafel and b) linear polarization plots of MS coupons with and without 2HBAP in 1.0 M HCl	70
4.21	a) Tafel and b) linear polarization plots of MS coupons with and without 2CHAP in 1.0 M HCl	70
4.22	Comparison of corrosion inhibition efficiency ($\eta_{pol}\%$) of the Schiff bases on MS in 1.0 M HCl	72
4.23	Current noise for MS in the absence and presence of Schiff bases (1mM) in 1.0 M HCl	73
4.24	Power spectral density (voltage and current) plots of MS in 1.0 M HCl in the presence a) blank b) 2HBAP c) DMCHHC d) 2CHAP e) DMCHDA and f) DMCHDP	74
4.25	Pitting index curve of MS in 1.0 M HCl in the presence a) blank b) 2HBAP c) DMCHHC d) 2CHAP e) DMCHDA and f) DMCHDP	75
4.26	SEM images of MS coupons before and after 24 h immersion a) bare b) blank (1.0 M HCl) c) treated with DMCHDP (1mM) in 1.0 M HCl and d) treated with DMCHDA (1 mM) in 1.0 M HCl	76
4.27	Frontier molecular orbitals a) HOMO and b) LUMO of DMCHDP	78
4.28	Frontier molecular orbitals a) HOMO and b) LUMO of DMCHDA	78
4.29	Frontier molecular orbitals a) HOMO and b) LUMO of DMCHHC	78
4.30	Frontier molecular orbitals a) HOMO and b) LUMO of 2HBAP	79
4.31	Frontier molecular orbitals a) HOMO and b) LUMO of 2CHAP	79
4.32	Optimized geometries of the Schiff bases a) DMCHDP b) DMCHDA c) DMCHHC d) 2HBAP and e) 2CHAP	79

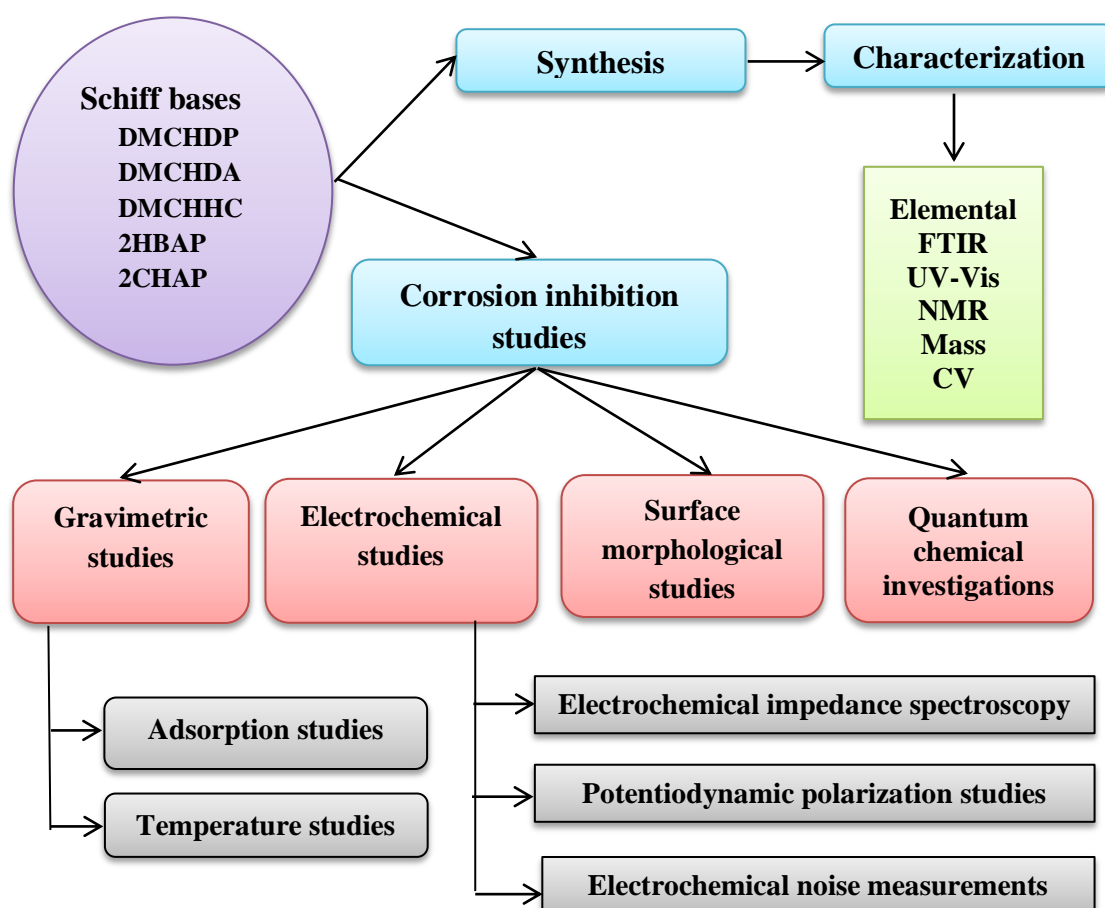
5.1	Comparison of corrosion rate of mild steel at different concentrations of the Schiff bases DMCHDP, DMCHDA, DMCHHC, 2HBAP and 2CHAP in 0.5 M H ₂ SO ₄	82
5.2	Comparison of corrosion inhibition efficiency ($\eta_w\%$) of the Schiff bases DMCHDP, DMCHDA, DMCHHC, 2HBAP and 2CHAP on MS in 0.5 M H ₂ SO ₄	82
5.3	Comparison of corrosion inhibition efficiency ($\eta_w\%$) of Schiff bases and their parent compounds on MS in 0.5 M H ₂ SO ₄	83
5.4	a) Langmuir adsorption isotherm of DMCHDP b) El-Awady adsorption isotherm of DMCHDA and c) Langmuir adsorption isotherm of 2CHAP on MS in 0.5 M H ₂ SO ₄ at 28 ^o C	85
5.5	Plot of a) log K vs 1000/T b) log K/T vs 1000/T with and without DMCHDP on MS in 0.5 M H ₂ SO ₄	86
5.6	Plot of a) log K vs 1000/T b) log K/T vs 1000/T with and without DMCHDA on MS in 0.5 M H ₂ SO ₄	87
5.7	Plot of a) log K vs 1000/T b) log K/T vs 1000/T with and without DMCHHC on MS in 0.5 M H ₂ SO ₄	87
5.8	Plot of a) log K vs 1000/T b) log K/T vs 1000/T with and without 2HBAP on MS in 0.5 M H ₂ SO ₄	87
5.9	Plot of a) log K vs 1000/T b) log K/T vs 1000/T with and without 2CHAP on MS in 0.5 M H ₂ SO ₄	88
5.10	a) Nyquist and b) Bode plots of MS coupons with and without DMCHDP in 0.5 M H ₂ SO ₄	89
5.11	a) Nyquist and b) Bode plots of MS coupons with and without DMCHDA in 0.5 M H ₂ SO ₄	89
5.12	a) Nyquist and b) Bode plots of MS coupons with and without DMCHHC in 0.5 M H ₂ SO ₄	90
5.13	a) Nyquist and b) Bode plots of MS coupons with and without 2HBAP in 0.5 M H ₂ SO ₄	90
5.14	a) Nyquist and b) Bode plots of MS coupons with and without 2CHAP in 0.5 M H ₂ SO ₄	90
5.15	Comparison of corrosion inhibition efficiency ($\eta_{EIS}\%$) of the Schiff bases on MS in 0.5 M H ₂ SO ₄	92
5.16	a) Tafel and b) linear polarization plots of MS coupons with and without DMCHDP in 0.5 M H ₂ SO ₄	93
5.17	a) Tafel and b) linear polarization plots of MS coupons with and without DMCHDA in 0.5 M H ₂ SO ₄	93
5.18	a) Tafel and b) linear polarization plots of MS coupons with and without DMCHHC in 0.5 M H ₂ SO ₄	93
5.19	a) Tafel and b) linear polarization plots of MS coupons with and without 2HBAP in 0.5 M H ₂ SO ₄	94
5.20	a) Tafel and b) linear polarization plots of MS coupons with and without 2CHAP in 0.5 M H ₂ SO ₄	94
5.21	Comparison of corrosion inhibition efficiency ($\eta_{pol}\%$) of the Schiff bases on MS in 0.5 M H ₂ SO ₄	96
5.22	UV-Vis spectra of a) 5,5-dimethyl-1,3-cyclohexanedione b) 2-aminophenol c) DMCHDP at 0 h and d) DMCHDP at 24 h in 0.5 M H ₂ SO ₄	97
5.23	UV-Vis spectra of a) 5,5-dimethyl-1,3-cyclohexanedione b) aniline	98

	c) DMCHDA at 0 h and d) DMCHDA at 24 h in 0.5 M H ₂ SO ₄	
5.24	Current noise for MS in the absence and presence of Schiff bases (1 mM) in 0.5M H ₂ SO ₄	98
5.25	Power spectral density (voltage and current) plots of MS in 0.5 M H ₂ SO ₄ in the presence of a) blank b) SA2AP c) DMCHHC d) DMCHDA e) DMCHDP and f) 2CHAP	99
5.26	Pitting index curves of MS in 0.5 M H ₂ SO ₄ in the presence of a) blank b) SA2AP c) DMCHHC d) DMCHDA e) DMCHDP and f) 2CHAP	100
5.27	SEM images of MS coupons before and after 24 h immersion a) bare b) blank (0.5 M H ₂ SO ₄) c) treated with DMCHDP (1mM) in 0.5 M H ₂ SO ₄ and d) treated with DMCHDA(1 mM) in 0.5 M H ₂ SO ₄	101
PART II CHELATION STUDIES		
8.1	Structures of a) ligand 3PHEP and b) its inner transition metal complexes	137
8.2	Structures of a) ligand 2PEHCT and b) its inner transition metal complexes	142
8.3	Structures of a) ligand 3TMAB and b) its inner transition metal complexes	147
PART III BIOLOGICAL STUDIES		
9.1	Micrograph of <i>S. aureus</i>	156
9.2	Micrograph of <i>E. faecalis</i>	157
9.3	Micrograph of <i>E. casseliflavus</i>	157
9.4	Micrograph of <i>E. coli</i>	158
9.5	Micrograph of <i>P. aeruginosa</i>	158
9.6	Micrograph of <i>E. hormaechei</i>	159
9.7	Representation of Gram's test	160
9.8	Structure of Penicillin	163
9.9	Structure of Ampicillin	163
9.10	Schematic representation of docking procedure	165
10.1	Representation of disc diffusion method	176
10.2	Structures of the target proteins in <i>S.aureus</i>	191
10.3	Structures of the target proteins in <i>E. coli</i>	192
11.1	Antibacterial activity of DMCHDP at different concentrations against <i>S. aureus</i>	195
11.2a	3D interaction diagram of DMCHDP with active site 3 of 2W9S	207
11.2b	3D interaction diagram of DMCHDA with active site 2 of 2W9S	207
11.2c	3D interaction diagram of DMCHHC with active site 1 of 1N67	207
11.2d	3D interaction diagram of 2HBAP with active site 1 of 2ZCO	207
11.2e	3D interaction diagram of 2CHAP with active site 1 of 4H8E	208
11.2f	3D interaction diagram of 3PHEP with active site 1 of 4H8E	208
11.2g	3D interaction diagram of 2PEHC with active site 2 of 1N67	208
11.2h	3D interaction diagram of 2PEHCT with active site 1 of 2W9S	208
11.2i	3D interaction diagram of 3TMAB with active site 2 of 1N67	209
11.2j	3D interaction diagram of 2PHEP with active site 3 of 2W9S	209
11.3a	2D interaction diagram of DMCHDP with active site 2 of 2W9S	209

11.3b	2D interaction diagram of DMCHDA with active site 2 of 2W9S	210
11.3c	2D interaction diagram of DMCHHC with active site 1 of 1N67	210
11.3d	2D interaction diagram of 2HBAP with active site 1 of 2ZCO	211
11.3e	2D interaction diagram of 2CHAP with active site 1 of 4H8E	211
11.3f	2D interaction diagram of 3PHEP with active site 1 of 4H8E	212
11.3g	2D interaction diagram of 2PEHC with active site 2 of 1N67	212
11.3h	2D interaction diagram of 2PEHCT with active site 2 of 2W9S	213
11.3i	2D interaction diagram of 3TMAB with active site 2 of 1N67	213
11.3j	2D interaction diagram of 2PHEP with active site 3 of 2W9S	214
11.4a	3D interaction diagram of DMCHDP with active site 2 of 2W6O	223
11.4b	3D interaction diagram of DMCHDA with active site 1 of 2MBR	223
11.4c	3D interaction diagram of DMCHHC with active site 2 of 2W6O	223
11.4d	3D interaction diagram of 2HBAP with active site 2 of 2VF5	223
11.4e	3D interaction diagram of 2CHAP with active site 1 of 2MBR	224
11.4f	3D interaction diagram of 3PHEP with active site 1 of 2MBR	224
11.4g	3D interaction diagram of 2PEHC with active site 4 of 1G2A	224
11.4h	3D interaction diagram of 2PEHCT with active site 2 of 1G2A	224
11.4i	3D interaction diagram of 3TMAB with active site 1 of 2MBR	225
11.4j	3D interaction diagram of 2PHEP with active site 1 of 2MBR	225
11.5a	2D interaction diagram of DMCHDP with active site 2 of 2W6O	225
11.5b	2D interaction diagram of DMCHDA with active site 1 of 2MBR	226
11.5c	2D interaction diagram of DMCHHC with active site 2 of 2W6O	226
11.5d	2D interaction diagram of 2HBAP with active site 2 of 2VF5	227
11.5e	2D interaction diagram of 2CHAP with active site 1 of 2MBR	227
11.5f	2D interaction diagram of 3PHEP with active site 1 of 2MBR	228
11.5g	2D interaction diagram of 2PEHC with active site 4 of 1G2A	228
11.5h	2D interaction diagram of 2PEHCT with active site 2 of 1G2A	229
11.5i	2D interaction diagram of 3TMAB with active site 1 of 2MBR	229
11.5j	2D interaction diagram of 2PHEP with active site 1 of 2MBR	230
11.6	Antibacterial activity of 2PEHCT, Nd(III)-2PEHCT and Sm(III)-2PEHCT at 500 μgdisc^{-1} against <i>E. faecalis</i>	233

PART I

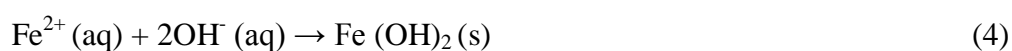
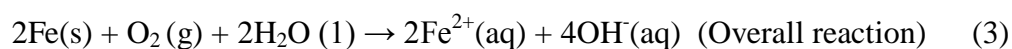
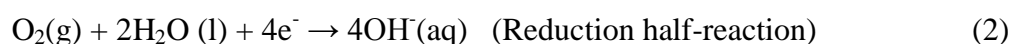
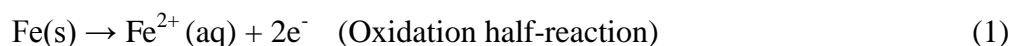
CORROSION INHIBITION STUDIES



CHAPTER 1

INTRODUCTION AND REVIEW

The term corrosion is generally used to describe the interaction of a material with its environment resulting into destruction of the material. It is a natural phenomenon which converts the metal into oxide, sulphide or hydroxide. Rusting of iron is a common example of corrosion. Rate of corrosion enhances in the presence of aggressive acid solutions. Acid solutions are generally used in industries for various purposes such as pickling, oil well acidification, cleaning, descaling etc [1-6]. Hydrochloric acid and sulphuric acid are the commonly used acids in industries. Among various metals mild steels are commonly used for construction purposes owing to its low cost, good weldability and mechanical properties [7-13]. Metallic corrosion is a major threat in industries due to excess use of acids. During the cleaning processes mild steel is attacked severely by the acid solution and gets corroded. As a result quality of the products and efficiency of plants get decreased. Steps involved in the rusting process are mentioned below. First step is the oxidation of iron into Fe^{2+} ion and reduction of oxygen existing in air into hydroxide ion. In the second step the Fe^{2+} and OH^- ions produced will combine to form hydroxide of iron $\text{Fe}(\text{OH})_2$, which on further reaction with oxygen and water present in air to form a reddish-brown solid of hydrated oxide of iron $\text{Fe}_2\text{O}_3 \cdot n\text{H}_2\text{O}$, which is generally called as rust. Mechanism of rusting is shown in Fig. 1.1.



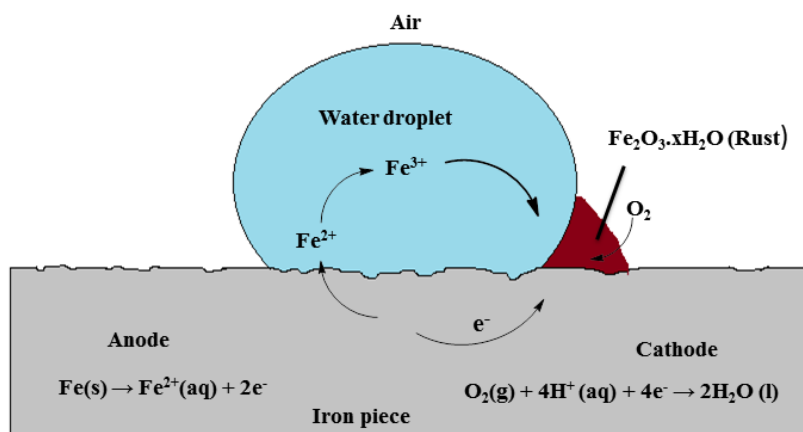


Fig. 1.1 Mechanism of rusting

Economic impact of corrosion

Corrosion is an inevitable process that has serious consequences on the economy of the world. The darkest side of corrosion in a country like India could be better understood if we account the total economic loss occurred in various sectors like infrastructure, utility services, production and manufacturing, defence and nuclear waste which is estimated to be around 1.52 lakh crores. This envisages the fact that corrosion has a deep root in the economic structure of a nation which most often remains unnoticed [14]. It is estimated that an average of 10% of the total metals produced worldwide is deteriorated due to corrosion. In industrialized nations the cost of corrosion is about 3-4% of their GDP. With the exponential economic growths of various sectors extend of corrosion is too increasing to worsen the situation. In countries like Japan and US, corrosion losses are estimated to be about 3% of their respective GDPs. Corrosion has a vital impact on the bottom line of industries, as damage due to corrosion results in increased maintenance cost, lower reliability of equipment, loss of production and poor product quality.

Economic cost of corrosion is classified into two i.e., direct cost and indirect cost. Direct cost is the quantitatively evaluated cost and it includes protection cost, research

and development, investment cost and corrosion inhibition whereas indirect cost is not quantitatively evaluated and it includes contamination of products, decrease in the efficiency of products, loss of revenue due to downtime, loss of products to spill and fire, environmental pollution etc. Estimate of the avoidable costs of corrosion ranges between 10-40%. Direct cost of corrosion is focused in most of the studies even though the impact of indirect cost on corrosion is greater. This is attributed to the difficulties in its estimation. Unfortunately, it is impossible to prevent corrosion, therefore controlling the rate of corrosion by adopting suitable cost effective methods is the most economical solution to its rising challenges [15].

Classification of corrosion

Corrosion is classified according to the nature of degradation of the metal.

Galvanic corrosion: It happens when metals of different substances are placed together in an aggressive electrolyte. A couple is formed between two metals, where one metal act as anode and the other as cathode. More active metal acts as anode and corrodes at an accelerated rate. Affected area is determined by studying the conductivity of the solution.

Uniform corrosion: Also defined as general corrosion which has uniform distribution throughout the surface of the metal. Destruction of protective coating on the metal surface often results in this type of corrosion.

Pitting corrosion: It is a class of localized corrosion results in the formation of small holes in metal. Corrosion of this kind is difficult to find out due to small size and hence more dangerous than uniform corrosion. When a pit is formed it grows into a cavity that takes on different shapes. Generally pits penetrate in the vertical direction from surface to bottom of the metal. It can be created due to non-uniformities in the structure of metal or due to damage of protective oxide film coating.

Crevice corrosion: Corrosion occurring in restricted spaces to which penetration of the working fluid from the environment is reduced. These restricted spaces in general are called crevices. Contact areas between parts, inside cracks and seams, under gaskets, spaces filled with deposits etc are examples of crevices.

Intergranular corrosion (cracking): Also defined as interdendritic or intercrystalline corrosion. It is the cracking preferentially occurring around the grain boundaries under tensile stress. Corrosion of this kind is generally identified using microstructure determination.

Microbial corrosion: This kind of corrosion is usually accelerated by microorganisms. Metal deterioration due to the corrosion process occurring as a result of metabolic activity of microorganisms in cold water systems is called microbiologically induced corrosion (MIC). Anaerobic bacteria will leads to this type of corrosion.

Filiform corrosion: Thread like type of corrosion which develops under protective coating on certain metals usually in humid atmospheres.

Fretting corrosion: Rapid corrosion that occurs at the interface between highly loaded metal surfaces contacted each other when subjected to slight vibrating motions.

High temperature corrosion: Deterioration of a metal due to heating. This can occur when a metal is subjected to a hot atmosphere in the presence of oxygen, sulfur or other compound capable of oxidizing the material.

Factors affecting corrosion

Significant two factors that considerably cause changes in corrosion are nature of metal and environment.

Nature of metal

- Physical state
- Passive character of metal

- Overvoltage
- Purity of metal
- Position in galvanic series
- Relative area of anodic and cathodic parts
- Nature of surface film
- Solubility of corrosion products
- Volatility of corrosion product

Nature of corroding environment

- Humidity of air
- Influence of pH
- Temperature
- Presence of impurities in atmosphere
- Conductance of the corroding medium
- Nature of ions present
- Polarization of electrodes
- Presence of suspended particles in atmosphere
- Flow velocity of process stream

Methods to prevent corrosion

Corrosion is categorized into different classes and they take place under different conditions. Since corrosion is a harmful process it is necessary to take measures to prevent it. Complete prevention of corrosion is difficult to achieve since it is possible only under ideal conditions. Corrosion is the destruction of metal due to its reaction with environment. Therefore the methods adopted to control the rate of corrosion modify the metal or environment.

Modification of metal

Selection of metals/alloys and proper designing: Noble metals and pure metals are corrosion resistant. Since noble metals are not used for general purposes and also such metals are not available in the purest form, their use is limited. Use of alloys which are corrosion resistant is more preferred for general purposes. Designing of equipment and structure is also very important. Simple design and structure is more preferred to control corrosion.

Monitoring the surface of metal: Rate of corrosion will increase when the surface of the metal is rough, crevices or holes is present and because of imperfections during production.

Cathodic protection: In order to control the rate of corrosion the metal surface is taken as cathode in the electrochemical cell. Due to the absence of anodic part on the metal, corrosion does not take place. This can be achieved by two methods such as sacrificial anode protection and impressed current cathodic protection.

Sacrificial anode protection: Electrochemical cell consists of an active metal as anode and metal to be protected as cathode. Hence corrosion will occur only on anode and the metal is protected. Thus the anode used for this purpose is called sacrificial anode. The corroded anodic part is replaced by the new one. Generally aluminium, zinc, magnesium and their alloys are used as sacrificial anode. Low investment cost is required and even economical when protection is required for short period.

Impressed current cathodic protection: System consisting of metal to be protected as cathode and the anode is connected to a DC source. Current is applied in the direction opposite to that of corrosion current to nullify it and to convert the corroding metal from anodic to cathodic nature. Replacement of anode is not required owing to its stable

nature. High investment cost is required and suitable when protection is required for long period.

Modification of environment

Deaeration: Large amount of oxygen dissolved in fresh water will leads to increase in the rate of corrosion. In this method, the dissolved oxygen is removed by agitating mechanically together with rise of temperature.

Coatings: Coating using paint is simple and cost-effective. Paint coatings will prevent the electrochemical charge transfer by acting as a boundary between metal and corrosive medium. Metal coating having high tendency to oxidize over another metal to be protected is called sacrificial coating.

Use of inhibitors: This is the most effective method for reducing the rate of corrosion in acid medium. Inhibitors minimize the corrosion process by raising cathodic or anodic polarization behavior, minimizing diffusion of ions to the metal surface and by raising electrical resistance of metallic surface. Based on the inhibition mechanism, corrosion inhibitors are classified into anodic, cathodic, mixed type and vapor phase inhibitors.

Anodic inhibitors: Also called passivating inhibitors. They protect the metal surface by creating a layer of oxide film on it. They alter the anodic reactions occurring in an electrochemical cell. Passivating inhibitors can be either oxidizing or nonoxidizing. Oxidizing inhibitor passivates metal in the absence of oxygen. Nitrite, chromate, nitrate etc are some examples. Non oxidizing inhibitor passivates metal in the presence of oxygen. Tungstate, molybdate, phosphate etc are some examples. The concentration of the inhibitor must be high in solution. Insufficient amount of inhibitor will leads to localized corrosion since the surface is not completely covered by the inhibitor.

Cathodic inhibitors: Inhibitors that minimizes the cathodic reaction and limit migration of ions to cathodic area. They inhibit by acting as cathodic poisons, cathodic

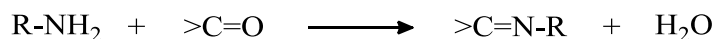
precipitates and oxygen scavengers. Sulphites, bicarbonates etc are some examples. Low concentration of inhibitor is required and hence more secure than anodic inhibitors.

Organic inhibitors: Organic inhibitors are used on a wide scale in industries. They are less toxic, had the ability to exist together with the protected metal, highly soluble and effective at different range of temperatures. They can act as anodic, cathodic or mixed inhibitor by adsorbing on the metal surface forming a film. Amines, quaternary ammonium salts, pyridine derivatives, amino acids, Schiff base, indazole, derivatives of imidazole, triazole, oxazol, thiadiazole, thiourea, thiazole and phtalimides, plant extracts and sulfonates are some examples of organic inhibitors. Schiff bases are well-known example for organic inhibitors. They are prepared by condensing an amino compound with aldehyde or ketone and having a general formula $R_2C=NR$. Literature survey revealed that Schiff bases are good corrosion inhibitors on comparing with the parent compounds from which they are synthesized. This is due to the participation of $-CH=N-$ group present in Schiff base molecules [16-18]. They can adsorb on the surface of the metal by means of both physical and chemical interaction [19-21]. Adsorption process is supported by structure of the inhibitor molecule, nature of metal surface and corrosive environment. The lone pair of electrons present on hetero atoms such as N, O and S, unsaturated π bonds, conjugated aromatic rings and planarity of the molecules are the most important characteristics that control adsorption of inhibitor molecules on the metal surface [22-25].

Schiff bases

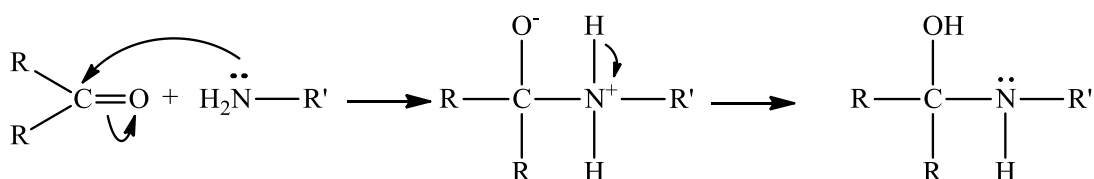
German chemist Hugo Schiff discovered Schiff base in 1864 [26]. Schiff bases are generally prepared by the condensation of carbonyl compounds (aldehyde/ketones) with aromatic or aliphatic primary amines. It is regarded as a nitrogen analogue of an

aldehyde or ketone where imine group substitutes C=O group and also known as imine or azomethine.

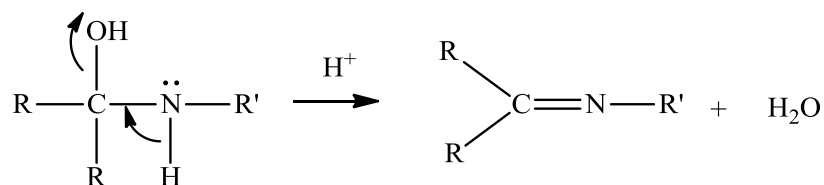


In the case of aldehydes the C=O group has less steric hindrance than ketone, hence it can form Schiff base more easily. Generally Schiff bases containing alkyl substituents can be easily polymerize and are unstable whereas that containing aryl substituents are stable due to effective conjugation. Schiff base formation is usually reversible and generally occurs upon heating or when acid or base is present. Generally Schiff base is formed through two steps. First step is the nucleophilic addition of primary amine to carbonyl group which leads to the formation of an unstable product carbinolamine. In the second step (rate determining step) acid catalyzed dehydration of the alcohol (carbinolamine) will take place. So the reaction involves an addition followed by an elimination reaction.

Step1: Carbinolamine formation



Step2: Acid catalyzed dehydration



Acid concentration had a great role in the synthesis of Schiff bases. Very high concentration of acid will lead to protonation of amines and hence loses its nucleophilicity. Also in acidic environment, the Schiff bases may sometimes hydrolyzed

back to its parent carbonyl compound and amine. Therefore mild acidic pH is preferable for Schiff base synthesis.

Denticity can vary from bidentate to polydentate in the case of Schiff base ligands. Donor atom present in it offers special capability to bind with metals. They can able to bind with various metal atoms and to stabilize metal atoms in different oxidation states. Incorporation of metals in the lattice of donor atoms will change the morphological, pharmacological and physiological properties of the Schiff base compounds. Their chelating ability with both transition and non-transition metal ions are very high. Sensitivity, selectivity, presence of azomethine group and synthetic flexibility of the Schiff base ligands makes them an important class of ligands.

Importance of Schiff bases

Schiff base ligands have extensive applications in various fields such as analytical, inorganic, organic and biological fields [27-30]. The lone pair of electrons in the sp^2 hybrid orbital of N atom in ($-C=NH-$) linkage present in Schiff bases enhances their biological and chemical importance [31-32]. They have excellent pharmacological activities and are widely used in pharmaceutical industry. Preparation of Schiff bases is comparatively easy, possess attractive features and have structural similarity with naturally occurring biological substances [33-34]. Large number of Schiff bases prepared from aromatic aldehydes and aromatic amines are used as fluorimetric analytical reagents [35]. Chiral Schiff bases are found to be a good catalyst in enantioselective Henry (nitro aldol) reaction [36]. The antibacterial, antitumor, antifungal, anti-inflammatory, catalytic, anti-HIV, anticonvulsant and antioxidant activities are reported in many literatures [37-44]. In many enzymatic reactions Schiff bases are found to be a prominent intermediate. Biochemical process involving such enzymatic reactions is condensation of primary amine of a lysine residue present in an enzyme with carbonyl

group present in the substrate forming Schiff base ligand [45]. Schiff bases have particularly significant applications in four types of reaction such as 1) hetero Diels-Alder reaction to furnish six membered nitrogen containing heterocyclic compounds 2) addition of organometallic reagents or hydride to C=N bond 3) skeletons for the building-up scaffolds, as the very famous salen scaffold, to be used as “privileged ligand” for the formation of the corresponding chiral salen metal complexes 4) Staudinger reaction with ketene to furnish biologically important β -lactam ring [46].

Malaria is a severe morbidity of humans and other animals. It is caused by protozoa of the genus *Plasmodium*. It is initiated by a bite from an infected female *Anopheles* mosquito, which introduces the *Plasmodium* through saliva into the circulatory system. In the blood, the protists travel to the liver to mature and reproduce. Typical symptoms of malaria include fever and headache, which in severe cases, can progress to coma and eventually death [47]. The imino-group of Schiff bases has shown valuable function to confer antimalarial activity. Schiff bases are also intermediate in bioprocesses such as transamination reaction [48]. The -C=N- present in Schiff bases can be easily reduced by complex metal hydrides and is a method for the formation of amino compounds. Similarly hydrogen cyanide addition to Schiff bases takes place easily and provides a feasible path for the formation of α -amino nitriles (Strecker synthesis). [1+2] Cycloaddition reactions of carbenoids and carbenes to Schiff bases are also reported in literature [49]. Another important characteristic of Schiff bases is their good chelating ability [50-53]. Azomethine group present in it has the potential to coordinate with almost all metals by coordinating through N atom. In order to reduce or prevent rate of corrosion of metallic substances in acidic environment corrosion inhibitors are widely used in industries. Azomethine linkage present in Schiff bases is responsible for the

complex formation with metal ion and thereby inhibits the corrosion. They create a barrier to moisture and oxygen by adsorbing on the surface of the metal [54].

Schiff bases as corrosion inhibitors in acid media- A review

Generally organic compounds having reactive centers such as hetero atoms, lone pair of electrons, aromatic rings, and delocalized π electrons are proved to be effective inhibitors of metallic corrosion in various environments. Schiff base is an organic compound satisfying all these features and found to be a potential corrosion inhibitor. Role of Schiff bases as an excellent corrosion inhibitor in various metals like mild steel, zinc, copper and aluminium in aggressive acid media like sulphuric acid, hydrochloric acid etc were already reported by researchers.

S. John et al. investigated the corrosion inhibition capacity of the compound 4-(N,N-dimethylaminobenzilidene)-3-mercapto-6-methyl-1,2,4-triazin(4H)-5-one (DAMMT) on mild steel in 1 M HCl using gravimetric method, electrochemical methods such as electrochemical impedance spectroscopy, potentiodynamic polarization (Tafel and linear polarization) and quantum chemical calculation [55]. Langmuir isotherm was found to be the best fit isotherm. It was found that DAMMT is an excellent inhibitor towards mild steel and also acts as a mixed type inhibitor. From the results it is clear that inhibition efficiency is found to increase with concentration and decreases with higher exposure time at 300 K. Structure of DAMMT is shown in Fig. 1.2.

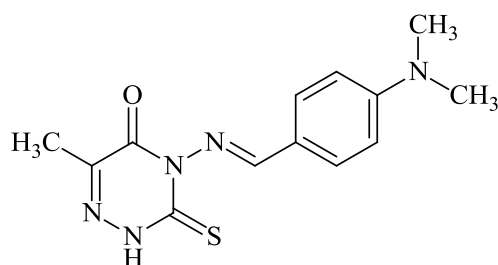


Fig. 1.2 Structure of DAMMT

The inhibiting nature of four Schiff bases, 2-((1Z)-1-aza-2-(2-pyridyl)vinyl)pyrimidine, 2-((1E)-2-aza-2-(1,3-thiazol-2-yl)vinyl)thiophene, 2-((1E)-2-aza-2-pyrimidine-2-ylvinyl)thiophene and 2-((1Z)-1-aza-2-(2-thienyl)vinyl)benzothiazole on the corrosion of carbon steel in 0.1 M HCl was investigated by A. Yurt et al. using electrochemical impedance studies and potentiodynamic polarization studies [56]. Polarization data revealed that all the four Schiff bases acted as anodic inhibitors. Inhibition efficiency was found to vary with the nature of substituent group present in the molecule. Temkin adsorption isotherm was the most-fit isotherm for all the Schiff bases. Study of impact of temperature on the corrosion inhibition efficiency showed that efficiency decreased with rise in temperature.

W. Li and co-workers studied the influence of two triazole derivatives 2,5-dichloro-acetophenone-O-1'-(1',3',4'-triazolyl)-methaneoxime (5-DTM) and 3,4-dichloro-acetophenone-O-1'-(1',3',4'-triazolyl)-methaneoxime (4-DTM) on corrosion of mild steel in 1 M HCl using weight loss, impedance and SEM studies [57]. Both triazole derivatives are found to exhibit good inhibition potency and acted as mixed type inhibitors. Excellent inhibition capacity was shown by these compounds at 1mM concentration according to weight loss studies. Results obtained from weight loss studies are in good agreement with electrochemical studies. Adsorption of triazole derivatives on MS in 1 M HCl was found to obey Langmuir adsorption isotherm.

K. M. Govindaraju et al. synthesized three Schiff bases of 4-amino-antipyrine and evaluated the influence of these Schiff bases (4-[(4-methoxy benzylidene)-amino]-antipyrine (AAAP), 4-[(benzylidene)-amino]-antipyrine (BAAP) and 4-[(4-hydroxy benzylidene)-amino]-antipyrine (SAAP)) and 4-amino-antipyrine (AAP) on corrosion of mild steel in acid media [58]. Techniques used for this purpose were weight loss, impedance, potentiodynamic polarization and FT-IR. From the studies, it is clear that the

Schiff bases are exhibiting very good inhibition capacity when compared to 4-amino-antipyrine. The order of efficiency is AAAP>SAAP>BAAP>AAP. All the Schiff bases acted as mixed type inhibitor according to polarization studies. Maximum inhibition potency of 90.83% was exhibited by AAAP at 0.8 mM concentration.

N. Kuriakose and co-workers synthesized thiophene-2-carbaldehyde tryptophan and investigated its corrosion inhibition capacity using weight loss and electrochemical studies on mild steel (MS) in 1 M HCl solution [59]. Results proved that the ligand is a very good inhibitor and efficiency increased with concentration. Freundlich isotherm was obeyed and evaluated thermodynamic parameters. Also it acted as mixed type inhibitor.

M. G. Hosseini et al. conducted electrochemical studies such as electrochemical impedance spectroscopy (EIS) and Tafel polarization to evaluate the inhibition of mild steel corrosion in 0.5 M H₂SO₄ solution by three Schiff bases N,N'-ethylen-bis(salicylideneimine) [S1], N,N'-isopropyl-bis(salicylideneimine) [S2] and N-acetyl acetone imine, N'-(2-hydroxybenzophenone imine)ortho-phenylen [S3] [60]. Maximum inhibition potency of ~97-98% was shown by these Schiff bases at 300 ppm concentration. S2 was more effective than the other two Schiff bases. The nature of adsorption is physical and obeyed Langmuir adsorption isotherm.

Theoretical and corrosion inhibition studies were done by I. Ahamad et al. to examine whether there is any relation between the results obtained from both studies [61]. The Schiff base 2-[2-(2-(3-phenylallylidene)hydrazine carbonothioyl)hydrazine carbonyl]benzoic acid acted as an excellent corrosion inhibitor for MS in 1 M hydrochloric acid medium. Maximum efficiency of about 99.5% is shown by the inhibitor at 1.369×10^{-6} M concentration. Protective film formation of the inhibitor on metal surface was confirmed by FTIR technique. Schiff base acted as a mixed type

inhibitor and the mechanism of adsorption is chemisorption. Parameters obtained from theoretical studies are in good agreement with that of corrosion studies.

Gravimetric, EIS, polarization and theoretical studies of three bis-Schiff bases (2-methoxybenzylidene)hydrazono)indolin-2-one (HZ-1), (2-hydroxybenzylidene)hydrazono)indolin-2-one (HZ-2) and (4-nitrobenzylidene)hydrazono)indolin-2-one (HZ-3)) of isatin was carried out by K. R. Ansari et al. to study the capability of reducing the corrosion of mild steel in 1.0 M HCl medium [62]. Order of inhibition efficiency was $\text{HZ-1} > \text{HZ-2} > \text{HZ-3}$. All the three inhibitors are mixed type and obeyed Langmuir adsorption isotherm. Surface morphological studies (SEM and EDX) were employed to confirm the protective film formation on metal surface. Quantum chemical and corrosion inhibition studies were in good correlation.

K. S. Shaju et al. synthesized the Schiff base anthracene-9(10H)-one-3-aminopropanoic acid (A9O3AP) and studied the effect of KI on its corrosion inhibition efficiency on mild steel in 0.5 M H_2SO_4 by means of weight loss, electrochemical impedance and potentiodynamic polarization studies [63]. Inhibition efficiency was found to increase with concentration and synergistic effect of KI was also observed. That is corrosion inhibition efficiency enhanced when KI is added. Freundlich and Langmuir isotherms were obeyed by inhibitor and inhibitor + KI on the metal surface. Thermodynamic parameters were also evaluated and it acted as mixed type inhibitor.

M. A. Quraishi et al. investigated the behaviour of five substituted dianils namely 1,4-di-dimethylaminobenzylideneaminophenylene (DDAP), 1,4-divanilledeneamino phenylene (DVAP), 1,4-disalicyledeneaminophenylene (DSAP), 1,4-dibenzylidene aminophenylene (DBAP) and 1,4-dicinnamylideneaminophenylene (DCAP) as inhibitor for mild steel corrosion in 1 N HCl and 1 N H_2SO_4 [64]. Among these compounds DCAP is the best inhibitor in both acid media. Variation of efficiency with concentration, nature

of the compound, immersion time and temperature were also evaluated. All inhibitors acted as mixed type inhibitors and obeyed Temkin adsorption isotherm.

Corrosion inhibition potency of three newly synthesized Schiff bases derived from aromatic aldehydes and L-lysine in 1 M HCl was evaluated using electrochemical, gravimetric, SEM, EDX and AFM methods by N. K. Gupta et al [65]. Efficiency was found to be increased with concentration and maximum inhibition efficiency of 2-amino-6-((4-dimethylamino)benzylideneamino)hexanoic acid at a concentration of 400 mgL^{-1} is 95.6%. Polarization data showed that all Schiff bases are cathodic inhibitors and obeyed Langmuir isotherm in hydrochloric acid medium.

Schiff bases of salicylaldehyde and cyclic ketones as corrosion inhibitors in acid media- A review

A. M. Abdel-Gaber and co-workers investigated the corrosion inhibition capacity of N,N' -bis(salicylaldehyde)-1,3-diaminopropane (Salpr) and its Co complex on steel in 1 M H_2SO_4 by EIS and polarization studies [66]. Stability of Co complex in acid media was examined by using spectrophotometry measurements. Adsorption behaviour was clarified using different isotherms. Results showed that Co complex has good corrosion inhibition effect than corresponding ligand. Structure of Salpr is shown in Fig. 1.3.

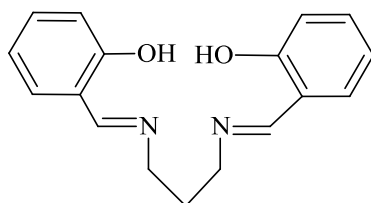


Fig. 1.3 Structure of Salpr

Corrosion inhibition of mild steel in 1 M HCl by Schiff bases derived from 4-amino antipyrine and salicylaldehyde/furfuraldehyde/anisaldehyde was evaluated using gravimetric and electrochemical studies by Balaji. M et al [67]. Results obtained from both studies were in good agreement and they inhibit corrosion by adsorbing on the

metal surface. Charge transfer resistance increased and double layer capacitance decreased with concentration. Polarization studies revealed that they are mixed type inhibitors.

S. P. Fakrudeena et al. synthesized the ligands N,N'-bis (3-methoxy salicylidene)-1,4-diaminophenylene (MSDP) and N,N'-bis(salicylidene)-1,4-diaminophenylene (SDP) [68]. Weight loss and SEM technique were used to evaluate the corrosion inhibition of SDP and MSDP on AA6061 and AA6063 alloy in 1 M HCl medium. Inhibition efficiency was found to increase with rise in concentration and alter with immersion time and solution temperature. Both Schiff bases obeyed Freundlich adsorption isotherm and MSDP was found to be an effective inhibitor than SDP.

Three Schiff bases have been derived from salicylaldehyde/p-chloroaniline, salicylaldehyde/N,N'-ethylenediamine and cinnamaldehyde/N,N'-ethylenediamine by P. Karuppasamy and co-workers [69]. The corrosion inhibition of these Schiff bases on mild steel in hydrochloric acid medium were evaluated using weight loss, impedance, potentiodynamic polarization, IR and UV-visible studies. Langmuir isotherm was obeyed by all the Schiff bases and they acted as mixed type inhibitors.

A. Barbosa da Silva et al. reported that the anti-corrosive behaviour of the reduced form (N,N'- bis(2-hydroxybenzyl)-1,2-ethylenediamine) is greater compared to N,N'-bis(salicylidene)-1,2-ethylenediamine (Salen) and mixture of parent compounds salicylaldehyde and ethylene diamine on carbon steel in 1 M HCl medium [70]. Corrosion monitoring was done by EIS, polarization study, spectrophotometry and corrosion potential measurements. Results showed similar inhibition efficiency for Salen and mixture of its corresponding parent compounds. This is attributed to the hydrolysis of Salen in acid medium. Structure of Salen is shown in Fig. 1.4.

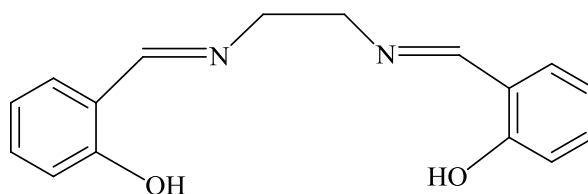


Fig. 1.4 Structure of Salen

R. Menaka et al. studied inhibition efficacy of Schiff base derived from chitosan and salicylaldehyde on mild steel in 1 M HCl medium adopting weight loss and electrochemical studies [71]. Characterization of the Schiff base was done by FTIR, Ultraviolet spectroscopy, elemental and SEM analysis. Thermal stability of the compound was also determined. Temkin isotherm is obeyed by the chitosan Schiff base and the adsorption is chemical in nature. SEM analysis confirmed the protective layer formation of the Schiff base on mild steel surface.

A novel Schiff base 2-((5-mercapto-1,3,4-thiadiazol-2-ylimino)methyl)phenol (MTMP) has been synthesized by R. Solmaz et al. and its inhibiting action on the corrosion of mild steel in 0.5 M HCl solution was investigated by weight loss and electrochemical studies [72]. Schiff base acted as a mixed inhibitor and obeyed Langmuir adsorption isotherm. Inhibition efficiency was concentration dependent and reached a maximum value of 97% at 1 mM. Structure of MTMP is shown in Fig. 1.5.

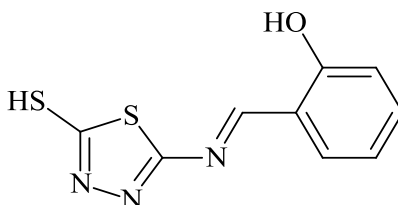


Fig. 1.5 Structure of MTMP

A. S. Fouda et al. synthesized N-3-hydroxyl-2-naphthoyl hydrazone derivatives of 2-acetophenone, α -tetralone, benzaldehyde and cyclohexanone and investigated corrosion inhibition efficiency of these derivatives on carbon steel in 0.5 M H₂SO₄ [73]. Corrosion monitoring techniques used were weight loss method and polarization

measurements. Study showed that these derivatives were mixed type inhibitors and obeyed Frumkin adsorption isotherm. Synergistic effect of KBr, KI and KSCN on enhancing the corrosion inhibition efficiency of the compounds was also studied.

Schiff bases of 2-aminophenol as corrosion inhibitors in acid media- A review

K. Veni and co-workers synthesized Schiff base derived from o-aminophenol and p-chlorobenzaldehyde and its transition metal complexes using grinding method [74]. Characterization was done using IR, UV, NMR, Mass and ESR spectroscopic techniques and molar conductivity studies. Corrosion inhibition study of the ligand and its complexes on mild steel surface were conducted using weight loss measurement in 0.1 M HNO₃. Promising inhibition efficiency was observed for the compounds.

Corrosion inhibition nature of the Schiff bases obtained by the condensation of 2-aminophenol with acrolein, 2-aminophenol with cinnamaldehyde and phenylene diamine with cinnamaldehyde on carbon steel in 0.5 N HCl were investigated using weight loss and electrochemical studies by M. Q. Mohammed [75]. IR, UV, ¹H NMR and CHN analysis were carried out for the characterization. Results obtained from both corrosion monitoring techniques are in good agreement and exhibiting good inhibition efficiency.

Y. B. Zemedet et al. studied corrosion inhibition efficiency of the Schiff base ligand (2E)-2-((5-((E)-(2-hydroxyphenylimino)methyl)thiophene-2-yl)methylene amino) phenol and its Co(II), Ni(II), Cu(II) and Zn(II) complexes using weight loss measurement in 0.1 M HCl for MS specimen [76]. Metal complexes are found to exhibit high inhibition efficiency than the ligands. The order of efficiency was [CoL(H₂O)₂] > [NiL(H₂O)₂] > [ZnL] > [CuL] > L, where L= ligand. Higher efficiency of complexes may be due to planarity and large size of the molecule. They inhibit the corrosion by adsorbing on the metal surface.

Gravimetric and electrochemical studies were adopted to evaluate inhibition efficiency of the ligands 2-(5-chloro-2-hydroxybenzylideneamino)phenol, 2-(2-hydroxybenzylideneamino)phenol and 2-(2-hydroxy-5-nitrobenzylideneamino)phenol against MS corrosion in 1 M HCl by S. K. Saha et al [77]. Surface morphological studies were carried out in the presence and absence of inhibitor to confirm the adsorption of ligand on metal. Corrosion inhibition efficiency is found to increase with increase in concentration of inhibitor. Polarization study revealed that they are mixed type inhibitors. All the ligands obeyed Langmuir adsorption isotherm on mild steel surface. Quantum chemical calculations were also carried out to determine the relation between structure of the molecule and the inhibition efficiency. There exist good interdependence between the experimental results and theoretical data.

Schiff bases of aniline as corrosion inhibitors in acid media- A review

P. Silku and co-workers synthesized and characterized acryloyl derivatives of Schiff base derived by the reaction of *p*-hydroxybenzaldehyde with aniline, *p*-nitroaniline, *p*-aminobenzoic acid, *p*-chloroaniline and *p*-methylaniline [78]. Spectroscopic tools like IR, UV-Vis, NMR and mass technique were adopted for characterization. UV-Vis study was done in three different solvents depending on the solubility of the ligand and derivatives. Corrosion inhibition efficiency of all the compounds on steel surface were investigated in 0.1 M NaOH, 0.1 M NaCl and 0.10 M H₂SO₄ medium with the aid of Tafel and cyclic voltammetric studies.

The corrosion inhibition efficiency of the Schiff bases N-(furfurilidene)-4-methyl aniline, N-(cinnamalidene)-4-methoxyaniline, N-(furfurilidene)-4-methoxyaniline, N-(salicylidene)-4-methoxyaniline and N-(cinnamalidene)-2-methylaniline on mild steel in H₂SO₄ was monitored using weight loss and thermometric methods by Upadhyay et al [79]. Results obtained from both methods are in good agreement and inhibition

efficiency depends on the concentration of inhibitor and acid medium. At highest concentration of Schiff base at the highest strength of acid, the inhibition efficiency is found to be maximum.

D. Daoud et al. investigated corrosion inhibition efficiency of the Schiff base synthesized from 4-[(4-aminophenyl)methyl]aniline and thiophene-3-carbaldehyde on mild steel X52 in 1 M HCl and 1 M H₂SO₄ with the aid of corrosion monitoring techniques such as weight loss, electrochemical impedance spectroscopy and potentiodynamic polarization studies [80]. Results showed that the synthesized Schiff base was an excellent corrosion inhibitor and the inhibition efficiency rise with inhibitor concentration. Langmuir adsorption isotherm was obeyed. Relation between inhibition efficiency of the studied Schiff base and quantum chemical calculation was also discussed using density functional theory (DFT) method.

M. Farsak and co-workers synthesized the Schiff base (E)-N-((E)-3-phenyl allylidene)-2-(phenylthio)aniline (2-PTA) and studied its corrosion inhibition efficiency on low carbon steel (LCS) in HCl medium for a wide range of temperature using electrochemical methods such as electrochemical impedance spectroscopy and potentiodynamic polarization studies [81]. The inhibitor 2-PTA is found to possess 99.8% corrosion inhibition efficiency after 120 h immersion time in 1 M HCl medium containing 2.5 mM inhibitor molecule. Results showed that the inhibitor 2-PTA was adsorbed on LCS to a larger extent at all temperatures. Tafel technique revealed that the inhibitor is cathodic controlled mixed type inhibitor at all temperature. Isotherm obeyed by 2-PTA on LCS is Langmuir adsorption isotherm. Larger value of K_{ads} also supports the higher adsorption ability of the inhibitor on metal surface. Structure of 2-PTA is shown in Fig. 1.6

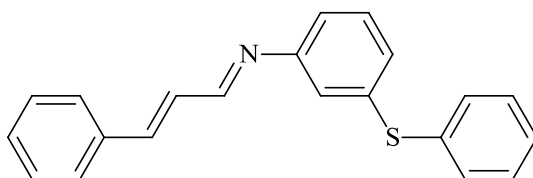


Fig. 1.6 Structure of 2-PTA

The effect of Schiff base (Z)-4-chloro-N-((2-chloroquinolin-3-yl) methylene) aniline (4-CCMA) on the corrosion of mild steel (MS) in 1 N HCl was examined using weight loss, impedance, potentiodynamic polarization and SEM analysis by Bhupendra M. Mistry et al [82]. Inhibition efficiency was found to rise with inhibitor concentration and exhibiting maximum efficiency of 99.04 % at 25 ppm of 4-CCMA. The inhibitor 4-CCMA serves as mixed type inhibitor according to polarization studies. Charge transfer resistance was found to increase with concentration of 4-CCMA in accordance with impedance study. Adsorption studies revealed that Langmuir adsorption isotherm was followed by the inhibitor. Impact of temperature on the corrosion inhibition of mild steel in 1 N HCl was also investigated in the range of temperature from 298-318 K. Structure of 4-CCMA is shown in Fig. 1.7.

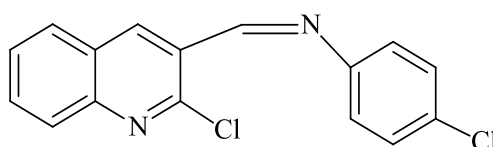


Fig. 1.7 Structure of 4-CCMA

Schiff bases of semicarbazide and thiosemicarbazide as corrosion inhibitors in acid media- A review

V. P. Raphael et al. carried out weight loss, EIS and polarization studies to determine the corrosion inhibition property of 3-acetylpyridinesemicarbazone (3APSC) on carbon steel in 1 M HCl [83]. From the results it is clear that 3APSC has significant inhibition even at low concentration. Adsorption obeyed Langmuir isotherm and it acted as mixed type inhibitor. Thermodynamic parameters such as activation energy, enthalpy

of corrosion and entropy of correction were also calculated. SEM analysis was also carried out to study the surface nature of the metal. Structure of 3APSC is shown in Fig. 1.8.

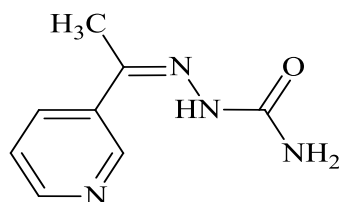


Fig. 1.8 Structure of 3APSC

Corrosion inhibition effect of mild steel in 1 M HCl by vanillinthiosemicarbazone and its ethyl and methyl derivatives were analysed using weight loss, impedance and potentiodynamic polarization studies by T. S. Franklin Rajesh and co-workers [84]. Inhibitors were found to exhibit good corrosion inhibition property even at 10^{-3} M concentration. Parent compounds were also subjected to corrosion inhibition studies. Result obtained from all the three methods are in good correlation. The three inhibitors are of mixed type and obeyed Langmuir adsorption isotherm.

Inhibiting nature of two semicarbazones (2-indolecarboxaldehyde/2-pyridine carboxaldehyde and semicarbazide hydrochloride) and four thiosemicarbazones (4-ethoxybenzaldehyde/ 4-hydroxybenzaldehyde/ 4-hydroxy-3-methoxybenzaldehyde/ 2-pyridinecarboxaldehyde and thiosemicarbazide) on the corrosion of carbon steel in 0.1 M HCl was investigated by C. M. Goulart et al. using electrochemical impedance spectroscopy, potentiodynamic polarization and molecular modelling at different inhibitor concentration [85]. Charge transfer resistance was found to increase with inhibitor concentration in impedance plots. Polarization studies revealed that the inhibitors acted as mixed type inhibitors.

V. P. Raphael and co-workers synthesized and characterized two heterocyclic semicarbazones (E)-2-((5-(4-nitrophenyl)-furan-2-yl)methylene)hydrazinecarboxamide

(NPFASC) and (E)-4-(5-((2-carbamoylhydrazano)methyl)furan-2-yl)benzoic acid (CPFASC) [86]. Corrosion inhibition capacity of the compounds on carbon steel surface in 1 M HCl medium by weight loss, EIS and polarizations studies were also investigated. Results showed that despite of non-planar structure of NPFASC, it is a more effective inhibitor than CPFASC. This is due to the reduction of NO_2 group present in NPFASC into NH_2 group when come close to metal surface in acid medium. Geometry of the molecule NPFASC will change in favour of corrosion inhibition as a result of this conversion. El-Awady and Freundlich isotherms were obeyed by NPFASC and CPFASC respectively. Surface morphological studies were also carried out using IR, AFM and SEM. Structure of CPFASC and NPFASC is shown in Fig. 1.9.

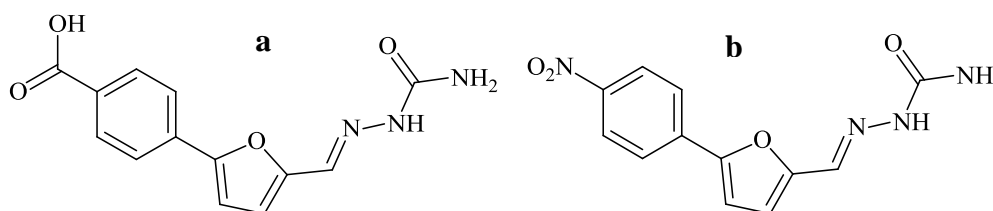


Fig. 1.9 Structure of a) CPFASC b) NPFASC

Three thiosemicarbazones and two semicarbazones such as 2-acetylpyridine-(4-methyl)thiosemicarbazone (2AP4MTSC), 2-acetylpyridinethiosemicarbazone (2APTSC), 2-acetylpyridine-(4-phenyl)thiosemicarbazone (2AP4PTSC), 2-acetylpyridine semicarbazone (2APSC) and 2-acetylpyridine-(4-phenyl)semicarbazone (2AP4PSC) were synthesized and their corrosion inhibition property was monitored using hydrogen evolution via the gasometric assembly at 30°C and 40°C in 5 M H_2SO_4 by P. C. Okafor and co-workers [87]. It is observed that thiosemicarbazones enhances the corrosion rate at low concentration and reduced the corrosion rate at higher concentrations. Semicarbazones enhanced the corrosion rate at all concentrations. Inhibition efficiency follows the order $2\text{AP4PTSC} > 2\text{AP4MTSC} > 2\text{APTSC} > 2\text{AP4PSC} > 2\text{APSC}$.

Dr. L. Ravikumar et al. evaluated corrosion inhibition efficiency of the Schiff bases r-2,c-6-diphenyl-t-3-methyl piperidine-4-one [S₁], r-2,c-6-diphenyl-t-3-methyl-N-methyl piperidine-4-one semicarbazone [S₂] and r-2,c-6-diphenyl-t-3-methyl piperidine-4-one semicarbazone [S₃] on mild steel in 1 M H₂SO₄ by means of weight loss, impedance, potentiodynamic polarization and scanning electron microscopic technique [88]. Inhibition efficiency was found to increase with concentration and at a concentration of about 7 mM, inhibition efficiency reaches a maximum value of 93-94% in all cases. The semicarbazone S₂ was more efficient than other two semicarbazones. The isotherm obeyed was Langmuir adsorption isotherm.

Scope and aims of present investigations

Corrosion is a serious issue that challenges scientists and researchers. The corrosion inhibition efficiency of a wide range of organic molecules has been screened by various researchers. Among them, Schiff bases are proven to be an effective corrosion inhibitor by adsorbing on the surface of the metal. The active part present in Schiff base molecules which is responsible for corrosion prevention is azomethine linkage. In addition to this, presence of lone pair of electrons on hetero atoms such as N, O and S, unsaturated π bonds, aromatic rings and planarity of the molecule are the most important characteristics that enhance adsorption of inhibitor molecules on the metal surface. Despite the fact that various Schiff base molecules have been screened for their corrosion inhibition potency, search for new Schiff base molecules for preventing corrosion has key importance in industrial and research fields.

In the present course of investigation it was proposed to carry out synthesis, characterization and checking corrosion inhibition efficiency of five Schiff base ligands derived from 5,5-dimethylcyclohexanone, salicylaldehyde and cyclohexanone with various amino compounds on mild steel in 1.0 M HCl and 0.5 M H₂SO₄ medium by

weight loss studies and electrochemical studies such as electrochemical impedance spectroscopy, potentiodynamic polarization studies and electrochemical noise measurements. Corrosion inhibition studies of the parent compounds also to be investigated to check the argument that the active part present in Schiff base molecules which is responsible for corrosion prevention is azomethine linkage. Corrosion inhibition mechanism is to be explored with the aid of adsorption isotherms. Thermodynamic parameters such as free energy of adsorption and adsorption equilibrium constant were also proposed to evaluate from adsorption isotherms.

Temperature dependent gravimetric corrosion investigations were employed to determine thermodynamic parameters such as activation energy (E_a), enthalpy of activation (ΔH^*), entropy of activation (ΔS^*) and Arrhenius parameter (A). Scanning electron microscopic analysis can be utilized to understand surface morphology of the mild steel specimens. Quantum chemical investigations will also perform to correlate the relationship between corrosion inhibition efficiency and electronic properties of the molecule.

CHAPTER 2

MATERIALS AND METHODS

This chapter mainly deals with general methods and reagents used for the preparation of Schiff bases, their characterization, composition of the metal specimen used and its preparation followed by the acid medium used for the study and the techniques adopted to evaluate rate of corrosion. Corrosion monitoring techniques used are gravimetric (weight loss) and electrochemical studies. Electrochemical studies involve electrochemical impedance spectroscopy (EIS), potentiodynamic polarization studies and electrochemical noise measurements. Also deals with techniques used for screening surface morphology and quantum chemical investigations.

Reagents

Chemicals such as 5,5-dimethyl-1,3-cyclohexanedione, salicylaldehyde, cyclohexanone, 2-aminophenol, semicarbazide hydrochloride and aniline were purchased from Merck.

Characterization techniques

The structures of the Schiff bases were formulated based on elemental analysis, spectral studies (FTIR, UV-Vis, NMR and Mass) and cyclic voltammetry.

Elemental (CHN) analysis

This analysis was done in order to estimate carbon, hydrogen and nitrogen present in inhibitor molecules. Products obtained after combustion of the sample were analyzed by microanalysis using Elementar make Vario EL III model CHNS analyser.

Fourier-transform infrared (FTIR) spectroscopy

Generally used for the determination of functional groups. Vibration of atoms is measured. In electromagnetic spectrum the region $4000-400\text{ cm}^{-1}$ belongs to IR region. KBr disc technique on a Shimadzu model FT-IR Spectrometer (Model IR affinity-1) was

used for recording IR spectra of Schiff bases. Useful for determining the various groups present in Schiff base molecules.

UV- visible spectroscopy

Shimadzu UV-Visible-1800 Spectrophotometer was used for recording electronic spectra of the Schiff bases. It gives an idea about geometry of the molecule. DMSO is used as solvent for UV-visible analysis.

NMR spectroscopy

The instrument BRUKER AVANCE III HD was used for ^1H NMR and ^{13}C NMR studies by taking dms o -d $_6$ as solvent.

Mass spectroscopy

Samples were prepared for taking mass spectra after purification by means of chromatographic method. Mass spectra were recorded using QP 2010 model Shimadzu GCMS.

Cyclic voltammetry (CV)

The electrochemical nature of the Schiff bases was investigated using cyclic voltammetric studies. Ivium compactstat-e electrochemical system was used for this study. A three electrode system consisting of glassy carbon, Ag-AgCl and platinum loop were used as working electrode, reference electrode and counter electrode respectively in this study [89]. 3 ml solution of the Schiff bases (0.1 mM) in DMSO was taken in the electrolytic cell and 2 ml of supporting electrolyte (tetra butyl ammonium hexa fluoro phosphate) (0.1 M) was added. Solution was kept unstirred and the cyclic voltammogram was recorded in the potential range 2.0 to -2.0 V at a scan rate of 0.02-0.1 V/s.

Corrosion inhibition studies

Details about composition of mild steel coupons, aggressive solutions and techniques adopted for monitoring corrosion inhibition capacity of the Schiff bases are described as follows.

Test specimen

Mild steel (MS) coupons having composition : C, 0.31%; Mn, 0.09%; S, 0.017%, P, 0.03%; Si, 0.03% and the rest Fe were cut into the dimension 1×1×0.96 cm and abraded with various grades of SiC papers (100, 220, 400, 600, 800, 1000, 1500 and 2000), washed with acetone, distilled water and dried. Area and thickness of each MS coupons were measured and weighed. Then it is immersed in 50 ml acid solutions at 28⁰C in hanging position with and without adding Schiff bases in different concentration using fishing lines.

Aggressive solution

Aggressive solutions of 1.0 M HCl and 0.5 M H₂SO₄ needed for the corrosion inhibition studies were prepared by diluting analytical grade acids (Merck) with de-ionized water. Schiff base solutions were prepared in aggressive solutions having a range of concentration 0.2-1.0 mM. The volume of the acidic solution used for gravimetric studies was 50 ml whereas 100 ml solution was used for electrochemical studies.

Gravimetric studies

In gravimetric study the mild steel specimen was immersed in 50 ml acid solutions at 28⁰C in hanging position with and without Schiff bases having different concentration using fishing lines. Weight loss of metal coupons was recorded after 24 h. Duplicate experiments were carried out and the average values were taken. Corrosion rate was obtained from gravimetric study. It is generally expressed in mmy⁻¹. Percentage of inhibition efficiency was then calculated from corrosion rates obtained. Equations

used for calculating corrosion rate and percentage of inhibition efficiency are given below [90-92].

$$v = \frac{KW}{DSt} \quad (1)$$

where $K = 87600$ (This is a factor used to convert cm/hour into mm/year), W , S , D , t denotes average weight loss of coupon (g), total area of specimen (cm^2), density of mild steel (g cm^{-3}), period of contact of metal with acid solution (h) respectively.

Density of MS specimen = 7.88g/cc.

Percentage of inhibition efficiency ($\eta_w\%$) was defined by

$$\eta_w\% = \frac{v_0 - v}{v_0} \times 100 \quad (2)$$

where v_0 and v represent corrosion rate of specimens in contact with the acid medium without and with inhibitor respectively.

Comparison of corrosion inhibition efficiency of Schiff bases with parent ketone/aldehyde and amine was carried out by weight loss studies of mild steel in 1.0 M HCl and 0.5 M H_2SO_4 at 28°C for 24 h. This comparative study was done in order to understand whether hydrolysis of Schiff base is taking place during the period of study and to determine the inhibition efficiency of the product obtained through hydrolysis.

Adsorption studies

Adsorption isotherms are used to illustrate the corrosion inhibition mechanism of molecules [93-94]. Isotherms give information regarding the nature of interaction between metal and Schiff bases. Langmuir, El-Awady, Frumkin, Temkin, Freundlich and Florry-huggin isotherms were the different adsorption isotherms considered for the study [95]. Most suitable isotherm was identified using correlation coefficient (R^2). Thermodynamic parameters obtained from adsorption isotherms are free energy of adsorption (ΔG_{ads}^0) and adsorption equilibrium constant (K_{ads}). Isotherm models considered for the study are given below

$$\text{Langmuir isotherm} \quad \frac{C}{\theta} = \frac{1}{K} + C \quad (3)$$

$$\text{Frumkin isotherm} \quad \log \frac{\theta}{(1-\theta)C} = \log K + g\theta \quad (4)$$

$$\text{Freundlich isotherm} \quad \theta = K_{ads}C \quad (5)$$

$$\text{El-awady isotherm} \quad \log \frac{\theta}{(1-\theta)} = \log K + y \log C \quad (6)$$

$$\text{Florry-huggin isotherm} \quad \log \frac{\theta}{C} = \log K + x \log (1 - \theta) \quad (7)$$

$$\text{Temkin isotherm} \quad \log \frac{\theta}{C} = \log K - g\theta \quad (8)$$

where θ , C , K is fractional surface coverage, concentration of the Schiff base and adsorption equilibrium constant respectively. The percentage of inhibition efficiency is related to fractional surface coverage as follows

$$\theta = \frac{\text{percentage of inhibition efficiency}}{100} \quad (9)$$

Relation between adsorption equilibrium constant K_{ads} and standard free energy of adsorption ΔG_{ads}^0 is given by [96-97]

$$\Delta G_{ads}^0 = -RT \ln(55.5 K_{ads}) \quad (10)$$

where 55.5 is the molar concentration of water, R and T represents universal gas constant and temperature in Kelvin respectively.

Temperature studies

Temperature dependent gravimetric corrosion investigations were done by keeping the MS specimen immersed in acidic solution with and without Schiff base molecule on a thermostat for a period of 24 h at temperatures 301 K, 313 K, 323 K and 333 K. Thermodynamic parameters such as activation energy (E_a), enthalpy of activation (ΔH^*), entropy of activation (ΔS^*) and Arrhenius parameter (A) were calculated using the

data obtained from the temperature study. Activation energy of metal dissolution was measured using an Arrhenius type equation given below [98-99]

$$K = A \exp(-E_a/RT) \quad (11)$$

where K, A, E_a , R and T represent corrosion rate, pre-exponential factor, activation energy, universal gas constant, temperature in Kelvin respectively. The plot of $\log K$ Vs $1000/T$ gives a straight line having slope and intercept as $-E_a/2.303R$ and $\log A$ respectively.

Thermodynamic parameters such as enthalpy of activation (ΔH^*) and entropy of activation (ΔS^*) were evaluated using transition state theory [100-101]

$$K = \left(\frac{RT}{Nh}\right) \exp\left(\frac{\Delta S^*}{R}\right) \exp\left(\frac{-\Delta H^*}{RT}\right) \quad (12)$$

where N is the Avogadro number and h is the Planck's constant. Value of ΔH^* was obtained from the slope $\left(\frac{-\Delta H^*}{2.303R}\right)$ whereas the value of ΔS^* was obtained from the intercept $\left(\log\left(\frac{R}{2.303Nh}\right) + \left(\frac{\Delta S^*}{2.303R}\right)\right)$ of the plot between $\log K/T$ vs $1/T$ for the metal dissolution in acid medium.

Electrochemical studies

Electrochemical methods are useful in determining the rate and mechanism of corrosion since it is an electrochemical phenomenon. Commonly used electrochemical methods for corrosion monitoring are electrochemical impedance spectroscopy (EIS), potentiodynamic polarization studies and electrochemical noise measurements. Polarization study involves Tafel and linear polarization analysis. The advantage of electrochemical studies over conventional gravimetric studies is that it takes less time for measurement. In the case of electrochemical investigations all the measurements were done with the help of computer and modern softwares. Thus the results obtained from

electrochemical measurements will be more accurate than conventional gravimetric measurements.

Ivium compactstat-e electrochemical system associated with a new version of iviumsoft software was utilized for the electrochemical measurements. This enables us to select suitable equivalent circuit, simulation of curve, calculation of current density and resistance more easily. A three electrode system, consisting of platinum electrode having 1 cm^2 area as counter electrode, saturated calomel electrode (SCE) as the reference electrode, metal specimen with an exposed area of 1 cm^2 as working electrode, were used for the studies.

Since corrosion is an electrochemical phenomenon, various corrosion parameters such as corrosion current density, corrosion potential, charge transfer resistance, values of anodic and cathodic slopes etc can be determined by analysing the charge transfer processes occurring at the electrode. Using these parameters we can calculate rate of corrosion and percentage of inhibition efficiency.

Electrochemical impedance spectroscopy (EIS)

Electrochemical impedance spectroscopy is the most useful technique for monitoring corrosion. The analyses were done with the help of suitable electrical circuit [102-105]. Fig. 2.1 shown below represents the most suitable circuit used for the study.

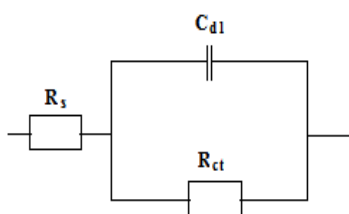


Fig. 2.1 Electrical circuit for impedance measurement

R_{ct} , R_s and C_{dl} represents charge transfer resistance, solution resistance and double layer capacitance respectively. Electrochemical spectra can be visualized with the help of two plots namely Nyquist and Bode plots.

Nyquist plot (Cole-Cole plot): A semicircle shaped curve is obtained by plotted the real part of impedance (Z') against imaginary part of impedance (Z'') as shown in Fig. 2.2. Higher limit of frequency reaches at the left side of the semicircle where it touches x axis and the lower limit of frequency reaches at the right side of the semicircle. Impedance at higher frequency is equal to solution resistance (R_s) whereas impedance at lower frequency is equal to the sum of solution resistance (R_s) and charge transfer resistance (R_{ct}). R_s is the resistance between reference and working electrode. it is also called ohmic resistance. Charge transfer resistance at the interface of electrode and solution is represented by R_{ct} . The ability to inhibit corrosion is expressed in terms of charge transfer resistance. R_{ct} value of the working electrode in contact with acid medium will be high in the presence of inhibitor whereas it has low value in the absence of inhibitor. Using this R_{ct} values we can calculate corrosion inhibition efficiency of the inhibitor molecules as shown in equation given below [106-108]

$$\eta_{EIS} \% = \frac{R_{ct} - R'_{ct}}{R_{ct}} \times 100 \quad (13)$$

where R_{ct} and R'_{ct} represents charge transfer resistance of working electrode in contact with the acid medium with and without inhibitor

Bode plot: In bode plot logarithm of frequency is plotted against logarithm of impedance and phase shift (Φ). The plot of $\log|Z|$ Vs $\log f$ is termed as impedance plot. $|Z| = \sqrt{Z'^2 + Z''^2}$. R_s and R_{ct} values are obtained from impedance plot. Break point of this curve should lie on a straight line (at intermediate frequency) whose slope will be -1. Extrapolation of this straight line to the y-axis at $f = 1$ or $\log f = 0$ give the value of C_{dl} .

$$|Z| = \frac{1}{C_{dl}} \quad (14)$$

Bode plot is more opted than Nyquist plot on account of its less measurement time. The combined impedance and Bode plot is shown in Fig. 2.3.

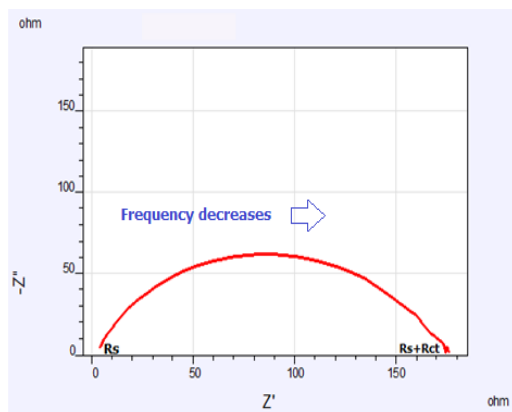


Fig. 2.2 Nyquist plot

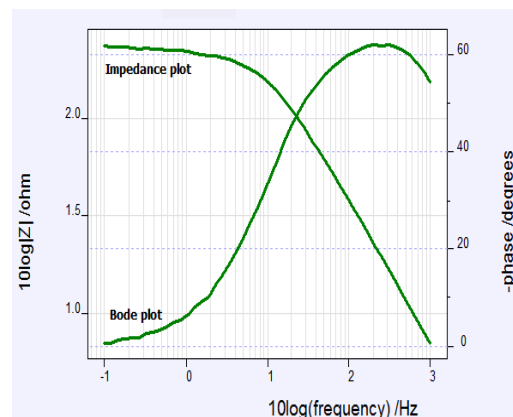


Fig. 2.3 Bode plot

Potentiodynamic polarization studies

Polarization method mainly deals with measurement of current generated as a function of potential or time by varying the potential of working electrode. Mainly the polarization techniques are of two types namely linear polarization and Tafel extrapolation method.

Tafel extrapolation method: This technique is based on mixed potential theory given by Wagner and Traud [109-110]. Reaction occurring in oxidation half-cell is the conversion of metal (M) into M^{2+} ion whereas in reduction half-cell H^+ ion is reduced to H_2 . Rate determining reaction is the cathodic reaction since it is slower than anodic reaction. In the case when both anodic and cathodic reaction occurring at same rate, charge accumulation will be absent. Mixed potential at this stage is called open circuit potential (OCP) which is designated as corrosion potential (E_{corr}). Current at this mixed potential is assigned as corrosion current density which is represented as i_{corr} . In order to obtain the applied current density (i_{app}) as a function of applied potential (E), the applied potential between working and reference electrode is controlled and scanned at constant rate. Tafel plot is shown in Fig. 2.4.

The Butler-Volmer equation describing polarization of reversible electrodes which are controlled by activation process is given below [111]

$$i_{app} = i_{corr} \left\{ \exp\left(\frac{\alpha_a}{RT}\right) zF(E - E_{corr}) - \exp\left(-\frac{\alpha_c}{RT}\right) zF(E - E_{corr}) \right\} \quad (15)$$

where i_{app} , i_{corr} , α_a and α_c denotes applied current density, corrosion current density, charge transfer coefficient for anodic reaction and charge transfer coefficient for cathodic reaction respectively. $E - E_{corr}$ is the polarization, which is the difference between applied potential and corrosion potential. z , F , R and T represent metal valence, Faraday constant, gas constant and temperature respectively.

For anodic polarization $E \gg E_{corr}$ and for cathodic polarization $E_{corr} \gg E$. The corresponding equations can be derived and from which anodic (b_a) and cathodic (b_c) slopes were obtained.

Corrosion inhibition efficiency is then determined using corrosion current density as described in equation given below [112-113]

$$\eta_{pol}\% = \frac{i_{corr} - i'_{corr}}{i_{corr}} \times 100 \quad (16)$$

where i_{corr} and i'_{corr} represents corrosion current density in the absence and presence of inhibitor respectively.

Linear polarization method: This method involves plotting applied current density as a linear function of electrode potential by displacing the potential by about 10 to 20 mV. Parameter measured in this technique is polarization resistance (R_p). Corrosion rate mainly depends on charge transfer process. The inhibitor adsorption on the metal surface will reduce the charge transfer process occurring between the metal and acid solution.

Relation between i_{corr} and polarization resistance is given by Stern and Geary equation as follows [114]

$$i_{corr} = \left[\frac{b_a b_b}{2.303(b_a b_b)} \right] \frac{\Delta i}{\Delta E} = \frac{B}{R_p} \quad (17)$$

where R_p is the polarization resistance which is equal to $\frac{\Delta E}{\Delta i}$ and B is a constant. There is a linear relationship between potential and i_{corr} . Polarization resistance is obtained from the slope of potential and current density near E_{corr} . Linear polarization plot is shown in Fig. 2.5. Corrosion rate is inversely proportional to polarization resistance. Corrosion inhibition efficiency is then determined using the equation given below [115]

$$\eta_{R_p} \% = \frac{R'_p - R_p}{R'_p} \times 100 \quad (18)$$

where R_p and R'_p denotes polarization resistance in the absence and presence of inhibitor respectively.

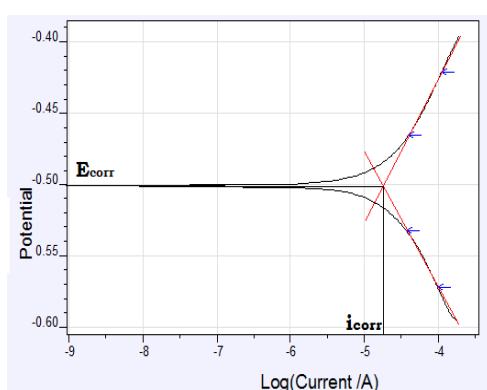


Fig. 2.4 Tafel plot

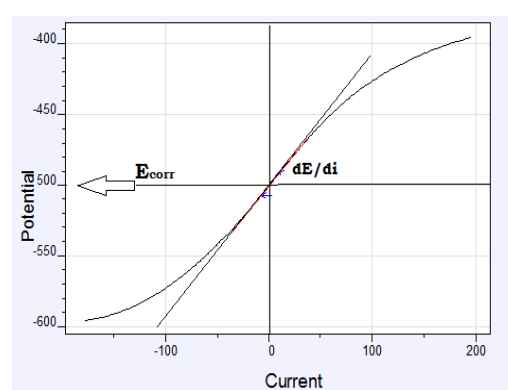


Fig. 2.5 Linear polarization plot

Electrochemical noise measurements

Electrochemical noise (ECN) measurement is a widely used technique in the field of corrosion engineering as a corrosion monitoring technique. Electrochemical noise is a common term used to indicate current and potential fluctuations. External current is not applied for measuring electrochemical noise. Noise is defined as undesirable disruption obscures with a preferred signal. It is a non-deterministic process which means that amplitude-time dependence of a specific source is not possible. Measurements were carried out in a three-electrode system consisting of two mild steel electrodes having 1 cm^2 area and a saturated calomel electrode [116-117]. The analysis was executed with the help of Ivium compactstat-e electrochemical system controlled by iviumsoft

software. All electrochemical noise analyses were performed for a period of 1200 s. The parameters mean value of current noise and pitting index were measured from noise plots. Mean value of current noise gives information regarding protective power of sample against corrosion and pitting index value helps to quantify localized pitting corrosion [118-120]. Current noise Vs. time plot and pitting index curve are shown in Fig 2.6a and b. Spectral analysis method is typically used to show noise signals as power spectral density (PSD) in the frequency domain. PSD plot is shown in Fig 2.6c. In order to convert time domain into frequency domain spectra two mathematical approaches used are fast Fourier transform (FFT) and maximum entropy method (MEM).

Frequency domain analysis: The basic principle is waveform of any complexity is taken into consideration as the addition of numerous sinusoidal waveforms of suitable relative phase, periodicity and amplitude [121-123]. In frequency domain analysis the depiction of a time depending process is called a spectrum. Parameter obtained from frequency domain analysis of a noise data is the power spectral density (PSD). Power spectral density is time independent and do not alter with time. Potential and current noise having greater amplitude indicates localized corrosion of metal.

Fast Fourier transform: Fast Fourier transform (FFT) is a faster machine calculation method of the complex Fourier series, based upon algorithms already existing. Mathematical properties of FFT are equivalent to that of traditional discrete Fourier transform. Leakage and aliasing are the two major problems accompanying analysis by FFT. The assumption of periodicity of finite time record in Fourier transform results leakage whereas too slow sampling rate introduced aliasing.

Maximum entropy method: Fourier transform is a major tool in all spectral analysis method [124]. But this is accurate only when long record length occurs. Spectral resolution is poor when the record length is short. Resolution can be enhanced in the case

of short length records by making use of Burg's maximum entropy method. This is achieved by extrapolating auto-correlation function and maximizing entropy of the probability density function in each step of the extrapolation. Burg's method is data dependent and nonlinear. The MEM is important in the various fields of science and technology.

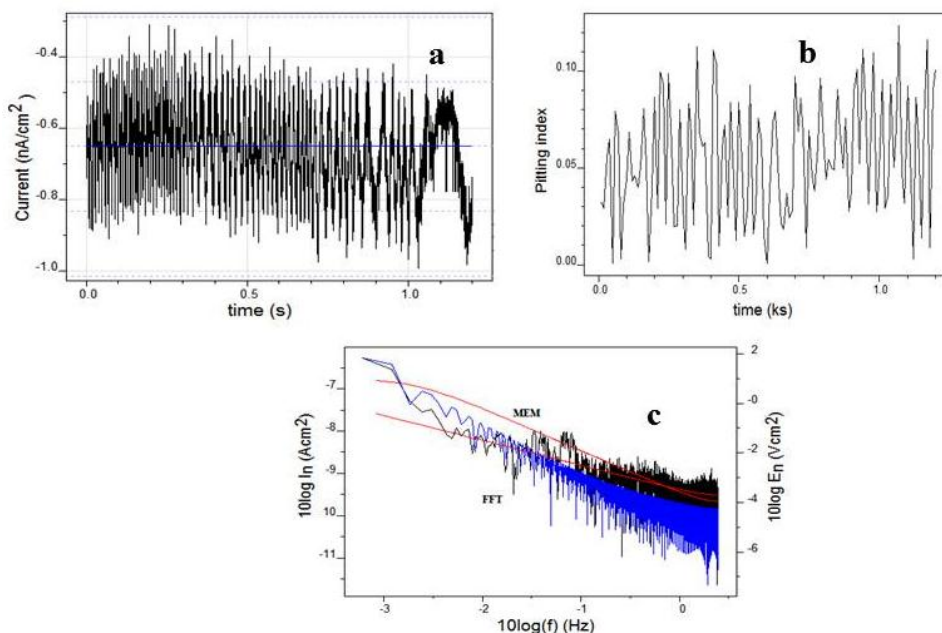


Fig. 2.6 a) Current noise Vs time plot b) pitting index curve c) PSD plot

Surface morphological studies

Surface morphological studies were done to understand the mechanism by which the Schiff base ligand decreases the corrosion rate. Surface morphology of mild steel specimens were determined using scanning electron microscope (JEOL Model JSM - 6390LV). SEM images of three set of specimens containing polished bare MS specimen, MS specimen immersed in acid solutions (1.0 M HCl and 0.5 M H₂SO₄) for 24 h (blank) and MS specimen immersed in acid solutions containing inhibitor molecule having 1 mM concentration were taken to evaluate the change occurring at the surface of the MS specimen before and after treatment with acid medium.

Quantum chemical investigations

The molecular structures were drawn with the help of Avogadro program. Density functional theory (DFT) method is employed for the geometry optimization of the molecules with the help of GAMESS software. B3LYP functional with a basis set of STO-3G was used for the studies. Combination of DFT and B3LYP will give good idea about the properties of the molecules related to their reactivity. This method is widely used to determine the relation between corrosion inhibition efficiency and electronic properties of the molecule [125-127]. Output is visualized using the program MacMolPlt output viewer. Parameters obtained from this study are highest occupied molecular orbital energy (E_{HOMO}), lowest unoccupied molecular energy (E_{LUMO}), energy gap (ΔE), electronegativity (χ), hardness (η) and number of electrons transferred from inhibitor molecule to Fe atom (ΔN). The parameters ΔE , χ , η and ΔN were calculated using the equations given below [128-129]

$$\Delta E = E_{\text{LUMO}} - E_{\text{HOMO}} \quad (19)$$

$$\chi = -1/2 (E_{\text{HOMO}} + E_{\text{LUMO}}) \quad (20)$$

$$\eta = 1/2 (E_{\text{HOMO}} - E_{\text{LUMO}}) \quad (21)$$

$$\Delta N = (\chi_{\text{Fe}} - \chi_{\text{inhib}}) / 2(\eta_{\text{Fe}} + \eta_{\text{inhib}}) \quad (22)$$

where $\eta_{\text{Fe}} = 0 \text{ eVmol}^{-1}$ and $\chi_{\text{Fe}} = 7 \text{ eVmol}^{-1}$

CHAPTER 3

SYNTHESIS AND CHARACTERIZATION OF SCHIFF BASES

This chapter deals with the synthesis and characterization of Schiff bases 2, 2'-(5,5-dimethylcyclohexane-1,3-diylidene)bis(azanylylidene)diphenol (DMCHDP), N,N'-(5,5-dimethylcyclohexane-1,3-diylidene)dianiline (DMCHDA), 2,2'-(5,5-dimethylcyclohexane-1,3-diylidene)bis(hydrazinecarboxamide) (DMCHHC), 2-((2-hydroxybenzylidene)amino)phenol (2HBAP) and 2-(cyclohexylideneamino)phenol (2CHAP). Elemental analysis, spectral studies such as Fourier transform infrared, UV- visible, NMR (^1H and ^{13}C) and mass spectroscopy and cyclic voltammetry are the characterization techniques employed for the derivation of structure of the synthesized Schiff bases.

Synthesis and characterization of 2,2'-(5,5-dimethylcyclohexane-1,3-diylidene)bis(azanylylidene)diphenol

Hot ethanolic solution of 5,5-dimethyl-1,3-cyclohexanedione (0.01 mol) was added dropwise to a stirred solution containing 0.02 mol of 2-aminophenol dissolved in ethanol. The mixture was refluxed for about 20 minutes and cooled. Brown coloured precipitate formed was filtered, washed with distilled water and dried. Yield of the inhibitor was 85%. M.P = 180°C .

Elemental and spectral analysis

Anal.calcd for $\text{C}_{20}\text{H}_{22}\text{N}_2\text{O}_2$: C, 74.53; H, 6.83; N, 8.69%. Found. C, 73.91; H, 6.74; N, 8.52%.

Characteristic stretching frequencies of various bonds in DMCHDP were observed in the IR spectrum. The azomethine moiety (C=N) was identified by the peak at 1600 cm^{-1} . A band at 3080 cm^{-1} was due to the aromatic C-H bond stretching vibration.

ν_{C-O} was observed at 1238 cm^{-1} . $\nu_{C=C}$ stretching vibration of the aromatic ring was observed at 1564 and 1514 cm^{-1} . A band at 3240 cm^{-1} indicates the stretching vibration of OH group. C-H bond of sp^3 hybridized carbon gave characteristic bands at 2960 and 2877 cm^{-1} . A peak at 1450 cm^{-1} corresponds to C-H bending vibration. In plane deformation was observed at 1147 , 1114 and 1037 cm^{-1} and out of plane deformation at 763 and 650 cm^{-1} .

Three distinct adsorption bands were observed in the UV-visible spectrum of DMCHDP. Peaks at 39682 cm^{-1} and 33784 cm^{-1} corresponds to $\pi \rightarrow \pi^*$ transition and the peak at 22936 cm^{-1} represents $n \rightarrow \pi^*$ transition.

Eight non-equivalent hydrogen atoms which were in different electronic environments gave corresponding characteristic peaks in the ^1H NMR spectrum. A peak obtained at $0.9\ \delta$ can be assigned to CH_3 group present in the cyclohexane ring. CH_2 group adjacent to the methyl group showed a peak at $2.0\ \delta$. Peak at $2.4\ \delta$ is assigned to the methylene proton in between two azomethine moieties. A broad peak at $9.8\ \delta$ corresponds to OH proton. Aromatic protons gave characteristic peaks at 6.8 - $7.1\ \delta$. The appearance of a weak broad signal at $8.4\ \delta$, due to the NH proton and peak at $4.8\ \delta$ due to olefinic CH, confirmed the existence of tautomerism. The structures of DMCHDP and its tautomer are given in Fig. 3.1.

Presence of eleven chemically different carbon atoms was confirmed by the ^{13}C NMR spectrum. Azomethine carbon was identified at 95.88 ppm . Aromatic carbons of the benzene ring exhibited six signals in the range 116.28 - 151.55 ppm . Methylene carbon atoms exhibited their peaks at 32.32 ppm and 49.78 ppm respectively. Methyl carbon atom exhibited a signal at 27.84 ppm .

In mass spectra molecular ion peak was absent. Base peak was observed at $m/z\ 216$, which is formed by the loss of amino phenolic moiety from the molecule. Loss

of one phenolic moiety resulted with a peak at m/z 231 which corresponds to $[C_{14}H_{19}N_2O]^+$. Peaks appeared at m/z 178, 160, 146, 133 and 109 were due to the fragments $[C_{11}H_{16}NO]^+$, $[C_9H_8N_2O]^+$, $[C_9H_{10}N_2]^+$, $[C_8H_7NO]^+$ and $[C_6H_9N_2]^+$ respectively.

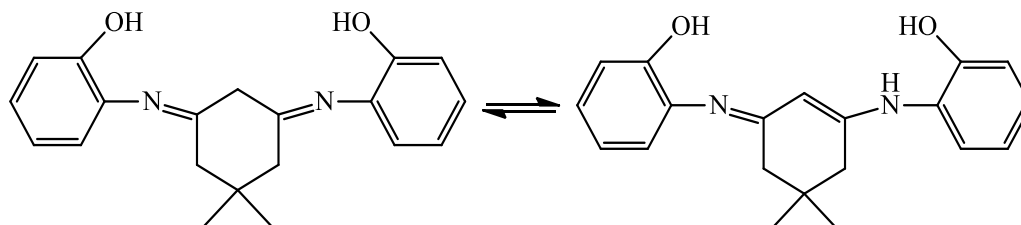


Fig. 3.1 Structures of DMCHDP and its tautomer

Cyclic voltammetric studies

Cyclic voltammogram of DMCHDP was recorded in the potential range 1.0 to -2.0 V at a scan rate of 0.10 V/s (Fig. 3.2a). There are three cathodic peaks (A, B and C) and three anodic peaks (D, E and F) in the forward and reverse scan respectively. Two cathodic peaks A and B observed at a potential of 0.376 V and -0.188 V respectively are due to the successive one electron reduction processes occurring at two azomethine moieties. Cathodic peak observed at a potential of -1.098 V is considered due to two electron reduction occurring at two azomethine moieties since, height of this peak is significantly higher than the other two cathodic peaks. Anodic peaks D and E observed at a potential of -0.421 V and -0.001 V are due to two successive one electron oxidation processes of the reduced form of DMCHDP. Though it is not clearly visible in voltammogram, the conversion of E to F takes place in two steps actually. Two stages having close oxidation potentials (0.3610 V and 0.4790 V) were more clearly visible in the voltammogram recorded at low scan rate (0.02 V/s). There are no counter cathodic and anodic peaks observed in this redox processes. This indicates the irreversible nature of the electron transfer processes. Cyclic voltammogram of DMCHDP at different scan

rates is given in Fig. 3.2b. Mechanism of redox process can be best viewed with the help of Fig. 3.3.

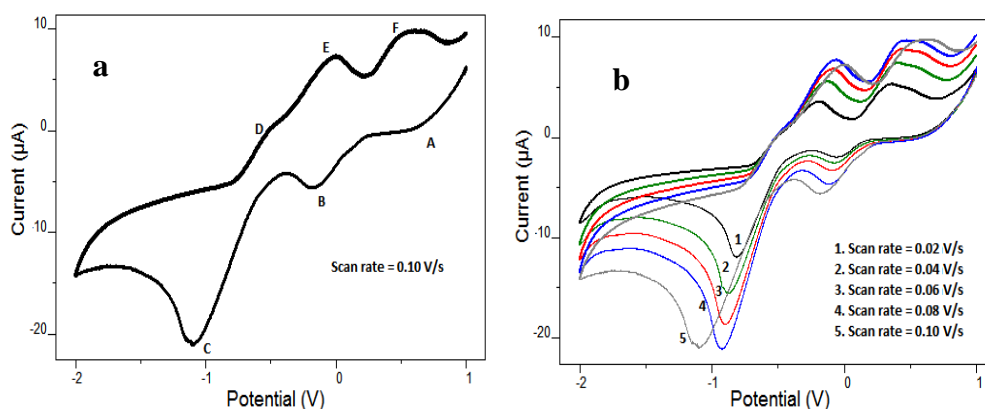


Fig. 3.2 Cyclic voltammogram of DMCHDP **a)** at a scan rate of 0.10 V/s **b)** at scan rates 0.02-0.10 V/s

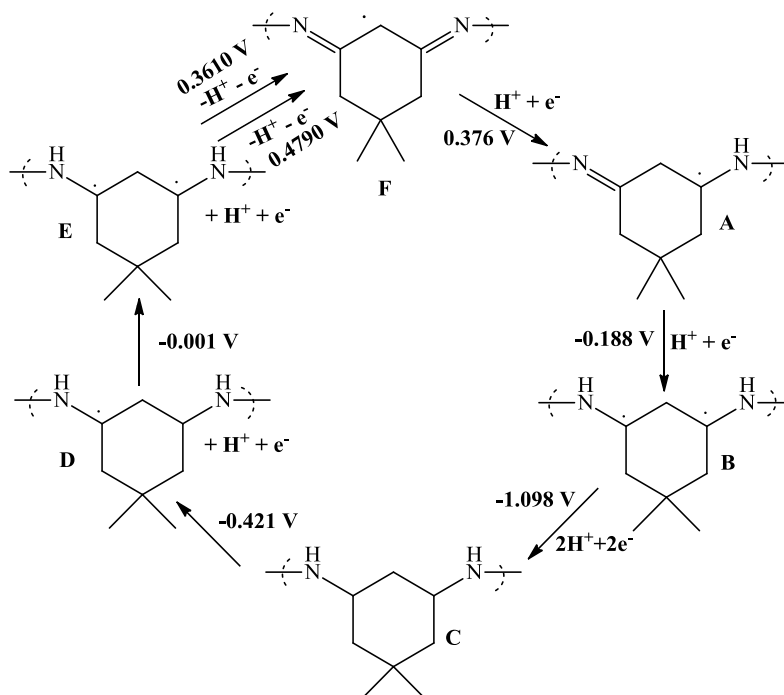


Fig. 3.3 Redox mechanism occurring at azomethine moiety of DMCHDP

Synthesis and characterization of N,N' -(5,5-dimethylcyclohexane-1,3-diyldene) dianiline

0.01 mol of 5,5-dimethyl-1,3-cyclohexanedione was dissolved in hot ethanol and added to a stirred ethanolic solution of 0.02 mol of aniline. Refluxed for 3 h and cooled. Yellow precipitate formed was filtered, washed with ethanol and recrystallized. Yield: 78%, M.P:152⁰C.

Elemental and spectral analysis

Anal.calcd for C₂₀H₂₂N₂: C, 82.7; H, 7.5; N, 9.6%. Found. C, 81.3; H, 6.9; N, 8.9%;

IR spectrum of DMCHDA exhibits several peaks corresponding to the stretching frequencies of various bonds. The formation of C=N linkage is proved by the stretching vibration at 1564 cm⁻¹. Peaks corresponding to ν_{C-N} were observed at 1249 cm⁻¹ and 1149 cm⁻¹. Peaks at 1529 cm⁻¹, 1440 cm⁻¹ and 1413 cm⁻¹ can be assigned to C=C vibrations of aromatic system. Stretching frequency due to NH vibration was identified as a broad peak at 3234 cm⁻¹. Peaks at 2949 cm⁻¹, 2879 cm⁻¹ and 2810 cm⁻¹ are due to the stretching vibration of sp³C-H bond. Aromatic C-H bond gave peak at 3055 cm⁻¹. In plane deformation was observed at 1033 cm⁻¹ and 1080 cm⁻¹. Out of plane deformation was observed at 707 cm⁻¹ and 759 cm⁻¹.

Peaks corresponding to $\pi \rightarrow \pi^*$ and $n \rightarrow \pi^*$ transition was observed at 39463 cm⁻¹ and 32020 cm⁻¹ respectively in the UV-visible spectrum of DMCHDA.

Seven distinct hydrogen atoms displayed seven independent signals in the ¹H NMR spectrum of DMCHDA. Methyl carbon exhibited a peak at 1.0 δ . The CH₂ carbons adjacent to the carbon containing methyl group and in between azomethine linkages displayed peaks at 2.3 δ , 2.1 δ and 5.5 δ respectively. Peaks at 7.2 δ and 7.0 δ are assignable to aromatic protons. Presence of peaks at 6.1 δ and 7.2 δ due to N-H and sp²C-H bonds proved the existence of tautomer. The structures of DMCHDA and its tautomer are shown in Fig. 3.4.

In the ¹³C NMR spectrum of DMCHDA the signal appeared at 28.35 ppm is due to methyl carbon. Azomethine carbon displayed a peak at 98.94 ppm. Peak at 32.88 ppm was assignable to the carbon containing methyl groups and the carbon present between two azomethine groups displayed a peak at 43.71 ppm. Signal at 50.35 ppm corresponds to the carbon adjacent to the carbon containing methyl groups. Carbon atoms present in

the aromatic ring displayed peaks at 123.86 ppm, 125.59 ppm, 129.39 ppm and 138.14 ppm.

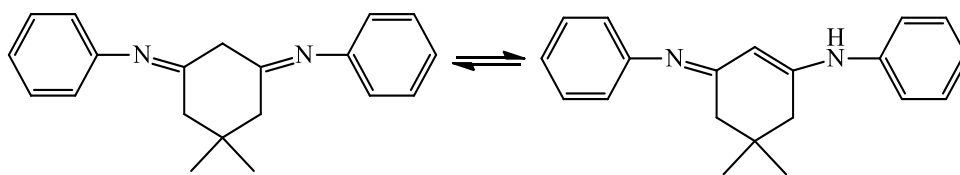


Fig. 3.4 Structures of DMCHDA and its tautomer

Presence of only one peak in the gas chromatogram indicates purity of the Schiff base formed. Molecular ion peak was absent. Base peak was observed at m/z 159 corresponds to the fragment $[C_{11}H_{13}N]^+$. Loss of one phenyl group resulted in the fragment $[C_{14}H_{19}N_2]^+$ at m/z 215. Peak at m/z 198 is due to the fragment $[C_{14}H_{16}N]^+$ formed by the loss of one aniline moiety and the peaks due to the fragments $[C_9H_8N]^+$, $[C_6H_6N]^+$, $[C_6H_5]^+$ were observed at m/z 130, 92 and 77 respectively.

Cyclic voltammetric studies

Cyclic voltammogram of DMCHDA was taken at a scan rate of 0.10 V/s in the potential range of 2.0 to -2.0 V in order to understand its electrochemical behaviour. Fig. 3.5 represents the cyclic voltammogram of DMCHDA at a scan rate of 0.10 V/s. On close examination two cathodic peaks marked as A and B and two anodic peaks marked as C and D are visible. Peaks A and B observed in the forward scan at 1.029 V and -0.671 V correspond to one electron reduction of the azomethine moiety. Peaks C and D appeared at -0.266 V and 0.994 V in the reverse scan are due to successive one electron oxidation of the reduced form of DMCHDA.

Synthesis and characterization of 2,2'-(5,5-dimethylcyclohexane-1,3-diyldene)bis(hydrazinecarboxamide)

To the stirred solution of semicarbazide hydrochloride (0.02 mol) dissolved in ethanol-water mixture, hot ethanolic solution of 5,5-dimethyl-1,3-cyclohexanedione was

added and refluxed for 15 min and dried. Then saturated solution of it was neutralized by adding very dilute NaOH solution to form bis semicarbazone. Yield = 70%.
M.P = 215⁰C

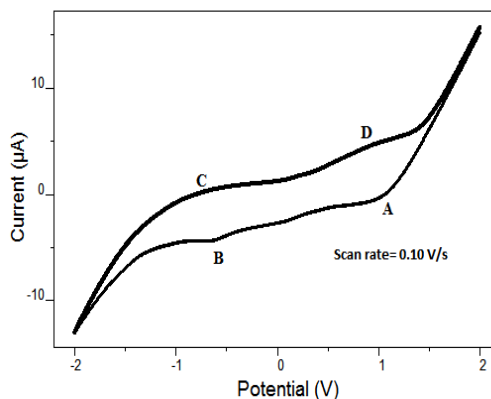


Fig. 3.5 Cyclic voltammogram of DMCHDA at a scan rate of 0.10 V/s

Elemental and spectral analysis

Anal.calcd for C₁₀H₁₈N₆O₂: C, 47.24; H, 7.08; N, 33.07%. Found. C, 46.58; H, 6.89; N, 33.84%;

In the IR spectra of DMCHHC, the peak due to azomethine moiety was observed at 1571 cm⁻¹. The peaks at 3468 cm⁻¹ and 3323 cm⁻¹ corresponds to stretching frequency of 1⁰ N-H groups whereas the peak due to 2⁰ N-H was observable at 3203 cm⁻¹. A peak at 1701 cm⁻¹ was assigned to stretching vibration of C=O group. Stretching frequency due to C-H and C-N vibrations were identified at 2954 cm⁻¹, 2903 cm⁻¹, 2873 cm⁻¹ and 1284 cm⁻¹ respectively. In plane bending was observed at 1099 cm⁻¹ and out of plane bending was observed at 763 cm⁻¹ and 705 cm⁻¹.

The peaks at 39370 cm⁻¹ and 33898 cm⁻¹ in the UV-visible spectrum of DMCHHC correspond to $\pi \rightarrow \pi^*$ and $n \rightarrow \pi^*$ transition respectively.

Five distinct peaks were obtained in the proton NMR spectrum of DMCHDC corresponding to five non-equivalent hydrogen atoms. Methyl protons gave a characteristic peak at 0.8 δ . Broad peaks observed at 6.5 δ and 9.4 δ was assigned to NH and NH₂ protons respectively. The CH₂ protons existing between two C=N groups

displayed a peak at 3.3 δ . The peak at 2.2 δ corresponds to CH_2 group adjacent to the carbon containing methyl group.

Six carbon atoms in various electronic environments displayed their characteristic peaks in the ^{13}C NMR spectrum. Azomethine carbon and carbonyl carbon displayed their peaks at 144.92 ppm and 157.55 ppm respectively. Peak at 27.45 ppm was assignable to methyl carbon and carbon atoms of methyl groups showed a peak at 28.34 ppm. The CH_2 carbon adjacent to the carbon containing methyl group and existing between two $\text{C}=\text{N}$ groups exhibited their peaks at 31.96 ppm and 46.19 ppm respectively. The structure of DMCHHC is shown in Fig. 3.6.

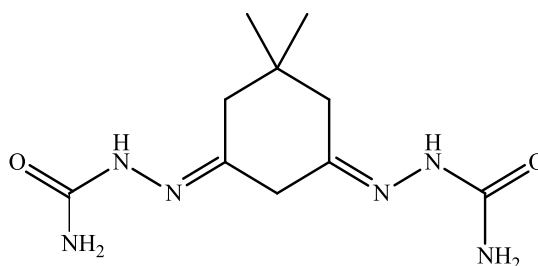


Fig. 3.6 Structure of DMCHHC

In the mass spectrum of the Schiff base molecular ion peak was observed at m/z 254. Base peak due to the fragment $[\text{C}_{10}\text{H}_{15}\text{N}_5\text{O}_2]^+$ was appeared at m/z 237, formed by the loss of NH_3 molecule from molecular ion. Loss of NH_2 moiety gave a signal at m/z 238. The fragments $[\text{C}_9\text{H}_{17}\text{N}_5\text{O}]^+$ and $[\text{C}_9\text{H}_{16}\text{N}_4\text{O}]^+$ were obtained by the loss of CONH and NCONH_2 moiety and displayed their peaks at m/z 211 and m/z 196 respectively. Appearance of peaks at m/z 194, 181, 164, 138 and 123 can be assigned to the fragments $[\text{C}_9\text{H}_{14}\text{N}_4\text{O}]^+$, $[\text{C}_9\text{H}_{15}\text{N}_3\text{O}]^+$, $[\text{C}_8\text{H}_{12}\text{N}_4]^+$, $[\text{C}_8\text{H}_{14}\text{N}_2]^+$ and $[\text{C}_8\text{H}_{13}\text{N}]^+$ respectively.

Cyclic voltammetric studies

Cyclic voltammogram of DMCHHC at a scan rate of 0.10 V/s is shown in Fig. 3.7. In the voltammogram, only two peaks having low intensities were appeared in

the forward scan. These peaks marked as A and B may be due to successive one electron reduction of the azomethine group present in the molecule. Absence of peaks corresponding to oxidation indicates that the electrochemical behaviour is more irreversible in nature.

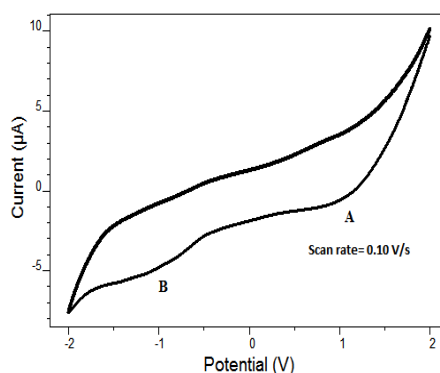


Fig. 3.7 Cyclic voltammogram of DMCHHC at a scan rate of 0.10 V/s

Synthesis and characterization of 2-((2-hydroxybenzylidene)amino)phenol

To the hot ethanolic solution of salicylaldehyde (0.01 mol), ethanolic solution of 2-aminophenol (0.01 mol) was added and refluxed for 2 h. Then concentrated, cooled and the orange-red precipitate formed was filtered and washed with ethanol. Yield = 88%. M.P = 178⁰C

Elemental and spectral analysis

Anal.calcd for C₁₃H₁₁NO₂: C, 73.23; H, 5.16; N, 6.57%. Found. C, 72.98; H, 5.23; N, 7.02%;

Characteristic stretching frequencies of the various bonds were observed in the IR spectrum of 2HBAP. A broad peak at 3322 cm⁻¹ was assigned to the OH group present in the molecule. Azomethine group has shown its stretching frequency at 1625 cm⁻¹ and ν_{C-N} was observed at 1215 cm⁻¹. The C=C present in the aromatic ring displayed peaks at 1598, 1527 and 1456 cm⁻¹ whereas the C-H bond in the aromatic ring displayed peak at 3045 cm⁻¹. In plane deformation was observed at 1014 cm⁻¹. Peaks at 904 and 732 cm⁻¹ were due to out of plane deformations.

The peaks corresponding to $\pi \rightarrow \pi^*$ and $n \rightarrow \pi^*$ transition were observed at 39062 cm^{-1} and 34014 cm^{-1} respectively in the UV-visible spectrum of 2HBAP.

In the ^1H NMR spectra of 2HBAP, the singlet at 13.8δ was assignable to the OH proton. The proton of the azomethine group displayed a signal at 9.7δ . Peaks at 7.4 , 6.8 , 6.10 and 7.4δ were exhibited by the protons of the ring present in salicylaldehyde moiety whereas the peaks at 8.95 , 7.61 , 9.95δ were due to the protons of the ring present in 2-aminophenol moiety.

Thirteen signals observed in the ^{13}C NMR spectrum may be attributed to thirteen different type carbon atoms present in the molecule. Signals due to carbons in the aromatic rings were observed in the range 116 - 160 ppm. Azomethine carbon displayed a peak at 161 ppm.

In mass spectrum, molecular ion peak was appeared at m/z 213. Base peak was observed at m/z 120 due to the fragment $[\text{C}_7\text{H}_6\text{NO}]^+$ formed by the loss of phenol moiety. Loss of OH group from the molecule leads to the fragment $[\text{C}_{13}\text{H}_{10}\text{NO}]^+$ and showed a signal at m/z 196. The peak at m/z 77 was due to phenyl cation and fragment ions such as $[\text{C}_6\text{H}_5\text{O}]^+$ and $[\text{C}_5\text{H}_5]^+$ exhibited their characteristic peaks at m/z 93 and 65 respectively. The structure of 2HBAP is shown in Fig. 3.8.

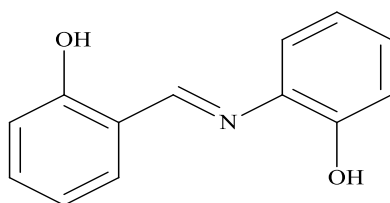


Fig. 3.8 Structure of 2HBAP

Cyclic voltammetric studies

Electrochemical response of the Schiff base, 2HBAP was studied by taking its cyclic voltammogram at a scan rate of 0.10 V/s in the potential range 2.0 to -2.0 V . Cyclic voltammogram of 2HBAP at a scan rate of 0.10 V/s is shown in Fig. 3.9. In the

figure three cathodic peaks (A, B and C) and two anodic peaks (D and E) were observed. Peaks A and C appeared at 0.312 V and -0.156 V may be due to successive one electron reduction processes occurring at azomethine moiety. Intensity of the cathodic peak C is high compared to other cathodic peaks. Thus the peak B displayed at -0.689 V may be attributed to the two phenolate/phenoxy radical since two OH groups are present in the molecule. Successive one electron oxidation processes of azomethine moiety are represented by less intense anodic peaks D and E at -0.393 V and 1.432 V respectively.

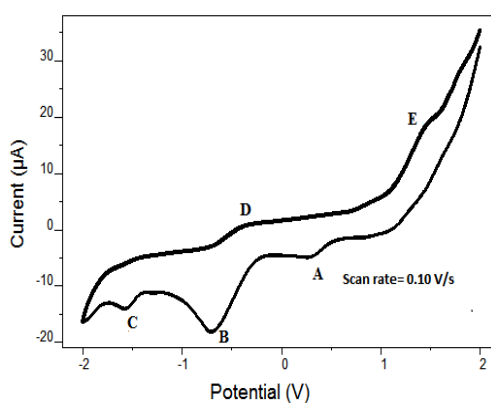


Fig. 3.9 Cyclic voltammogram of 2HBAP at a scan rate of 0.10 V/s

Synthesis and characterization of 2-(cyclohexylideneamino)phenol

To the hot ethanolic solution of cyclohexanone (0.01 mol), ethanolic solution of 2-aminophenol (0.01 mol) was added and refluxed for 2 h. Then concentrated, cooled and the brown precipitate formed was filtered and washed with ethanol. Yield =72%. M.P= 128⁰C.

Elemental and spectral analysis

Anal.calcd for C₁₂H₁₅NO: C, 76.19; H, 7.93; N, 7.40%. Found. C, 76.10; H, 7.19; N, 7.68%;

In the Fourier transform infrared spectrum of the Schiff base absorption peak appeared at 1602 cm⁻¹ was assigned to C=N stretching vibration. ν_{C-N} and ν_{N-H} were observed at 1267 cm⁻¹ and 3304 cm⁻¹ respectively. Also the appearance of $\nu_{C=C}$ at 1510

and 1495 cm^{-1} proved the existence of tautomer. Stretching vibration due to OH group was displayed at 3375 cm^{-1} . The C-H stretching vibration of aromatic ring and cyclohexanone ring were observed at 3051 and 2956 cm^{-1} . Peak at 1080 cm^{-1} was due to in plane deformation whereas the peaks at 896 and 742 cm^{-1} represent out of plane deformation.

Absorption bands observed in the electronic spectrum of 2CHAP at 39526 and 34013 cm^{-1} represent $\pi \rightarrow \pi^*$ and $n \rightarrow \pi^*$ transitions respectively.

Eight characteristics peaks were observed in the proton NMR spectrum of 2CHAP corresponding to eight different type protons. The OH proton displayed a peak at $5.1\ \delta$. Protons of the aromatic ring showed peaks in the range 6.4 - $7.8\ \delta$ whereas the protons of the cyclohexane ring displayed peaks at 1.9 , 2.3 and $3.8\ \delta$.

In the ^{13}C NMR spectrum of 2CHAP nine distinct signals were observed. Azomethine carbon displayed a peak at 128.75 ppm . Aromatic ring carbons displayed peaks at 116 ppm , 119 ppm , 121 ppm , 125.34 ppm , 129.73 ppm and 144.28 ppm . Carbon atoms of cyclohexane ring system showed peaks in the range 25.20 ppm - 100.82 ppm . The structure of 2CHAP is shown in Fig. 3.10.

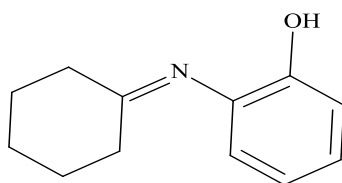


Fig. 3.10 Structure of 2CHAP

In the mass spectrum of the Schiff base 2CHAP, the molecular ion peak was absent. Base peak was observed at $m/z\ 109$ due to the fragment $[\text{C}_6\text{H}_7\text{NO}]^+$. Peaks appeared at m/z values 80 and 64 correspond to the fragment $[\text{C}_6\text{H}_8]^+$ and $[\text{C}_5\text{H}_4]^+$ respectively.

Cyclic voltammetric studies

Cyclic voltammogram of 2CHAP at a scan rate of 0.10 V/s is shown in Fig. 3.11.

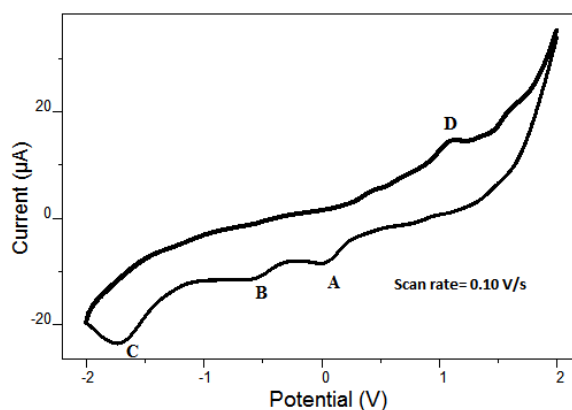


Fig. 3.11 Cyclic voltammogram of 2CHAP at a scan rate of 0.10 V/s

During the forward scan three cathodic peaks and during the reverse scan one anodic peak was observed. Peaks A and B at -0.021 V and -0.554 V may be due to successive one electron reduction of azomethine moiety and the peak C at -1.703 V is due to phenolate/phenoxy radical. The anodic peak at 1.093 V can be attributed to one electron oxidation of azomethine moiety.

CHAPTER 4

CORROSION INHIBITION STUDIES OF SCHIFF BASES IN 1.0 M HCl MEDIUM

Investigations on corrosion inhibition efficiency of the Schiff bases 2,2'-(5,5-dimethylcyclohexane-1,3-diylidene)bis(azanylylidene)diphenol (DMCHDP), N,N'-(5,5-dimethylcyclohexane-1,3-diylidene)dianiline (DMCHDA), 2,2'-(5,5-dimethylcyclohexane-1,3-diylidene)bis(hydrazinecarboxamide) (DMCHHC), 2-((2hydroxybenzylidene)amino) phenol (2HBAP), 2-(cyclohexylideneamino)phenol (2CHAP) having concentration in the range 0.2-1.0 mM on mild steel were conducted in 1.0 M HCl. Mild steel specimens were prepared as per ASTM standards. Corrosion monitoring techniques employed for the study are gravimetric (weight loss) and electrochemical studies (electrochemical impedance spectroscopy, potentiodynamic polarization studies and electrochemical noise measurements). To illustrate the mechanism of inhibition by Schiff base molecule adsorption studies were also carried out. Thermodynamic parameters of corrosion of mild steel such as activation energy (E_a), enthalpy of activation (ΔH^*), entropy of activation (ΔS^*) and Arrhenius factor (A) were evaluated using temperature dependent gravimetric investigations. Surface morphology of mild steel specimens were also determined using scanning electron microscope. Quantum chemical studies were done to illustrate the efficiency of these Schiff bases as corrosion inhibitor on mild steel in acid medium.

Weight loss studies

Parameters of corrosion such as rate of corrosion and corrosion inhibition efficiency obtained by weight loss studies carried out on mild steel specimens in 1.0 M HCl using Schiff bases (DMCHDP, DMCHDA, DMCHHC, 2HBAP and 2CHAP) at different concentrations for 24 h are shown in Table 4.1 and Table 4.2 respectively. Data

clearly showed that the rate of corrosion decreased with the concentration of Schiff bases in all cases except for 2HBAP. Comparison of corrosion rate of mild steel at different concentrations of the Schiff bases DMCHDP, DMCHDA, DMCHHC, 2HBAP and 2CHAP in 1.0 M HCl are shown in Fig. 4.1.

Table 4.1 Rate of corrosion of MS in mmy^{-1} with and without Schiff bases DMCHDP, DMCHDA, DMCHHC, 2HBAP and 2CHAP in 1.0 M HCl

Conc (mM)	Schiff base				
	DMCHDP	DMCHDA	DMCHHC	2HBAP	2CHAP
0.0	7.304	7.304	7.304	7.304	7.304
0.2	1.207	1.411	1.208	12.134	5.443
0.4	1.088	1.285	1.130	10.827	3.953
0.6	0.523	1.017	0.960	10.385	3.642
0.8	0.464	0.873	0.617	9.075	2.692
1.0	0.437	0.538	0.507	9.074	1.490

Table 4.2 Corrosion inhibition efficiency ($\eta_w\%$) of Schiff bases DMCHDP, DMCHDA, DMCHHC, 2HBAP and 2CHAP on MS in 1.0 M HCl

Conc (mM)	Schiff base				
	DMCHDP	DMCHDA	DMCHHC	2HBAP	2CHAP
0.2	83.46	80.67	83.45	-66.13	25.47
0.4	85.09	82.39	84.52	-48.23	45.86
0.6	92.83	86.07	86.84	-42.18	50.12
0.8	93.63	88.04	91.54	-24.25	63.14
1.0	94.01	92.63	93.05	-24.23	79.60

The ligands DMCHDP, DMCHDA and DMCHHC have high corrosion inhibition efficiency compared to 2HBAP and 2CHAP. Also the inhibition efficiency of these three ligands is greater than 80% at all studied concentrations. At 1 mM concentration, maximum efficiency of about 94.01%, 92.63% and 93.05% was reached by DMCHDP, DMCHDA and DMCHHC respectively. As the concentration increases, number of molecules required to block the reaction sites also increases. As a result corrosion inhibition efficiency increased with concentration. Comparison of corrosion

inhibition efficiency of the Schiff bases DMCHDP, DMCHDA, DMCHHC, 2HBAP and 2CHAP on MS in 1.0 M HCl are shown in Fig. 4.2.

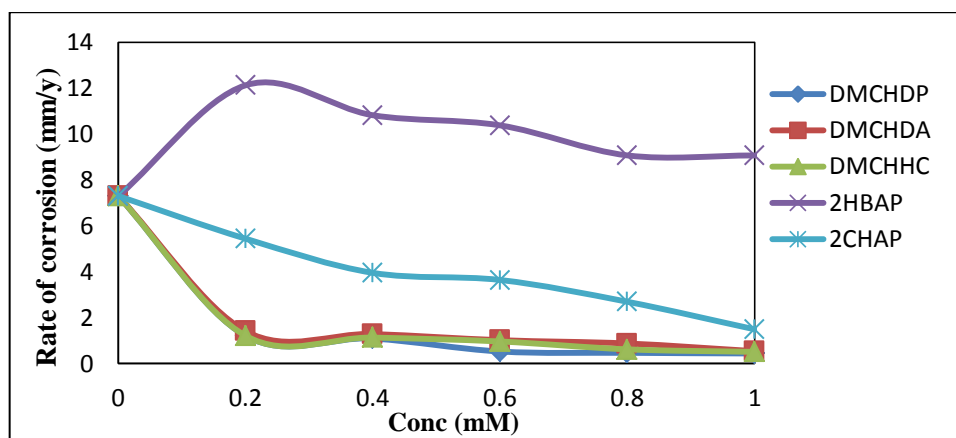


Fig. 4.1 Comparison of corrosion rate of mild steel at different concentrations of the Schiff bases DMCHDP, DMCHDA, DMCHHC, 2HBAP and 2CHAP in 1.0 M HCl

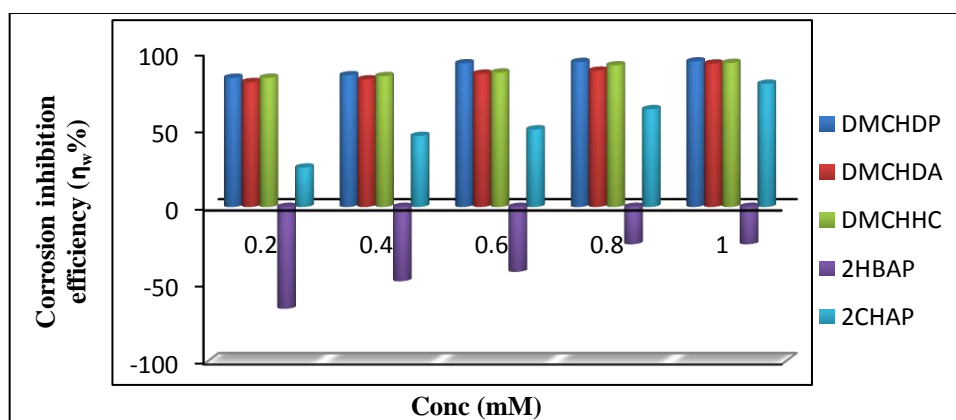


Fig. 4.2 Comparison of corrosion inhibition efficiency ($\eta_w\%$) of the Schiff bases DMCHDP, DMCHDA, DMCHHC, 2HBAP and 2CHAP on MS in 1.0 M HCl

Presence of azomethine ($>C=N-$) groups and aromatic rings are responsible for the enhanced activity of DMCHDP and DMCHDA. In addition, the hydroxyl group present in DMCHDP enhanced its efficiency. In DMCHHC azomethine group and hetero atoms such as N and O are responsible for the high inhibition capacity.

But in 2HBAP, even though the rate is decreasing with rise in concentration, it is higher than the blank specimen. As a result 2HBAP exhibits antagonistic nature on corrosion. Antagonistic effect of 2HBAP may be due to any one of the following reasons

or their combined effects: 1) evolution of hydrogen as a result of catalytic action of the compound adsorbed on metal 2) decrease of overpotential for cathodic processes 3) formed complex is easily soluble and it lowered the overpotential for cathodic processes.

Comparison between $\eta_w\%$ of Schiff bases with its parent compounds

In order to compare the corrosion inhibition efficiency of the Schiff bases with the corresponding aldehydes/ketones and amines from which they synthesized, weight loss measurement of the parent compounds were also conducted at concentrations 0.2 mM, 0.6 mM and 1.0 mM. The aldehyde, ketone and amines used for the synthesis are salicylaldehyde (SAY), 5,5-dimethyl-1,3-cyclohexanedione (DM), cyclohexanone (CH), 2-aminophenol (2AP), aniline (AN) and semicarbazide (SZ). Results are shown in Table 4.3. Comparison of corrosion inhibition efficiency of parent compounds and Schiff bases on MS in 1.0 M HCl are shown in Fig. 4.3.

Table 4.3 Corrosion inhibition efficiency ($\eta_w\%$) of Schiff bases and their parent compounds on MS in 1.0 M HCl

Compounds	Conc (mM)		
	0.2	0.6	1.0
DM	-85.40	-70.67	-42.56
2AP	-98.50	-67.76	-65.68
AN	-70.19	-8.46	25.70
SZ	-140.38	-133.79	-133.56
SAY	-111.73	-80.13	-60.47
CH	-136.78	-130.44	-109.77
DMCHDP	83.46	92.83	94.01
DMCHDA	80.67	86.07	92.63
DMCHHC	83.45	86.84	93.05
2HBAP	-66.13	-42.18	-24.23
2CHAP	25.47	50.12	79.60

From the table it is clear that the parent compounds have antagonistic effect on corrosion and inhibition efficiency of all the Schiff bases is remarkably higher than the

parent compounds. This is due to the participation of electron rich $>C=N-$ group present in the Schiff base ligands in the corrosion inhibition process.

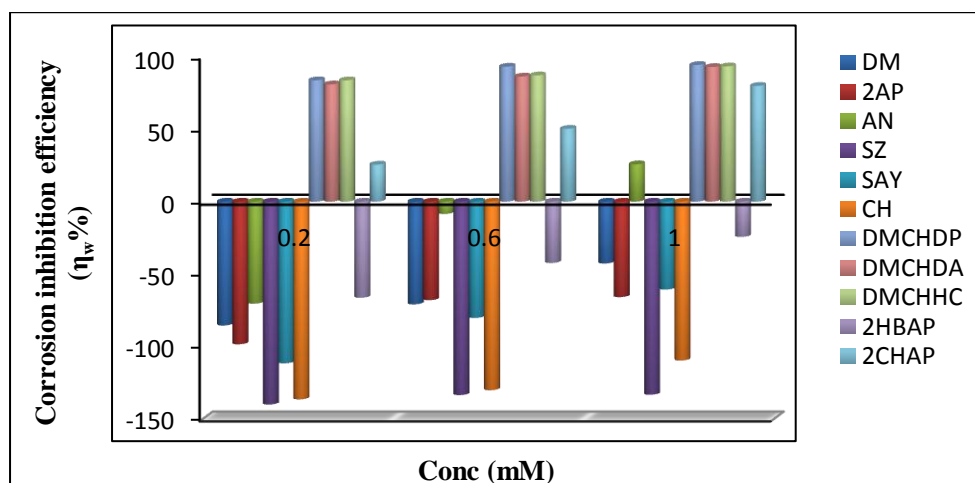


Fig. 4.3 Comparison of corrosion inhibition efficiency ($\eta_w\%$) of Schiff bases and their parent compounds on MS in 1.0 M HCl

Adsorption studies

Adsorption isotherms are useful to elucidate information regarding structural and thermodynamic parameters of the electrical double layer. Corrosion inhibition property of the organic compounds on MS surface is mainly due to adsorption. Therefore it is essential to understand the mode of adsorption that gives information regarding interaction of inhibitor molecule and MS surface. For this purpose different isotherms such as Langmuir, El-Awady, Frumkin, Temkin, Freundlich, and Florry-huggin isotherms were plotted and the best fit one was identified using correlation coefficient (R^2). Correlation coefficients obtained for the Schiff bases in various isotherms are given in Table 4.4.

Thermodynamic parameters obtained from the study are free energy of adsorption (ΔG_{ads}^0) and adsorption equilibrium constant (K_{ads}). Adsorption study clearly showed that the three Schiff bases DMCHDP, DMCHDA and DMCHHC were found to obey Langmuir adsorption isotherm whereas 2HBAP and 2CHAP obeyed Frumkin adsorption isotherm on MS surface in 1.0 M HCl medium.

Table 4.4 Correlation coefficients of the Schiff bases derived from various adsorption isotherms

Isotherm	Correlation coefficient (R^2)				
	DMCHDP	DMCHDA	DMCHHC	2HBAP	2CHAP
Langmiur	0.9988	0.9969	0.9979	0.9299	0.8522
Freunlich	0.8540	0.9762	0.9534	0.9066	0.9684
Frumkin	0.9541	0.9634	0.9421	0.9450	0.9756
Temkin	0.8522	0.8553	0.8221	0.9007	0.9331
El-Awady	0.8725	0.7968	0.8021	0.8996	0.9185
Florry Huggin	0.8479	0.7552	0.7695	0.7241	0.6145

Thermodynamic parameters obtained from the analysis of isotherms are given in Table 4.5 and the adsorption isotherms of Schiff base molecules on MS surface in 1.0 M HCl medium are described in Fig. 4.4.

Table 4.5 Thermodynamic parameters for the adsorption of DMCHDP, DMCHDA, DMCHHC, 2HBAP and 2CHAP on MS in 1.0 M HCl

Parameter	Schiff base				
	DMCHDP	DMCHDA	DMCHHC	2HBAP	2CHAP
Correlation coefficient (R^2)	0.9988	0.9969	0.9979	0.9450	0.9756
K_{ads}	20000	16666.66	20000	3333.33	2385.61
ΔG_{ads}^0 (kJmol^{-1})	-34.86	-34.40	-34.86	-30.37	-29.53

The ΔG_{ads}^0 values upto -20 kJmol^{-1} indicate that the interaction of charged molecule and charged metal surface is electrostatic in nature (physisorption) while if its value is more negative than -40 kJmol^{-1} indicates the presence of co-ordinate type bond between Schiff base molecules and metal surface (chemisorption). Negative values of ΔG_{ads}^0 in all case indicate spontaneity of the process. In the case of Schiff bases subjected to adsorption studies the ΔG_{ads}^0 values varies from $-29.53 \text{ kJmol}^{-1}$ to $-34.86 \text{ kJmol}^{-1}$. This indicates that the adsorption behaviour of all Schiff bases involves both electrostatic and chemical interaction. High value of adsorption equilibrium constant (K_{ads}) of DMCHDP, DMCHDA and DMCHHC than the other two Schiff base ligands indicates strong interaction of them on MS surface.

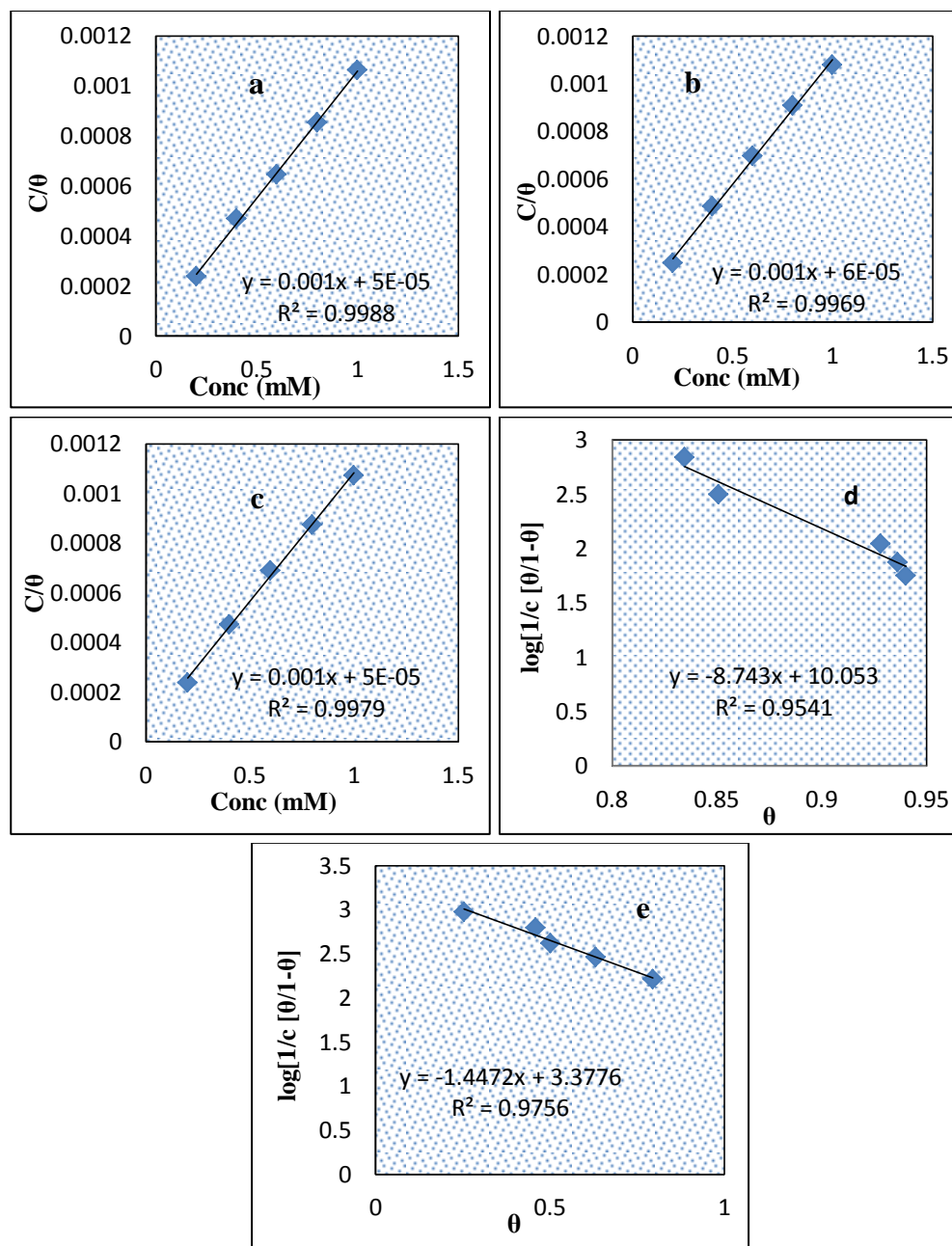


Fig. 4.4 Langmuir adsorption isotherm of a) DMCHDP b) DMCHDA and c) DMCHHC and Frumkin adsorption isotherm of d) 2HBAP and e) 2CHAP on MS in 1.0 M HCl at 28°C

Temperature studies

Temperature dependent gravimetric investigations definitely benchmark the mode of corrosion inhibition process. Degree of corrosion is dependent on temperature, remarkably in acid media associated with hydrogen evolution. In the present work, the impact of temperature on the inhibition process was investigated using weight loss

studies for 24 h in 1.0 M HCl with and without Schiff bases (DMCHDP, DMCHDA, DMCHHC, 2HBAP and 2CHAP) at temperatures 301 K, 313 K, 323 K and 333 K.

Activation energy of metal dissolution was measured using an Arrhenius type equation given below

$$K = A \exp(-E_a/RT) \quad (1)$$

where K, A, E_a , R and T represents corrosion rate, pre-exponential factor, activation energy, universal gas constant, temperature in Kelvin respectively.

Straight lines obtained by plotting log K vs 1/T for MS specimens in acid, with and without Schiff bases are shown in Fig. 4.5- 4.9a.

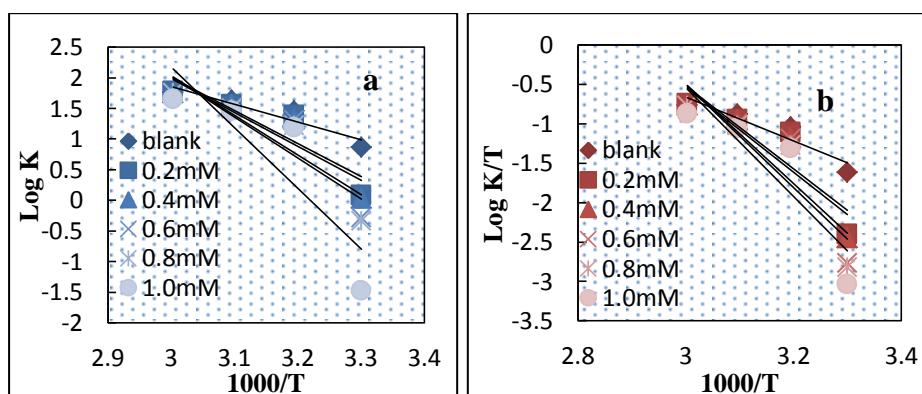


Fig.4.5 Plot of a) log K vs 1000/T b) log K/T vs 1000/T with and without DMCHDP on MS in 1.0 M HCl

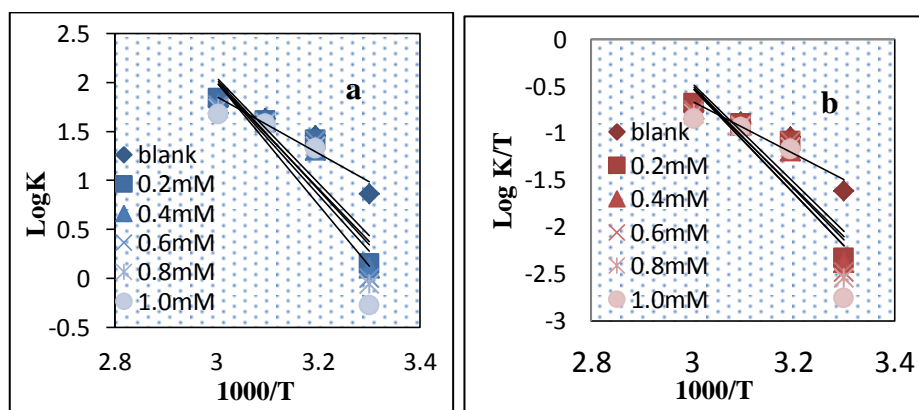


Fig. 4.6 Plot of a) log K vs 1000/T b) log K/T vs 1000/T with and without DMCHDA on MS in 1.0 M HCl

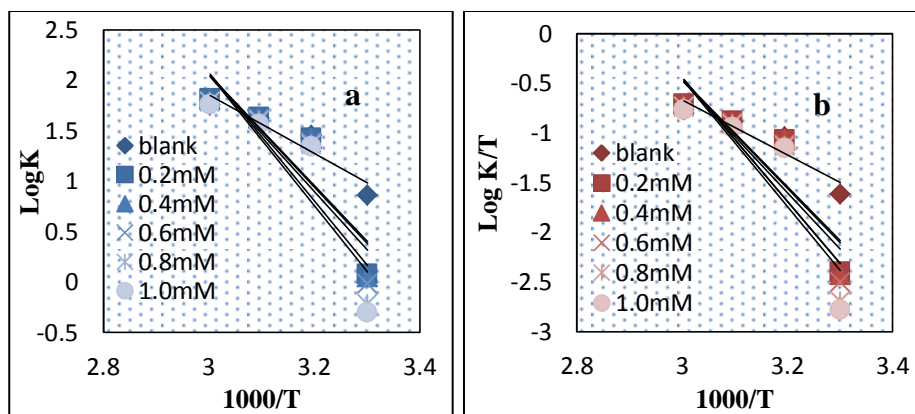


Fig. 4.7 Plot of a) $\log K$ vs $1000/T$ b) $\log K/T$ vs $1000/T$ with and without DMCHHC on MS in 1.0 M HCl

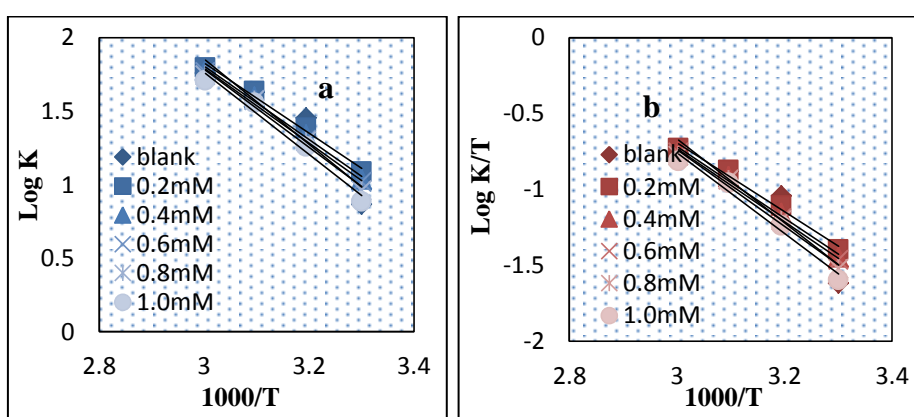


Fig. 4.8 Plot of a) $\log K$ vs $1000/T$ b) $\log K/T$ vs $1000/T$ with and without 2HBAP on MS in 1.0 M HCl

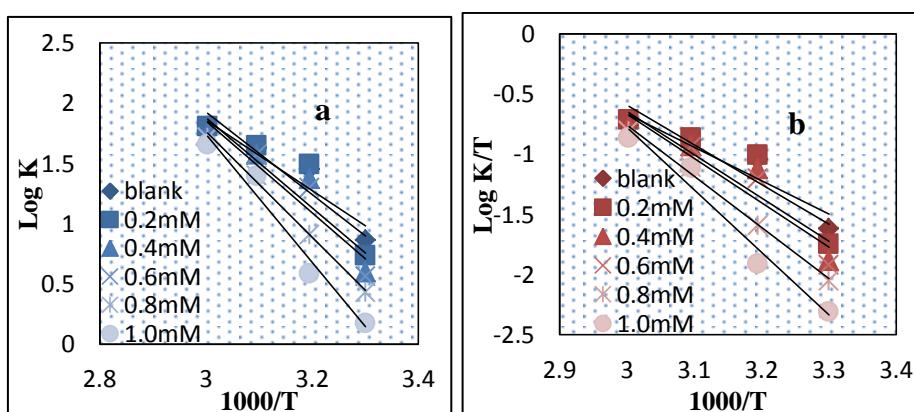


Fig. 4.9 Plot of a) $\log K$ vs $1000/T$ b) $\log K/T$ vs $1000/T$ with and without 2CHAP on MS in 1.0 M HCl

Activation energy needed for the metal dissolution in 1.0 M HCl was obtained from the slope of these plots. Thermodynamic parameters such as enthalpy (ΔH^*) and entropy (ΔS^*) were evaluated using transition state theory (equation 2).

$$K = \left(\frac{RT}{N_h}\right) \exp\left(\frac{\Delta S^*}{R}\right) \exp\left(\frac{-\Delta H^*}{RT}\right) \quad (2)$$

where N is the Avogadro number and h is the Planck's constant. Value of ΔH^* was obtained from the slope $\left(\frac{-\Delta H^*}{2.303R}\right)$ whereas the value of ΔS^* was obtained from the intercept $\left(\log\left(\frac{R}{2.303Nh}\right) + \left(\frac{\Delta S^*}{2.303R}\right)\right)$ of the plot between $\log K/T$ vs $1/T$ for the metal dissolution in 1.0 M HCl (see Fig. 4.5- 4.9b). The values of parameters such as activation energy (E_a), Arrhenius factor (A), enthalpy of activation (ΔH^*) and entropy of activation (ΔS^*) are given in Table 4.6

Table 4.6 Thermodynamic parameters of corrosion of MS with and without Schiff bases in 1.0 M HCl

Schiff base	Conc (mM)	E_a (kJ mol ⁻¹)	A	ΔH^* (kJ mol ⁻¹)	ΔS^* (J mol ⁻¹ K ⁻¹)
DMCHDP	Blank	55.67	3.81×10^{10}	53.03	-44.26
	0.2	103.04	1.40×10^{18}	100.40	100.59
	0.4	105.58	3.38×10^{18}	102.94	107.92
	0.6	123.53	2.43×10^{21}	120.89	162.60
	0.8	127.55	1.01×10^{22}	124.91	174.49
	1.0	134.58	1.16×10^{23}	131.94	194.77
DMCHDA	0.2	102.76	1.41×10^{18}	100.12	100.64
	0.4	103.55	1.68×10^{18}	100.91	102.10
	0.6	107.13	6.44×10^{18}	104.48	113.26
	0.8	109.73	1.56×10^{19}	107.09	120.65
	1.0	119.48	5.24×10^{20}	116.83	149.65
DMCHHC	0.2	105.97	4.63×10^{18}	103.39	110.54
	0.4	107.16	7.06×10^{18}	104.52	114.05
	0.6	110.70	2.49×10^{19}	108.06	124.54
	0.8	122.27	1.74×10^{21}	119.63	159.85
	1.0	125.31	4.99×10^{21}	122.67	168.58
2HBAP	0.2	45.92	1.06×10^9	43.28	-74.05
	0.4	47.86	2.03×10^9	45.23	-68.66
	0.6	48.64	2.59×10^9	46.00	-66.61
	0.8	51.00	6.00×10^9	48.36	-59.64
	1.0	53.57	1.44×10^9	50.09	-52.35
2CHAP	0.2	65.71	1.68×10^{12}	63.08	-12.76
	0.4	71.32	1.13×10^{13}	68.68	3.03
	0.6	73.06	2.00×10^{13}	70.42	7.82
	0.8	84.06	8.63×10^{14}	81.43	39.12
	1.0	101.81	4.97×10^{17}	99.18	91.97

It was observed that the activation energy of corrosion in the presence of Schiff bases was higher, compared to metal dissolution without Schiff bases in 1.0 M HCl. Endothermic character of metal dissolution process was reflected from the positive sign of enthalpy. It is also observed that ΔH^* and ΔS^* increased with rise in concentration of inhibitors. Activation energy and enthalpy of corrosion is high in the case of DMCHDP, DMCHDA and DMCHHC compared to 2HBAP and 2CHAP. High corrosion inhibition efficiency of the Schiff bases DMCHDP, DMCHDA and DMCHHC is supported by this observation. Randomness of activated complex goes up with rise in concentration of Schiff bases and ΔS^* acquired positive values.

Electrochemical impedance spectroscopy

The nature of corrosion inhibition of Schiff bases on MS in 1.0 M HCl was evaluated using electrochemical impedance spectroscopy at 28⁰C. Impedance spectra (Nyquist and Bode plots) of MS in the absence and presence of Schiff bases at various concentrations in 1.0 M HCl are shown in Fig. 4.10, 4.11, 4.12, 4.13 and 4.14.

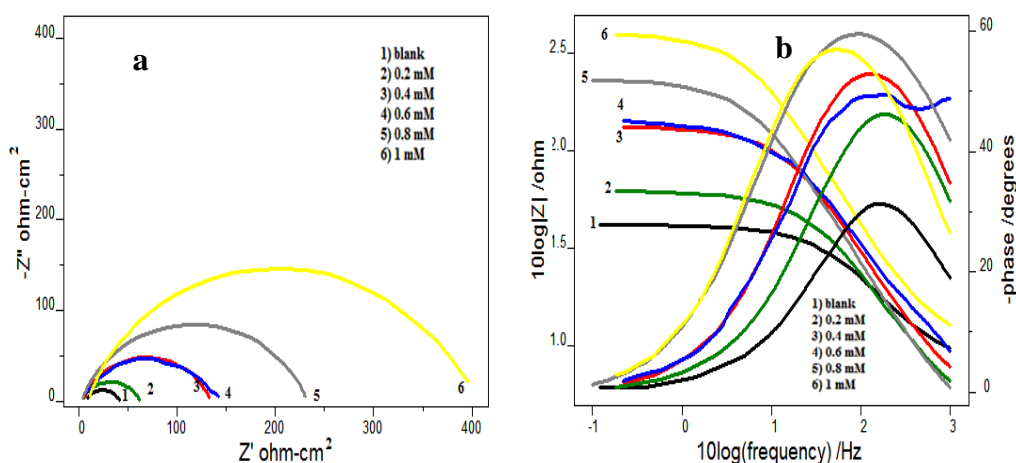


Fig. 4.10 a) Nyquist and b) Bode plots of MS coupons with and without DMCHDP in 1.0 M HCl

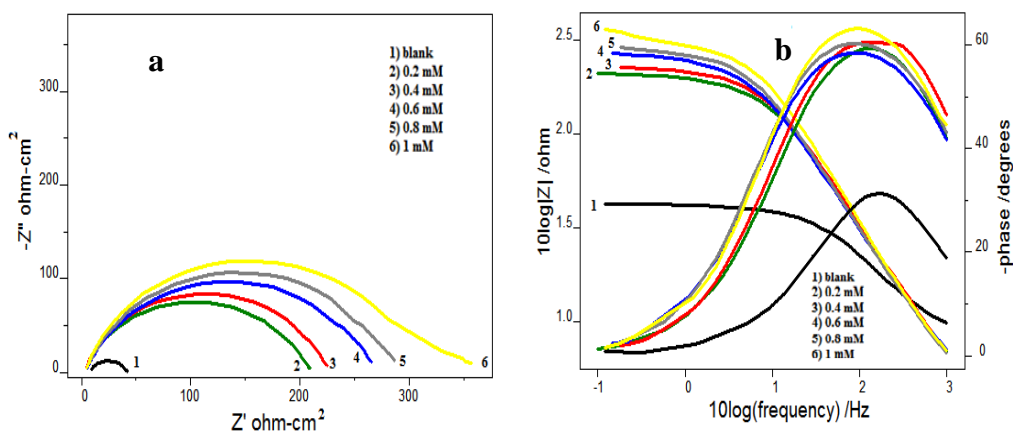


Fig. 4.11 a) Nyquist and b) Bode plots of MS coupons with and without DMCHDA in 1.0 M HCl

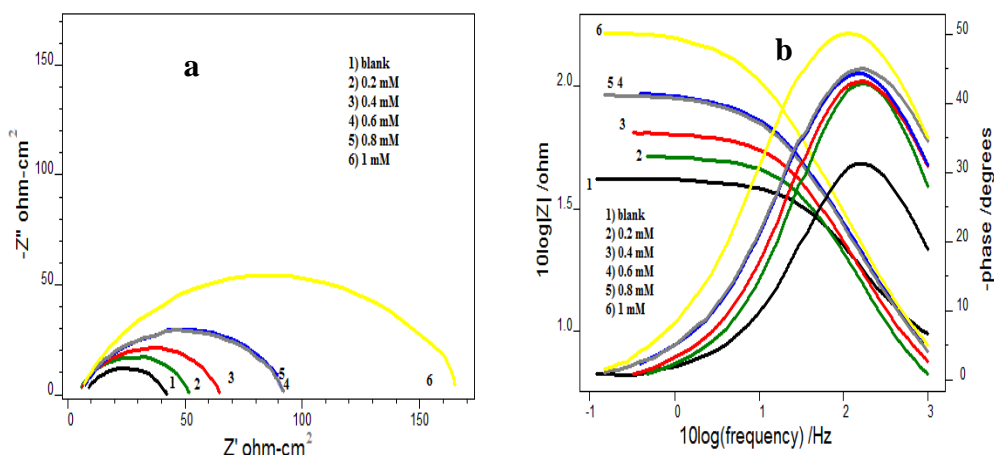


Fig. 4.12 a) Nyquist and b) Bode plots of MS coupons with and without DMCHHC in 1.0 M HCl

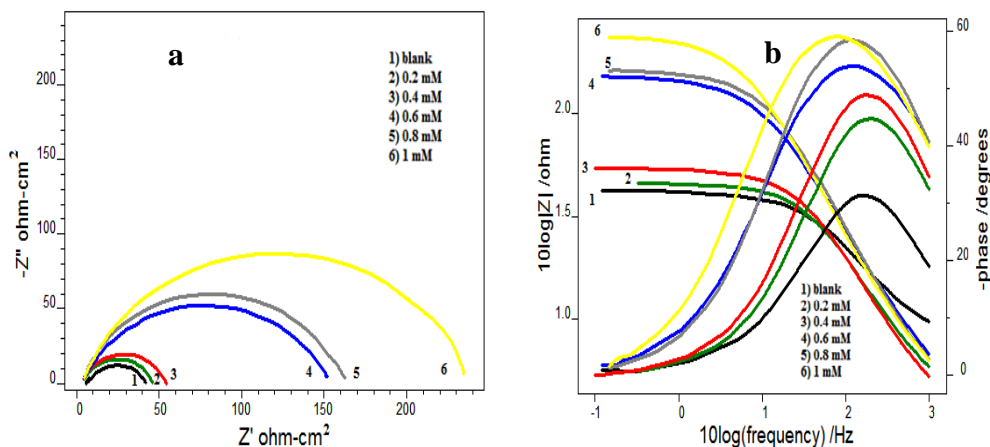


Fig. 4.13 a) Nyquist and b) Bode plots of MS coupons with and without 2HBAP in 1.0 M HCl

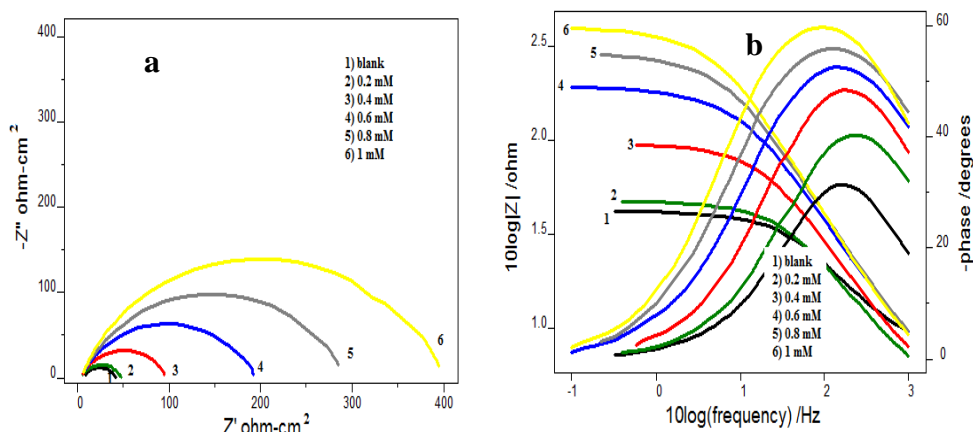


Fig. 4.14 a) Nyquist and b) Bode plots of MS coupons with and without 2CHAP in 1.0 M HCl

Impedance spectra showed a significant change on addition of Schiff bases at various concentrations. Nyquist plots of blank and treated specimen with Schiff bases have similar shape but different size. This indicates that the mechanism of dissolution of metal is same in both cases. Size of the Nyquist plots was found to be increased with rise in concentration of Schiff bases, which indicates that the impedance of MS increased when the concentration increased.

Equivalent circuit used to fit the Nyquist plots (Randles circuit) is shown in Fig. 4.15. The circuit consist of a double layer capacitance C_{dl} , solution resistance R_s and charge transfer resistance R_{ct} . Constant phase element (CPE) is inserted into the circuit in preference to pure double layer capacitance to lower the effects due to deformities on the surface of metal as shown in Fig. 4.15. The impedance of CPE can be expressed as

$$Z_{CPE} = \frac{1}{Y_0(j\omega)^n} \quad (3)$$

where Y_0 is the magnitude of CPE, n is the exponent (phase shift), ω is the angular frequency and j is the imaginary unit. Based on the values of n , CPE can be capacitance, inductance and resistance. It is observed that the values of n is between 0.75 and 1.0, and indicates the nature of capacitance of CPE. Impedance data such as R_{ct} , C_{dl} and the percentage of inhibition efficiency ($\eta_{EIS}\%$) of the Schiff bases are listed in Table 4.7.

Table 4.7 Impedance data of MS coupons with and without Schiff bases in 1.0 M HCl

Schiff base	Conc (mM)	C_{dl} (μFcm^{-2})	R_{ct} (Ωcm^2)	$\eta_{\text{EIS}}\%$
Blank	0.0	105	29.1	-
	0.2	97.7	50.5	42.37
	0.4	82.8	114	74.47
	0.6	82.0	117	75.12
	0.8	112	202	85.59
	1.0	64.6	349	91.66
DMCHDP	0.2	81.8	181	83.92
	0.4	81.6	200	85.45
	0.6	99.4	232	87.45
	0.8	92.9	253	88.49
	1.0	65.4	308	90.55
DMCHDA	0.2	104	40.6	28.32
	0.4	103	50.9	42.83
	0.6	99.5	72.8	60.03
	0.8	105	73.2	60.24
	1.0	103	136	85.95
DMCHHC	0.2	102	37.4	22.19
	0.4	106	45.2	35.62
	0.6	109	77.62	77.62
	0.8	88.8	79.2	79.21
	1.0	118	86.1	86.08
2HBAP	0.2	96.6	36.2	19.61
	0.4	81.4	76.6	62.01
	0.6	78.3	158	81.58
	0.8	75.8	241	87.92
	1.0	75.8	338	91.39
2CHAP	0.2	96.6	36.2	19.61
	0.4	81.4	76.6	62.01
	0.6	78.3	158	81.58
	0.8	75.8	241	87.92
	1.0	75.8	338	91.39

On observing the results charge transfer resistance (R_{ct}) was found to be increased with concentration whereas capacitance (C_{dl}) value is reduced in the case of all Schiff bases. Charge transfer resistance has an inverse relationship with corrosion rate and is a measure of transfer of electrons across exposed metal surface. Decrease in C_{dl} values is due to the lowering of local dielectric constant and/or increase in thickness of electrical double layer. Corrosion inhibition efficiency ($\eta_{\text{EIS}}\%$) is also found to be increased with concentration. In contradiction to weight loss studies, all the Schiff bases are good inhibitors of corrosion according to impedance measurement. Antagonistic effect on corrosion is exhibited by 2HBAP in weight loss studies. Impedance studies showed that

2HBAP has appreciable corrosion inhibition efficiency. This may be due to the less immersion time in the case of electrochemical studies (30 min) compared to weight loss studies (24 h). Factors such as catalytic action of the adsorbed compound and lowering of overpotential which leads to the antagonistic nature of 2HBAP may predominate only after the time taken for electrochemical analysis.

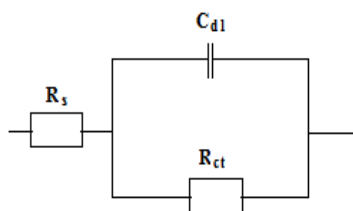


Fig. 4.15 The equivalent circuit used to fit the Nyquist plots

Maximum inhibition efficiency of about 91.66%, 90.55%, 85.95%, 86.08% and 91.39% was exhibited by the Schiff bases DMCHDP, DMCHDA, DMCHHC, 2HBAP and 2CHAP respectively at 1 mM concentration. Comparison of corrosion inhibition efficiency ($\eta_{\text{EIS}}\%$) of the Schiff bases on MS in 1.0 M HCl was shown in Fig. 4.16.

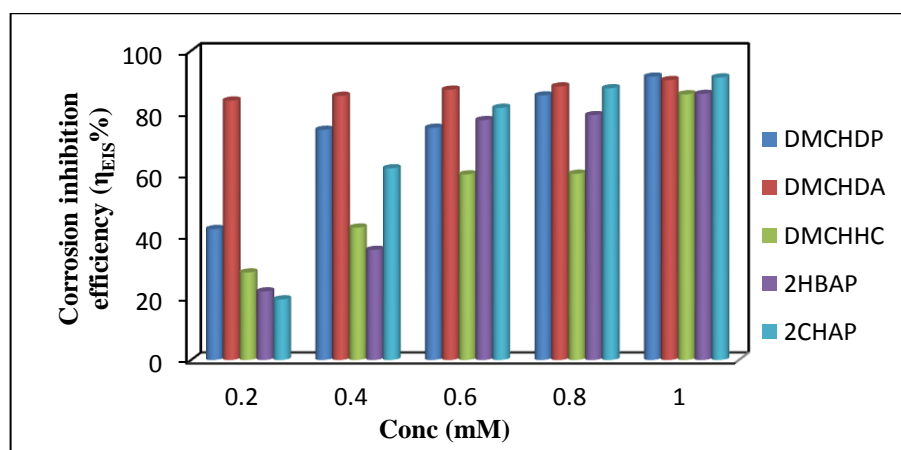


Fig. 4.16 Comparison of corrosion inhibition efficiency ($\eta_{\text{EIS}}\%$) of the Schiff bases on MS in 1.0 M HCl

Potentiodynamic polarization studies

Corrosion inhibition efficiency was also monitored using potentiodynamic polarization studies. This method mainly deals with measurement of current generated as a function of potential or time by varying the potential of working electrode. Two types of polarization techniques such as Tafel and linear polarization were employed for this

purpose. Corrosion current density (I_{corr}) and polarization resistance (R_p) were the main parameters obtained from Tafel and linear polarization techniques respectively. The Tafel and linear polarization plots of the Schiff bases are shown in Fig. 4.17, 4.18, 4.19, 4.20 and 4.21. Polarization data such as corrosion potential (E_{corr}), corrosion current density (I_{corr}), cathodic slope (b_c), anodic slope (b_a), polarization resistance (R_p) and inhibition efficiencies ($\eta_{\text{pol}}\%$ and $\eta_{R_p}\%$) of the Schiff bases in 1.0 M HCl are given in Table 4.8.

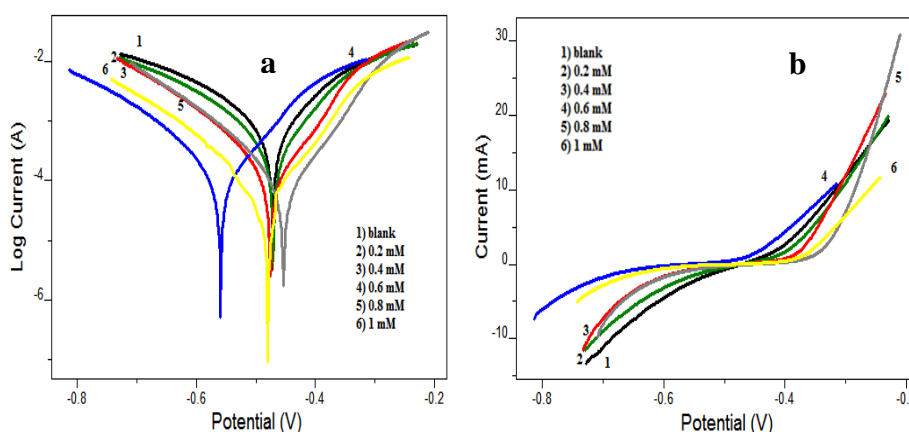


Fig. 4.17 a) Tafel and b) linear polarization plots of MS coupons with and without DMCHDP in 1.0 M HCl

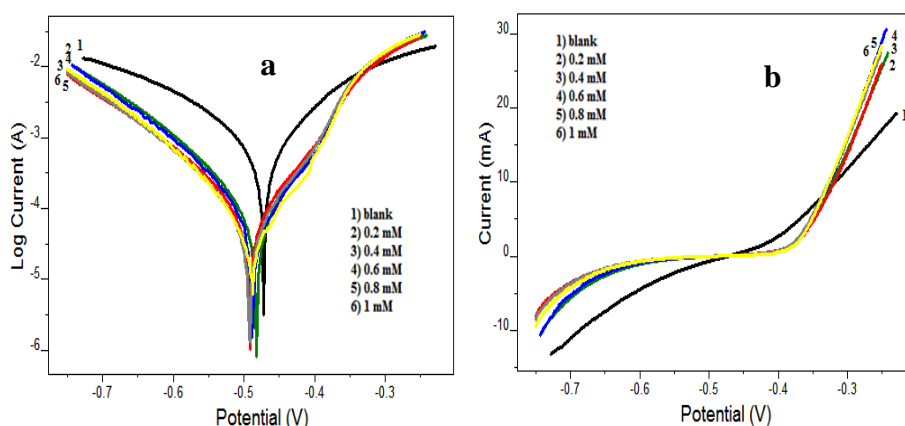


Fig.4.18 a) Tafel and b) linear polarization plots of MS coupons with and without DMCHDA in 1.0 M HCl

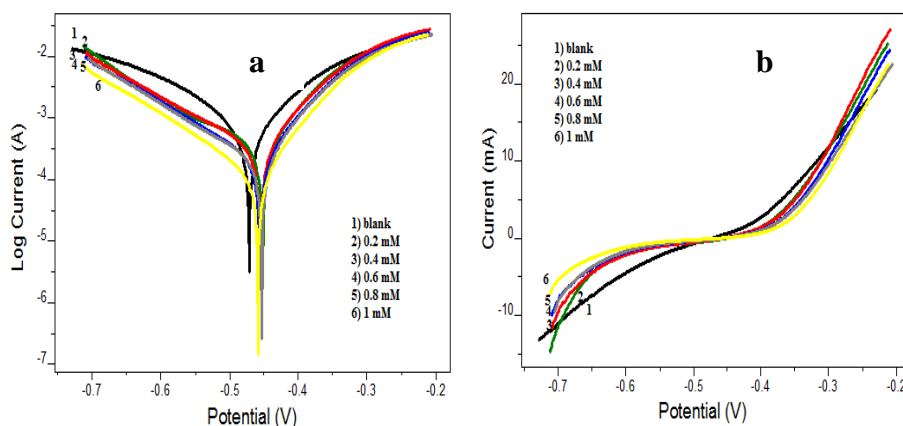


Fig. 4.19 a) Tafel and b) linear polarization plots of MS coupons with and without DMCHHC in 1.0 M HCl

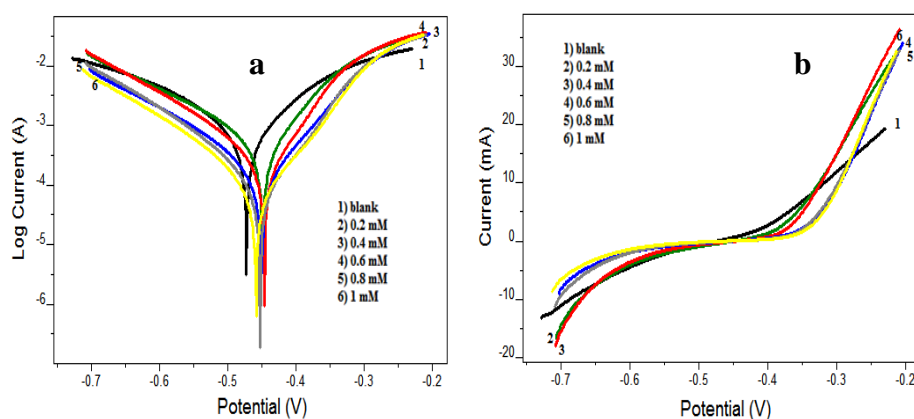


Fig. 4.20 a) Tafel and b) linear polarization plots of MS coupons with and without 2HBAP in 1.0 M HCl

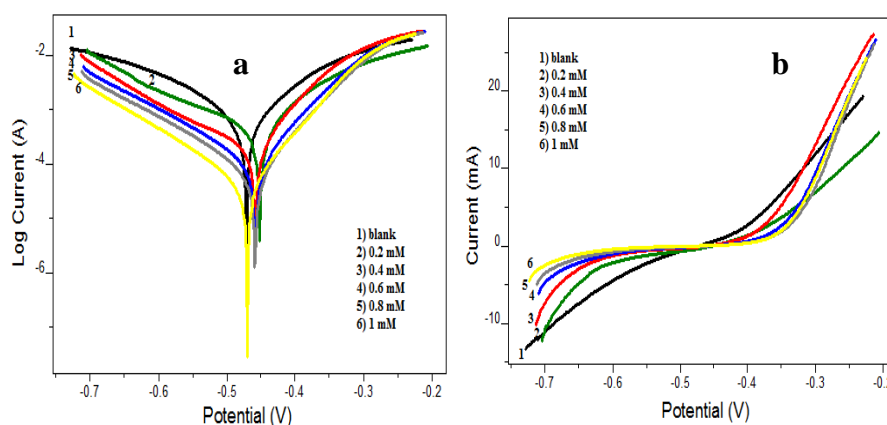


Fig. 4.21 a) Tafel and b) linear polarization plots of MS coupons with and without 2CHAP in 1.0 M HCl

Table 4.8 Polarization data of MS coupons with and without Schiff bases in 1.0 M HCl

Schiff base	Tafel data					Polarization data		
	Conc (mM)	E_{corr} (mV)	I_{corr} ($\mu\text{A}/\text{cm}^2$)	b_a (mV/dec)	$-b_c$ (mV/dec)	$\eta_{\text{pol}}\%$	R_p (Ω)	$\eta_{\text{Rp}}\%$
Blank	0.0	-477.3	1160	172	212	-	35.58	-
	0.2	-473.5	640	138	185	44.82	53.56	33.57
	0.4	-461.4	172	83	141	85.21	132.8	73.21
DMCHDP	0.6	-547.2	163	104	150	85.97	187.6	81.03
	0.8	-432.2	98.9	73	135	91.47	207.6	82.86
	1.0	-471.5	59.5	79	130	94.87	360	90.12
DMCHDA	0.2	-468.8	101	73	128	91.31	201.1	82.31
	0.4	-468.9	84.3	71	139	92.73	241.4	85.26
	0.6	-461.1	74	63	126	93.62	247.8	85.64
	0.8	-469.5	67.4	65	129	94.19	278.6	87.23
	1.0	-461.9	51.1	59	121	95.59	335.3	89.39
DMCHHC	0.2	-502.1	461	145	156	60.26	70.82	49.76
	0.4	-454.9	442	133	161	61.89	71.53	50.26
	0.6	-487.4	319	125	148	72.50	92.48	61.53
	0.8	-494.1	309	132	142	73.36	96.26	63.04
	1.0	-458.3	174	108	143	85.00	153.2	76.77
2HBAP	0.2	-469.1	767	134	179	33.88	43.34	17.9
	0.4	-464.4	444	110	149	61.72	61.77	42.39
	0.6	-441.2	193	87	156	83.36	125.6	71.67
	0.8	-442	128	77	132	88.96	165.8	78.54
	1.0	-435	93.3	70	139	91.95	215.7	83.5
2CHAP	0.2	-494.4	605	185	183	47.84	66.18	46.24
	0.4	-504.3	281	123	144	75.77	102.7	65.35
	0.6	-468.8	132	92	147	88.62	187.0	80.97
	0.8	-461.7	83.6	83	146	92.79	275.4	87.08
	1.0	-468.7	46.4	74	133	96.00	444.1	91.99

From the polarization data it is evident that corrosion current density decreased and polarization resistance increased with the concentration of Schiff bases. As a result percentage of corrosion inhibition efficiency was increased. Metal dissolution will be hindered by the adsorbed molecules by inhibiting the anodic or/and cathodic processes of corrosion. On evaluating polarization plots, there is a considerable difference in the slope

of the Tafel lines both in the presence and absence of Schiff base molecules. All the Schiff bases were found to affect both anodic and cathodic sites of corrosion and hence act as mixed type inhibitors. Tafel data revealed that all Schiff bases are good inhibitors of corrosion and the results are in good agreement with that of impedance data. Comparison of corrosion inhibition efficiency ($\eta_{\text{pol}}\%$) of the Schiff bases on MS in 1.0 M HCl is shown in Fig. 4.22.

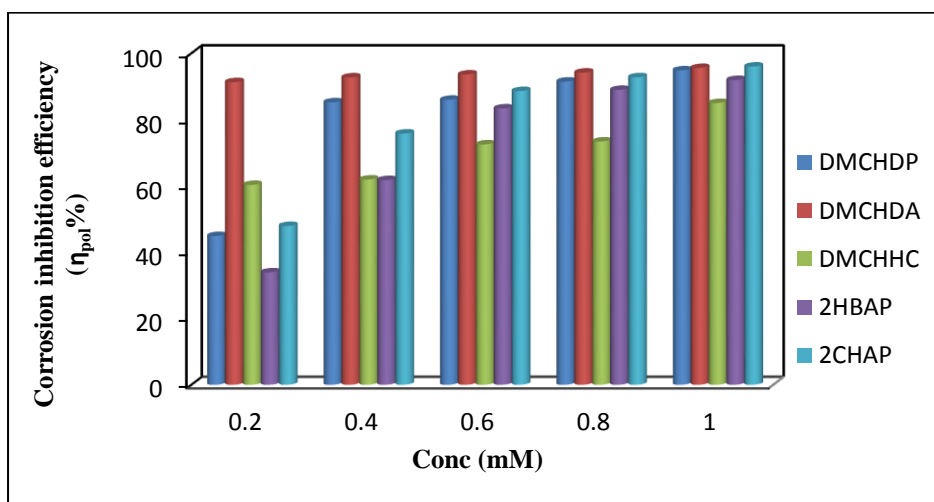


Fig. 4.22 Comparison of corrosion inhibition efficiency ($\eta_{\text{pol}}\%$) of the Schiff bases on MS in 1.0 M HCl

Electrochemical noise measurements

Electrochemical noise measurements were carried out in a three-electrode system consisting of two mild steel electrodes having 1 cm^2 area and a saturated calomel electrode. The analysis was executed with the help of Ivium compactstat-e electrochemical system controlled by iviumsoft software. All electrochemical noise analyses were performed for a period of 1200s.

Current noise for MS in the absence and presence of Schiff bases (1 mM) in 1.0 M HCl are shown in Fig. 4.23. From the figure, it is clear that blank specimen exhibits higher mean value of current noise in respect of the specimen dipped in an acid medium containing Schiff base molecules. This reflects the high protective power of Schiff bases in 1.0 M HCl medium.

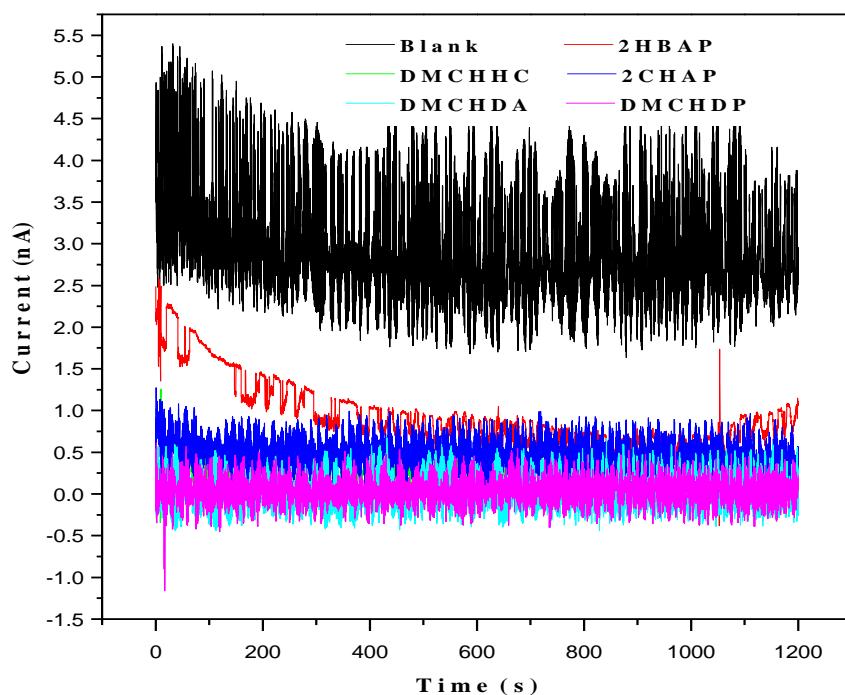


Fig. 4.23 Current noise for MS in the absence and presence of Schiff bases (1 mM) in 1.0 M HCl

Frequency domain analysis of noise measurement gave the PSD (power spectral density) plots of different systems, which is represented in Fig. 4.24. On detailed evaluation of PSD plots, it is evident that at all frequencies, the values of current noise are comparatively large for blank metal specimen than for metal immersed in acid solution containing Schiff base molecules. This suggests that localised corrosion of mild steel is occurring in acid solution without Schiff base molecule. Pitting index is a measure of resisting power to localised pitting corrosion. Pitting index curves are shown in Fig. 4.25. Amplitude of the pitting index curve corresponding to blank metal specimen is lower than metal specimens treated with acid solution containing Schiff base molecules. This implies that acid solution containing a Schiff base molecule has higher resistance to pitting corrosion.

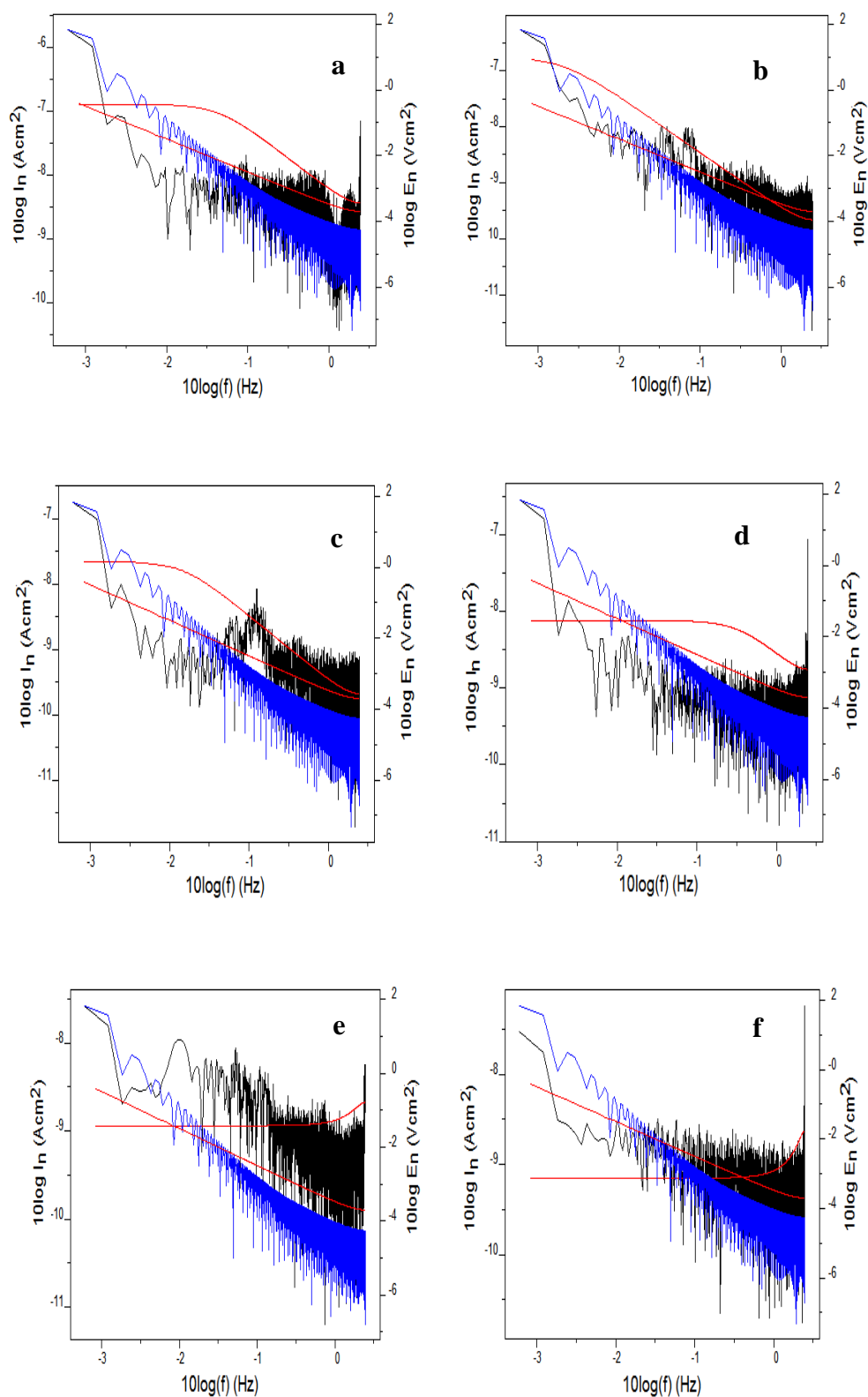


Fig. 4.24 Power spectral density (voltage and current) plots of MS in 1.0 M HCl in the presence a) blank b) 2HBAP c) DMCHHC d) 2CHAP e) DMCHDA and f) DMCHDP

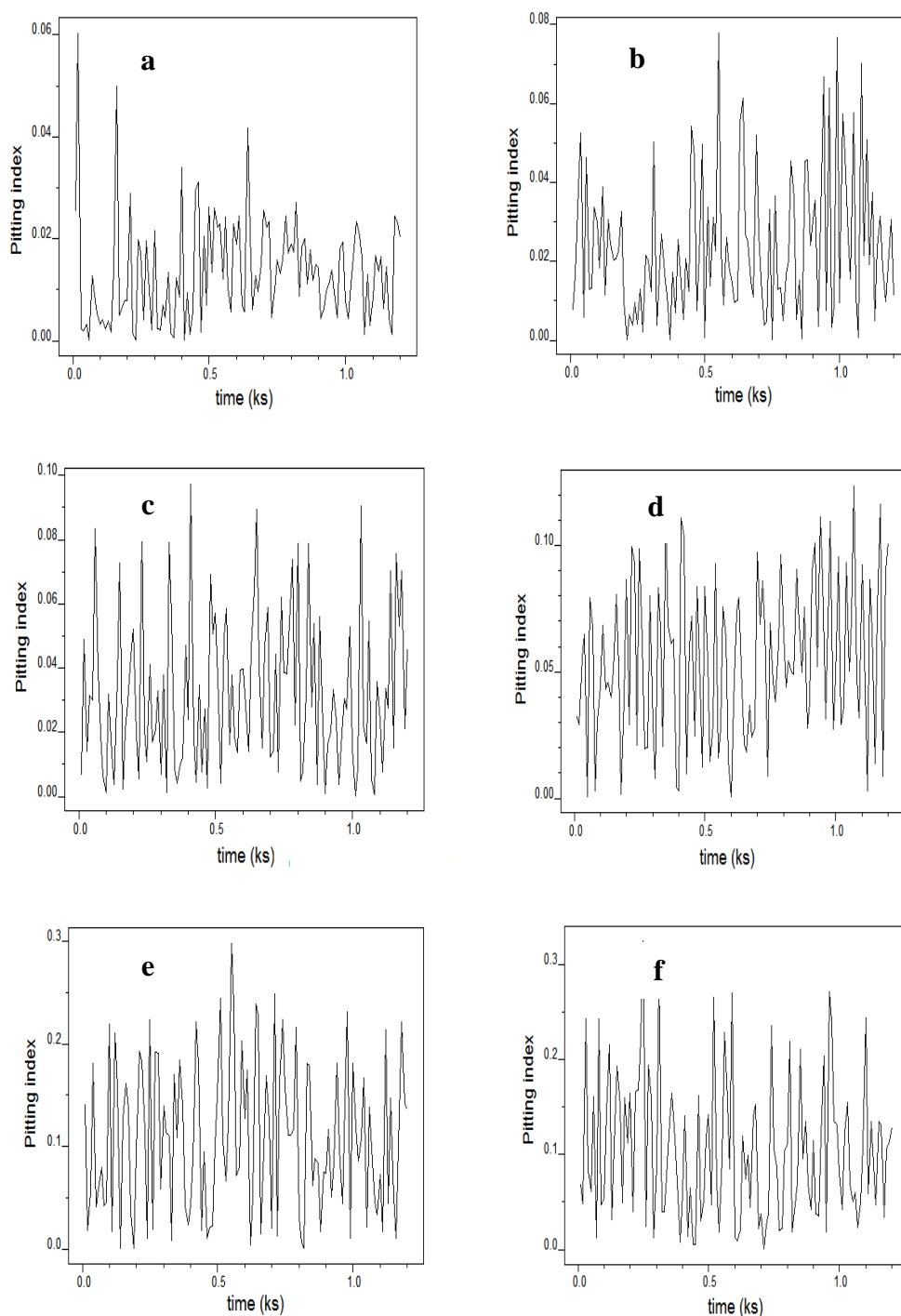


Fig. 4.25 Pitting index curve of MS in 1.0 M HCl in the presence a) blank b) 2HBAP c) DMCHHC d) 2CHAP e) DMCHDA and f) DMCHDP

Surface morphological studies

The surface morphological studies of the MS coupons were done by scanning electron microscope. Fig. 4.26(a-d) represents the SEM images of bare metal and in the

presence and absence of Schiff bases DMCHDP and DMCHDA (1.0 mM). Morphological studies clearly established that the surface of polished mild steel coupon before treatment in acid solution was smooth and not corroded as shown in Fig. 4.26a.

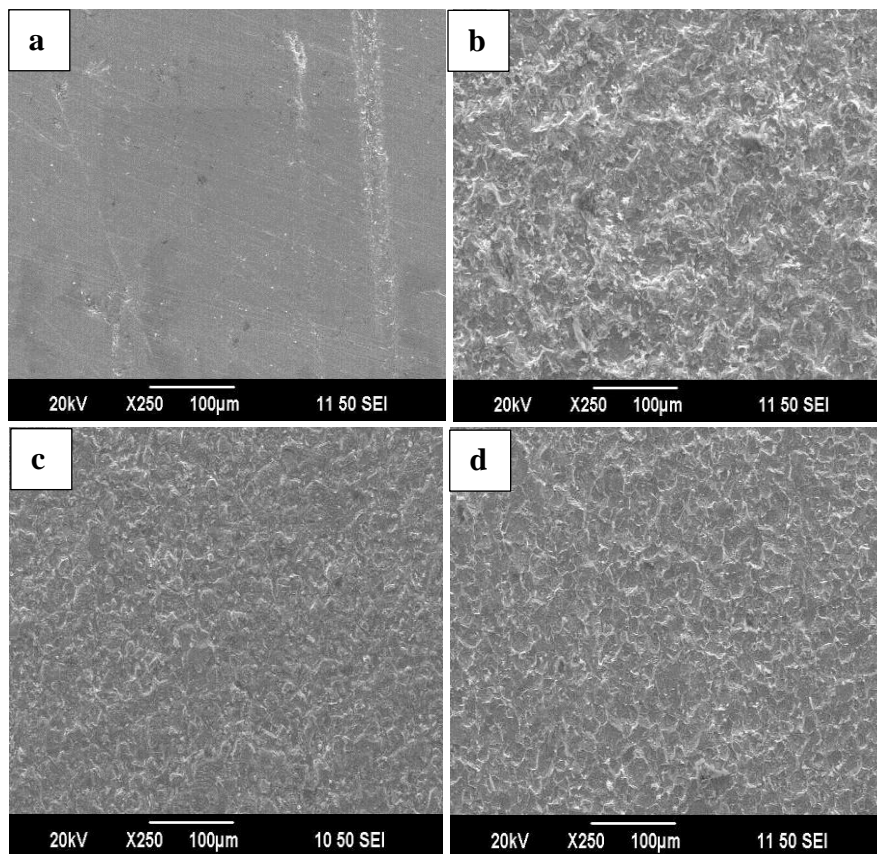


Fig. 4.26 SEM images of MS coupons before and after 24 h immersion a) bare b) blank (1.0 M HCl) c) treated with DMCHDP (1 mM) in 1.0 M HCl d) treated with DMCHDA (1 mM) in 1.0 M HCl

Significant change in the surface morphology was noticed after immersion in aggressive medium without Schiff bases (Fig. 4.26b). It is clear from the Fig. 4.26b, c and d that corrosion is more prominent in the case of MS coupon immersed in acid solution in the absence of Schiff bases. However in the presence of 1.0 mM concentration of DMCHDP and DMCHDA, rate of corrosion was decreased and the surface deterioration has been reduced (Fig. 4.26 c and d). This is due to the surface coverage of the Schiff bases molecule containing imine group. Aromatic rings and the azomethine linkage play great role in preventing dissolution of the metal and thereby protecting the mild steel from corrosion.

Quantum chemical investigations

Density functional theory (DFT) method is powerful theoretical tool for understanding the corrosion inhibition mechanism of organic molecules. There is a strong relationship between the energy gap of HOMO and LUMO with hardness and softness in accordance with HSAB concept. Inhibitor is defined as soft base when the energy gap between HOMO and LUMO is small and thus it have a tendency to coordinate with metals which are soft acid. Softness will increase when the corrosion inhibition tendency is high. In the electronic configuration $[\text{Ar}]4s^23d^6$ of Fe atom the 3d orbital is only partially filled. Thus this 3d orbital will bind with HOMO of the Schiff base molecule. Also the electrons in the filled 4s orbital are donated to LUMO of Schiff bases. Hence the Schiff base is adsorbed on the surface of the metal by the interaction of Fe atom orbital (4s and 3d) with HOMO and LUMO of Schiff bases. When the energy of LUMO decreases the energy gap will also decreases and as a result corrosion inhibition efficiency increases. In the present study the corrosion inhibition efficiency of five Schiff base ligands DMCHDP, DMCHDA, DMCHHC, 2HBAP and 2CHAP were evaluated using quantum chemical parameters. The values of parameters are shown in Table 4.9.

Table 4.9 Quantum chemical parameters of the Schiff base molecules calculated using DFT method

Schiff base	E_{HOMO} (eV)	E_{LUMO} (eV)	ΔE (eV)	χ (eV)	η (eV)	ΔN
DMCHDP	-1.7959	-0.1632	1.6327	0.9795	0.8163	3.687
DMCHDA	-1.6326	0.0544	1.6870	0.7891	0.8435	3.681
DMCHHC	-1.9047	-0.1904	1.7142	1.4075	0.8568	3.263
2HBAP	-3.2925	1.0612	4.3537	1.1156	2.1781	1.350
2CHAP	-3.0748	1.8503	4.9250	0.6122	2.4620	1.297

From the table it is clear that the energy gap between HOMO and LUMO is low in the case of DMCHDP, DMCHDA and DMCHHC on comparing with 2HBAP and 2CHAP. Thus the corrosion inhibition capacity of the ligands DMCHDP, DMCHDA and

DMCHHC will be high than the other two ligands. This result is in good agreement with that obtained from weight loss studies. Frontier molecular orbitals of the Schiff bases are shown in Fig. 4.27, 4.28, 4.29, 4.30 and 4.31. Optimized geometries of the Schiff bases are given in Fig 4.32.

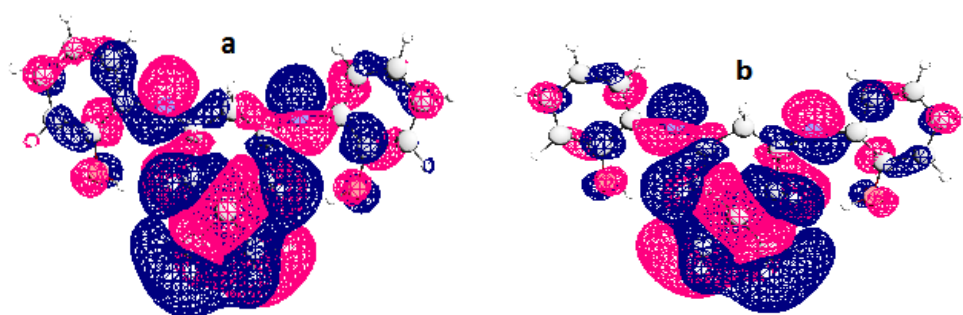


Fig. 4.27 Frontier molecular orbitals a) HOMO and b) LUMO of DMCHDP

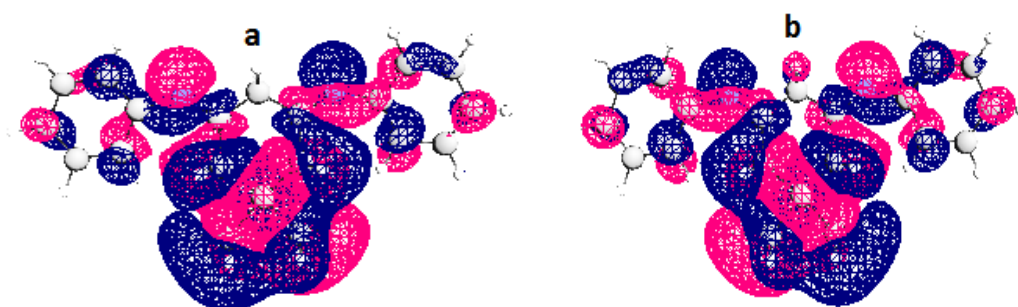


Fig. 4.28 Frontier molecular orbitals a) HOMO and b) LUMO of DMCHDA

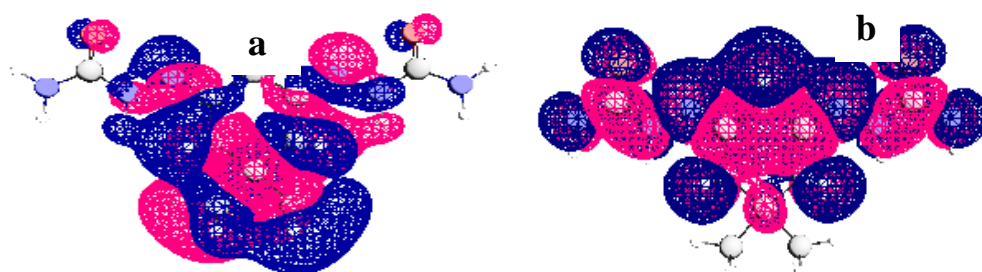


Fig. 4.29 Frontier molecular orbitals a) HOMO and b) LUMO of DMCHHC

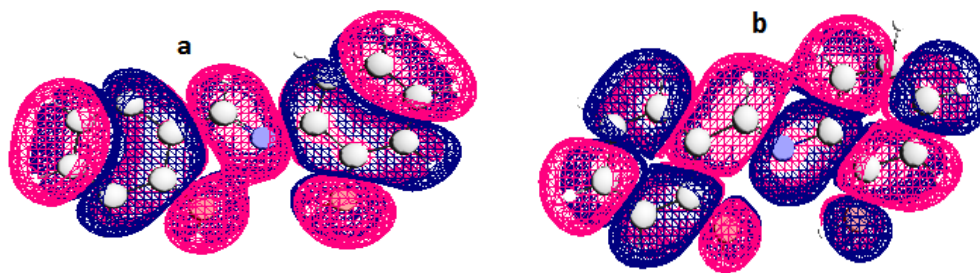


Fig. 4.30 Frontier molecular orbitals a) HOMO and b) LUMO of 2HBAP

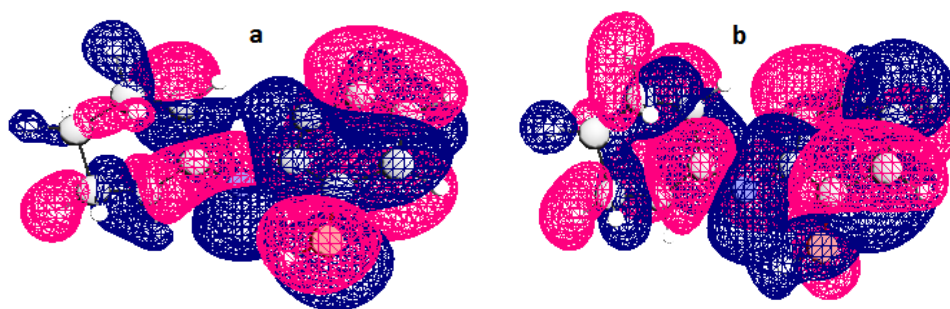


Fig. 4.31 Frontier molecular orbitals a) HOMO and b) LUMO of 2CHAP

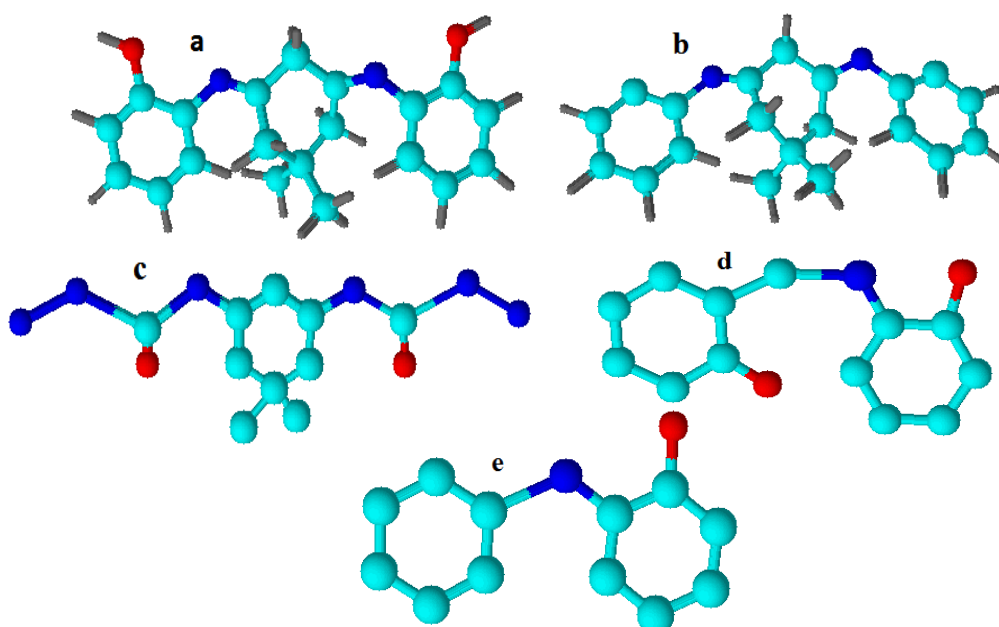


Fig. 4.32 Optimized geometries of the Schiff bases a) DMCHDP b) DMCHDA c) DMCHHC d) 2HBAP and e) 2CHAP

CHAPTER 5

CORROSION INHIBITION STUDIES OF SCHIFF BASES IN 0.5 M H₂SO₄ MEDIUM

Corrosion inhibition efficiency of the Schiff bases 2,2'-(5,5-dimethylcyclohexane-1,3-diylidene)bis(azanylylidene)diphenol (DMCHDP), N,N'-(5,5-dimethylcyclohexane-1,3-diylidene)dianiline (DMCHDA), 2,2'-(5,5-dimethylcyclohexane-1,3-diylidene)bis(hydrazinecarboxamide) (DMCHHC), 2-((2hydroxybenzylidene)amino)phenol (2HBAP), 2-(cyclohexylideneamino)phenol (2CHAP) on mild steel were also conducted 0.5 M H₂SO₄. 0.2-1.0 mM concentration of Schiff bases was used for the study. Gravimetric (weight loss) and electrochemical studies such as electrochemical impedance spectroscopy, potentiodynamic polarization studies and electrochemical noise measurements were employed for monitoring corrosion inhibition efficiency. Adsorption isotherm, impact of temperature and surface morphology were also evaluated in this chapter.

Weight loss studies

The weight loss of the MS specimen at 24 h interval in 0.5 M H₂SO₄ in the absence and presence of Schiff bases (DMCHDP, DMCHDA, DMCHHC, 2HBAP and 2CHAP) at different concentrations were determined. Corrosion rate and inhibition efficiency were calculated, which is depicted in Table 5.1 and 5.2 respectively.

On close examination of the results, it is found that the rate of corrosion of MS specimen immersed in 0.5 M H₂SO₄ was higher (35.20 mmy⁻¹) than that immersed in acid solution containing Schiff base molecules. Also the corrosion rate was found to be decreased with concentration of Schiff base molecules. Comparison of corrosion rate of mild steel at different concentrations of the Schiff bases DMCHDP, DMCHDA, DMCHHC, 2HBAP and 2CHAP in 0.5 M H₂SO₄ are shown in Fig. 5.1. Corrosion

inhibition efficiency of the Schiff bases increased with rise in concentration of Schiff base molecules. Inhibition efficiency of the Schiff bases except 2HBAP was lower in 0.5 M H₂SO₄ compared to the inhibition efficiency in 1.0 M HCl at all concentrations. This may be attributed to the aggressive nature of 0.5 M H₂SO₄.

Table 5.1 Rate of corrosion of MS in mmy⁻¹ with and without Schiff bases DMCHDP, DMCHDA, DMCHHC, 2HBAP and 2CHAP in 0.5 M H₂SO₄

Conc (mM)	Schiff base				
	DMCHDP	DMCHDA	DMCHHC	2HBAP	2CHAP
0.0	35.20	35.20	35.20	35.20	35.20
0.2	19.80	24.16	28.77	22.66	26.82
0.4	7.87	10.33	26.55	22.48	18.82
0.6	7.49	6.81	20.04	21.88	18.15
0.8	2.97	4.39	18.29	17.06	11.66
1.0	2.65	4.40	16.96	15.66	9.77

Table 5.2 Corrosion inhibition efficiency ($\eta_w\%$) of Schiff bases DMCHDP, DMCHDA, DMCHHC, 2HBAP and 2CHAP on MS specimen in 0.5 M H₂SO₄

Conc (mM)	Schiff base				
	DMCHDP	DMCHDA	DMCHHC	2HBAP	2CHAP
0.2	43.73	31.36	18.25	35.61	23.79
0.4	77.63	70.62	24.55	36.13	46.50
0.6	78.70	80.64	43.05	37.81	48.41
0.8	91.54	87.50	48.03	51.52	66.85
1.0	92.46	87.52	51.81	55.49	72.23

Corrosion inhibition efficiency of DMCHDP and DMCHDA were higher compared to other three Schiff bases. This may be due to the presence of azomethine groups, aromatic rings and hetero atoms. The maximal values of corrosion inhibition efficiency on the MS surface by 1 mM concentration of DMCHDP and DMCHDA were found to be 92.46% and 87.52% respectively. Comparison of corrosion inhibition efficiency of the Schiff bases DMCHDP, DMCHDA, DMCHHC, 2HBAP and 2CHAP on MS in 0.5 M H₂SO₄ were shown in Fig. 5.2.

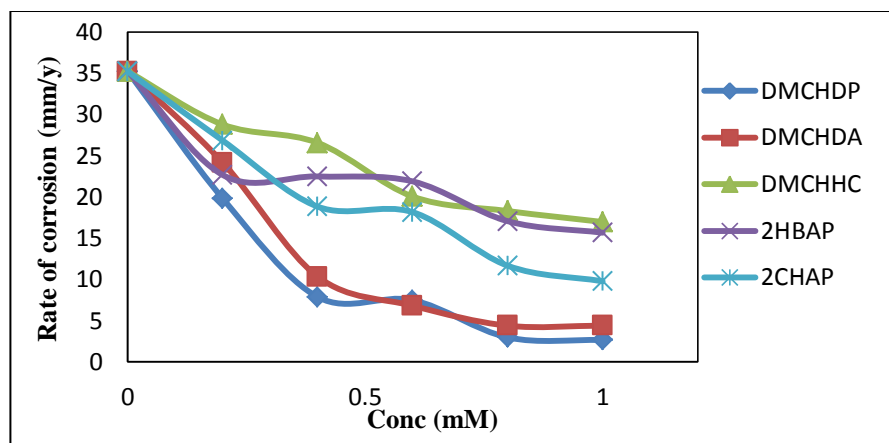


Fig. 5.1 Comparison of corrosion rate of mild steel at different concentrations of the Schiff bases DMCHDP, DMCHDA, DMCHHC, 2HBAP and 2CHAP in 0.5 M H₂SO₄

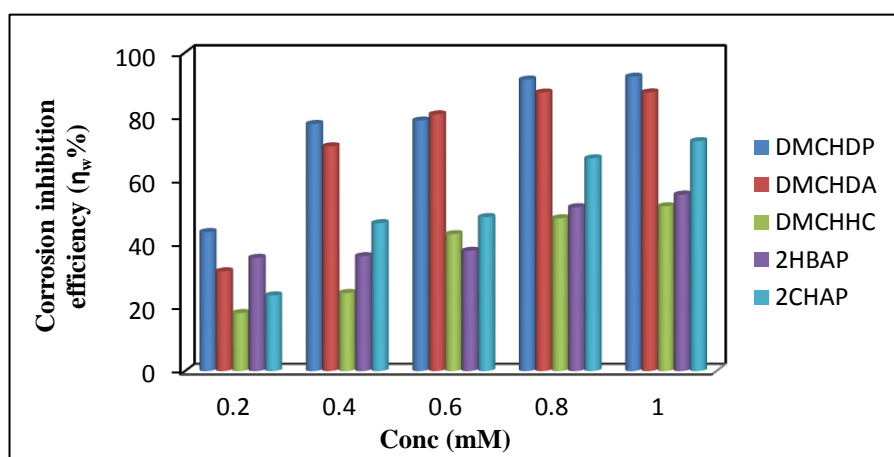


Fig. 5.2 Comparison of corrosion inhibition efficiency ($\eta_w\%$) of the Schiff bases DMCHDP, DMCHDA, DMCHHC, 2HBAP and 2CHAP on MS in 0.5 M H₂SO₄

Comparison between $\eta_w\%$ of Schiff bases with its parent compounds

In order to correlate the corrosion inhibition efficiency of Schiff bases with parent compounds such as salicylaldehyde (SAY), 5,5-dimethyl-1,3-cyclohexanedione (DM), cyclohexanone (CH), 2-aminophenol (2AP), aniline (AN) and semicarbazide (SZ), weight loss measurements of mild steel specimens were conducted in 0.5 M H₂SO₄ and the efficiencies are given in Table 5.3. Corrosion inhibition efficiency of Schiff bases was higher than the parent compounds. It is due to the involvement of >C=N- group present in the Schiff base molecule during adsorption phenomena. Comparison of corrosion

inhibition efficiencies of Schiff bases and their parent compounds on MS in 0.5 M H₂SO₄ are shown in Fig. 5.3.

Table 5.3 Corrosion inhibition efficiency of Schiff bases and their parent compounds on MS in 0.5 M H₂SO₄

Compounds	Conc (mM)		
	0.2	0.6	1.0
DM	29.50	38.68	56.23
2AP	21.14	25.22	29.86
AN	28.26	29.70	43.04
SZ	-9.42	-8.32	-5.39
SAY	6.10	10.41	20.66
CH	0.83	1.57	6.57
DMCHDP	43.73	78.70	92.46
DMCHDA	31.36	80.64	87.50
DMCHHC	18.25	43.05	51.81
2HBAP	35.61	37.81	55.49
2CHAP	23.79	18.15	9.77

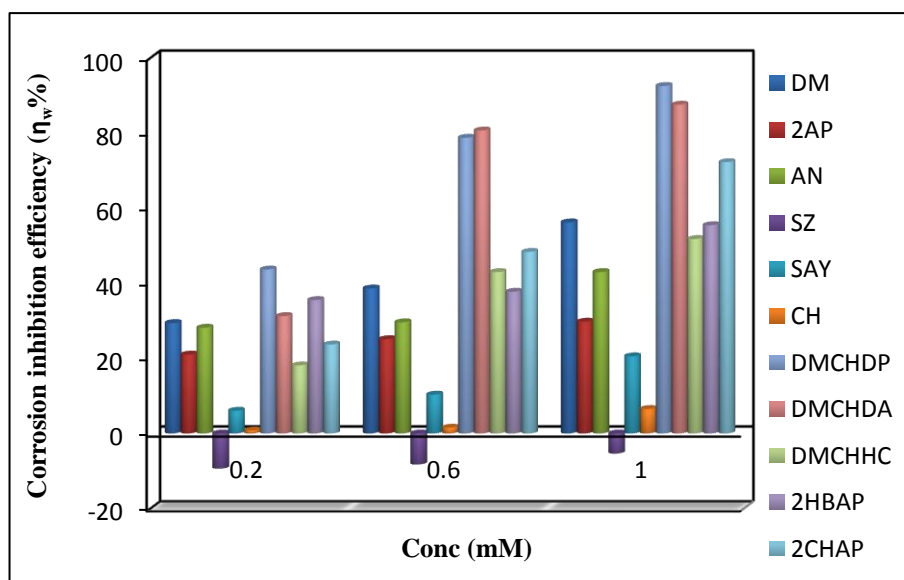


Fig. 5.3 Comparison of corrosion inhibition efficiency ($\eta_w\%$) of Schiff bases and their parent compounds on MS in 0.5 M H₂SO₄

Adsorption studies

Mechanism of the inhibition of corrosion of MS in 0.5 M H₂SO₄ can be elucidated with the help of adsorption isotherms. Langmuir, Temkin, El-Awady, Florry-huggin, Freundlich and Frumkin adsorption isotherms were considered, and the best

suites isotherm was determined by calculating the correlation coefficient (R^2). Correlation coefficients obtained for the Schiff bases in various isotherms are given in Table 5.4. Thermodynamic parameters obtained from the study are free energy of adsorption (ΔG_{ads}^0) and adsorption equilibrium constant (K_{ads}). From the results it is clear that Langmuir isotherm was obeyed by the Schiff bases DMCHDP and 2CHAP whereas El-Awady isotherm was obeyed by DMCHDA. None of the isotherms considered to study the mechanism of inhibition was obeyed by DMCHHC and 2HBAP. Thermodynamic parameters obtained from the analysis of isotherms are given in Table 5.5 and the adsorption isotherms of Schiff base molecule on MS surface in 0.5 M H_2SO_4 medium are described in Fig. 5.4.

Table 5.4 Correlation coefficients of the Schiff bases derived from various isotherms

Isotherm	Correlation coefficient (R^2)				
	DMCHDP	DMCHDA	DMCHHC	2HBAP	2CHAP
Langmuir	0.9728	0.8592	0.3781	0.8464	0.9997
Freunlich	0.7949	0.7556	0.5881	0.8008	0.6217
Frumkin	0.8801	0.8449	0.2995	0.6101	0.9136
Temkin	0.9233	0.9189	0.5882	0.6441	0.8163
El-Awady	0.9485	0.9606	0.6046	0.6454	0.8986
Florry Huggin	0.8345	0.5999	0.0073	0.3808	0.8812

Table 5.5 Thermodynamic parameters for the adsorption of DMCHDP, DMCHDA, DMCHHC, 2HBAP and 2CHAP on MS in 0.5 M H_2SO_4

Parameter	Schiff base		
	DMCHDP	DMCHDA	2CHAP
Correlation coefficient	0.9728	0.9606	0.9997
K_{ads}	3333.33	1613968.88	33333.33
ΔG_{ads}^0 (kJmol^{-1})	-30.37	-45.84	-36.13

Negative values of ΔG_{ads}^0 in all case indicate spontaneity of the process. The value of ΔG_{ads}^0 for DMCHDP and 2CHAP were -30.37 and -36.13 kJmol^{-1} respectively. This indicates that the adsorption behaviour of these molecules involves both

physisorption and chemisorption. In the case of DMCHDA ΔG_{ads}^0 value was -45.84kJmol^{-1} , which indicates the presence of co-ordinate type bond between DMCHDA and metal surface (chemical interaction).

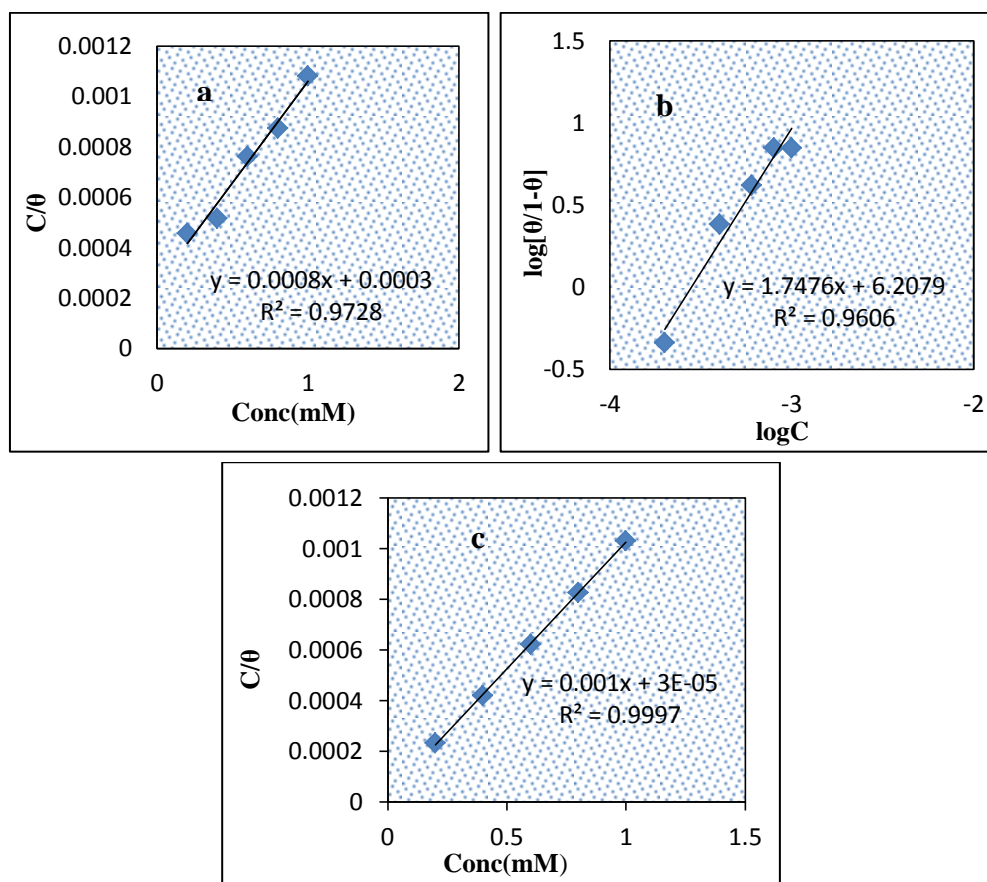


Fig. 5.4 a) Langmuir adsorption isotherm of DMCHDP b) El-Awady adsorption isotherm of DMCHDA and c) Langmuir adsorption isotherm of 2CHAP on MS in 0.5 M H_2SO_4 at 28°C

Temperature studies

Impact of temperature on the rate of corrosion was investigated using weight loss studies at temperatures 301 K, 313 K, 323 K and 333 K. The activation energy of metal dissolution was calculated using an Arrhenius type equation given below

$$K = A \exp(-E_a/RT) \quad (1)$$

where A, K, R, T and E_a denote pre-exponential factor, corrosion rate, universal gas constant, temperature in Kelvin and activation energy respectively. Activation energy required for the dissolution of metal was obtained from the slope of the plot $\log K$ vs $1/T$

for MS specimens in acid media, with and without Schiff base molecules (Fig. 5.5-5.9a). Thermodynamic parameters such as enthalpy (ΔH^*) and entropy (ΔS^*) changes were evaluated using transition state theory (equation 2)

$$K = \left(\frac{RT}{Nh}\right) \exp\left(\frac{\Delta S^*}{R}\right) \exp\left(\frac{-\Delta H^*}{RT}\right) \quad (2)$$

where h and N are Planck's constant and Avogadro number respectively. The slope, $\frac{-\Delta H^*}{2.303R}$ and intercept, $\log\left(\frac{R}{2.303Nh}\right) + \left(\frac{\Delta S^*}{2.303R}\right)$ were obtained by plotting $\log K/T$ vs $1/T$ (Fig. 5.5-5.9b). Table 5.6 represents the activation energy and thermodynamic parameters such as entropy of activation (ΔS^*) and enthalpy of activation (ΔH^*). It was observed that the activation energy of metal dissolution was high in the case of acid solution containing Schiff base molecules. Also, it was found that E_a increased with concentration of Schiff base, which implies that dissolution of the metal was reduced with respect to the rise in Schiff base concentration. Activation energy of corrosion in 0.5 M H_2SO_4 is less compared to that in 1.0 M HCl. This indicates that the corrosion is more pronounced in 0.5 M H_2SO_4 due to its high aggressive nature. Positive sign of the enthalpy of activation indicates the endothermic nature of metal dissolution. ΔH^* and ΔS^* values were found to increase along with rise in concentration of Schiff bases.

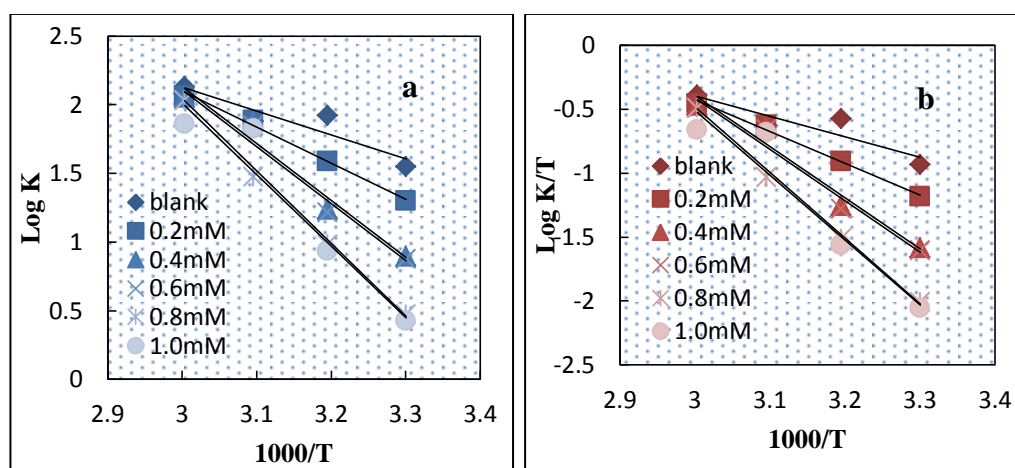


Fig. 5.5 Plot of a) $\log K$ vs $1000/T$ b) $\log K/T$ vs $1000/T$ with and without DMCHDP on MS in 0.5 M H_2SO_4

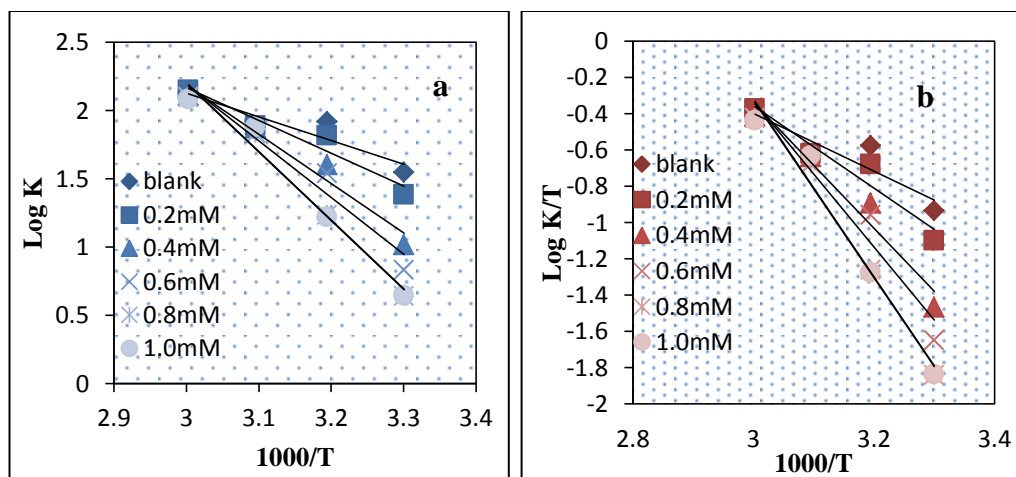


Fig. 5.6 Plot of a) $\log K$ vs $1000/T$ b) $\log K/T$ vs $1000/T$ with and without DMCHDA on MS in $0.5 \text{ M H}_2\text{SO}_4$

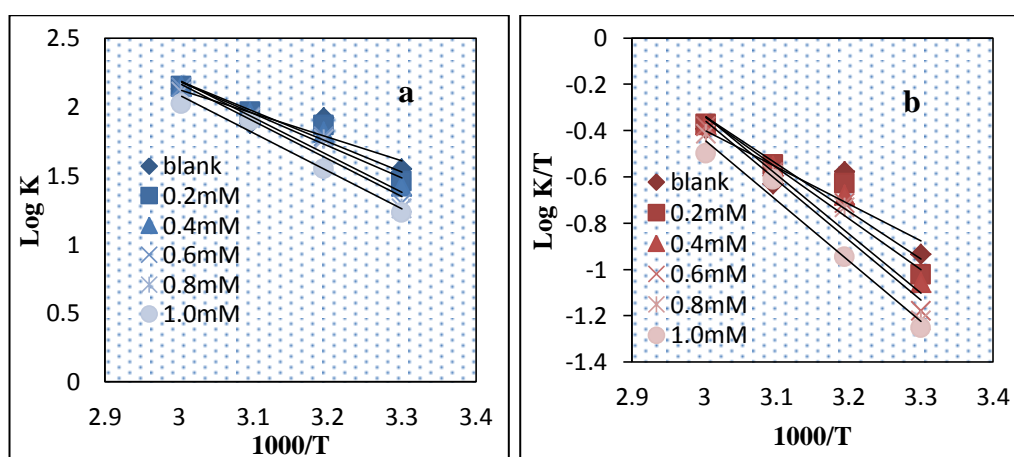


Fig. 5.7 Plot of a) $\log K$ vs $1000/T$ b) $\log K/T$ vs $1000/T$ with and without DMCHHC on MS in $0.5 \text{ M H}_2\text{SO}_4$

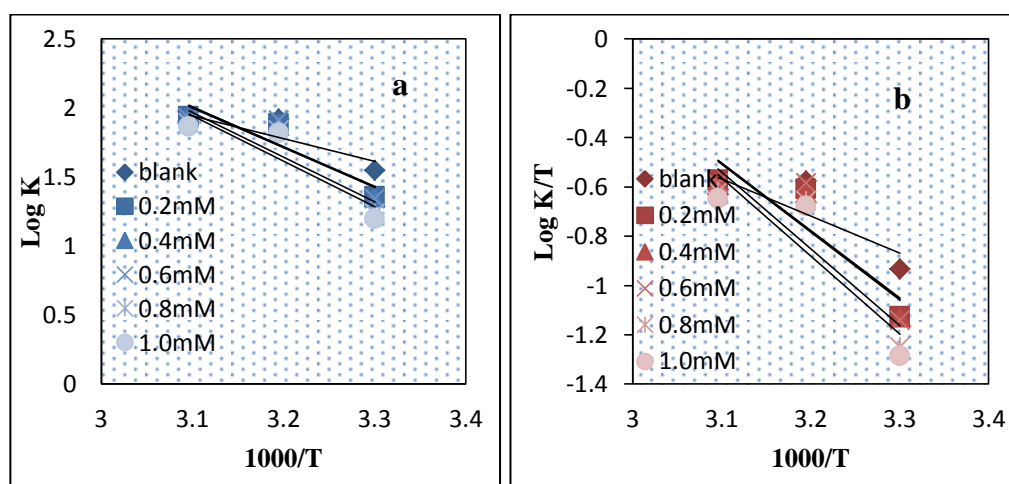


Fig. 5.8 Plot of a) $\log K$ vs $1000/T$ b) $\log K/T$ vs $1000/T$ with and without 2HBAP on MS in $0.5 \text{ M H}_2\text{SO}_4$

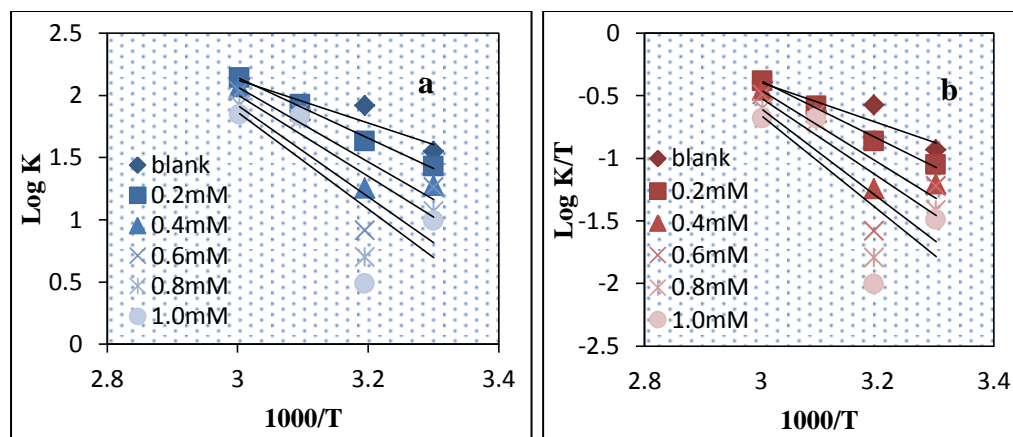


Fig. 5.9 Plot of a) $\log K$ vs $1000/T$ b) $\log K/T$ vs $1000/T$ with and without 2CHAP on MS in 0.5 M H_2SO_4

Table 5.6 Thermodynamic parameters of corrosion of MS with and without Schiff bases in 0.5 M H_2SO_4

Schiff base	Conc (mM)	E_a ($kJ\ mol^{-1}$)	A	ΔH^* ($kJ\ mol^{-1}$)	ΔS^* ($J\ mol^{-1}K^{-1}$)
DMCHDP	Blank	33.1	2.08×10^7	30.5	-106.71
	0.2	50.24	9.31×10^9	47.60	-55.97
	0.4	79.40	3.73×10^{14}	76.76	32.15
	0.6	79.43	3.58×10^{14}	76.79	31.81
	0.8	99.57	4.09×10^{17}	96.93	90.36
	1.0	100.93	7.21×10^{17}	98.29	95.07
DMCHDA	0.2	46.10	2.46×10^9	43.46	-67.03
	0.4	69.12	1.04×10^{13}	66.48	2.38
	0.6	79.66	4.75×10^{14}	77.02	34.16
	0.8	96.33	1.96×10^{17}	93.69	84.25
	1.0	96.58	2.18×10^{17}	93.94	85.13
DMCHHC	0.2	42.23	6.38×10^8	39.59	-78.26
	0.4	44.90	1.67×10^9	42.26	-70.29
	0.6	51.81	2.04×10^{10}	49.17	-49.44
	0.8	52.43	2.43×10^{10}	49.79	-48.01
	1.0	52.92	2.39×10^{10}	50.28	-48.15
2HBAP	0.2	54.99	8.09×10^{10}	52.39	-37.86
	0.4	55.21	8.69×10^{10}	52.61	-37.27
	0.6	55.22	8.83×10^{10}	52.62	-37.14
	0.8	62.13	1.07×10^{12}	59.53	-16.42
	1.0	63.05	1.43×10^{12}	60.45	-14.02
2CHAP	0.2	46.77	2.96×10^9	44.13	-65.50
	0.4	57.67	1.26×10^{11}	55.03	-34.28
	0.6	62.45	6.14×10^{11}	59.81	-21.14
	0.8	70.22	8.36×10^{12}	67.58	0.56
	1.0	74.59	3.57×10^{13}	71.95	12.64

Electrochemical impedance spectroscopy

Ivium compactstat-e electrochemical system associated with a new version of iviumsoft software was utilized for the electrochemical measurements. A three electrode system, consisting of platinum electrode having 1 cm^2 area as counter electrode, saturated calomel electrode (SCE) as the reference electrode, metal specimen with an exposed area of 1 cm^2 as working electrode, were used for the studies. Impedance spectra (Nyquist and Bode plots) of MS in the absence and presence of Schiff bases at various concentrations in $0.5 \text{ M H}_2\text{SO}_4$ are shown in Fig. 5.10, 5.11, 5.12, 5.13 and 5.14.

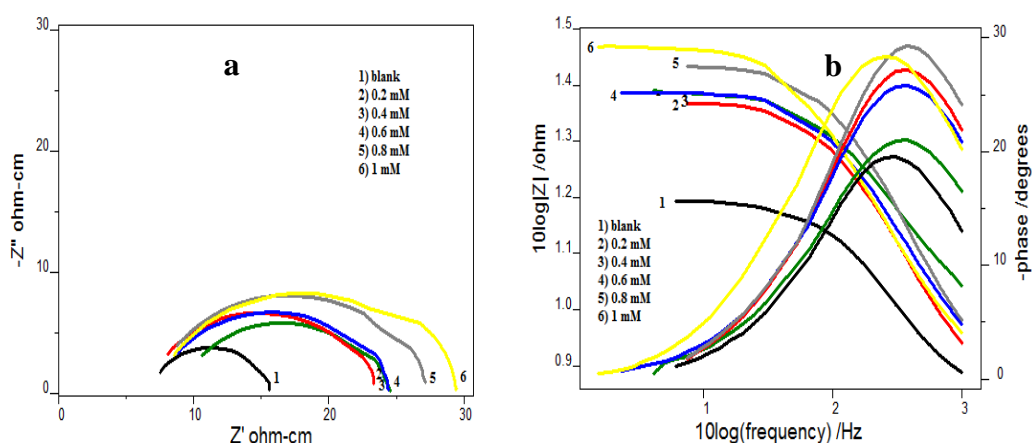


Fig. 5.10 a) Nyquist and b) Bode plots of MS coupons with and without DMCHDP in $0.5 \text{ M H}_2\text{SO}_4$

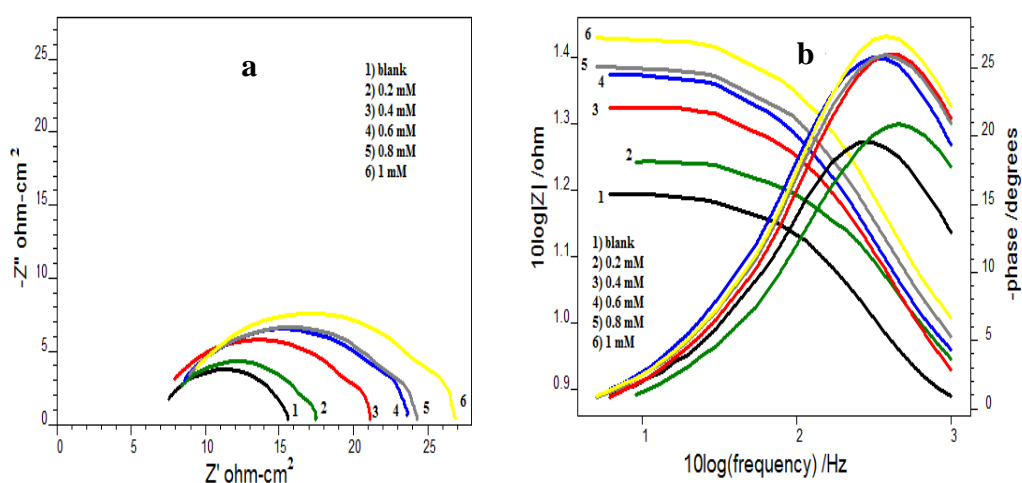


Fig. 5.11 a) Nyquist and b) Bode plots of MS coupons with and without DMCHDA in $0.5 \text{ M H}_2\text{SO}_4$

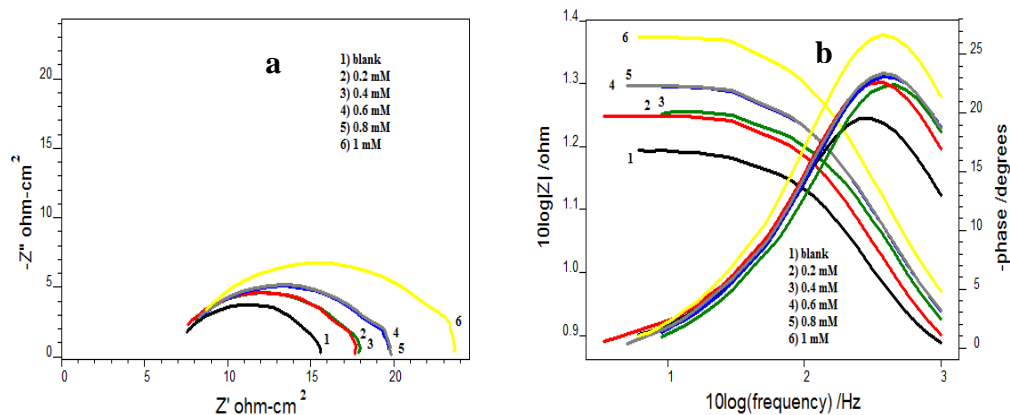


Fig. 5.12 a) Nyquist and b) Bode plots of MS coupons with and without DMCHHC in 0.5 M H_2SO_4

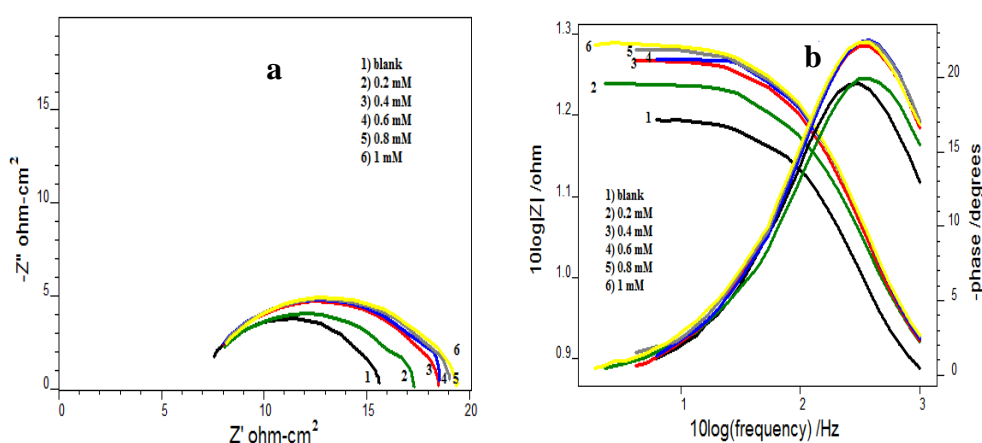


Fig. 5.13 a) Nyquist and b) Bode plots of MS coupons with and without 2HBAP in 0.5 M H_2SO_4

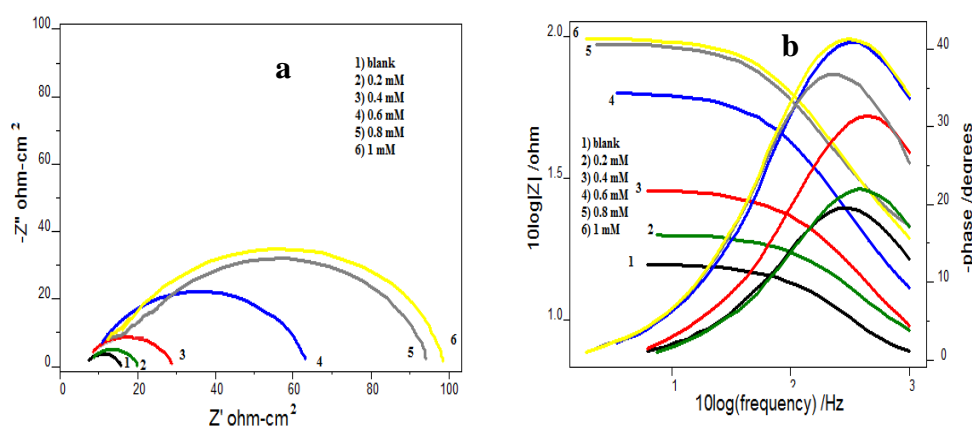


Fig. 5.14 a) Nyquist and b) Bode plots of MS coupons with and without 2CHAP in 0.5 M H_2SO_4

Electrochemical impedance data such as R_{ct} , C_{dl} and the percentage of inhibition efficiency ($\eta_{EIS}\%$) of the Schiff bases are listed in Table 5.7. From the data it is established that charge transfer resistance of the blank solution ($7.96 \Omega cm^2$) is less than

that of the solution containing Schiff base molecule. Also charge transfer resistance (R_{ct}) was found to increase and capacitance (C_{dl}) was reduced with increase in concentration of Schiff bases. As a result corrosion inhibition efficiency ($\eta_{EIS}\%$) was also increased with concentration.

Table 5.7 Impedance data of MS coupons with and without Schiff bases in 0.5 M H_2SO_4

Schiff base	Conc (mM)	C_{dl} (μFcm^{-2})	R_{ct} (Ωcm^2)	$\eta_{EIS}\%$
Blank	0.0	113	7.9	-
DMCHDP	0.2	72.8	13.1	39.23
	0.4	66.5	14.6	45.48
	0.6	67.7	14.9	46.57
	0.8	53.2	17.5	54.51
	1.0	83.9	19.3	58.76
DMCHDA	0.2	72.6	9.10	12.53
	0.4	66.6	12.8	37.81
	0.6	71.6	14.3	44.33
	0.8	62.3	14.7	45.85
	1.0	54.6	16.7	52.33
DMCHHC	0.2	72.0	9.86	19.26
	0.4	85.7	9.91	19.68
	0.6	71.4	11.1	28.28
	0.8	72.0	11.2	28.93
	1.0	60.4	14.6	45.48
2HBAP	0.2	94.5	8.88	10.36
	0.4	86.1	10.2	21.96
	0.6	80.9	10.3	22.71
	0.8	83.1	10.5	24.19
	1.0	87.3	10.8	26.29
2CHAP	0.2	72.8	10.9	26.97
	0.4	49.4	19.1	58.32
	0.6	33.2	48.8	83.69
	0.8	27.1	70.2	88.66
	1.0	23.2	77.1	89.67

Maximum inhibition efficiencies of about 58.76%, 52.33%, 45.48%, 26.29% and 89.67% were exhibited by the Schiff bases DMCHDP, DMCHDA, DMCHHC, 2HBAP and 2CHAP respectively at 1 mM concentration. Inhibition efficiency of all the Schiff bases is lower compared to the EIS measurements in 1.0 M HCl medium. Minimum efficiency of about 26.97% was exhibited by 2CHAP at 0.2 mM concentration while at

1.0 mM concentration, maximum efficiency of 89.67% was achieved. According to gravimetric analysis DMCHDP and DMCHDA have appreciable corrosion inhibition efficiency. In contrary to this observation, the inhibition efficiency is low at all concentrations according to EIS measurements. Comparison of corrosion inhibition efficiency ($\eta_{\text{EIS}}\%$) of the Schiff bases on MS in 0.5 M H_2SO_4 was shown in Fig. 5.15.

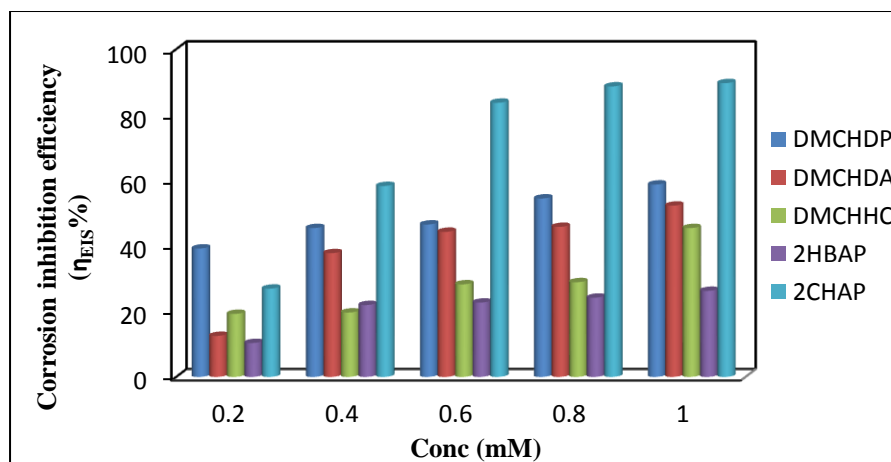


Fig. 5.15 Comparison of corrosion inhibition efficiency ($\eta_{\text{EIS}}\%$) of the Schiff bases on MS in 0.5 M H_2SO_4

Potentiodynamic polarization studies

Tafel and linear polarization studies were carried out to understand the effect of Schiff bases towards polarization of metal specimens. Polarization parameters such as corrosion current density (I_{corr}) and polarization resistance (R_p) were measured using this technique and then inhibition efficiency ($\eta_{\text{pol}}\%$ and $\eta_{R_p}\%$) was calculated using these parameters. Tafel and linear polarization plots of the Schiff bases are shown in Fig. 5.16, 5.17, 5.18, 5.19 and 5.20. Polarization data such as corrosion potential (E_{corr}), corrosion current densities (I_{corr}), cathodic slope (b_c), anodic slope (b_a), polarization resistance (R_p) and inhibition efficiency ($\eta_{\text{pol}}\%$ and $\eta_{R_p}\%$) of the Schiff bases in 0.5 M H_2SO_4 are listed in Table 5.8.

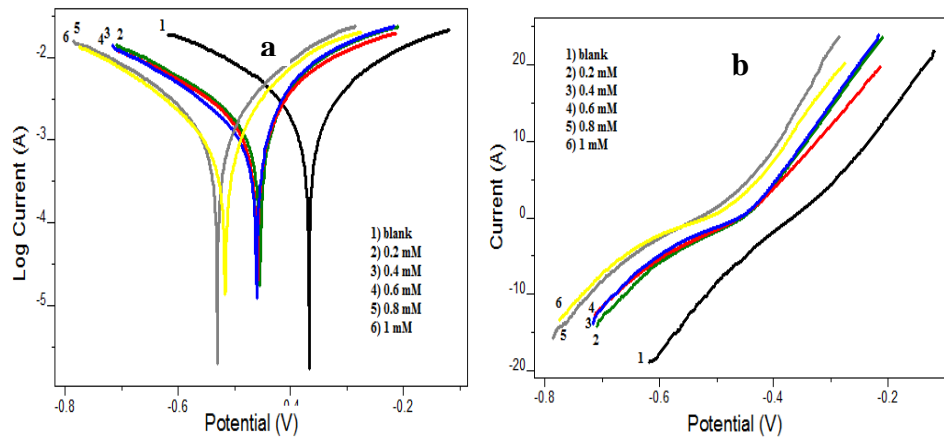


Fig. 5.16 a) Tafel and b) linear polarization plots of MS coupons with and without DMCHDP in 0.5 M H_2SO_4

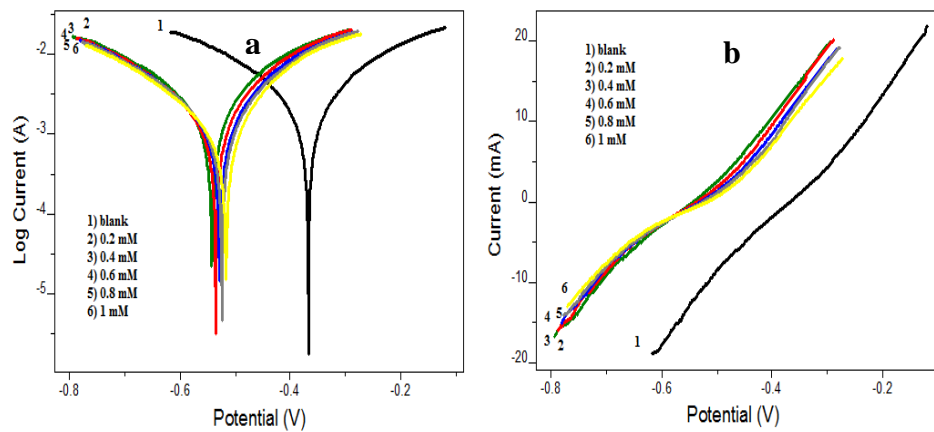


Fig. 5.17 a) Tafel and b) linear polarization plots of MS coupons with and without DMCHDA in 0.5 M H_2SO_4

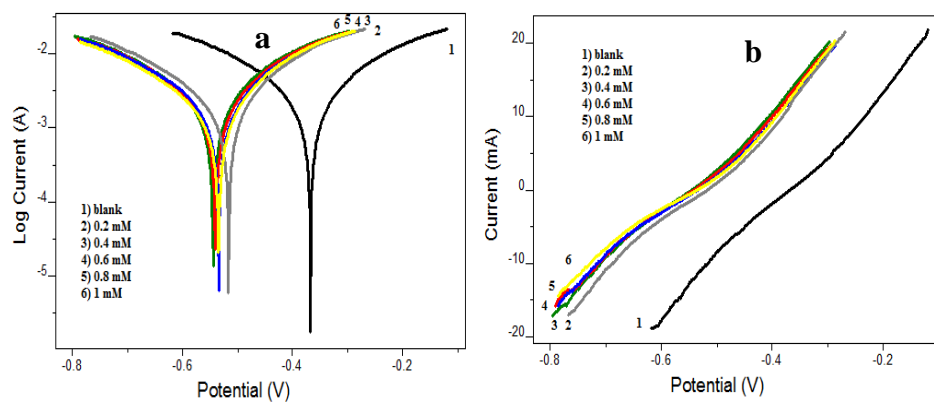


Fig. 5.18 a) Tafel and b) linear polarization plots of MS coupons with and without DMCHHC in 0.5 M H_2SO_4

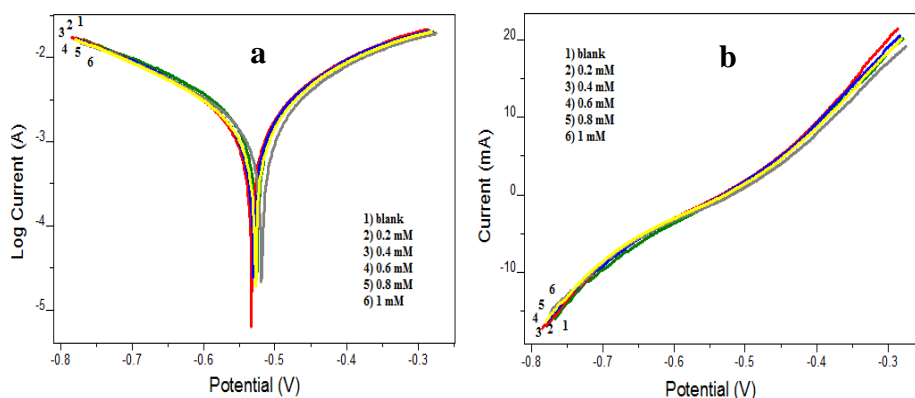


Fig. 5.19 a) Tafel and b) linear polarization plots of MS coupons with and without 2HBAP in 0.5 M H₂SO₄

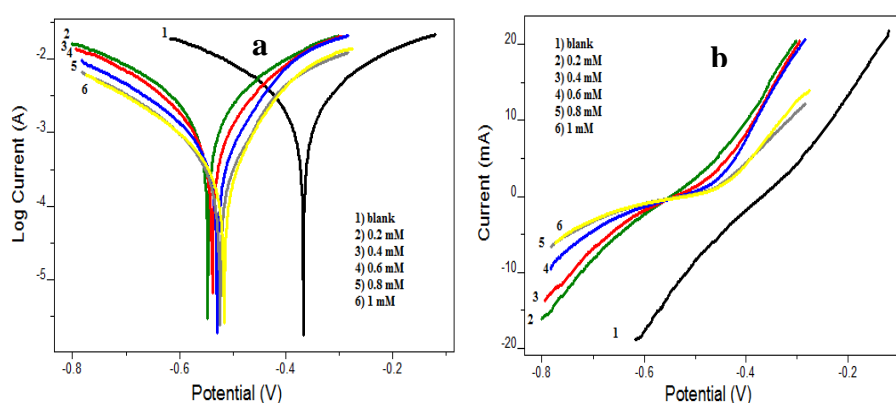


Fig. 5.20 a) Tafel and b) linear polarization plots of MS coupons with and without 2CHAP in 0.5 M H₂SO₄

Polarization data reveals that corrosion current density increased and polarization resistance decreased with the rise in concentration of Schiff bases. As a result, the percentage of inhibition efficiency also increased. A maximum inhibition efficiency ($\eta_{\text{pol}}\%$) of 50.79%, 44.33%, 28.4%, 24.32% and 81.41% were shown by DMCHDP, DMCHDA, DMCHHC, 2HBAP and 2CHAP respectively at 1 mM concentration. The b_a and b_c values indicated that addition of Schiff bases to acid media affected both cathodic and anodic parts of the curves and hence acted as a mixed type inhibitor. Comparison of corrosion inhibition efficiency ($\eta_{\text{pol}}\%$) of the Schiff bases on MS in 0.5 M H₂SO₄ were shown in Fig. 5.21. Impedance and polarization data are in good agreement. Considerable difference was noticed between the corrosion inhibition efficiency of DMCHDP and

DMCHDA in gravimetric and electrochemical studies (EIS and potentiodynamic polarization) in 0.5 M H₂SO₄ medium.

Table 5.8 Polarization data of MS coupons with and without Schiff bases in 0.5 M H₂SO₄

Schiff base	Tafel data					Polarization data		
	Conc (mM)	E _{corr} (mV)	I _{corr} (μA/cm ²)	b _a (mV/dec)	-b _c (mV/dec)	η _{pol} %	R _p (Ω)	η _{RP} %
Blank	0	-374.3	2528	241	242	-	20.74	-
	0.2	-500.5	2282	253	243	9.73	23.61	12.16
	0.4	-496.3	2058	257	251	18.47	25.59	18.95
DMCHDP	0.6	-514.5	1957	244	219	22.59	26.76	22.49
	0.8	-538.3	1563	185	222	38.17	28.04	26.03
	1	-539.9	1244	185	205	50.79	33.91	38.83
DMCHDA	0.2	-559.7	2329	250	236	7.87	22.63	8.35
	0.4	-556.3	1832	224	213	27.53	25.87	19.83
	0.6	-547.2	1735	220	226	31.37	27.93	25.74
	0.8	-539.1	1557	206	224	38.41	29.9	30.64
	1	-543.1	1408	210	212	44.33	32.52	36.22
DMCHHC	0.2	-556.1	2348	244	243	7.12	22.54	7.98
	0.4	-557.1	2145	240	229	15.15	23.52	11.82
	0.6	-549.8	2127	240	243	15.86	23.76	12.71
	0.8	-529.4	2102	220	233	16.85	24.63	15.79
	1	-551.3	1810	219	231	28.4	27.02	23.24
2HBAP	0.2	-525.9	2269	250	238	10.24	23.35	11.18
	0.4	-544.4	2010	221	237	20.49	24.71	16.07
	0.6	-543.3	2002	223	237	20.8	24.89	16.67
	0.8	-537.7	1914	229	244	24.29	26.16	20.72
	1	-545.8	1913	228	233	24.32	26.79	22.58
2CHAP	0.2	-552.3	1909	217	233	24.49	25.55	18.83
	0.4	-539.6	1233	173	215	51.23	33.74	38.53
	0.6	-536.5	754	142	209	70.17	48.77	57.47
	0.8	-536.4	530	155	205	79.03	72.28	71.31
	1	-532.2	470	143	201	81.41	77.29	73.16

Evaluated corrosion inhibition efficiency of these two Schiff bases according to gravimetric studies in H₂SO₄ medium was higher than that of EIS and potentiodynamic polarization investigations. By using UV-visible spectroscopy, it was confirmed that

slow hydrolysis of DMCHDP and DMCHDA is occurring in 0.5 M H₂SO₄ medium.

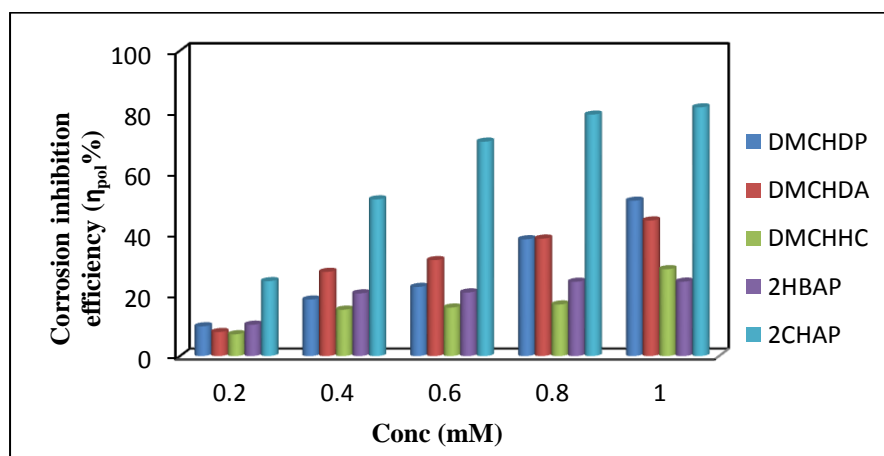


Fig. 5.21 Comparison of corrosion inhibition efficiency ($\eta_{\text{pol}}\%$) of the Schiff bases on MS in 0.5 M H₂SO₄

Fig. 5.22 represents the UV-Vis spectra of DMCHDP and its corresponding parent compounds in 0.5 M H₂SO₄. In the figure 5-5-dimethyl-1,3-cyclohexanedione and 2-aminophenol exhibited peaks at 259 nm and 268 nm respectively. The peak at 290 nm due to DMCHDP is shifted to 265 nm when UV-Vis spectrum of DMCHDP was taken after immersion time of 24 h. This indicates the formation of 2-aminophenol molecule. It can be assumed that large number of Schiff bases didn't undergo appreciable structural degradation for 1-2 h and thus exhibit poor corrosion inhibition potency on MS according to electrochemical studies. On keeping DMCHDP for a period of 24 h it can be imagined that partial hydrolysis takes place (for one C=N linkage only). This structural degradation of DMCHDP may be highly beneficial to interact effectively on the MS surface, since the bulky nature of the molecule is appreciably lowered. Electron rich aromatic ring and the C=N linkage now can make coordinate type bonds with the surface metal atoms easily. Thus after a period of 24 h, DMCHDP molecule showed much enhanced corrosion inhibition efficiency on MS surface.

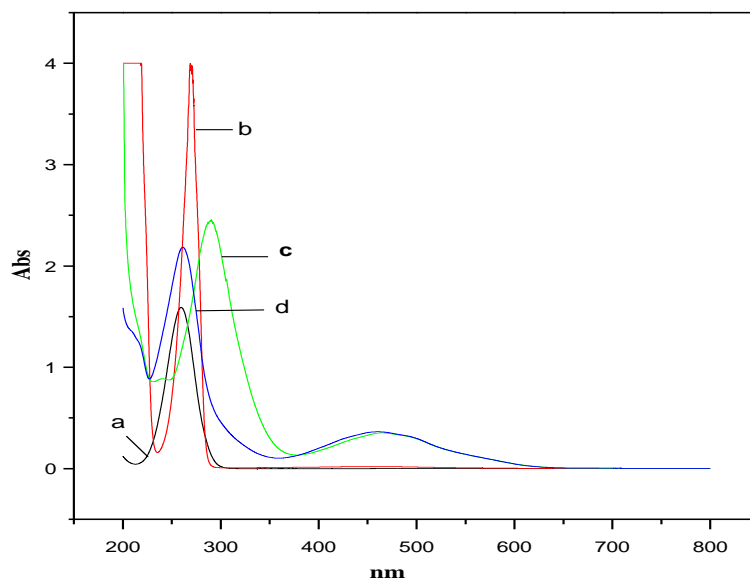


Fig. 5.22 UV-Vis spectra of a) 5,5-dimethyl-1,3-cyclohexanedione b) 2-aminophenol c) DMCHDP at 0 h and d) DMCHDP at 24 h in 0.5 M H₂SO₄

Fig. 5.23 represents the UV-Vis spectra of DMCHDA and its corresponding parent compounds in 0.5 M H₂SO₄. In the case of DMCHDA complete hydrolysis of the molecule takes place and the parent compounds 5-5-dimethyl-1,3-cyclohexanedione (Dm) and aniline (An) regenerated were responsible for the high inhibition efficiency. The peak of 5-5-dimethyl-1,3-cyclohexanedione at 259 nm is observed in the UV-Vis spectrum of DMCHDA after immersion time of 24 h in 0.5 M H₂SO₄. Peak due to aniline at 252 nm may be merged. Parent compounds itself have appreciable inhibition efficiency in 0.5 M H₂SO₄ (Table 5.3). Enhanced inhibition efficiency of DMCHDA in gravimetric study than electrochemical study was attributed to the net effect of inhibition efficiency of both parent compounds formed during hydrolysis. Even though there is a probability for hydrolysis in 1.0 M HCl medium the corrosion inhibition efficiency of DMCHDP and DMCHDA in gravimetric and electrochemical studies follows the same trend. This may be due to the higher adsorption tendency of these Schiff bases on Cl⁻ ion, which is strongly bind to mild steel surface instead of its hydrolysis.

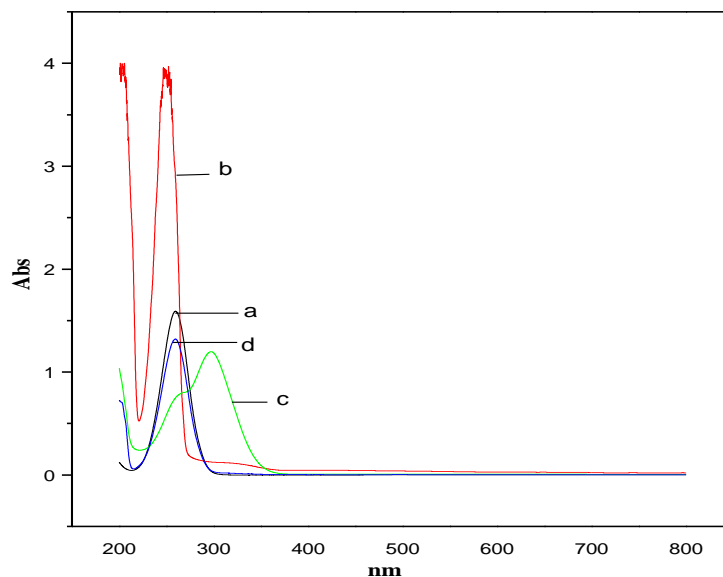


Fig. 5.23 UV-Vis spectra of a) 5,5-dimethyl-1,3-cyclohexanedione b) aniline c) DMCHDA at 0 h and d) DMCHDA at 24 h in 0.5 M H_2SO_4

Electrochemical noise measurements

The parameters mean value of current noise and pitting index were measured from noise plots. Mean value of current noise gives information regarding protective power of sample against corrosion and pitting index value helps to quantify localized pitting corrosion. Current noise for MS in the absence and presence of Schiff bases (1 mM) in 0.5 M H_2SO_4 is shown in Fig. 5.24.

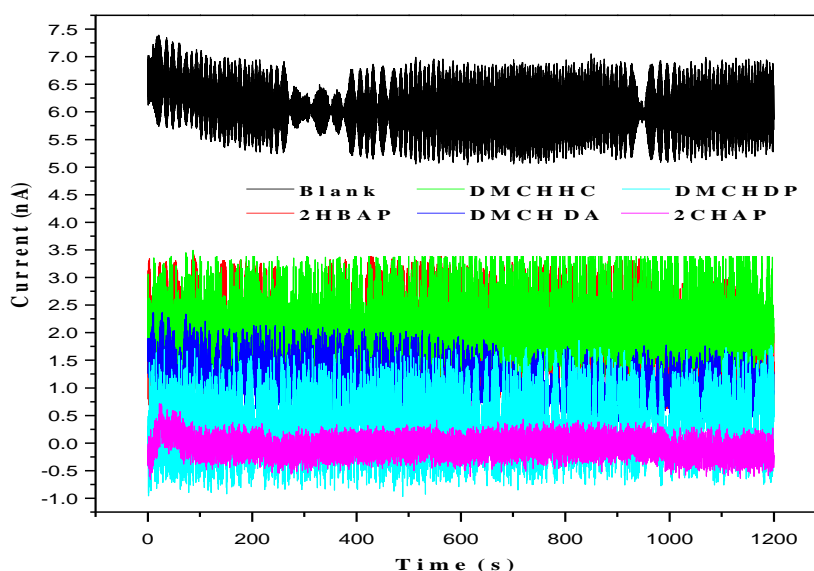


Fig. 5.24 Current noise for MS in the absence and presence of Schiff bases (1 mM) in 0.5 M H_2SO_4

From the figure, it is clear that blank specimen exhibits higher mean value of current noise in respect of the specimen dipped in an acid medium containing Schiff base molecules, and the mean value of current noise in 0.5 M H_2SO_4 was greater than in 1.0 M HCl medium, which reflects the greater protective power of Schiff bases in 1.0 M HCl medium. PSD plot is shown in Fig 5.25.

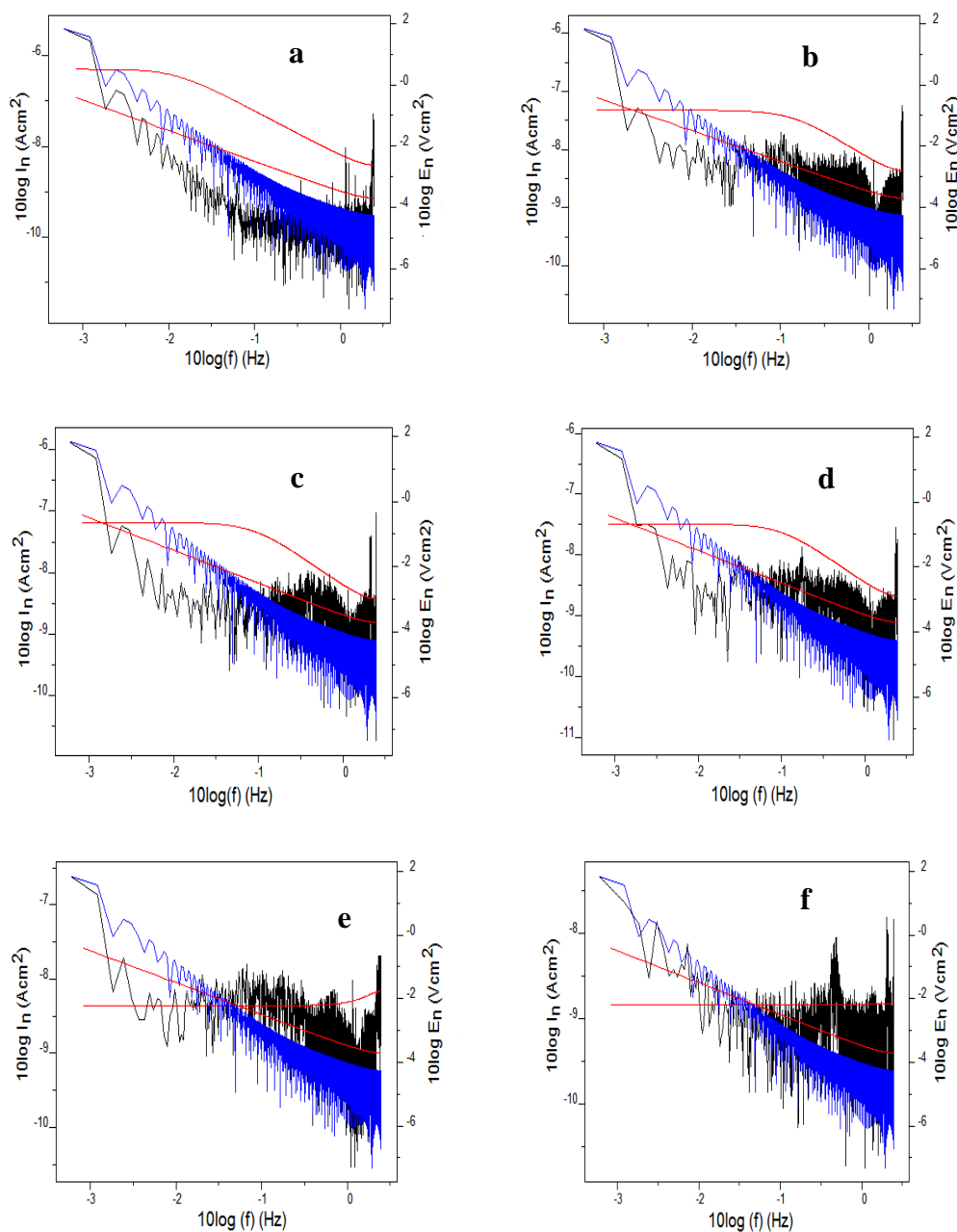


Fig. 5.25 Power spectral density (voltage and current) plots of MS in 0.5 M H_2SO_4 in the presence of a) blank b) 2HBAP c) DMCHHC d) DMCHDA e) DMCHDP and f) 2CHAP

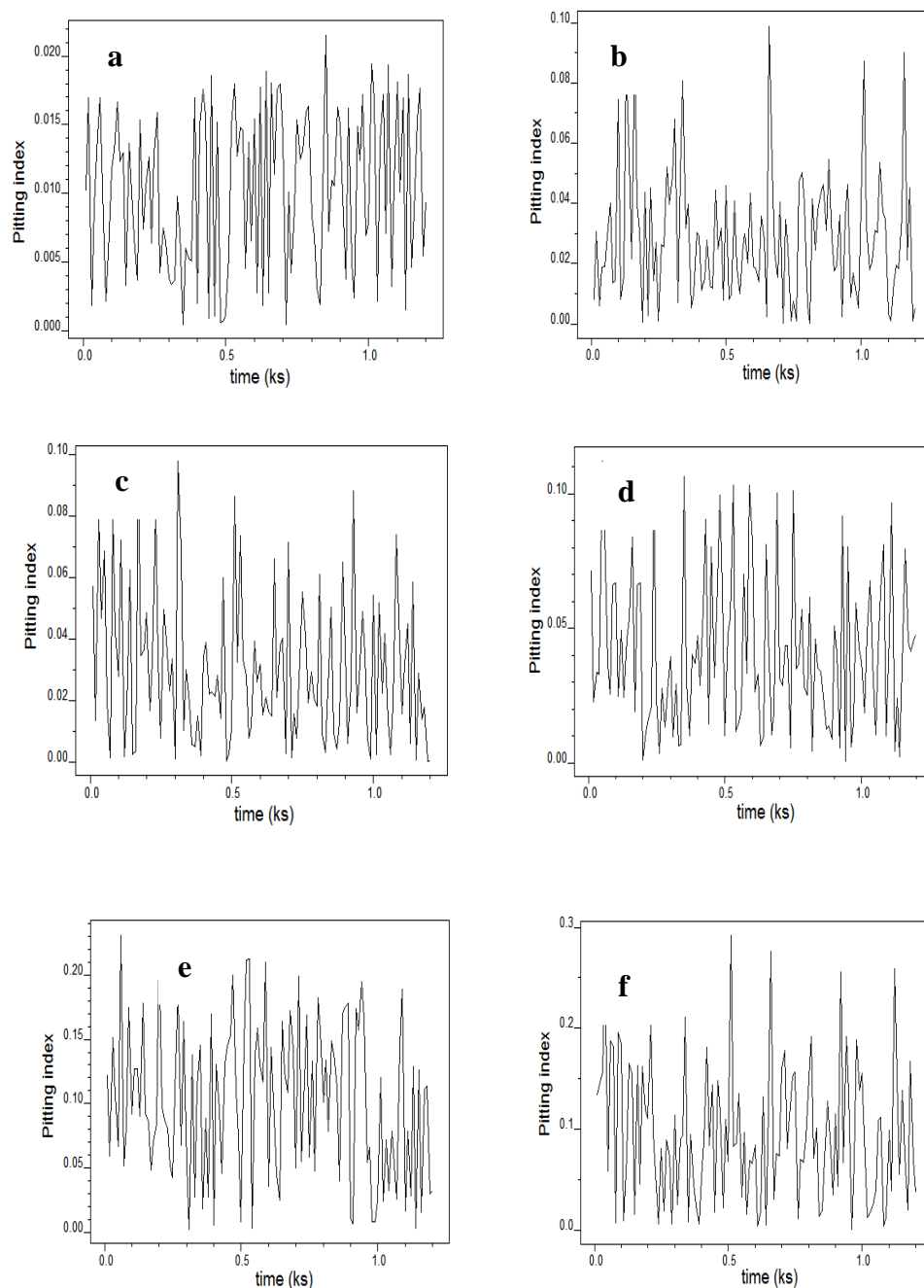


Fig. 5.26 Pitting index curves of MS in 0.5 M H₂SO₄ in the presence of a) blank b) 2HBAP c) DMCHHC d) DMCHDA e) DMCHDP and f) 2CHAP

The values of current noise are comparatively large for blank metal specimen than for metal immersed in acid solution containing Schiff base molecules at all frequencies. Thus localised corrosion is happening in the absence of Schiff base molecule. Pitting index curves are shown in Fig. 5.26. Amplitude of the pitting index curve corresponding to blank metal specimen is lower than metal specimens treated with

acid solution containing Schiff bases. Thus the acid solution containing Schiff base molecule has high resistance to corrosion.

Surface morphological studies

In order to determine the surface morphology of MS coupons, scanning electron microscopy was conducted. Fig. 5.27(a-d) represents the SEM images of bare metal, mild steel coupon in 0.5 M H_2SO_4 , MS treated with DMCHDP (1 mM) and MS treated with DMCHDA (1 mM) respectively.

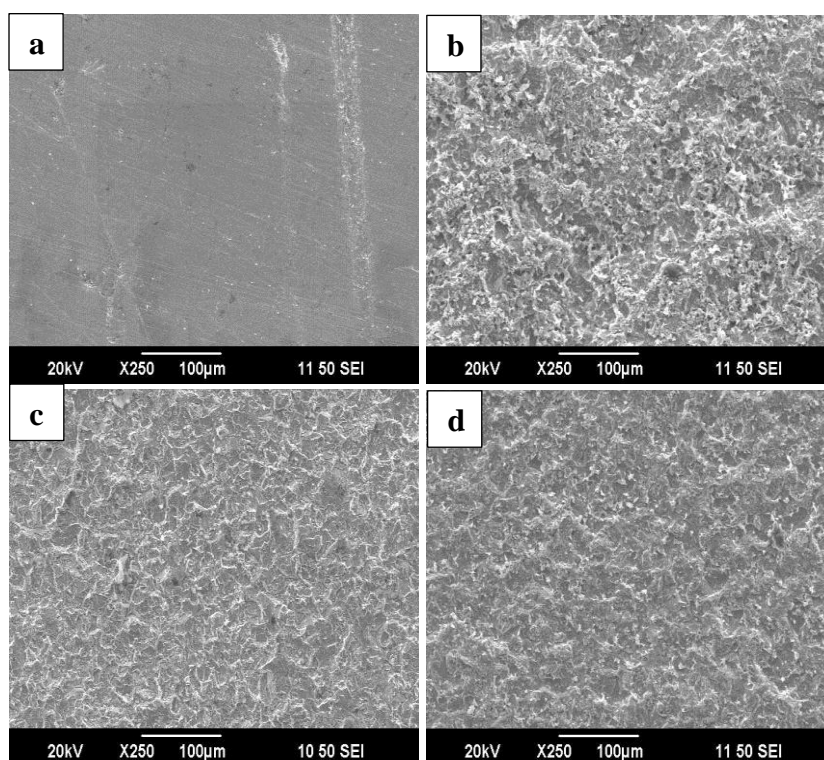


Fig. 5.27 SEM images of MS coupons before and after 24 h immersion a) bare b) blank (0.5 M H_2SO_4) c) treated with DMCHDP (1 mM) in 0.5 M H_2SO_4 and d) treated with DMCHDA(1 mM) in 0.5 M H_2SO_4

There exists a remarkable difference between the surface of a polished mild steel specimen and the one treated with acid solution. It is clear that the mild steel surface reacted with acid medium is erratic and rough in nature. A remarkable change in the surface morphology of MS was observed after adding Schiff base molecule into 0.5 M H_2SO_4 medium. In the presence of 1 mM concentration of DMCHDP and DMCHDA the

corrosion rate was found to decrease and the surface became less corroded. This is a clear indication of the formation of a protective layer of Schiff base molecules on mild steel surface.

SUMMARY

In this part synthesis and characterization of the Schiff bases such as 2,2'-(5,5-dimethylcyclohexane-1,3-diylidene)bis(azanylylidene)diphenol (DMCHDP), N,N'-(5,5-dimethylcyclohexane-1,3-diylidene)dianiline (DMCHDA), 2,2'-(5,5-dimethylcyclohexane-1,3-diylidene)bis(hydrazinecarboxamide) (DMCHHC), 2-((2hydroxybenzylidene)amino) phenol (2HBAP) and 2-(cyclohexylideneamino)phenol (2CHAP) were carried out. Elemental analysis, spectral studies such as FTIR, UV-visible, NMR (^1H and ^{13}C) and mass spectroscopy and cyclic voltammetric studies were employed for the structural elucidation.

Corrosion inhibition efficiency of these Schiff bases on mild steel was also investigated in 1.0 M HCl and 0.5 M H_2SO_4 . The concentration of the Schiff bases used for the study lies in the range of 0.2-1.0 mM. Corrosion inhibition efficiency of the synthesized Schiff bases was evaluated using gravimetric method and electrochemical methods such as electrochemical impedance spectroscopy (EIS), potentiodynamic polarization studies and electrochemical noise measurements. Evaluation of adsorption phenomenon on the mild steel surface was carried out using various adsorption isotherms to verify the mechanism of inhibition and surface morphological studies were performed to confirm the adsorption behaviour. Effect of temperature on the corrosion inhibition efficiency as well as quantum chemical calculations was also done.

Data revealed that corrosion inhibition capacity of the Schiff bases derived from 5,5-dimethylcyclohexane-1,3-dione such as DMCHDP, DMCHDA and DMCHHC was high compared to that of 2HBAP and 2CHAP in 1.0 M HCl. Also the inhibition efficiency of these three inhibitors is greater than 90% at 1 mM concentration according to weight loss studies. Azomethine, hydroxyl group and presence of hetero atoms present in these Schiff bases are responsible for their higher efficiency. In the case of all Schiff

bases except 2HBAP, rate of corrosion is less than that of blank specimen and is found to be decreasing with rise in concentration, which established the antagonistic nature of 2HBAP on corrosion. Adsorption study revealed that the Schiff bases DMCHDP, DMCHDA and DMCHHC obey Langmuir adsorption isotherm whereas 2HBAP and 2CHAP follow Frumkin adsorption isotherm on mild steel in 1.0 M HCl. According to impedance and polarization studies all the Schiff bases have appreciable inhibition efficiency, and act as mixed type inhibitors towards mild steel corrosion.

In 0.5 M H₂SO₄ the corrosion inhibition efficiency of all the Schiff bases except 2HBAP are less compared to that in 1.0 M HCl according to weight loss study. This can be attributed to the aggressive nature of sulphuric acid medium. The inhibition efficiency of DMCHDP and DMCHDA was high than other Schiff bases according to weight loss study. Also it was observed that the inhibition efficiency of these two Schiff bases reduced considerably in impedance and potentiodynamic polarization measurements. Comparatively high efficiency observed in weight loss measurement may be attributed to hydrolysis of DMCHDP and DMCHDA in sulphuric acid medium. DMCHDP undergo partial hydrolysis whereas DMCHDA undergo complete hydrolysis which was clearly observed in UV-visible spectra taken after 24 h immersion of mild steel specimen in inhibitor solutions. High inhibition efficiency upon hydrolysis can be explained by the lowering of steric nature in the case of DMCHDP whereas it may be because of the formation of parent compounds having appreciable inhibition efficiency, in the case of DMCHDA. Schiff bases DMCHDP and 2CHAP obeyed Langmuir adsorption isotherm whereas DMCHDA followed El-Awady isotherm. In sulphuric acid medium also all the Schiff bases acted as mixed type inhibitors, towards the mild steel corrosion.

Temperature-dependent gravimetric analysis showed that the activation energy of corrosion was high in both acid solutions containing Schiff base molecules. Also it was

observed that activation energy increased with rise in concentration of Schiff bases. Positive value of enthalpy of corrosion reflects the endothermic nature of corrosion. Surface morphological study established the protective nature of Schiff bases on mild steel surface. Electrochemical noise measurement was also carried out to examine the inhibition capacity.

REFERENCES

1. Z. Tao, S. Zhang, W. Li and B. Hou, *Ind. Eng. Chem. Res.* 49, 2593-2599 (2010).
2. S. John and A. Joseph, *Mater. Chem. Phys.* 133, 1083-1091 (2012).
3. S. Deng, X. Li and H. Fu, *Corros. Sci.* 53, 3596-3602 (2011).
4. K. R. Ansari and M. A. Quraishi, *Corros. Sci.* 95, 62-70 (2015).
5. I. Ahamad, R. Prasad and M. A. Quraishi, *J. Solid State Electrochem.* 14, 2095-2105 (2010).
6. K. C. Emregül and O. Atakol, *Mater. Chem. Phys.* 83, 373-379(2004).
7. D. Gopi, K. M. Govindaraju and L. Kavitha, *J. Appl. Electrochem.* 40, 1349-1356 (2010).
8. X. Wang, H. Yang and F. Wang, *Corros. Sci.* 53, 113-121 (2011).
9. M. P. Chakravarthy and K. N. Mohana, *ISRN Corrosion.* 2014, 1-13 (2014).
10. A. K. Singh, S. K. Shukla, M. Singh and M. A. Quraishi, *Mater. Chem. Phys.* 129, 68-76 (2011).
11. K. Ramya, R. Mohan, K. K. Anupama and A. Joseph, *Mater. Chem. Phys.* 149, 632-647 (2015).
12. A. K. Singh, S. K. Shukla, M. A. Quraishi and E. E. Ebenso, *J. Taiwan Inst. Chem. Eng.* 43, 463-472 (2012).
13. X. Wang, Y. Wang, Q. Wang, Y. Wan, X. Huang and C. Jing, *Int. J. Electrochem. Sci.* 13, 5228-5242 (2018).
14. N. G. Thompson, M. Yunovich and D. Dunmire, *Corros. Rev.* 25, 247-261 (2007).
15. O. S. I. Fayomi, I. G. Akande and S. Odigie, *J. Phys.: Conf. Ser.* 1378, 1-8 (2019).

16. K. S. Jacob and G. Parameswaran, *Corros. Sci.* 52, 224-228(2010).
17. K. S. Shaju, K. J. Thomas and V. P. Raphael, *Orient. J. Chem.* 30, 807-813 (2014).
18. R. Solmaza, E. Altunbas and G. Kardas, *Mater. Chem. Phys.* 125, 796-801 (2011).
19. H. Keles, M. Keles, I. Dehri, and O. Serindag, *Mater. Chem. Phys.* 112, 173-179 (2008).
20. P. Lowmunkhong, D. Ungthararak and P. Sutthivaiyakit, *Corros. Sci.* 52, 30-36 (2010).
21. M. Paulson Binsi, K. Thomas Joby, K. Ragi, C. Varghese Sini and J. Reeja, *Curr. Chem. Lett.* 9, 1-12 (2019).
22. K. Mallaiya, R. Subramaniam, S. S. Srikandan, S. Gowri, N. Rajasekaran and A. Selvaraj, *Electrochim. Acta.* 56, 3857-3863 (2011).
23. K. R. Ansari, M. A. Quraishi and A. Singh, *Corros. Sci.* 79, 5-15 (2014).
24. N. Soltani, M. Behpour, S. M. Ghoreishi and H. Naeimi, *Corros. Sci.* 52, 1351-1361 (2010).
25. E. E. Oguzie, *Mater. Lett.* 59, 1076-1079 (2005).
26. H. Schiff, *Justus Liebigs Ann. Chem.* 131, 118-119 (1864).
27. D. N. Dhar and C. L. Taploo, *J. Sci. Ind. Res.* 41, 501-506 (1982).
28. E. Bayer, *Angew. Chem. Int. Ed.* 3, 325-332 (1964).
29. F. Feigl, *Spot Tests in Organic Analysis*, Elsevier, New York, NY, USA, 2, (1958).
30. P. Przybylski, A. Huczynski, K. Pyta, B. Brzezinski and F. Bartl, *Curr. Org. Chem.* 13, 124-148 (2009).
31. P. Singh, R. L. Goel and B. P. Singh, *J. Indian Chem. Soc.* 52, 958-959 (1975).

-
32. Elmali, M. Kabak and Y. Elerman, *J. Mol. Struct.* 477, 151-158 (2000).
33. A. Chawla, K. Kuldeep, P. Chawla and R. K. Dhawan, *J. Res. Appl. Nat. Soc. Sci.* 1, 85-92 (2015).
34. A. Fattah-alhosseini and M. Noori, *Measurement.* 94, 787-793 (2016).
35. M. N. Ibrahim and S. E. A. Sharif, *E-J. Chem.* 4, 531-535 (2007).
36. M. Colak, T. Aral, H. Hosgoren and N. Demirel, *Tetrahedron: Asymmetr.* 18, 1129–1133 (2007).
37. S. Kumar, D. N. Dhar, and P. N. Saxena, *J. Sci. Ind. Res.* 68, 181-187 (2009).
38. M. S. Karthikeyan, D. J. Prasad, B. Poojary, K. S. Bhat, B. S. Holla and N. S. Kumari, *Bioorg. Med. Chem.* 14, 482-489 (2006).
39. L. Heinisch, E. Roemer, P. Jutten, W. Haas, W. Werner and U. Mollmann, *J. Antibiot.* 52, 1029-1041 (1999).
40. W. Rehman, M. K. Baloch, B. Muhammad, A. Badshah and K. M. Khan, *Chin. Sci. Bull.* 49, 119-122 (2004).
41. M. S. Alam, J. -H. Choi and D. -U. Lee, *Bioorg. Med. Chem.* 20, 4103-4108 (2012).
42. D. Sriram, P. Yogeewari, N. S. Myneedu and V. Saraswat, *Bioorg. Med. Chem. Lett.* 16, 2127-2129 (2006).
43. A. K. Chaubey and S. N. Pandeya, *Int. J. Pharmtech. Res.* 4, 590-598 (2012).
44. Y. -F. Li and Z. -Q. Liu, *Eur. J. Pharm. Sci.* 44, 158-163 (2011).
45. Dr. A. Xavier and N. Srividhya, *IOSR J. Appl. Chem.* 7, 6-15 (2014).
46. W. Qin, S. Long, M. Panunzio and B. Stefano, *Molecules.* 18, 12264-12289 (2013).
47. P. Rathelot, P. Vanelle, M. Gasquet, F. Delmas, M. P. Crozet, P. Timon-David and J. Maldonado, *Eur. J. Med. Chem.* 30, 503-508 (1995).
-

-
48. B. Witkop and T. W. Beiler, *J. Am. Chem. Soc.* 76, 5589-5597 (1954).
 49. M. S. Novikov, A. F. Khlebnikov, O. V. Besedin and R. R. Kostikov, *Tetrahedron Lett.* 42, 533-535 (2001).
 50. I. N. Booyesen, S. Maikoo, M. P. Akerman and B. Xulu, *Polyhedron.* 79, 250-257 (2014).
 51. N. K. Chaudhary and P. Mishra, *Bioinorg. Chem. Appl.* 2017, 1-13 (2017).
 52. B. K. Singh, A. Prakash, H. K. Rajour, N. Bhojak and D. Adhikari, *Spectrochim. Acta A.* 76, 376-383 (2010).
 53. M. El-Behery and H. El-Twigry, *Spectrochim. Acta A.* 66, 28-36 (2007).
 54. S. Li, S. Chen, S. Lei, H. Ma, R. Yu and D. Liu, *Corros. Sci.* 41, 1273-1287 (1999).
 55. S. John, B. Joseph, K. K. Aravindakshan and A. Joseph, *Mater. Chem. Phys.* 122, 374-379 (2010).
 56. A. Yurt, A. Balaban, S. Ustün Kandemir, G. Bereket and B. Erk, *Mater. Chem. Phys.* 85, 420-426 (2004).
 57. W. Li, Q. He, S. Zhang, C. Pei and B. Hou, *J. Appl. Electrochem.* 38, 289-295 (2008).
 58. K. M. Govindaraju, D. Gopi and L. Kavitha, *J. Appl. Electrochem.* 39, 2345-2352 (2009).
 59. N. Kuriakose, J. T. Kakkassery, V. P. Raphael and S. K. Shanmughan, *Indian J. Mater. S.* 2014, 1-6 (2014).
 60. M. G. Hosseini, M. Ehteshamzadeh and T. Shahrabi, *Electrochim. Acta.* 52, 3680-3685 (2007).
 61. I. Ahamad, C. Gupta, R. Prasad and M. A. Quraishi, *J. Appl. Electrochem.* 40, 2171-2183 (2010).
-

62. K. R. Ansari and M. A. Quraishi, *J. Ind. Eng. Chem.* 20, 2819-2829 (2014).
63. K. S. Shaju, K. J. Thomas, V. P. Raphael and A. Paul, *ISRN Corrosion*. 2012, 1-8 (2012).
64. M. A. Quraishi and D. Jamal, *Mater. Chem. Phys.* 78, 608–613 (2003).
65. N. K. Gupta, C. Verma, M. A. Quraishi and A. K. Mukherjee, *J. Mol. Liq.* 215, 47-57 (2016).
66. A. M. Abdel-Gaber, M. S. Masoud, E. A. Khalil and E. E. Shehata, *Corros. Sci.* 51, 3021-3024 (2009).
67. M. Balaji, N. Chandrasekar, G. Sharmila and R. Manivannan, *Int. J. Res. Eng. Technol.* 4, 51-64 (2016).
68. S. P. Fakrudeen, H. C. Ananda murthy and V. B. Raju, *J. Chil. Chem. Soc.* 57, 1364-1371 (2012).
69. P. Karuppasamy, M. Ragu, J. Thiruppathy, M. Ganesan, T. Rajendran and V. K. Sivasubramanian, *Int. J. Multidiscip. Res. Dev.* 1, 14-24 (2014).
70. A. Barbosa da Silva, E. D. Elia and J. Antonio da Cunha Ponciano Gomes, *Corros. Sci.* 52, 788-793 (2010).
71. R. Menaka and S. Subhashini, *J. Adhes. Sci. Technol.* 30, 1622-1640 (2016).
72. R. Solmaza, E. Altunbas and G. Kardas, *Mater. Chem. Phys.* 125, 796-801 (2011).
73. A. S. Fouda and S. A. EL-Sayyad, *Anti-Corros. Method M.* 58, 63-69 (2011).
74. K. Veni, A. D. Karthik, K. Geetha and D. Shakila, *IOSR J. Pharm.* 2, 62-68 (2017).
75. M. Q. Mohammed, *J. Basrah Researches.* 37, 116-130 (2011).
76. Y. B. Zemedede, D. Nithyakalyani and S. Ananda Kumar, *Int. J. Med. Res.* 2, 128-141 (2016).

-
77. S. K. Saha, A. Dutta, P. Ghosh, D. Sukulc and P. Banerjee, *Phys. Chem. Chem. Phys.* 17, 5679-5690 (2015).
78. P. Silku, S. Ozkinali, Z. Ozturk, A. Asan and D. A. Kose, *J. Mol. Struct.* 1116, 72-83 (2016).
79. R. K. Upadhyay, S. Anthony and S. P. Mathur, *Russ. J. Electrochem.* 43, 238-241 (2007).
80. D. Daoud, T. Douadi, S. Issaadi and S. Chafaa, *Corros. Sci.* 79, 50-58 (2014).
81. M. Farsak, H. Keles and M. Keles, *Corros. Sci.* 98, 223-232 (2015).
82. B. M. Mistry and S. Jauhari, *Res. Chem. Intermed.* 41, 6289-6307 (2014).
83. V. P. Raphael, K. J. Thomas, K. S. Shaju and A. Paul, *Res. Chem. Intermed.* 40, 2689-2701 (2013).
84. T. S. Franklin Rajesh, A. Sheik Mideen, J. Karthikeyan and S. Anitha, *Int. J. Appl. Bioeng.* 6, 2810-2815 (2012).
85. C. M. Goulart, A. Esteves-Souza, C. A. Martinez-Huitle, C. J. F. Rodrigues, M. A. M. Maciel and A. Echevarria, *Corros. Sci.* 67, 281-291 (2013).
86. V. P. Raphael, J. T. Kakkassery, K. S. Shaju and S. Varghese, *Int. J. Ind. Chem.* 8, 49-60 (2016).
87. P. C. Okafor, E. E. Oguzie, G. E. Iniama, M. E. Ikpi and U. J. Ekpe, *Global J. Pure Appl. Sci.* 14, 89-95 (2008).
88. Dr. L. Ravikumar, Dr .G. Rathika and R. Punitha, *Int. J. Adv. Res. Technol.* 2, 3137-3143 (2013).
89. N. Raman, S. Ravichandran, and C. Thangaraja, *J. Chem. Sci.* 116, 215-219 (2004).
90. Y. Meng, W. Ning, B. Xu, W. Yang, K. Zhang, Y. Chen, L. Li, X. Liu, J. Zheng and Y. Zhang, *RSC Adv.* 7, 43014-43029 (2017).
-

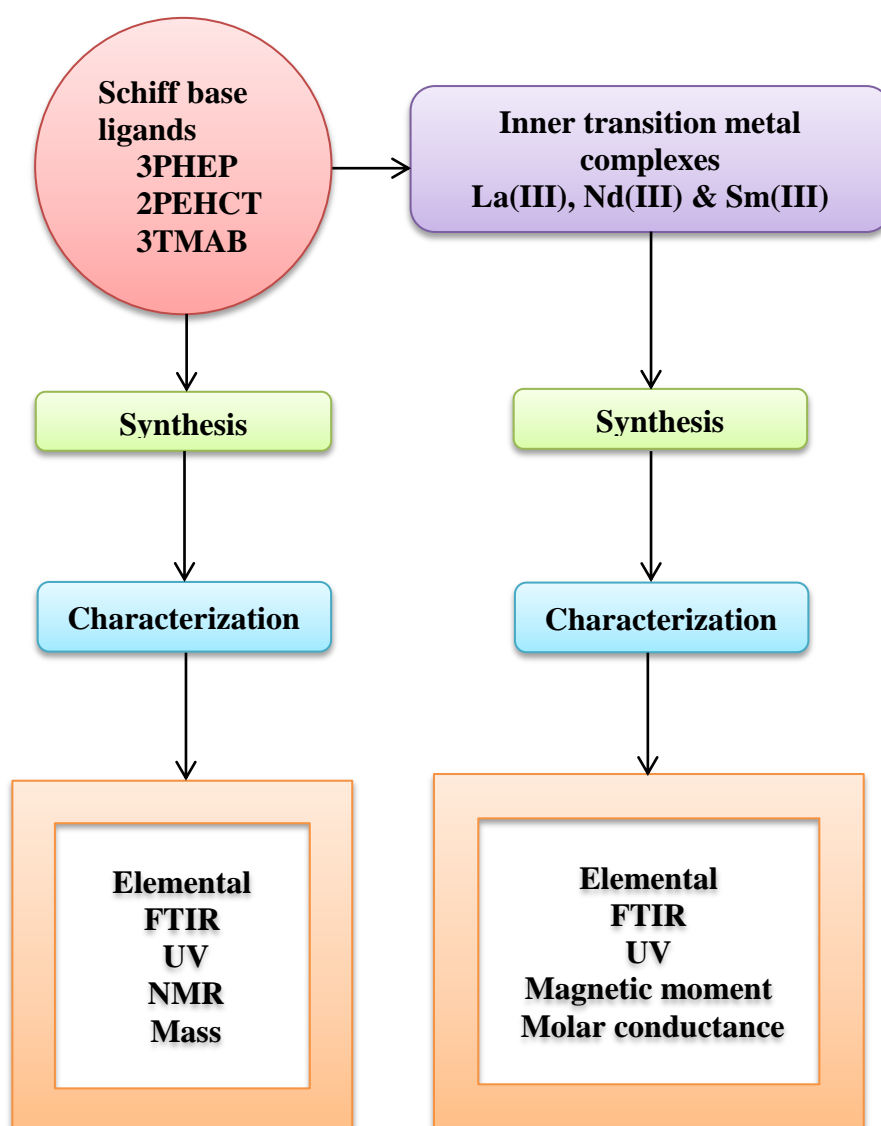
-
91. A. Dandia, S. L. Gupta, M. A. Quraishi, and P. Singh, *ACS Sustain. Chem. Eng.* 1, 1303-1310 (2013).
 92. A. A. Farag, M. A. Migahed and A. M. Al-Sabagh, *Egypt. J. Pet.* 24, 307-315 (2015).
 93. S. Issaadi, T. Douadi, A. Zouaoui, S. Chafaa, M. A. Khan and G. Bouet, *Corros. Sci.* 53, 1484-1488 (2011).
 94. X. Li, S. Deng, H. Fu and T. Li, *Electrochim. Acta.* 54, 4089–4098 (2009).
 95. A. Ghanbari, M. M. Attar and M. Mahdavian, *Mater. Chem. Phys.* 124, 1205-1209 (2010).
 96. S. A. Umoren, *J. Appl. Polym. Sci.* 119, 2072-2084 (2011).
 97. H. Ashassi-Sorkhabi, B. Shaabani and D. Seifzadeh, *Electrochim. Acta.* 50, 3446-3452 (2005).
 98. G. E. Badr, *Corros. Sci.* 51, 2529-2536 (2009).
 99. D. K. Yadav, M. A. Quraishi and B. Maiti, *Corros. Sci.* 55, 254-266 (2012).
 100. Z. Tao, W. He, S. Wang, S. Zhang and G. Zhou, *Corros. Sci.* 60, 205-213 (2012).
 101. P. Singh, V. Srivastava and M. A. Quraishi, *J. Mol. Liq.* 216, 164-173 (2016).
 102. Y. Tang, X. Yang, W. Yang, R. Wana, Y. Chen and X. Yin, *Corros. Sci.* 52, 1801-1808 (2010).
 103. A. R. Sathiya Priya, V. S. Muralidharan and A. Subramania, *Corrosion.* 64, 541-552 (2008).
 104. C. Verma, M. A. Quraishi, E. E. Ebenso, I. B. Obot and A. El Assry, *J. Mol. Liq.* 219, 647-660 (2016).
 105. E. E. Elemike, D. C. Onwudiwe, H. U. Nwankwo and E. C. Hosten, *J. Mol. Struct.* 1136, 253-262 (2017).
-

-
106. N. K. Gupta, M. A. Quraishi, C. Verma and A. K. Mukherjee, *RSC Adv.* 6, 102076-102087 (2016).
 107. A. Y. Musa, A. B. Mohamad, A. A. H. Kadhum, M. S. Takriff and L. T. Tien, *Corros. Sci.* 53, 3672-3677 (2011).
 108. L. Li, Q. Qu, W. Bai, F. Yang, Y. Chen, S. Zhang and Z. Ding, *Corros. Sci.* 59, 249-257 (2012).
 109. R. Baboian, “*Corrosion Tests and Standards: Application and Interpretation*”, ASTM stock NO: MNL-20, 2nd edn. (1998).
 110. C. Wagner and W. Z. Traud, *Z. Elektrochem.* 44, 391 (1938).
 111. T. Badea, M. Nicola, I. D. Vaireanu, I. Maior and A. Cojocaru, “*Electrochimie si Corozione, Matrixrom, Bucuresti*”, 150 (2005).
 112. A. Pandey, B. Singh, C. Verma and E. E. Ebenso, *RSC Adv.* 7, 47148-47163 (2017).
 113. P. P. Kumari, S. A. Rao and P. Shetty, *Procedia Mater. Sci.* 5, 499-507 (2014).
 114. M. Dekker, “*Electrochemical Techniques in Corrosion, Science and Engineering*”, New York (2003).
 115. I. Ahamad, R. Prasad and M. A. Quraishi, *Mater. Chem. Phys.* 124, 1155-1165 (2010).
 116. Y. J. Tan, S. Bailey and B. Kinsella, *Corros. Sci.* 38, 1681-1695 (1996).
 117. F. Mansfeld, Z. Sun, C. H. Hsu and A. Naguib, *Corros. Sci.* 43, 341-352 (2001).
 118. J. Smulko, K. Darowicki and A. Zieliński, *Electrochem. Commun.* 4, 388-391 (2002).
 119. S. Abd El Wanees, A. Abd and M. Abdel Azzem, *Int. J. Electrochem. Sci.* 3, 104-117 (2008).
 120. J. F. Chen and W. F. Bogaerts, *Corros. Sci.* 37, 1839-1842 (1995).

121. H. Ashassi-Sorkhabi, D. Seifzadeh and M. Raghibi-Boroujeni, *Arab. J. Chem.* 9, S1320–S1327 (2016).
122. A. M. Homborg, R. A. Cottis and J. M. C. Mol, *Electrochim. Acta.* 222, 627-640 (2016).
123. A. M. Homborg, E. P. M. van Westing, T. Tinga, X. Zhang, P. J. Oonincx, G. M. Ferrari, J. H. W. de Wit and J. M. C. Mol, *Corros. Sci.* 66, 97-110 (2013).
124. S. F. Burch, S. F. Gull and J. Skilling, *Comput. Vision, Graph. Image Processing.* 23, 113-128 (1983).
125. K. F. Al-Azawi, S. B. Al-Baghdadi, A. Z. Mohamed, A. A. Al-Amiery, T. K. Abed, S. A. Mohammed, A. A. H. Kadhum and A. B. Mohamad, *Chem. Cent. J.* 10, 1-9 (2016).
126. T. Arslan, F. Kandemirli, E. E. Ebenso, I. Love and H. Alemu, *Corros. Sci.* 51, 35-47 (2009).
127. E. E. Ebenso, D. A. Isabirye and N. O. Eddy, *Int. J. Mol. Sci.* 11, 2473-2498 (2010).
128. P. M. Nouri and M. M. Attar, *Bull. Mater. Sci.* 38, 499-509 (2015).
129. M. M. Kabanda, L. C. Murulana, M. Ozcan, F. Karadag, I. Dehri, I. B. Obot and E. E. Ebenso, *Int. J. Electrochem. Sci.* 7, 5035-5056 (2012).

PART-II

CHELATION STUDIES



CHAPTER 6

INTRODUCTION AND REVIEW

Coordination chemistry, an important field in chemistry, mainly deals with study of coordination compounds. Coordination compounds consist of a central metal ion surrounded by a group of atoms called ligands. Upon dissolution they do not ionize into its constituents of which they are made; instead they give complex ions. Various characteristic properties are shown by coordination compounds and it depends on the kind of ligand and nature of metal ion. Theory of coordination compounds was proposed by Alfred Werner in 1893 and he got Nobel Prize for this in 1913. If there is two or more donor atoms present in ligand, then it can form bond with the metal resulting in the formation of rings. Such complexes are called chelates. Bond formed between metal and the ligand can either be covalent or ionic according to the nature of metal and ligand molecule. Stability of chelates depends upon number and size of the ring formed during chelation. In the case of saturated rings five membered chelate is stable, whereas in the case of rings containing double bonds six membered ring is favorable [1]. Normally the donor atoms present in chelating agents are O, N and S.

There are so many coordination compounds exist in nature. For example chlorophyll, vitamin B₁₂ and haemoglobin are coordination compounds of magnesium, cobalt and iron respectively. Formation of bond between metal ion and donor atom takes place with or without replacing hydrogen atom. The organic functional groups such as carboxylic (-COOH), oxime (>C=N-OH), sulphonic (-SO₃H), imine (>C=N-H), phenolic (-OH), thiophenolic (-SH) groups etc can form metal bond by replacing hydrogen atom, whereas the groups such as alcoholic (-OH), ether (-O-), thiol (-SH), carbonyl (>C=O), thiocarbonyl (>C=S), thioether (-S-), primary amine (NH₂), secondary amine (NHR), tertiary amine (NR₂), alkyl imine (>C=N-R) etc can form metal bond without replacing

hydrogen atom. Coordination compounds have applications in the field of photography, metallurgy, textile dyeing, industry, toxicology, material science, medicinal chemistry, bioinorganic chemistry, ceramics, electroplating, photonics etc [2-6]. Even though there are so many ligands available, the contribution of Schiff bases in the evolution of coordination chemistry is most remarkable [7-9]. Detailed discussion on Schiff bases are well documented in chapter 1.

Schiff base complexes - A review

Literature survey revealed that research in the field of Schiff bases and their complexes are going on extensively due to wide range of applications in various fields. Presence of azomethine nitrogen in Schiff bases is responsible for its coordinating ability with metal ions.

Schiff bases are multipurpose ligand, which are important in several fields. The metal complexes of Schiff bases are also used extensively owing to their versatile applications such as biological activities such as antibacterial, antitumor, antifungal, anti-inflammatory, antimalarial, antiproliferative, antipyretic, antianxiety activity etc, catalytic activity, antioxidant activity, precursor for metal chalcogenide etc. Review on these versatile applications of Schiff base complexes were carried out by many researchers [10-17]

S. M. Ben-saber and co-workers prepared and characterized Fe(III), Ni(II), Co(II) and Zn(II) complexes of Schiff base synthesized from o-aminobenzoic acid and p-dimethylaminobenzaldehyde [18]. IR, UV, CHN analysis and molar conductance measurement were used as characterization tools. Results showed that 1:1 stoichiometry exist between metal and ligand, non-electrolytic nature of complexes, coordination of ligand to the central metal atom through O atom of carboxyl group of the 2-aminobenzoic acid moiety and azomethine nitrogen. Geometry suggested for Fe(III)

and Zn(II) complexes were octahedral and tetrahedral respectively whereas Co(II) and Ni(II) complexes possess square planar geometry.

A. Pradhan et al. carried out a review study of the Schiff bases derived from the amino compounds such as 4-aminobenzene sulphonamide, 2-aminobenzthiazole, 4-amino salicylic acid, 4-aminophenol, aniline, semicarbazide, thiosemicarbazide, 4-aminoantipyrine, o-phenylenediamine, 2-aminothiophenol, 2-aminopyrazine, p-anisidine, s-benzylthiocarbamate and some of its complexes [19]. Ni(II), Cu(II), Co(II), Mn(II), Zn(II), Cd(II), Hg(II), VO(II), Pd(II), Pt(II), U(IV), Zr(II) and Sb(II) are the metal ions used for the complex formation. Antimicrobial activity of the Schiff bases and the complexes were also discussed.

M. Sahin and co-workers synthesized Cu(II), Ni(II), Pb(II) and Zn(II) complexes of assymetrical Schiff base ligands prepared by using 2-hydroxy-1-naphthaldehyde and 1,2-phenylenediamine, 9-anthracenecarboxaldehyde and 4-methyl-1,2-phenylenediamine [20]. Structures were predicted on the basis of elemental analysis, FT-IR, NMR, UV-Vis, ESR, XRD and fluorescence studies. Antimicrobial activity of the ligand and complexes were screened against the bacterial strains such as *Staphylococcus aureus*, *Streptococcus mutans*, *Enterococcus faecalis*, *Pseudomonas aeruginosa* and *Escherichia coli* using broth micro dilution methods. Some of the complexes have better antimicrobial activity than the corresponding ligands.

A. M. Abu-Dief et al. carried out review on applications of Schiff bases and their transition metal complexes [21]. Biological activities such as antibacterial, antifungal, anticancer, antioxidant and antiviral activity of various Schiff bases and their complexes were discussed. Use of the Schiff base complexes as catalyst in reactions such as polymerization, reduction of thionyl chloride, oxidation of organic compounds, reduction

reactions of ketones, aldol reaction, epoxidation of alkenes, Henry reaction and synthesis of bis(indolyl) methanes were also discussed.

L. H. Abdel-Rahman et al. studied Fe(II) complexes of five Schiff bases obtained by the reaction of o-hydroxynaphthaldehyde with L-histidine, L-alanine, L-arginine, L-aspartic acid and L-phenylalanine [22]. Complexes were characterized by means of conventional tools. Results showed that L-histidine Schiff base is tetradentate whereas all other Schiff bases are tridentate with ONO coordinating sites. Octahedral geometry was assigned for all the complexes. Teratogenicity, interaction with CT-DNA, antibacterial and antifungal activity of the complexes were also tested. Metal complexes showed good activity than the corresponding ligands.

A. B. Deilami et al. has done reactions of VO(acac)₂ and CuCl₂·2H₂O with the Schiff base 5-bromo-2-((allylimino)methyl)phenol to form complexes of type CuL₂ and [VOL₂]_n [23]. Characterization of these complexes was done on the basis of FT-IR, elemental analysis, UV-Vis, and XRD data. From single crystal XRD the copper complex is found to be a four coordinate one and vanadium complex is found to be six coordinate. Electrochemical behaviour and DFT calculations of the complexes were also carried out.

In 2011, S. M. Islam et al. synthesized Cu(II) complex of 4-acetylpyridine thiosemicarbazone and characterized by UV-vis diffuse reflectance spectroscopy (DRS), Fourier transform infrared spectroscopy (FT-IR), scanning electron microscope (SEM) and thermogravimetric analysis (TGA) [24]. Catalytic activity of this copper complex in the oxidation of alkanes, alkenes and aromatic alcohols using H₂O₂ as oxidant was evaluated for homogenous and heterogeneous systems. Better catalytic activity is exhibited in heterogeneous system. The *in vitro* antibacterial activity of the ligand and

complex was also evaluated against the bacterial strains *Escherichia coli* and *Staphylococcus aureus*.

A review on the synthesis of various symmetrical and assymetrical Schiff bases and their transition metal complexes were done by I. P. Ejidike and co-workers [25]. The applications of Schiff bases and their complexes such as antifungal, anticancer, antioxidant and antibacterial activity were also considered for discussion.

N. Mahalakshmi et al. studied DNA cleavage and antimicrobial activity of VO(II), Ni(II), and Cu(II) complexes of a binuclear Schiff base derived from 2-aminobenzaldehyde and 3,3',4,4'-tetraminobiphenyl [26]. Cyclic voltammetry, fluorescence spectroscopy and viscosity measurements were employed to study the interaction of complexes with CT-DNA. The bacterial strains *Staphylococcus aureus*, *Klebsiella pneumonia* and *Escherichia coli* were used for the study of antimicrobial activity. Activity of the complexes was found to be higher than the Schiff base ligand.

X. Zhong and co-workers reported the antitumor activity of Cu(II), Zn(II), Ni(II), Mn(II) and Co(II) complexes of a bis-Schiff base ligand obtained from thiosemicarbazide and 2,3-butanedione [27]. Cu(II) complex has highest antitumor activity than the other four complexes.

S. K. Tadavi et al. prepared manganese, cobalt and nickel complexes with a new Schiff base derivative of 1,2-diaminopropane and 2-hydroxy-6-isopropyl-3-methyl benzaldehyde [28]. Structure of the complexes was confirmed using elemental analysis, cyclic voltammetry, XRD, SEM-EDX and spectral studies. Structure of the nickel complex was found to be dimeric and square planar. Synthesized compounds were also screened for antioxidant, DNA cleavage and antimicrobial activity.

A detailed review of the catalytic activity of the polymer supported Schiff base complexes were published by K. C. Gupta and co-workers [29]. Catalytic activity of the

polymer supported Schiff bases is found to be higher than the unsupported Schiff bases. Fe(III), Ni(II), Zn(II), Co(II) and Cu(II) complexes have been applied as catalysts for oxidation of phenol and epoxidation of cyclohexene. Mn(II) complexes showed good catalytic activity in heterogeneous and homogenous condition in the oxidation of alkanes and alkenes. Very high catalytic activity was exhibited by polymer supported Fe(III) complex of Schiff bases than the other polymer supported complexes and unsupported analogues. Similarly for the oxidation of cyclo-octene molybdenum carbonyls, complexes of Schiff bases and Ru(III), Fe(III) salen complexes were found to be active catalysts. Polymer-supported Schiff base complexes were also exhibiting catalytic activity in the oxidation of adamantane, styrene, benzyl alcohol, stilbene, limonene, benzene and its alkyl derivatives. In the case of high temperature reactions, moisture and thermal stability were responsible for the high activity of polymer supported Schiff base complexes. They also evaluated recyclability of the polymer supported analogues.

M. Maneiro and co-workers prepared substituted N,N'-bis(salicylidene)-1,2-diimino-2-methylethane and its Mn(II) and Mn(III) complexes, having general formula $[\text{Mn}^{\text{II}}\text{L}(\text{H}_2\text{O})_2]$ and $[\text{Mn}^{\text{III}}\text{L}(\text{H}_2\text{O})_n(\text{ClO}_4)]$ [30]. Electron withdrawing substituent on phenyl ring will result to form Mn(II) complexes while Mn(III) oxidation state was exhibited when the ligands hold electron donating substituent on the benzenoid part. The peroxidase activity of these Schiff bases is high compared to the other Schiff base complexes of manganese. This can be attributed to the structural peculiarity of the complex that allows coordination of H_2O_2 substrate molecule to the manganese.

N. Raman et al. reviewed structural characteristics and biological investigations of transition metal complexes synthesized from 4-aminoantipyrine based Schiff bases [31]. Synthesis, magnetic, structural characteristics, spectral, redox, DNA cleavage and antimicrobial study of the complexes were discussed.

Zn(II) and Pb(II) complexes of 2,4-dibromo-6-((E)-(mesitylimino)methyl) phenol and 2-((E)-(2,6-diisopropylphenylimino)methyl)-4,6-dibromophenol were synthesized and their catalytic, luminescence and antibacterial activities were explored by Z. -Q. Feng et al. [32]. Characterization was done by means of thermogravimetric analysis, elemental analysis, IR-spectroscopy, single and powder XRD studies. Zn(II) and Pb(II) complexes possess tetrahedral and square planar geometry respectively. Photoluminescence was displayed by the complexes in solid state. Pb(II) complex was used as a catalyst in the Suzuki reaction of phenylboronic acid with 4-bromoanisole. Penicillin was used as the standard to compare the antibacterial activity of the complexes.

S. Kumar and co-workers carried out a detailed review on catalytic role of Schiff base and their complexes in several biological systems, dyes and pigments [33]. Their use as molecular oxygen detector and in food packages and birth control were also described.

I. R. Parrey et al. synthesized Cu complex of L-histidine and 2-carboxyaldehyde by template method [34]. Structure of the complex was confirmed using some physicochemical techniques. Catalytic activity of the complex in liquid phase hydroxylation of phenols was monitored. Effect of temperature, amount of catalyst, and amount of oxidant in the catalytic activity were also studied.

Rare earth metals in coordination chemistry

The elements from lanthanum ($Z=57$) to lutetium ($Z=71$) are generally named as lanthanides. They are also known as rare earth elements and have similar chemical properties. In lanthanides, the 4f sub-orbital is progressively filled. Due to lanthanide contraction there is a steady decrease in the ionic radius on going from lanthanum to lutetium. Separation of lanthanide ions is very complex owing to their

similarity in the chemical properties. Solvent extraction method, ion exchange chromatography and counter current exchange method are used for their separation. General properties of lanthanides are; 1) silvery white soft metal 2) hardness increasing with atomic number 3) very high boiling point and melting point 4) strong reducing agent 5) most of them are paramagnetic and 6) under UV light many of them fluoresces.

Lanthanides exhibit a wide range of coordination number and hence their reactivity is high compared to transition metals [35]. Here steric factor of the ligands determine the geometry instead of crystal field effects [36]. Crystal field splitting is low and electronic spectra are sharp on comparing with that of transition metals. Anionic ligands containing highly electronegative donor atoms are preferred by lanthanides. The oxidation state generally shown by the lanthanides is +3. Large coordination number is a unique feature of lanthanides compared to transition metals. Coordination number of 3d transition metals is normally 4 and 6 whereas in the case of lanthanide complexes it is 8 or 9. This is because the ionic radius of lanthanides is high compared to transition metals. Crystal field stabilization energy of transition metals is very high compared to that of lanthanide ions. As a result lanthanide complexes exhibit coordination number in the range 3 to 12 and the coordinating bonds become non directional. Now a days lanthanide Schiff base complexes have great significance owing to their relevance in the various fields of research such as material science, medicinal, inorganic chemistry etc. Apart from transition metal complexes, detailed investigations on inner transition metal complexes of Schiff bases were also reported extensively.

Rare earth metal complexes of Schiff bases - A review

Complexes of Pr(III), Sm(III), Gd(III), Tb(III), Er(III) and Yb(III) of a Schiff base derived from 5-bromosalicylaldehyde and threonine were synthesized and characterized by L. Logu and co-workers [37]. $[\text{Ln}(\text{L})(\text{NO}_3)_2(\text{H}_2\text{O})]\text{NO}_3$ (where

L= Schiff base ligand) is the general formula of the complexes. Spectral studies revealed that the ligand is tridentate with ONO donor atoms. Fluorescence study of Sm(III), Er(III) and Tb(III) complexes, antibacterial, antifungal and antioxidant properties of all the complexes were investigated.

B. Erk et al. synthesized N,N'-bis(o-hydroxyaryl)aldimino Schiff bases and its uranium(VI) complexes [38]. Structural determination was done by IR, UV and elemental analysis. Polymeric structure was observed and it is due to the strong interaction between ligand and ion. Solubility of the complexes was found to be low and decomposition point is found to be high.

K. Prajapati and co-workers conducted a review study on lanthanide ion complexes of various organic compounds including Schiff base ligands [39]. Biological importance of these ligands and complexes were also discussed. Review study pointed out that the lanthanide complexes of Nd, Gd and Ce ions exhibits high antifungal activity whereas Nd, Yb and Eu complexes exhibit high anticancer activity.

P. S. Mansingh et al. synthesized complexes of type $[\text{UO}_2(\text{HL})\text{X}_2]$, $[\text{UO}_2(\text{HL}')\text{X}_2]$ (where X=Cl, NCS, CH_3COO , I, NO_3) and $[\text{Th}(\text{L}')_2\text{X}_2]$ (where X= NCS, I, NO_3) using the Schiff bases obtained by the *in situ* condensation of N,N-dimethylethylenediamine with o-hydroxy naphthaldehyde (HL') and salicylaldehyde (HL) [40]. IR spectra confirmed the facts that the acetate and nitrate groups are bonded in bidentate manner, ligands in tridentate manner and thiocyanate as N-bonded unidentate isothiocyanate group. PMR spectra were utilized to confirm the binding mode of the ligands and thermogravimetric analysis was done to check the stability of the complexes.

A series of Ln(III) ions such as Pr(III), Sm(III), Gd(III), Tb(III), Er(III) and Yb(III) were used for the complex formation with a Schiff base derived from

5-bromosalicylaldehyde and leucine by L. Lekha and co-workers [41]. Characterization was done using elemental analysis, mass spectrometry, thermal analysis, EPR, FT-IR and UV-vis spectra. IR spectra revealed that the ligand is tridentate and coordinate with metal ion through one oxygen and one nitrogen donor atoms. Coordination number of the complexes is found to be 8 and the stoichiometry of the complexes is 1:1. Fluorescence property and TG-DTA were also studied. For the oxidation of aniline and its substituted derivatives, Gd(III) complex is acting as an efficient catalyst.

P. A. Vigato carried out a review on lanthanide and actinide complexes of macrocyclic and acyclic Schiff base ligands [42]. [1+1], [2+2] and [3+3] macrocycles were used to form complexes with metal ions. The complex formation was confirmed by NMR and X-ray study.

A series of actinide metal complexes of thorium(IV) and dioxouranium(VI) with Schiff base ligands 4-[N(salicylaldehyde)amino]antipyrine and 4-[N(cinnamaldehyde)amino]antipyrine were synthesized and characterized using conventional methods by R. K. Agarwal and co-workers [43]. Coordination sites of the ligand (azomethine nitrogen and carbonyl oxygen) were confirmed using IR spectroscopy. XRD studies and thermogravimetric analysis of some of the complexes were also reported.

Two lanthanide complexes of Schiff base derived from lysine and o-vanillin were synthesized and characterized by J. -P. Cheng et al. [44]. $[[\text{Gd}(\text{HL})(\text{H}_2\text{O})_2\text{NO}_3](\text{NO}_3)(\text{H}_2\text{O})]$ and $[[\text{La}(\text{HL})(\text{H}_2\text{O})_2\text{NO}_3](\text{NO}_3)(\text{H}_2\text{O})]$ are the general formula of the complexes. Ligand is tetradentate and coordinates with the metal atom through two carboxylic oxygen atoms, phenolic oxygen and azomethine nitrogen. Antibacterial activity of the complexes against *Staphylococcus aureus*, *Bacillus subtilis* and *Escherichia coli* and the interaction with calf thymus DNA was also evaluated.

Y. M. Issa and co-workers synthesized La(III) and Ce(III) complexes of thio-Schiff base derivatives having general formula $[ML_2(H_2O)X].2H_2O$ [45]. Where M= Ln (III) ion, X= ClO_4^- or Cl^- and L=Schiff base ligand. Studies have been done on water of hydration, thermal stability and coordinated water molecules.

La(III), Nd(III) and Dy(III) complexes of Schiff base formed by the reaction of 1-naphthylamine with 3-nitro benzaldehyde and 4-methoxy benzaldehyde was synthesized and characterized by S. P. Idhol et al. [46]. The *in vitro* antibacterial studies against bacteria such as *Staphylococcus aureus*, *Escherichia coli*, *Basillus subtilis* and *Salmonella typhi* and antifungal studies against *Pencillium Crysogenum* and *Aspergillus niger* were also carried out. Results showed that antimicrobial activity of the complexes were greater than the corresponding Schiff base ligands.

R. Yerrasani et al. synthesized a mesogenic Schiff base ligand N,N'-di-(4'-octyloxybenzoate)salicylidene-1,12-diaminododecane and its La(III), Pr(III), Nd(III), Sm(III), Eu(III), Tb(III) and Dy(III) complexes [47]. Thermal stability and phase transition behaviour were investigated using the techniques thermogravimetric analysis, temperature-dependent Raman spectroscopy, polarizing optical microscopy and scanning calorimetry. Emission property and bonding behaviour of the synthesized complexes were also evaluated using IR, electronic, fluorescence and NMR spectral studies.

Rare earth metal complexes of heterocyclic Schiff bases - A review

S. Agnihotri et al. reported dioxouranium(VI) and thorium(IV) complexes of two Schiff base ligands obtained by the reaction of p-hydroxyl benzaldehyde, p-trimethoxy benzaldehyde and 2-amino pyridine [48]. Structures of the ligands and complexes were confirmed using elemental analysis, spectral studies, thermogravimetric methods and conductance measurements. Toxic effects of the complexes were also monitored.

Three Schiff base ligands were synthesized by the condensation of *o*-phenylenediamine, 2-aminopyridine and *p*-phenylenediamine with 5,7-dihydroxy-6-formyl-2-methylbenzopyran-4-one by A. L. El-Ansary and co-workers [49]. La(III), Nd(III) and Er(III) complexes of the Schiff bases were also prepared and characterized using IR, electronic absorption, elemental analysis, ¹H-NMR and molar conductance studies. Thermogravimetric analysis showed that the product obtained upon degradation is metallic oxide. Fluorescence study of Nd(III) and Er(III) complexes were also investigated in dimethylformamide (DMF).

A series of lanthanide complexes having general formula [Ln₂L(H₂O)₄(NO₃)₄](NO₃)₂·2H₂O (Ln= Ln³⁺, Pr³⁺, Nd³⁺, Gd³⁺ and Er³⁺) were synthesized using the Schiff base ligand *N,N'*-bis-(2-thiophenecarboxaldimine)-3,3'-diaminobenzidene (L) by M. Shakir and co-workers [50]. Elemental analysis, FT-IR, UV-Vis, ¹H NMR, fluorescence, mass spectroscopy, SEM, EDX and thermal analysis were used as characterization tools. Results confirmed that the coordination number of the complexes was 8 and the stoichiometry between ligand and metal was 1:2. Anticancer activity of both ligand and complexes were also monitored towards the cell lines human breast cancer cell lines (MCF-7) and human cervical cancer cell lines (HeLa). Activity of the complexes was high compared to that of respective ligand.

DNA binding affinity and cytotoxic activity of the complexes having general formula [LnL(NO₃)₂]NO₃ (where Ln= Sm, Eu, La), prepared using the Schiff base ligand ethylenediiminobi(6-hydroxychromone-3-carbaldehyde), was investigated by B. -D. Wang et al. [51]. Characterization of the complexes was done on the basis of elemental analysis, spectral studies (IR, UV-Vis, NMR, Mass, fluorescence), molar conductivity and TG-DTA. HepG2 cancer cell lines were used to study cytotoxic activity and calf thymus DNA was used for DNA binding study. Results showed that ligand has

good cytotoxic activity against HepG2 cancer cell lines. Also Eu(III) and Sm(III) complexes have high DNA binding affinity.

Antimicrobial activity of a series of lanthanide ion [La(III), Ce(III), Pr(III), Nd(III), Sm(III) and Gd(III)] complexes of a Schiff base 4-hydroxy-3-(1-{2-(2-hydroxy-benzylidene)-aminophenylimino}-thyl)-6-methy-pyran-2-one have been screened by V. A. Shelke et al. [52]. Elemental analysis, ^1H NMR spectra, FTIR, conductometry, UV-visible, thermal analysis, magnetic susceptibility and X-ray diffraction studies were carried out for the structural confirmation of the complexes. Results showed that ligand behaves as dibasic tetradentate with ONNO donor atoms. Stoichiometry of the complexes was found to be 1:1 and possess distorted octahedral geometry. XRD study suggests that La(III) and Ce(III) complexes belongs to monoclinic crystal system whereas Pr(III) and Nd(III) complexes belongs to orthorhombic crystal system. TGA/DTA was also studied and Horowitz–Metzger and Coats–Redfern methods were used to determine the kinetic parameters. Strains used for the antimicrobial studies were *Staphylococcus aureus*, *Bacillus* sp., *Escherichia coli*, *Trichoderma*, *Fusarium oxysporum* and *Aspergillus niger*.

La(III), Ce(III), Nd(III), Er(III) and Gd(III) complexes of the Schiff base salicylaldehyde L-phenylalanine (KHL) and o-phenanthroline (Phen) were synthesized and characterized by X. U. Dongfang et al. [53]. Anticancer activity of the complexes against K562 tumor cell was tested using flow cytometry and methyl thiazolyl tetrazolium (MTT) colorimetry. Results showed that the complexes inhibit the growth of K562 tumor cell.

Eight lanthanide [La(III), Pr(III), Nd(III), Sm(III), Eu(III), Gd(III), Dy(III) and Y(III)] complexes of the Schiff base derived from indole-3-acetic acid were synthesized, characterized and the plant growth activity test were carried out by Ganesh N. Naik and

co-workers [54]. Ligand is monobasic tridentate and coordinate with metal atom through azomethine nitrogen, carbonyl oxygen and hydroxyl oxygen. Results of plant growth activity showed that the complexes enhanced the activity on complex formation at 1×10^{-6} M concentration.

Antimicrobial activity of the La(III), Pr(III), Nd(III), Sm(III) and Eu(III) complexes of the Schiff base o-hydroxyacetophenone-7-chloro-4-quinoline was investigated by K. S. Abou-melha et al [55]. Characterization of the ligand and complexes were done using various physicochemical methods. Antibacterial activity against *Staphylococcus aureus* and *Escherichia coli* and antifungal activity against *Candida albicans* were screened. High antimicrobial activity was observed for the compounds.

Scope and aims of present investigations

Rare earth complexes with Schiff base ligands have been extensively investigated due to their versatile structures, interesting coordination and wide pharmacological applications. Many research works in this field have proved the antibacterial, antifungal, anti-inflammatory and even anticancer activities of various Schiff base complexes.

In the present course it is aimed to synthesize and characterize three potential heterocyclic Schiff base ligands such as 3-(1-(2-phenylhydrazono)ethyl)pyridine (3PHEP), 2-(1-(pyridine-3-yl)ethylidene)hydrazine carbothioamide (2PEHCT) and 3-((thiophen-2-ylmethylene)amino)benzoic acid (3TMAB). Lanthanide complexes of La(III), Nd(III) and Sm(III) are also to be synthesized and characterized. Elemental analysis, metal percentage estimation, spectral studies such as FTIR, UV-Vis, NMR (^1H and ^{13}C) and mass, magnetic moment studies and molar conductance measurement will be explored as characterization tools, in order to derive the geometry and structures of the ligands and complexes.

CHAPTER 7

MATERIALS AND METHODS

General methods and reagents used for the preparation of Schiff base ligands, their inner transition metal complexes and the techniques used for their characterization are briefly described in this section.

Reagents

Analar grade samples were used for the synthesis of Schiff bases. Thiosemicarbazide, thiophene-2-carbaldehyde and 3-aminobenzoic acid were obtained from Fluka. 3-acetylpyridine and phenylhydrazine hydrochloride were purchased from Merck. Lanthanide metal oxides such as La_2O_3 , Nd_2O_3 and Sm_2O_3 were received from Sigma-Aldrich.

Characterization techniques

Techniques used for the structure elucidation of the ligand and complexes are as follows.

Elemental (CHN) analysis

CHN analysis of ligands and metal chelates were done to estimate the percentage of carbon, hydrogen and nitrogen present in it. Elementar make Vario EL III model CHN analyzer was used for this purpose.

Estimation of metal

Pyrolysis as well as volumetric/gravimetric method was adopted for this purpose. In the former method an empty crucible of known weight about 0.1 g of the metal complex was taken and strongly heated for 2 h using an electric Bunsen. Upon heating metal complexes were converted to corresponding oxides and the organic particles were burnt off. After cooling weight of the crucible was measured and then metal percentage was calculated using weight of metal oxide formed.

Metal percentage of complexes was also determined by means of EDTA complexometric titration. Metal complexes of known amount are allowed to digest in concentrated nitric acid. Metal complexes will decompose in this stage. Then this solution is transferred quantitatively into a volumetric flask and makes up to a standard volume. Standard EDTA solution was also prepared. Then pipette out known volume of the metal solution into a titration flask and added four drops of 1:1 ammonia. Metal ions will precipitate as its hydroxide. It is then dissolved in dilute nitric acid and 10 ml buffer solution (CH_3COONa and CH_3COOH) was added to maintain $\text{pH} = 5$. Pyridine and xylene orange was added two and four drops respectively to the buffered solution of metal. Then the solution is titrated against 0.01 M EDTA till the color changes from red to yellow.

Spectral studies

KBr disc technique was used for recording IR spectra of ligands and complexes on a Shimadzu model FT-IR Spectrometer (Model IR affinity-1). Useful for determining the various groups present in ligand and metal complexes and to establish the coordination between metal and ligand.

To get idea about geometry of the molecules electronic spectra of the ligands and metal complexes were recorded in a Shimadzu UV-Visible-1800 Spectrophotometer. Proton and ^{13}C NMR spectra of the ligands in dmsO-d_6 was recorded using the instrument BRUKER AVANCE III HD. QP 2010 model Shimadzu GCMS was used to record mass spectra of ligand.

Magnetic moment studies

Magnetic susceptibilities of the complexes were measured by means of Gouy method. $\text{Hg}[\text{Co}(\text{NCS})_4]$ was used as calibrant. The apparatus Sherwood, UK (Mark 1) was used for the measurement. Diamagnetic corrections were applied using Pascal

constants taking into consideration, the magnetic contribution by various atoms and structural units. Effective magnetic moments were calculated from the corrected susceptibilities using the equation

$$\mu_{\text{eff}} = 2.84 \Psi_M \quad (1)$$

where Ψ_M is the molar susceptibility corrected for diamagnetism and T is the absolute temperature [56-57]. Theoretical magnetic moments were calculated using the formula

$$\mu_{\text{eff}} = g S(S + 1) \quad (2)$$

where g is the gyro magnetic ratio and S the total spin quantum number

Molar conductance studies

Molar conductance studies of the metal chelates were done using ELICO conductivity meter. Cell constant was maintained as 1 in all measurements [58]. 10^{-3} M concentration of metal complex solution in DMSO solvent at $30 \pm 2^\circ\text{C}$ was used for measurements. This parameter gave an idea about the electrolytic nature of the complexes.

CHAPTER 8

STUDIES ON INNER TRANSITION METAL COMPLEXES OF HETEROCYCLIC SCHIFF BASES

Three heterocyclic Schiff bases such as 3-(1-(2-phenylhydrazono)ethyl)pyridine (3PHEP), 2-(1-(pyridine-3-yl)ethylidene)hydrazine carbothioamide (2PEHCT) and 3-((thiophen-2-ylmethylene)amino)benzoic acid (3TMAB) were synthesized and characterized by means of elemental analysis and spectral studies such as FTIR, UV-visible, NMR (^1H and ^{13}C) and Mass spectroscopy. Chelating ability of these Schiff base ligands were proved by synthesizing inner transition metal complexes of La(III), Nd(III) and Sm(III). Elemental (CHN) analysis, FTIR, UV-visible, magnetic moment, estimation of metal and molar conductance studies were used for the characterization of the metal complexes.

This chapter is divided into three sections. Section I deals with synthesis and characterization of the Schiff base ligand 3-(1-(2-phenylhydrazono)ethyl)pyridine (3PHEP) and its inner transition metal complexes. Section II consist of synthesis and characterization of the Schiff base ligand 2-(1-(pyridine-3-yl)ethylidene)hydrazine carbothioamide (2PEHCT) and its inner transition metal complexes. Synthesis and characterization of the Schiff base ligand 3-((thiophen-2-ylmethylene)amino)benzoic acid (3TMAB) and its inner transition metal complexes were discussed in the section III.

Section I

La(III), Nd(III) and Sm(III) complexes of 3-(1-(2-phenylhydrazono)ethyl)pyridine

This section deals with synthesis and characterization of the Schiff base ligand 3-(1-(2-phenylhydrazono)ethyl)pyridine (3PHEP) and its inner transition metal complexes of lanthanum, neodymium and samarium.

Synthesis and characterization of 3PHEP and its inner transition metal complexes

Equimolar amount of ethanolic solution of 3-acetylpyridine and phenylhydrazine hydrochloride was dissolved in ethanol-water (3:1) mixture and refluxed for 4 h. Solution is then evaporated to dryness and cooled slowly. Yellow coloured precipitate formed was filtered and washed with minimum amount of ethanol. Then melting point was determined after recrystallization from ethanol. 81% yield is obtained and melting point is found to be 245⁰C.

Ln(III) nitrate solution was first prepared by digesting Ln₂O₃ (0.01 mol) in con HNO₃ thrice. After digestion and evaporation, the residue is cooled and added 20 ml ethanol. This ethanolic nitrate solution was then refluxed for 3 h, after adding ethanolic solution of 3PHEP (0.02 mol) into it. Then allowed to cool and added dilute ammonia (1:20) dropwise till a turbidity is formed. Magnetically stirred the solution and the precipitate formed was filtered, washed with ethanol and dried over anhydrous calcium chloride.

Elemental analysis

Results of microanalytical, magnetic and conductance data of 3PHEP and its inner transition metal complexes are shown in Table 8.1. Experimental and calculated values are in good agreement. From the data it is clear that 1:1 stoichiometry exist between 3PHEP and metal ions.

FTIR spectral studies

Stretching frequencies corresponding to different bonds in 3PHEP were observed in its IR spectrum. Broad peak at 3265 cm^{-1} corresponds to the N-H stretching frequency. Formation of C=N linkage is proved by the stretching vibration at 1593 cm^{-1} . Also a peak corresponding to $\nu_{\text{C-N}}$ was observed at 1048 cm^{-1} . C=C present in the aromatic rings displayed an emerged spectrum of peaks having range $1540\text{-}1600\text{ cm}^{-1}$. Stretching frequencies in the range $3030\text{-}3100\text{ cm}^{-1}$ corresponds to aromatic C-H bond stretching and in plane deformation of the pyridine ring was shown at 621 cm^{-1} and 667 cm^{-1} .

Lowering of C=N stretching frequency of complexes in comparison to 3PHEP clearly confirmed the coordination between imine nitrogen of ligand and metal. Presence of water molecules in the complexes was shown by the additional peaks in the range $3328\text{-}3426\text{ cm}^{-1}$. Also the peaks observed in the range $1300\text{-}1500\text{ cm}^{-1}$ signified the existence of coordinated nitrate ion in complexes with unidenticity. New peaks in the range $610\text{-}690\text{ cm}^{-1}$ and $530\text{-}550\text{ cm}^{-1}$ are a clear indication of the M-N and M-O bonds formed in the complexes. Characteristic infrared absorption frequencies (cm^{-1}) of 3PHEP and its inner transition metal complexes are given in Table 8.2.

Electronic spectral studies

In the electronic spectra of 3PHEP two peaks were observed. Peak at 29239 cm^{-1} corresponds to $n \rightarrow \pi^*$ transition and the peak at 32679 cm^{-1} corresponds to $\pi \rightarrow \pi^*$ transition. On comparing the electronic spectra of the complexes with that of ligand it is observed that there is bathochromic shift for the absorption bands in the case of the complexes, which clearly indicates that the Schiff base ligand is coordinated to metal ion.

NMR spectral studies

Nine non-equivalent protons were observed in the proton NMR spectrum of 3PHEP. Methyl protons displayed a singlet at 2.3 δ . Weak and broad singlet at 9.8 δ corresponds to the proton present in the NH group of phenylhydrazine portion. Protons present in the benzenoid and pyridine ring exhibited signals in the range 6.7-7.3 δ and 8.7-9.0 δ respectively.

Eleven chemically different carbon atoms present in 3PHEP showed 11 distinct signals in the ^{13}C NMR spectrum. Methyl carbon displayed a peak at 12.53 ppm. Peak at 137.99 ppm corresponds to the carbon atom of azomethine group. Quaternary carbon atom present in the pyridine ring and benzenoid ring displayed a signal at 134.88 ppm and 145.07 ppm respectively. Remaining carbon atoms of both ring showed signals in the range 113-140 ppm.

Mass spectral studies

Molecular ion peak was appeared at m/z 211 in the mass spectrum of 3PHEP, which is also appeared to be as the base peak, reflects the stability of the ligand molecule. In addition to M peak, M+1 peak is observed at m/z 212 in the intensity ratio 100:14 which confirms the presence of thirteen carbon atoms in the ligand molecule. The fragments $[\text{C}_5\text{H}_4\text{N}]^+$ and $[\text{C}_6\text{H}_6\text{N}]^+$ displayed signals at m/z 78 and 92 respectively. These fragments have the relative natural abundance of 56 and 55 respectively. Secondary fragments such as $[\text{C}_4\text{H}_3]^+$ and $[\text{C}_5\text{H}_5]^+$ formed from the pyridine fragment showed signal at m/z 51 and 65 respectively.

Magnetic moment studies

Geometry prediction of the complexes is possible by magnetic moment measurement. La^{3+} ($4f^0$) with zero unpaired electron is found to be diamagnetic whereas neodymium and samarium complexes are found to be paramagnetic. Sm^{3+} ion has an odd

electronic configuration, $[\text{Xe}]4f^5$ labelled as Kramer's ion and exhibited μ_{eff} 1.72 BM as expected. Neodymium ion which has 3 unpaired electron exhibited magnetic moment value 4.09 BM. Thus octahedral geometry is assigned for all the complexes.

Molar conductance studies

Molar conductance of all the complexes was studied in DMSO. The value of molar conductance was found to be in between $2\text{-}5 \Omega^{-1}\text{cm}^2\text{mol}^{-1}$. This indicates that outside the coordination sphere, no counter ions were present and thus possess non-electrolytic nature.

Table 8.1 Microanalytical, magnetic and conductance data of 3PHEP and its inner transition metal complexes

Parameter	3PHEP (L)	*Complex		
		La(III)	Nd(III)	Sm(III)
Colour	Yellow	brown	brown	brown
Yield	82	70	61	66
Molecular weight	211	554	559	565
Melting point ($^{\circ}\text{C}$)	245	>300	>300	>300
M% Found	-	24.98	26.82	25.88
(Cald.)	-	(25.09)	(25.76)	(26.55)
C% Found	72.44	29.01	26.99	28.12
(Cald.)	(73.92)	(28.15)	(27.90)	(27.61)
H% Found	5.99	2.18	2.97	3.01
(Cald.)	(6.16)	(2.70)	(2.68)	(2.65)
N% Found	19.15	16.04	14.84	14.27
(Cald.)	(19.90)	(15.16)	(15.02)	(14.86)
μ_{eff} (BM)	-	Diamagnetic	4.09	1.72
Molar conductance ($\Omega^{-1}\text{cm}^2\text{mol}^{-1}$)	-	5	2	3
Geometry	-	Octahedral	Octahedral	Octahedral

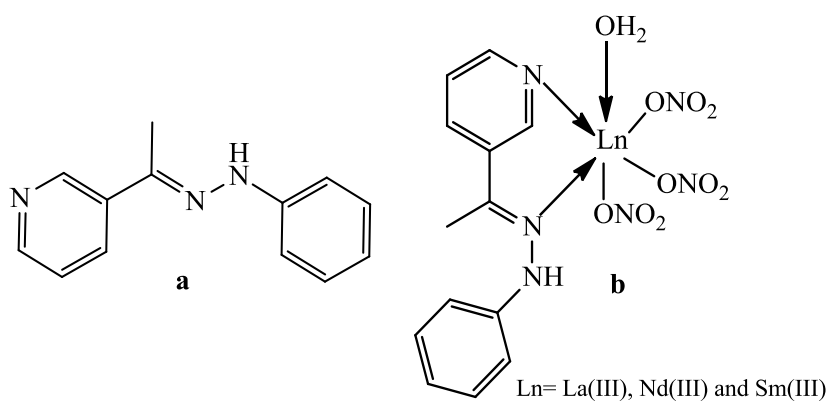
* $[\text{LnL}(\text{NO}_3)_3(\text{H}_2\text{O})]$ where Ln=La(III), Nd(III) and Sm(III)

Based on the physicochemical data, octahedral geometry was assigned to all these chelates where the ligand 3PHEP is behaving as zerovalent bidentate with NN donor sites. Structures of the ligand 3PHEP and its inner transition metal complexes are represented in Fig 8.1.

Table 8.2 Characteristic infrared absorption frequencies (cm^{-1}) of 3PHEP and its inner transition metal complexes

Assignment	3PHEP	*Complex		
	(L)	La(III)	Nd(III)	Sm(III)
$\nu_{\text{H}_2\text{O}}$	-	3426	3328	3410
ν_{NH}	3265	3228	3228	3227
$\nu_{\text{C}=\text{N}}$	1593	1573	1570	1584
$\nu_{\text{C}=\text{C}}$	1540	1404	1393	1503
ν_{NO_3}	-	1394, 1427	1388, 1456	1391, 1449
$\nu_{\text{C}-\text{N}}$	1048	1033	1048	1013
In plane bending	941	927	913	903
Out of plane bending	856	844	856	864
$\nu_{\text{M}-\text{N}}$	-	612	667	683
$\nu_{\text{M}-\text{O}}$	-	538	543	534

* $[\text{LnL}(\text{NO}_3)_3(\text{H}_2\text{O})]$ where Ln=La(III), Nd(III) and Sm(III)

**Fig. 8.1** Structures of a) ligand 3PHEP and b) its inner transition metal complexes

Section II

La(III), Nd(III) and Sm(III) complexes of 2-(1-(pyridine-3-yl)ethylidene)hydrazine carbothioamide

Synthesis and characterization of the Schiff base ligand 2-(1-(pyridine-3-yl)ethylidene)hydrazine carbothioamide (2PEHCT) and its of inner transition metal complexes are explained in this section.

Synthesis and characterization of 2PEHCT and its inner transition metal complexes

3-acetylpyridine and thiosemicarbazide in the ratio 1:1 in ethanol were mixed and refluxed for 3 h. After evaporation to dryness the solution was allowed to cool slowly. Pale yellow coloured precipitate formed was filtered and washed with minimum amount of ethanol. Recrystallized from ethanol and melting point was determined. Yield of 2PEHCT was found to be 79% and it melts at 205⁰C.

Ln₂O₃ (0.01 mol) was decomposed with con HNO₃ thrice and heated to prepare Ln(III) nitrate. Concentrated, cooled and added 20 ml ethanol. Ethanolic solution of 2PEHCT (0.02 mol) was added to this ethanolic nitrate solution and refluxed for 3 h. Dilute ammonia was added dropwise in the ratio 1:20 till a turbidity is formed after cooling the ethanolic mixture. Then stirred the solution magnetically and the precipitate formed was filtered, washed with ethanol and dried over anhydrous calcium chloride.

Elemental analysis

Percentage of C, H and N as well as the metal content were estimated by microanalytical methods. The results of microanalytical, magnetic and conductance data of 2PEHCT and its inner transition metal complexes are shown in Table 8.3. There is a good correlation between observed and calculated values of elemental analysis. 1:1 stiochiometry exist between metal and ligand in all complexes.

FTIR spectral studies

IR spectrum of 2PEHCT consists of characteristic stretching frequencies corresponding to various bonds. Peak observed at 1612 cm^{-1} is due to the presence of azomethine group. Stretching frequency due to NH vibration was identified at 3201 cm^{-1} as a medium band. Terminal amino group exhibited symmetrical and asymmetric vibrations and the corresponding peaks were observed at 3246 cm^{-1} and 3385 cm^{-1} . C=S vibration was identified at 880 cm^{-1} . A very weak band at 2466 cm^{-1} is a clear evidence for the existence of tautomeric form of the ligand, with thiol moiety.

In complexes the stretching frequencies of the azomethine group were found to be lowered due to its involvement in complexation. Additional bands in the range $3424\text{-}3474\text{ cm}^{-1}$ and $1313\text{-}1477\text{ cm}^{-1}$ implies the coordination of water and nitrate molecules in the complexes respectively. Appearance of M-N and M-S bands in the spectrum of complexes is very much in favor to the coordination of N and S atom to the metal. Characteristic infrared absorption frequencies (cm^{-1}) of 2PEHCT and its inner transition metal complexes are given in Table 8.4.

Electronic spectral studies

In the electronic spectra of 2PEHCT two peaks were observed. The peak at 31347 cm^{-1} corresponds to $n \rightarrow \pi^*$ transition and the adsorption frequency at 31948 cm^{-1} implies $\pi \rightarrow \pi^*$ transition. In the case of complexes these peaks are found to shift to higher wavelength. This is a clear proof for the formation of complexes.

NMR spectral studies

In the proton NMR spectrum of 2PEHCT eight distinct signals were observed. The signal at $2.3\ \delta$ is due to methyl protons. Protons in the terminal NH_2 of the thiosemicarbazide moiety exhibited a broad peak at $3.4\ \delta$. A singlet observed at $8.1\ \delta$ was assigned to NH proton present in the thiosemicarbazide part. SH proton displayed a

peak at 10.3 δ . This is due to the existence of tautomeric structure of the molecule.

Protons in the pyridine ring exhibited signals in the range 7.4-9.2 δ .

Table 8.3 Microanalytical, magnetic and conductance data of 2PEHCT and its inner transition metal complexes

Parameter	2PEHCT (L'H)	*Complex		
		La(III)	Nd(III)	Sm(III)
Colour	Pale yellow	Cream	Grey	Off white
Yield	70%	65%	68%	59%
Molecular weight	194	492	497	503
Melting point ($^{\circ}\text{C}$)	205	>300	220	235
M% Found	-	27.95	29.13	28.98
(Cald.)	-	(28.19)	(28.92)	(29.76)
C% Found	48.55	19.26	18.89	19.58
(Cald.)	(49.49)	(19.51)	(19.31)	(19.08)
H% Found	4.99	2.45	3.25	3.09
(Cald.)	(5.15)	(2.64)	(2.61)	(2.58)
N% Found	29.22	18.35	15.86	17.28
(Cald.)	(28.9)	(17.07)	(16.90)	(16.69)
μ_{eff} (BM)	-	Diamagnetic	3.51	1.40
Molar conductance ($\Omega^{-1}\text{cm}^2\text{mol}^{-1}$)	-	3	40	5
Geometry	-	Octahedral	Octahedral	Octahedral

*[LnL'(NO₃)₂(H₂O)₂] where Ln=La(III), Nd(III) and Sm(III)

¹³C NMR spectrum of 2PEHCT consists of eight signals corresponding to eight chemically distinct carbon atoms. Methyl carbon exhibited its signal at 13.72 ppm. The signal at 145.55 ppm is due to azomethine carbon. Quaternary carbon present in the pyridine ring displayed a signal at 133.23 ppm. The other carbon atoms of the pyridine ring appeared at 149.67 ppm, 123.23 ppm, 133.94 pmm and 147.74 ppm. Signal at 179.08 ppm is assigned to the carbon atom present in the thiosemicarbazone moiety.

Magnetic moment studies

Information's concerning the geometry of the complexes was obtained from the magnetic moment measurement. Magnetic moment values of Nd(III) and Sm(III)

complexes are found to be 3.51 BM and 1.40 BM respectively, whereas La(III) complex is diamagnetic. Octahedral geometry is assigned for all complexes.

Molar conductance studies

Molar conductance measurement was done for all complexes and is given in Table 8.3. Molar conductance values of the complexes are in the range of 3-40 $\Omega^{-1}\text{cm}^2\text{mol}^{-1}$. These values suggest non-electrolytic behaviour and absence of counter ions outside the coordination sphere of metal chelates.

On the basis of spectral, elemental and magnetic data, octahedral geometry with 1:1 stoichiometry between ligand and metal is assigned to all the Ln complexes. 2PEHCT behaved monovalent bidentate ligand with NS donor sites. Structures of the ligand 2PEHCT and its inner transition metal complexes are represented in Fig 8.2.

Table 8.4 Characteristic infrared absorption frequencies (cm^{-1}) of 2PEHCT and its inner transition metal complexes

Assignment	2PEHCT (L H)	*Complex		
		La(III)	Nd(III)	Sm(III)
$\nu_{\text{H}_2\text{O}}$	-	3424	3430	3474
ν_{NH}	3264	3211	3249	3267
$\nu_{\text{C=N}}$	1612	1574	1609	1604
$\nu_{\text{C=C}}$	1508, 1583	1498, 1543	1470, 1528	1503, 1588
ν_{NO_3}	-	1416, 1313	1414, 1313	1477, 1414
$\nu_{\text{C-S}}$	1132	1113	1089	1089
In plane bending	1012	980	973	973
Out of plane bending	701	722	761	701
$\nu_{\text{M-N}}$	-	601	642	622
$\nu_{\text{M-O}}$	-	548	581	504
$\nu_{\text{M-S}}$	-	473	481	486

*[LnL'(NO₃)₂(H₂O)₂] where Ln=La(III), Nd(III) and Sm(III)

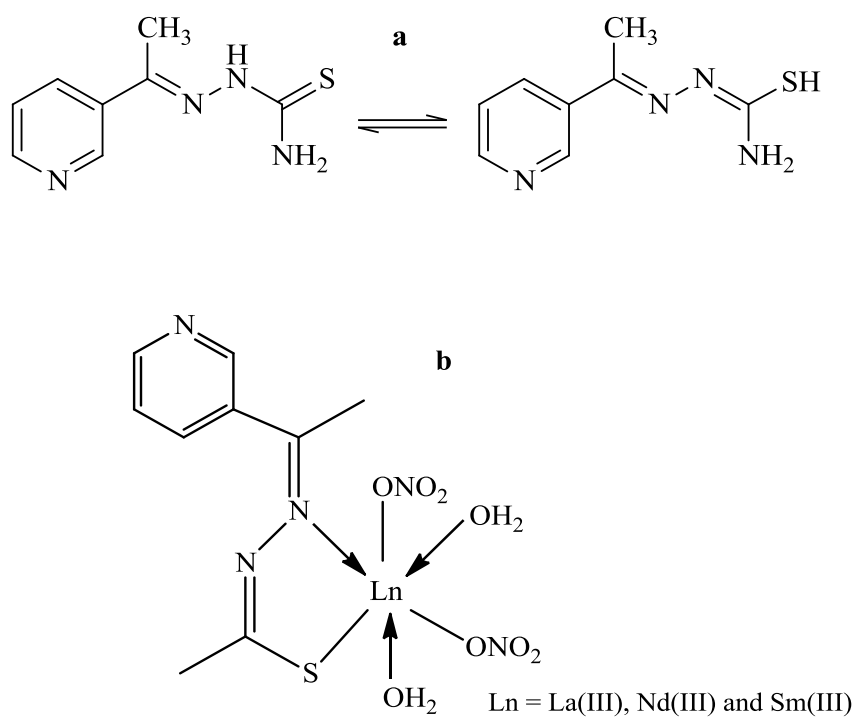


Fig. 8.2 Structures of a) ligand 2PEHCT and b) its inner transition metal complexes

Section III

La(III), Nd(III) and Sm(III) complexes of 3-((thiophen-2-ylmethylene)amino)benzoic acid

This section deals with synthesis and characterization of the Schiff base ligand 3-((thiophen-2-ylmethylene)amino)benzoic acid (3TMAB) and its inner transition metal complexes

Synthesis and characterization of 3TMAB and its inner transition metal complexes

Ethanol solution of thiophene-2-carbaldehyde was added to solution of 3-aminobenzoic acid in ethanol and refluxed for 3 h. Solution was then evaporated and cooled to obtain pale yellow coloured precipitate, which was filtered and washed with minimum amount of ethanol. Recrystallization from ethanol resulted in 82% yield of the product. Melting point was found to be 136⁰C

Nitrate solution of lanthanide ions were prepared by heating 0.01 mol of its oxides (Ln₂O₃) in con HNO₃. Volume of the solution is then reduced, cooled and 20 ml ethanol was added. Then the solution was refluxed for 3 h after adding 0.02 mol of 3TMAB dissolved in ethanol. Resulting mixture is then cooled and added dilute ammonia (1:20) drop wise till a turbidity is formed. Precipitate was formed when the solution is magnetically stirred, which was filtered, washed with ethanol and dried over anhydrous calcium chloride.

Elemental analysis

The stoichiometry present between metal and ligand is obtained from elemental analysis data. Results of elemental analysis are shown in Table 8.5. From the data it is clear that 1:1 stoichiometry exist between metal and ligand.

FTIR spectral studies

In the IR spectrum of 3TMAB the peak observed at 1612 cm^{-1} is due to the presence of azomethine group. A scalloped band is obtained for OH group at 3000 cm^{-1} . A signal at 1689 cm^{-1} corresponds to the asymmetric stretching vibration of COO group. A signal at 1292 cm^{-1} was assignable to $\nu_{\text{C-O}}$. In plane deformation was observed at 1197 cm^{-1} and out of plane deformation was observed at 717 and 914 cm^{-1} . Stretching frequency due to sp^2 hybridized C-H bond was shown at 3062 cm^{-1} .

In complexes the involvement of azomethine group in coordination with metal was confirmed by the shift of its stretching frequency to lower value. Also the asymmetric stretching vibration of COO group is also shifted, which indicates coordination of carboxylate group to the metal. The presence of new signal around 1450 cm^{-1} and 3400 cm^{-1} in complexes confirmed the presence of coordinated nitrate and water molecule. Also the appearance of stretching frequencies corresponding to M-O and M-N confirmed the formation of complex. Characteristic infrared absorption frequencies (cm^{-1}) of 3TMAB and its inner transition metal complexes are given in Table 8.6.

Electronic spectral studies

Two separate peaks observed at 32154 cm^{-1} and 39062 cm^{-1} in the electronic spectra of 3TMAB correspond to $\text{n} \rightarrow \pi^*$ and $\pi \rightarrow \pi^*$ transition. In the case of complexes bathochromic shift was occurred for these bands which are a clear evidence for the complex formation.

NMR spectral studies

In the proton NMR spectra of 3TMAB, signal at $12.9\ \delta$ correspond to the proton present in the COOH group. A broad signal at $3.2\ \delta$ was assignable to the proton in azomethine carbon. Protons of the aromatic ring and thiophene ring showed signal in the range $7.7\text{-}8.8\ \delta$ and $7.1\text{-}7.7\ \delta$ respectively.

^{13}C NMR spectrum of 3TMAB displayed 12 peaks corresponding to 12 chemically distinct carbon atoms. Azomethine carbon displayed a peak at 154.99 ppm. Carbon atom of carboxyl group showed a peak at 167.03 ppm. Peaks due to protons of the benzene ring and thiophene ring were appeared in the range 129-151 ppm and 120-129 ppm respectively.

Magnetic moment studies

Idea about the geometry of the complexes was obtained from the magnetic moment measurement. Magnetic moment values of Nd(III) and Sm(III) complexes are found to be 3.73 BM and 1.51 BM respectively, whereas La(III) complex is diamagnetic. Octahedral geometry is assigned for all complexes.

Table 8.5 Microanalytical, magnetic and conductance data of 3TMAB and its inner transition metal complexes

Parameter	3TMAB (L'H)	*Complex		
		La(III)	Nd(III)	Sm(III)
Colour	Pale yellow	Pale brown	Dark brown	Light brown
Yield	70%	62%	58%	52%
Molecular weight (MW)	231	529	534	540
Melting point ($^{\circ}\text{C}$)	136	>300	220	245
M% Found	-	25.98	26.01	27.25
(Cald.)	-	(26.28)	(26.97)	(27.78)
C% Found	63.84	27.11	27.01	25.95
(Cald.)	(62.34)	(27.22)	(26.96)	(26.66)
H% Found	3.81	2.68	2.38	2.18
(Cald.)	(3.90)	(2.26)	(2.24)	(2.22)
N% Found	7.04	8.01	7.48	8.08
(Cald.)	(6.06)	(7.94)	(7.86)	(7.77)
μ_{eff} (BM)	-	Diamagnetic	3.73	1.51
Molar conductance ($\Omega^{-1}\text{cm}^2\text{mol}^{-1}$)	-	15	49	41
Geometry	-	Octahedral	Octahedral	Octahedral

*[LnL''(NO₃)₂(H₂O)₂] where Ln=La(III), Nd(III) and Sm(III)

Molar conductance studies

Molar conductance measurement was done for all complexes and is given in Table 8.5. The molar conductance value of the complexes is in the range of 15-50 $\Omega^{-1} \text{ cm}^2 \text{ mol}^{-1}$. These values suggest non-electrolytic behaviour and absence of counter ions outside the coordination sphere of metal chelates.

Table 8.6 Characteristic infrared absorption frequencies (cm^{-1}) of 3TMAB and its inner transition metal complexes

Assignment	3TMAB (L'H)	*Complex		
		La(III)	Nd(III)	Sm(III)
$\nu_{\text{H}_2\text{O}}$		3382	3393	3427
ν_{COO} (asym)	1689	1615	1614	1614
$\nu_{\text{C=N}}$	1579	1565	1570	1561
ν_{COO} (sym)	1524	1515	1521	1510
ν_{NO_3}	-	1501, 1403	1498, 1394	1492, 1394
$\nu_{\text{C-O}}$	1292	1291	1291	1291
In plane bending	1197	1188	1039	1039
Out of plane bending	914, 717	893, 752	901, 814	901, 814
$\nu_{\text{M-N}}$	-	682	673	673
$\nu_{\text{M-O}}$	-	423	492	498

*[LnL'(NO₃)₂(H₂O)₂] where Ln=La(III), Nd(III) and Sm(III)

From the characterization data the ligand 3TMAB coordinates with metal through NO donor sites and acted as monovalent bidentate ligand. Also it was noticed that 1:1 stoichiometry exist between all metal and ligand and possess octahedral geometry. Structure of the ligand 3TMAB and its inner transition metal complexes are represented in Fig 8.3.

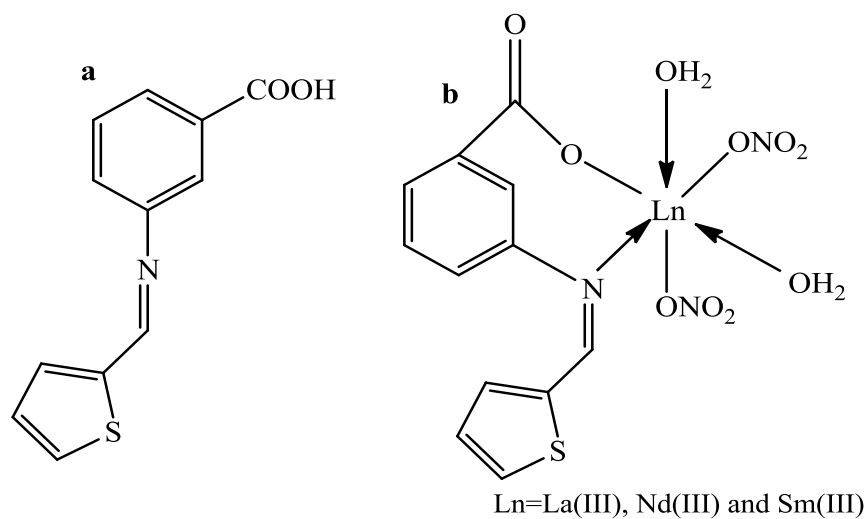


Fig. 8.3 Structures of a) ligand 3TMAB and b) its inner transition metal complexes

SUMMARY

Synthesized three heterocyclic Schiff bases derived from 3-acetylpyridine and thiophene-2-carbaldehyde such as 3-(1-(2-phenylhydrazono)ethyl)pyridine (3PHEP), 2-(1-(pyridine-3-yl)ethylidene)hydrazine carbothioamide (2PEHCT) and 3-((thiophen-2-ylmethylene)amino)benzoic acid (3TMAB) and their characterization were done by CHN analysis, spectral studies such as FTIR, UV-visible, NMR (^1H and ^{13}C) and mass spectroscopy. The inner transition metal complexes of these heterocyclic Schiff bases were synthesized to check their chelating ability. The complexes were also subjected to characterization by means of elemental (CHN) analysis, FTIR, UV, magnetic moment, estimation of metal and molar conductance measurements and structures were formulated.

Chelating ability of the heterocyclic Schiff bases 3PHEP, 2PEHCT and 3TMAB was explored by synthesizing inner transition metal complexes with metal ions of Lanthanum, Neodymium and Samarium. It was observed that 1:1 stoichiometry exists between metal and ligand in the case of all complexes. Ligand 3PHEP acted as zerovalent bidentate ligand and coordinates through azomethine nitrogen and the nitrogen atom present in the pyridine ring while the other two, 2PEHCT and 3TMAB were behaved as monovalent bidentate ligands but their coordination sites are different. 2PEHCT coordinates through azomethine nitrogen and sulphur atom where as in 3TMAB azomethine nitrogen and oxygen of the carboxylate group are the coordination sites.

On the basis of physicochemical data, octahedral geometry was assigned to La(III), Nd(III) and Sm(III) complexes of all these ligands. Diamagnetic behaviour was found for La(III) complexes, whereas Nd(III) and Sm(III) complexes are paramagnetic

as expected. Molar conductance data suggested that all the complexes are non-electrolytic in nature.

Presence of coordinated water molecules in all the chelates is evident by the appearance of additional broad peaks at almost 3400 cm^{-1} in the FTIR spectra. Nitrate ions with unidentate nature are present in all the complexes. Based on physicochemical data the general structure $[\text{LnL}(\text{NO}_3)_3(\text{H}_2\text{O})]$ is assigned to lanthanide complexes derived from Schiff base, 3PHEP while the lanthanide chelates derived from 2PEHCT and 3TMAB possess the general formula $[\text{LnL}(\text{NO}_3)_2(\text{H}_2\text{O})_2]$.

REFERENCES

1. P. Pfeiffer, *Angew. Chem.* 53, 93-98 (1940).
2. N. Raman, A. Kulandaisamy, A. Shunmugasundaram and K. Jeyasubramanian, *Transit. Met. Chem.* 26, 131-135 (2001).
3. E. Hadjoudis, M. Vittorakis and I. Moustakali-Mavridis, *Tetrahedron.* 43, 1345-1360 (1987).
4. T. Yoshikuni, *J. Mol. Catal. A: Chem.* 148, 285-288 (1999).
5. E. J. Hadjoudis, *Photochem.* 17, 355-363 (1981).
6. B. A. Uzoukwu, P. U. Adiukwu, S. S. Al-Juaid, P. B. Hitchcock and J. D. Smith, *Inorg. Chim. Acta.* 250, 173-176 (1996).
7. S. Yamada, *Coord. Chem. Rev.* 1, 415-423 (1966).
8. R. H. Holm and M. J. O'connor, *Prog. Inorg. Chem.* 14, 241-395 (1971).
9. R. H. Holm, G. W. Ewerett (Jr.) and A. Chakkravorty, *Prog. Inorg. Chem.* 7, 83-214 (1966).
10. S. A. Dalia, F. Afsan, Md. S. Hossain, Md. N. Khan, C. M. Zakaria, Md. Kudrat-E-Zahan and Md. M. Ali, *Int. J. Chem.* 6, 2859-2866 (2018).
11. M. S. More, P. G. Joshi, Y. K. Mishra and P. K. Khanna, *Mater. Today Chem.* 14, 1-22 (2019).
12. K. Divya, G. M. Pinto and A. F. Pinto, *Int. J. Curr. Pharm. Res.* 9, 27-30 (2017).
13. W. Al-Zoubi, A. A. S. Al-Hamdani and M. Kaseem, *Appl. Organometal. Chem.* 30, 810-817 (2016).
14. A. Prakash and D. Adhikari, *Int. J. Chemtech Res.* 3, 1891-1896 (2011).
15. C. M. da Silva, D. L. da Silva, L. V. Modolo, R. B. Alves, M. A. de Resende, C. V. B. Martins, A. de Fatima, *J. Adv. Res.* 2, 1-8 (2012).

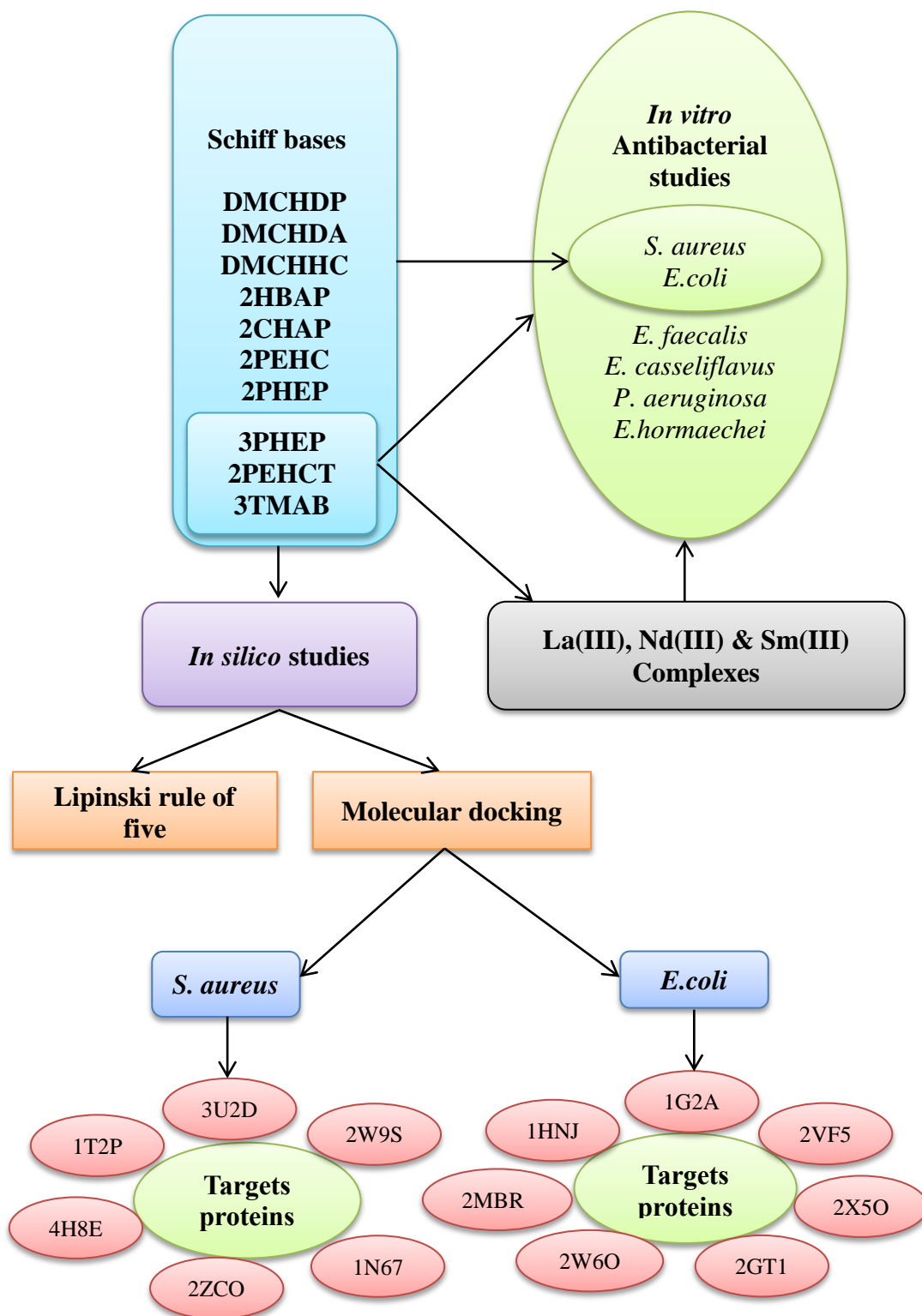
-
16. R. Drozdak, B. Allaert, N. Ledoux, I. Dragutan, V. Dragutan and F. Verpoort, *Adv. Synth. Catal.* 347, 1721-1743 (2005).
 17. S. Akhter, H. U. Zaman, S. Mir, A. M. Dar and S. Shrivastava, *Eur. Chem. Bull.* 6, 475-483 (2017).
 18. S. M. Ben-saber, A. A. Maihub, S. S. Hudere and M. M. El-ajaily, *Microchem. J.* 81, 191-194 (2005).
 19. A. Pradhan and A. Kumar, *Chem. Process. Eng. Res.* 35, 84-86 (2015).
 20. M. Sahin, N. Kocak, D. Erdenay and U. Arslan, *Spectrochim. Acta A.* 103, 400-408 (2013).
 21. A. M. Abu-Dief and I. M. A. Mohamed, *Beni-Seuf Univ. J. Basic Appl. Sci.* 4, 119-133 (2015).
 22. L. H. Abdel-Rahman, R. M. El-Khatib, L. A. E. Nassr, A. M. Abu-Dief, F. El-Din Lashin, *Spectrochim. Acta A.* 111, 266-276 (2013).
 23. A. B. Deilami, M. Salehi, A. Amiri and A. Arab, *J. Mol. Struct.* 1181, 190-196 (2019).
 24. S. M. Islam, A. S. Roy, P. Mondal, M. Mubarak, S. Mondal, D. Hossain, S. Banerjee and S. C. Santra, *J. Mol. Catal. A-Chem.* 336, 106-114 (2011).
 25. I. P. Ejidike and P. A. Ajibade, *Rev. Inorg. Chem.* 35, 191-224 (2015).
 26. N. Mahalakshmi and R. Rajavel, *Arab. J. Chem.* 7, 509-517 (2010).
 27. X. Zhong, J. Yi, J. Sun, H. -L. Wei, W. -S. Liu and K. -B. Yu, *Eur. J. Med. Chem.* 41, 1090-1092 (2006).
 28. S. K. Tadavi, A. A. Yadav and R. S. Bendre, *J. Mol. Struct.* 1152, 223-231 (2018).
 29. K. C. Gupta, A. K. Sutar and C. -C. Lin, *Coord. Chem. Rev.* 253, 1926-1946 (2009).
-

-
30. M. Maneiro, M. R. Bermejo, M. I. Fernandez, E. Gomez-Forneas, A. M. Gonzalez-Noya and A. M. Tyryshkin, *New J. Chem.* 27, 727-733 (2003).
 31. N. Raman, S. J. Raja and A. Sakthivel, *J. Coord. Chem.* 62, 691-709 (2009).
 32. Z. -Q. Feng, X. -L. Yang and Y. -F. Ye, *Sci. World J.* 2013, 1-9 (2013).
 33. S. Kumar, D. N. Dhar and P. N. Saxena, *J. Sci. Ind. Res. India.* 68, 181-187 (2009).
 34. I. R. Parrey and A. A Hashmi, *Mor. J. Chem.* 3, 147-151 (2015).
 35. C. Meenakshi, V. Ramamoorthy, S. Shivkolunthu and S. Muthusubramanian, *Indian J. Chem.* 40 (A), 207-210 (2001).
 36. M. G. B. Drew, *Coord. Chem. Rev.* 24, 179-275 (1977).
 37. L. Logu, K. R. Kamatchi, H. Rajmohan, S. Manohar, R. Gurusamy and E. Deivanayagam, *Appl. Organometal. Chem.* 29, 90-95 (2014).
 38. B. Erk, *Inorg. Chim. Acta.* 167, 91-95 (1990).
 39. K. Prajapati, P. Prajapati, M. Brahmhatt and J. Vora, *Res. J. Life Sci. Bioinform. Pharm. Chem. Sci.* 4, 804-813 (2018).
 40. P. S. Mansingh and K. S. Dash, *Indian J. Chem.* 34A, 904-907 (1995).
 41. L. Lekha, K. K. Raja, G. Rajagopal and D. Easwaramoorthy, *J. Organomet. Chem.* 753, 72-80 (2014).
 42. P. A. Vigato, *Inorg. Chim. Acta.* 139, 39-48 (1987).
 43. R. K. Agarwal, K. Arora and P. Dutt, *Synth. React. Inorg. Met. -Org. Chem.* 24, 301-324 (1994).
 44. J. -P. Cheng, Q. -Y. Lin, R. -D. Hu, W. -Z. Zhu, H. -Q. Li and D. -H. Wang, *Cent. Eur. J. Chem.* 7, 105-110 (2009).
 45. Y. M. Issa, H. M. Abdel Fattah and A. A. Soliman, *J. Therm. Anal.* 42, 1175-1184 (1994).
-

46. S. P. Idhol and Dr. R. E. Khadsan, *Int. J. Ind. Chem and Biotec.* 1, 1-5 (2015).
47. R. Yerrasani, M. Karunakar, R. Dubey, A. K. Singh, R. Nandi, Ranjan K. Singh and T. R. Rao, *J. Mol. Liq.* 216, 510-515 (2016).
48. S. Agnihotri and K. Arora, *E-J Chem.* 7, 1045-1054 (2010).
49. A. L. El-Ansary and N. S. Abdel-Kader, *Int. J. Inorg. Chem.* 2012, 1-13 (2012).
50. M. Shakir, A. Abbasi, M. Faraz and A. Sherwani, *J. Mol. Struct.* 1102, 108-116 (2015).
51. B. -D. Wang, Z. -Y. Yang, D. -D. Qin and Z. -N. Chen, *J. Photochem. Photobiol.* 194, 49-58 (2008).
52. V. A. Shelke, S. M. Jadhav, V. R. Patharkar, S. G. Shankarwar, A. S. Munde and T. K. Chondhekar, *Arab. J. Chem.* 5, 501-507 (2012).
53. XU. Dongfang, MA. Shuzhi, DU. Guangying, HE. Qizhuang and SUN. Dazhi, *J. Rare Earths.* 26, 643-647 (2008).
54. G. N. Naik, A. H. Pathan, R. P. Bakale, S. G. Ligade and K. B. Gudasi, *J. Chem.* 3, 149-157 (2013).
55. K. S. Abou-Melha and H. Faruk, *J. Coord. Chem.* 61, 1862-1874 (2008).
56. B. N. Figgis, J. Lewis, "Modern Coordination Chemistry", Interscience, New York (1960).
57. P. W. Selwood, "Magnetochemistry", Interscience, New York (1958).
58. L. Coury, *Conductance Measurements Part 1: Theory. Current Separations*, 18, 91-96 (1999).

PART- III

BIOLOGICAL STUDIES



CHAPTER 9

INTRODUCTION AND REVIEW

The research in the field of therapeutics is of great importance for the improvement of the quality of human life and for reducing human diseases. A vast number of diseases are caused by pathogenic organisms. Pathogens are microorganisms that are harmful to human body. Bacteria, virus, fungus, prion, protozoa, viroid etc are the different types of pathogens. Our body has the ability to defense against potential pathogens. Microbial infections are drastically increased in living beings due to multi drug resistant microorganisms. Even though a large number of antibiotics and chemotherapeutic agents are available to resist such microorganisms, the development of efficient novel chemotherapeutic agents is vital in the medical field [1-3].

Bacteria are microscopic organisms having cell walls. It is the first form of life in earth [4-5]. They have different shapes such as round, cylindrical and spiral. Round shaped bacteria are termed as cocci, whereas cylindrical and spiral bacteria are called as bacilli and spirilla respectively. Bacteriology is the branch deals with the study of bacteria. Even though they are essential in many processes like nitrogen fixation, some of them are pathogenic and cause infective diseases. Bacteria are generally categorized into two, namely gram-positive and gram-negative bacteria.

Gram-positive bacteria

Gram-positive bacteria are a bacterium that retains the violet colour of the stain used in Gram staining method. *Bacillus thuringiensis*, *Staphylococcus aureus*, *Bacillus subtilis*, *Enterococcus faecalis*, *Enterococcus casseliflavus* etc are examples for gram-positive bacteria

Staphylococcus aureus

S. aureus is a round-shaped bacterium which is a member of Firmicutes [6]. In Greek the meaning of the term Staphyle is ‘bunch of grapes’ and kokkos is berry. This name is given since the bacteria is forming grape like clusters. Cell wall of these species is amorphous and tough. Thickness of the cell wall is about 20-40 nm. Cytoplasm is present under the cell wall which is



Fig. 9.1 Micrograph of *S. aureus*

surrounded by cytoplasmic membrane. Major component of the cell wall is the peptidoglycan (50% of cell wall mass). The other component that contributes 40% of cell wall mass is teichoic acids. Remaining 10% of cell wall mass consists of exoproteins, surface proteins and peptidoglycan hydrolases.

Naturally this bacterium is found in nasopharynx of the human body and on skin. *S. aureus* can cause infections of nose, skin, vagina, urethra and gastrointestinal tract [7-8]. They are non-sporing, non-motile and few strains are capsulated. Nearly 50% of human population is carriers of *S. aureus*. It can grow in the temperature range 7-48.5⁰C (optimum temperature 30-37⁰C, pH of about 4.2-9.3 (optimum 7-7.5) and in the presence of upto 15% NaCl concentration. This helps them to grow in various food items. Micrograph of *S. aureus* is shown in Fig. 9.1.

Enterococcus faecalis

Enterococcus is a class of bacteria that is generally present in gut and bowel, vaginal tract and in oral cavity. Enterococcus when present in small amounts does not have any life threatening problems. Bacterial infection spreads throughout the body especially in people with unhealthy conditions which can cause even death [9]. Temperature range for the growth of Enterococcus is 10-42⁰C. Of the approximately 17

types of *Enterococcus* species, the most common species found in human body are *E. faecalis* and *E. faecium*. *Enterococcus faecalis* is a gram-positive bacterium which was formerly known as *Streptococcus faecalis*. The *E. faecalis* genome consists of 3.22 million base pairs with 3,113 protein-coding genes. These bacteria



Fig. 9.2 Micrograph of *E. faecalis*

will penetrate to human body through urine, blood and wounds which may cause infection [10]. Micrograph of *E. faecalis* is shown in Fig. 9.2.

Enterococcus casseliflavus

Enterococcus casseliflavus is a rare non-faecium, non-faecalis, vancomycin-resistant enterococcus (VRE) that is responsible for up to 2% of all enterococcal infections [11]. A large number of infections such as urinary tract infections, bacteremia, endocarditis, meningitis, septic arthritis, hematogenous osteomyelitis, pneumonia, pelvic, intra-abdominal and soft tissue infections will be caused by enterococci. Micrograph of *E. casseliflavus* is shown in Fig. 9.3.

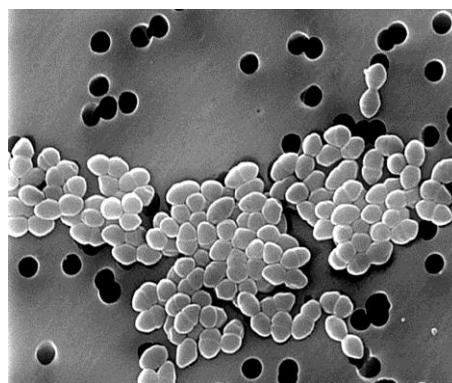


Fig. 9.3 Micrograph of *E. casseliflavus*

Gram-negative bacteria

Gram-negative bacteria are a bacterium that does not retain the violet colour of the stain used in the Gram staining method. *Escherichia coli*, *Enterobacter aerogenes*, *Proteus vulgaris*, *Pseudomonas aeruginosa*, *Enterobacter hormaechei* etc are examples for gram-negative bacteria.

Escherichia coli

In 1885 a German bacteriologist Theodor Escherich discovered *E. coli* in human colon. Normally found in intestines and in gut of some animals. They are rod-shaped, anaerobic and commonly found in intestines. It belongs to the genus *Escherichia*. The volume, length and diameter of the cell are $0.6\text{--}0.7\ \mu\text{m}^3$, $2.0\ \mu\text{m}$ and $0.25\text{--}1.0\ \mu\text{m}$ respectively. The cell wall consists of a thin peptidoglycan layer and an outer membrane. They are motile, non-capsulated, non-spore former and produce peritrichous flagella. Optimum temperature required for the growth is $15\text{--}45^\circ\text{C}$. Few of them are pathogenic and the species which are not harmful will prevent colonization, helps in digestion and produce vitamin K and B₁₂ [12-13]. Neonatal meningitis, urinary tract infections and gastroenteritis are the infections caused by *E. coli* in human. The symptoms are nausea, abdominal cramps, constant fatigue and diarrhea. Micrograph of *E. coli* is shown in Fig. 9.4.

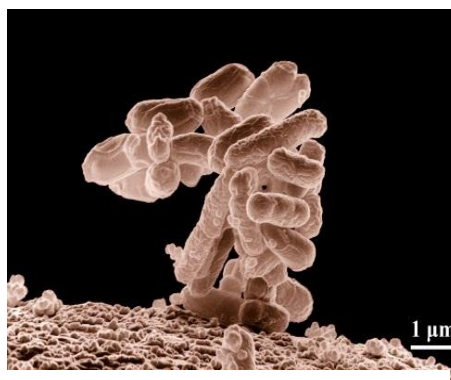


Fig. 9.4 Micrograph of *E. coli*

Pseudomonas aeruginosa

It is a rod-shaped gram-negative bacterium, $0.5\text{--}0.6$ by 1.5 microns which are aerobic, motile with polar flagella, non-spore forming, nonfermentive, toxigenic and invasive. They appear as singly or in pairs or as short chains. This bacterium is considered as opportunistic and it infects urinary tract, wounds, burns and cause blood infections [14]. It is generally known for its high resistant capacity to antibiotics [15] and for its characteristic water-soluble pigment as pyoverdine

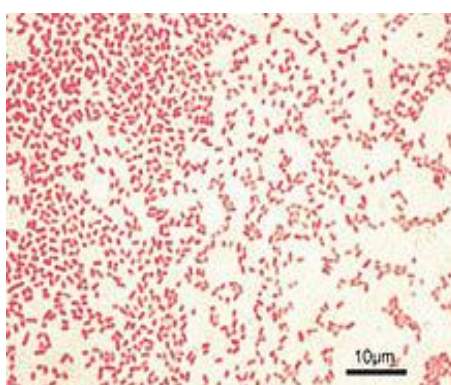


Fig. 9.5 Micrograph of *P. aeruginosa*

(yellow and fluorescent), pyocyanin (blue), pyomelanin (brown) and pyorubin (red). Temperature of about 37⁰C or 42⁰C is favorable for its growth. In 1882 it is first isolated from green pus by Gessard. They have fruity, sweet-grape smell, sometimes corn/taco-like odor. They are found in hot tubs, moist environment such as water and soil, fresh fruits and vegetables, lakes, rivers, streams, respiratory therapy equipment, dialysis tubing, catheters and portable water sources like sinks and showers. Micrograph of *P. aeruginosa* is shown in Fig. 9.5.

Enterobacter hormaechei

Enterobacter hormaechei is a new species belongs to *Enterobacteriaceae* family.

It is previously called as Enteric Group 75 [16].

Enterobacter hormaechei is named in honor of Estenio Hormaeche, a Uruguayan microbiologist who (with P. R. Edwards) proposed and defined the genus *Enterobacter*. They are rod shaped, anaerobic, motile and non-spore forming. It is a

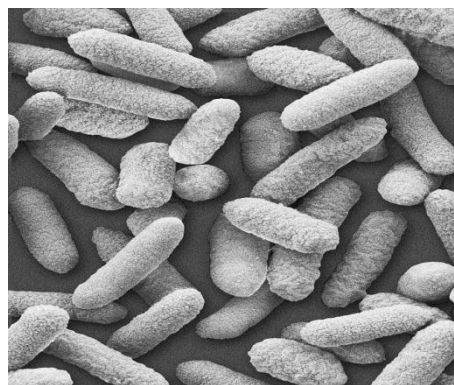


Fig. 9.6 Micrograph of *E. hormaechei*

member of coliform group of bacteria. Optimum

temperature for the growth is 44.5⁰C in the presence of bile salts. It can cause infections in respiratory and urinary tracts. They are oxidase reductase, ferment glucose with acid production and reduce nitrates to nitrites. Micrograph of *E. hormaechei* is shown in Fig. 9.6

Gram's method

Gram's method is used to classify the bacteria into two groups based on the difference in the cell walls [17]. This technique was named after a Danish bacteriologist Hans Christian Gram. Gram-positive bacteria consist of a thick peptidoglycan layer whereas in gram-negative bacteria peptidoglycan layer is thin and contains two outer

layers. In this method the bacteria is first stained with crystal violet dye and washed with absolute alcohol and water. Then it is again stained with a pink coloured dye safranin. A gram-positive bacterium retains the violet colour whereas a gram-negative bacterium gets the pink colour. This is due to the structural dissimilarity of the bacterial cell wall. A thick peptidoglycan layer present in the cell wall of gram-positive bacteria is responsible for retaining the violet colour of the dye. In the case of gram-negative bacteria the layer present outside the lipid will never bind the violet stain and get washed away during the staining processes. Schematic representation of Gram's test is shown in Fig. 9.7.

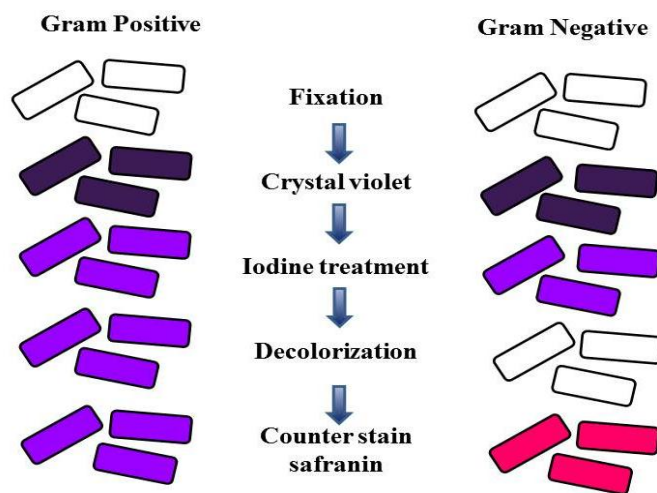


Fig. 9.7 Representation of Gram's test

Factors affecting the growth of bacteria

There are several factors that control the growth of bacteria. Nutrient concentration, pH, temperature, presence of salt and ions, gaseous concentration and light are some of the factors influencing the bacterial growth.

Nutrition concentration

The presence of substance promoting the growth of bacteria in the culture media will enhance the growth of bacteria. Nutrient concentration required for the growth of various bacteria is different. Rate of bacterial growth increases upto a certain level with increase in concentration of nutrient. After that the growth rate remains constant.

pH

Change in pH will affect the ionic properties of its cell. Therefore change in pH will affect the growth of bacteria. The suitable pH for the bacterial growth is in the range 6.5-7.5.

Temperature

Temperature range of about 0 to 85⁰C is suitable for the survival of bacteria. The death rate of bacteria will be enhanced when the temperature is suddenly reduced, and even kill the bacteria at a lower temperature. If the water content in the medium where bacterial growth is high, low temperature is required to kill the bacteria. Bacteria are categorized into three depending on temperature range required for the growth as psychrophilic, mesophilic and thermophilic (Table 9.1).

Table 9.1 Classification of bacteria based on the temperature range required for the growth

Temperature (⁰ C)	Psychrophilic	Mesophilic	Thermophilic.
Minimum	0 ⁰ C	5-25 ⁰ C	25-45 ⁰ C
Optimum	15 ⁰ C	18-45 ⁰ C	55 ⁰ C
Maximum	30 ⁰ C	30-50 ⁰ C	60-93 ⁰ C

Minimum temperature and maximum temperature are the lowest and highest temperature that allows the growth of bacteria. Optimum temperature is the temperature at which bacterial growth is maximum. Solidification of cell membrane occurs below minimum temperature and denaturation of enzymes and cellular proteins occur above maximum temperature. As a result there is no bacterial growth below minimum and above maximum temperature. The optimum temperature for psychrophilic, mesophilic and thermophilic bacteria are 15⁰C, 18-45⁰C and 55⁰C respectively.

Salt and ions

Metal ions like Zn^{2+} , Ca^{2+} , Fe^{2+} , K^+ etc are required by the bacteria for the synthesis of enzymes and proteins. NaCl is not required for most bacteria however for halophilic bacteria such as *Archeobacteria*, high salt concentration is required.

Gaseous concentration

Oxygen and CO_2 has an important role in the growth of bacteria. O_2 is needed for aerobic respiration. Hence obligate aerobic bacteria will sustain in the presence of O_2 whereas it is harmful to anaerobic bacteria. CO_2 is required for capnophilic bacteria such as *Helicobacter pylori* and *Campylobacter*.

Light

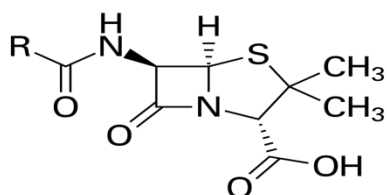
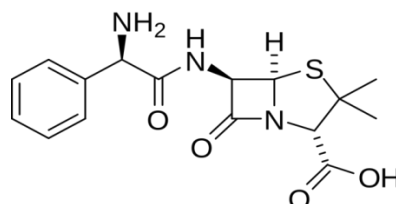
Visible light is not harmful to bacterial cells whereas non visible rays like infrared and UV-visible rays have an adverse effect on bacterial cells.

Antibacterial agents

Antibiotics are the commonly used antibacterial agents [18]. They are substances generated by one microorganism that selectively inhibits the growth of another. They inhibit by disrupting different targets present in the bacteria and cell surface, by blocking the growth of new proteins and by inhibiting DNA replication. They are classified into various groups such as beta-lactams, glycopeptides, macrolides and ketolides, aminoglycosides, tetracyclines and glycylicyclines, quinolones, lincosamides, streptogramins, oxalidinones, lipopeptides, polymixins, ansamycins and sulfa drugs. The examples of antibiotics belong to these groups and their mechanism of action is shown in Table 9.2. Structure of antibiotics penicillin and ampicillin are given in Fig. 9.8 and 9.9 respectively.

Table 9.2 Classification of antibiotics with examples and their mechanism of action

Group	Examples	Mechanism of action
Beta-lactams	Penicillins, Cephalosporins, Carbapenems, Ampicillin	Inhibit cell wall synthesis
Glycopeptides	Vancomycin, Teichoplanin, Telavancin	
Macrolides and ketolides	Azithromycin, Telithromycin, Erythromycin, Clarithromycin	Inhibit protein synthesis
Aminoglycosides	Gentamicin, Amikacin, Tobramycin, Netilmicin, Streptomycin	
Tetracyclines and Glycylcyclines	Tetracycline, Tigecycline, Doxycycline, Minocycline	
Lincosamides	Clindamycin	
Streptogramins	Quinupristin/ dalfopristin	
Oxalidinones	Linezolid	Destroys cell membrane structure
Ansamycins	Rifampicin	
Lipopeptides	Daptomycin	
Polymixins	Colistin Polymixin B	Inhibit DNA synthesis
Sulfa drugs	Sulfamethoxazoletrimethoprim	
Quinolones	Ciprofloxacin, Norfloxacin Levofloxacin, Moxifloxacin	Inhibit DNA gyrase

**Fig. 9.8** Structure of Penicillin**Fig. 9.9** Structure of Ampicillin

Molecular docking

Molecular docking is a key tool in the field of molecular biology and modern drug design. It is an *in silico* approach used to explore drug-receptor interactions [19-21]. Main aim is to predict the best-fit orientation of the drug molecule that binds to a specified protein target of interest in order to find out the activity and affinity of the drug molecule. Computer-aided drug design is a fast, automatic and very low cost process that can be done either by structure based drug design (SBDD) or ligand based drug design (LBDD) [22]. Ligand based drug design is an indirect method which have been used

when a series of ligand molecules having good activity is known and structural information about target is not available. Methods employed for this are pharmacophore modelling and quantitative structure activity relationship (QSAR). Former model designed to identify the ligand structures needed for target binding and the latter one is to suggest molecular similarity and biological activity. QSAR is based on the principle that structurally similar chemicals are likely to have similar physicochemical and biological properties. Structure based drug design is mainly based on the three dimensional structure of the target. If any target is not available it can be created by using homology modeling. Using the structure of the target, we can predict the binding affinity of drug molecules to the target. The most common method used for SBDD is molecular docking.

The vital steps involved in docking are prediction of conformation, position and orientation of the ligands within the target sites and evaluation of binding energy. Its default search function is based on Lamarckian Genetic Algorithm (LGA), a hybrid genetic algorithm with local optimization that uses a parameterized free-energy scoring function to estimate binding energy. Docking efficiency is high if the location of binding site is known before docking. In the lack of information about binding site, online servers or cavity detection programs such as POCKET, GRID, PASS, SurfNet and MMC have been used to identify active sites within target proteins. Docking without any idea about the active site is called blind docking. Schematic representation of docking procedure is shown in Fig. 9.10.

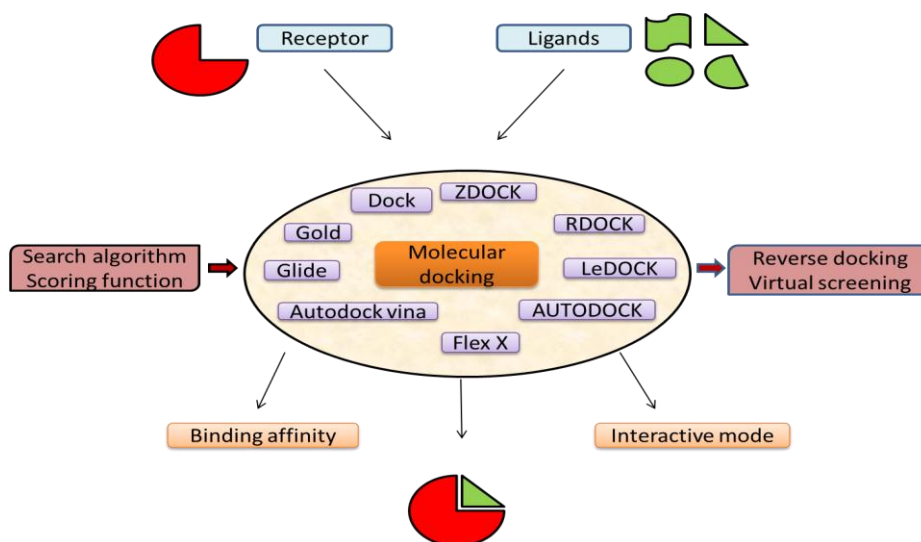


Fig. 9.10 Schematic representation of docking procedure

Schiff bases and its metal complexes as antibacterial agents – A review

Schiff base ligands and their metal chelates have wide application in the field of biology. They are found to be effective antibacterial, antifungal, antimalarial, antiinflammatory, antioxidant agents. Its ability to prevent the bacterial growth is well reported.

S. A. Patil and coworkers synthesized and characterized Cu(II), Co(II) and Ni(II) complexes of the Schiff bases derived from 8-acetyl-7-hydroxy-4-methylcoumarin and meta substituted thiosemicarbazides [23]. Characterization was done using spectral, thermal, magnetic and cyclic voltammetric studies. The antibacterial (*Escherichia coli*, *Bascillus subtilis*, *Staphilococcus aureus*, and *Salmonella typhi*), antifungal (*Aspergillus Niger*, *Candida albicans* and *Cladosporium*) and DNA cleavage activities of the complexes were also evaluated. It is found that Schiff bases and complexes are active against *E. coli*, *S. aureus* and *S. typhi*. All complexes exhibited enhanced activity against *S. typhi*. Another important observation is that antifungal activity of the Schiff bases and complexes is high compared to their antibacterial activity.

B. K. Singh et al. investigated antimicrobial activity of the Schiff base 2-aminophenol-pyrrole-2-carboxaldehyde and its Cd(II), Zn(II), Pb(II) and Sn(II)

complexes against two bacterium *E. coli* and *S. aureus* using agar well-diffusion method [24]. Coordination of ligand with metal was established using IR and NMR (^1H) spectroscopy. Chloramphenicol is used as the standard antibiotic to compare the activity of synthesized compounds. Ligand, Zn(II) and Cd(II) complexes are more active against *E. coli* whereas other complexes are active against *S. aureus*. Also the activity of Zn(II) complexes were higher than other complexes in both bacterial strains.

Cyclic voltammetry (CV) and antimicrobial activity of Cu^{II} , Mn^{II} , Co^{II} , Ni^{II} , VO^{II} and Zn^{II} complexes of two Schiff bases acetoacetanilido-4-aminoantipyrinyl-2-aminophenol and acetoacetanilido-4-aminoantipyrinyl-2-aminothiophenol were carried out by N. Raman et al [25]. Structure of the metal complexes were confirmed by spectroscopic techniques (IR, UV, ^1H NMR and ESR), magnetic moment measurement and microanalytical data. Microorganisms used for the antimicrobial activity were *Staphylococcus aureus*, *Bacillus subtilis*, *Pseudomonas aeruginosa*, *Salmonella typhi*, *Shigella fleneri*, *Rhizoctonia bataicola*, *Klebsiella pneumoniae* and *Aspergillus niger*.

V. B. Badwaik and co-workers synthesized Fe(II), Ni(II), Cd(II), Mn(II), Cu(II), $\text{UO}_2(\text{VI})$, Zn(II) and Co(II) complexes of Schiff base derived from glycine and 2-hydroxy-5-methylacetophenone [26]. Characterization was done using IR, ESR, electronic spectroscopic techniques, electrical conductance, analytical, thermogravimetric analysis and magnetic susceptibility measurements. Antibacterial activity is tested against both gram-positive and gram-negative bacterium using disc diffusion method. 10 mg/L is the concentration of the compounds taken for the study in DMSO. Both ligand and complexes have less activity than the standard antibiotic streptomycin. Inhibitory power of the ligand enhanced upon chelation.

Z. H. Chohan et al. synthesized Schiff base derived from amino-5-hydroxypyridine and salicylaldehyde and its Co(II), Ni(II) Cu(II), and Zn(II) metal

complexes [27]. Characterization was done on the basis of analytical, physical and spectral data. *S. aureus*, *Klebsiella pneumoniae*, *E. coli*, *Proteus vulgaris* and *P. aeruginosa* were the bacterial strains used for screening antibacterial activity. Effect of anions in the antibacterial activity of the complexes was also monitored by preparing same metal complexes having different anions such as nitrate, chloride, acetate and sulphate. Activity of the complexes is enhanced when the anion are present in the order nitrate>oxalate>chloride>sulphate.

The synthesis and characterization of two novel Schiff bases N,N'-bis (acetophenone)ethylenediamine, N,N'-bis(4-nitrobenzaldehyde)ethylenediamine and their transition metal complexes (Zn(II) and Cd(II)) were done by A. Prakash and co-workers [28]. IR spectra indicate the bonding of ligand with metal through acetate and azomethine moiety. The *in vitro* studies were carried out to determine the antibacterial potential of the synthesized ligands and metal chelates. Both ligands and complexes are found to possess good antibacterial properties.

The antibacterial activity (*in vitro*) of the Schiff base N,N'-bis(pyrrrole-2-carbaldehyde)ethylenediamine and its Ni(II), Mn(II), Cu(II) and Co(II) complexes were evaluated using the bacterial strains *E. coli* and *S.aureus* by B. K. Singh et al [29]. Spectral, electrochemical and magnetic studies were used for characterization. The *in vitro* inhibitory activity of the metal chelates were high than the ligand. Also Ni(II) complex was found to more active than the other complexes.

Ti(III), Mn(III), MoO(V), Ru(III), V(III), MoO₂(VI), and UO₂(VI) complexes of the Schiff base derived from 2-aminophenol and 1-phenyl-2,3-dimethyl-4-(4-iminopentan-2-one)-pyrazolin-5-one were synthesized and characterized by A. Saxena and co-workers [30]. Geometry of all the complexes is found to octahedral. Antibacterial activity of both ligand and complexes were done against *B. subtilis* and *S. aureus*. The

nature of metal ion has influence on antibacterial activity. Order of activity against *B. subtilis* and *S. aureus* was Mn(III) > MoO(V) > MoO₂(VI) > Ru(III) > UO₂(VI) > V(III) > Ti(III) and MoO(V) > MoO₂(VI) > UO₂(VI) > Ru(III) > Mn(III) > V(III) > Ti(III) respectively

L. Lekha and co-workers synthesized Sm(III), Pr(III), Tb(III), Gd(III), Yb(III) and Er(III) complexes of sodium salt of 2-[(5-bromo-2-hydroxy-benzylidene)-amino]-3-hydroxypropionic acid [31]. General formula of the complexes was [Ln(L)(NO₃)₂(H₂O)]NO₃. Elemental analysis, UV–Vis, conductivity measurements, fluorescence study, FT-IR and mass spectrometry were used as characterization techniques. Antibacterial activity of the Schiff base and complexes were also carried out against *E. coli*, *P. aeruginosa*, *P. vulgaris* and *S. aureus* by means of agar diffusion method. Results showed that the activity of the Ln(III) complexes of the ligand is high compared to the corresponding ligand. That is activity is enhanced upon chelation. Also the Sm(III) and Gd(III) complexes showed exceptional activity compared to other complexes.

Seven Ln(III) complexes of the tetradentate Schiff base (N,N'-bis(1-naphthaldimine)-o-phenylenediamine) was synthesized and their antibacterial activity against *Staphylococcus aureus*, *Shigella dysenteriae*, *Escherichia coli*, *Serratia marcescens* and *Pseudomonas aeruginosa* using micro-broth dilution and agar well diffusion was done by W. M. Al Momani et al [32]. La(III), Nd(III) and Gd(III) complexes were more active than two standard antibiotics used against *Pseudomonas aeruginosa*. Pr(III) and La(III) complexes were effective against *Staphylococcus aureus* whereas complex of Sm(III) is effective against *Serratia marcescens*. Minimum inhibitory concentration observed is 1.95-250.00 µg/mL. Dy(III) and Er(III) showed no remarkable activity in comparison with the two standard antibiotics used.

S. Alghool et al. synthesized the Schiff base (3,5-di-tert-butyl-2-hydroxybenzyl) amino]acetic acid and its La(III), Gd(III), Ce(IV), Sm(III) and Nd(III) complexes [33]. Characterization was done by elemental analyses, IR, UV-visible, FAB-mass, magnetic measurement, molar conductance measurements and NMR spectral studies. Antibacterial and antifungal activity of the complexes was also evaluated. Antibacterial activity was screened against the bacterial strains *S. aureus* and *E. coli* whereas the antifungal activity was screened against *A. flavus* and *C. albicans*. Tetracycline and Amphotericin B are the standard antibiotics used in antibacterial and antifungal studies respectively. Results showed that the activity of the complexes was less compared to that of ligands.

Synthesis, characterization and antibacterial activity of the seven lanthanide complexes of a tridentate Schiff base derived from 2-aminopyrimidine and 2-hydroxyacetophenone were carried out by K. Mohanan and co-workers [34]. Luminescence, thermal decomposition, XRD and DNA cleavage study was also conducted. *E. coli*, *B. magaterium*, *S. typhi* and *S. aureus* were the bacterial species used for the study. Both the ligand and complexes have *in vitro* growth inhibitory activity with MIC values in the range 20–60 µg/mL. The *in vitro* growth inhibitory activity of the complexes were high than ligands.

Z. A. Taha et al. synthesized eight novel Ln(III) complexes (Ln(III) = Dy, Nd, Gd, Tb, Sm, Er, Pr and La) of bis-(salicyladehyde)-1,3-propylenediimine and characterized using elemental analysis, molar conductivity measurements, spectral studies and thermogravimetric analysis (TGA) [35]. Sm(III), Dy(III) and Tb(III) ions have characteristic luminescence, which indicates that the ligand is efficient for absorbing and transfer energy to metal. Most of the Ln(III) complexes have antibacterial activity against various pathogenic bacteria and are higher than the corresponding ligand. This is attributed to the increase in lipophilic nature of the metal when coordinated with

ligand. Activity of ligand is high against *Pseudomonas aereuginosa* and *S. dysenteriae* whereas inactive against *P. vulgaris*. Also many of the complexes are more active than the standard antibiotics such as cephalexin and cephradine.

A novel Schiff base by the condensation of 3-aminopyridine and 8-formyl-7-hydroxy-4-methyl-coumarin and its nine Ln(III) complexes were synthesized by V. Mutalik et al [36]. In addition to characterization studies, fluorescence study, antibacterial, antifungal and antitubercular activities were also studied. *E. coli* and *S. aureus* were the bacterial strains whereas *C. Albicans* and *A. Niger* were the fungi used for the study. Antimicrobial activity of the complexes was found to be greater than that of ligand.

Nine novel lanthanide complexes of the Schiff base 5-bromosalicylidene-4-amino-3-mercapto-1,2,4-triazine-5-one (BrSAMT) having the general formula $[Ln(L)(ONO_2)(H_2O)_2]$ were synthesized and characterized by A. S. Ramasubramanian and co-workers [37]. Spectral, magnetic, thermal and molar conductance studies confirmed the coordination sites of the ligand. Antibacterial activity against gram-negative bacteria such as *E. coli*, *Salmonella typhi*, *Shigella flexneri* and *Pseudomonas aeruginosa* was shown by La, Yb and Eu complexes.

S. Alghool et al. synthesized and characterized an amino acid Schiff base N-(2-hydroxybenzyl)-L-methionine acid and its La(III), Th(IV) and Ce(IV) complexes [38]. Structure of the compounds was confirmed by elemental, spectral and molar conductivity measurements. Both ligand and complexes were screened for antifungal and antibacterial activity. Antibacterial activity was screened against the bacterial strains *S. aureus* and *E. coli* whereas the antifungal activity was screened against *A. flavus* and *C. albicans*. Tetracycline and amphotericin B were the standard antibiotics used in antibacterial and

antifungal studies respectively. Results showed that the activity of the complexes is less compared to that of ligands.

Molecular docking studies with proteins as targets – A review

A series of 3-((1-benzyl-1H-1,2,3-triazol-4-yl)methoxy)-2-(4-fluorophenyl)-4H-chromen-4-ones were synthesized and characterized by Vidya S. Dofe et al [39]. The characterization was done by IR, NMR (^1H and ^{13}C) and Mass spectroscopy. All the compounds were subjected to *in vitro* antibacterial study against *Escherichia coli*, *Staphylococcus aureus*, *Pseudomonas aeruginosa* and *Bacillus subtilis* and antifungal activity against *Candida tropicalis*, *Candida albicans* and *Candida glabrata* by micro broth dilution method. Molecular docking study was also done to elucidate the binding at the active site. Docking studies were carried out using Glide v6.2 and the results showed that there is a good binding interaction.

A. Bharathi and co-workers synthesized six novel dihydropyrimido[4,5-*a*]acridin-2-amines and the structures were analysed using FTIR, EIMS, NMR (^1H and ^{13}C) and single crystal XRD studies [40]. The molecular docking and *in vitro* antidiabetic activity of the compounds on α -glucosidase and α -amylase activity were also evaluated. Docking studies were performed using AutoDock 4.0. The *in vitro* studies are in good agreement with docking studies.

G. Sabbagh et al. carried out docking studies of fifty flavonoids with β -ketoacyl acyl carrier proteinsynthase I (KAS I) present in *E. coli* using iGemdock v2.1 [41]. Among the flavonoids taken, two of them named isorhamnetin and genistein are found to exhibit binding energy of about -132.42 kcal/mol and -135.76 kcal/mol. This is comparable with the binding energy of the standard drugs cerulenin (-99.64 kcal/mol) and thiolactomicin (-90.26 kcal/mol). They are also found to obey Lipinski rule of five to predict druglikeness.

Antibacterial activity of fourteen novel quinioline based chalcones obtained by the condensation of 2,7-dichloro-8-methyl-3-formyl quinoline and acetophenone/acetylthiophenes, were carried out against 3 gram-positive and 3 gram-negative bacteria by M. I. Abdullah et al [42]. Bioassay and computational (theoretical and docking) studies were also carried out. The chalcones having bromo or chloro substituent are found to have high antibacterial activity. Docking study showed that the binding energy of chalcones having high interaction with DNA gyrase is -8.18 and -8.88 kcal/mol respectively.

Antifungal and antibacterial studies of the imidazole and pyrazole based compounds prepared by one-pot reaction, was carried out by F. Abrigach and co-workers [43]. Results showed that the compounds have efficient antifungal activity rather than antibacterial activity. This observation is also supported by lipophilicity study and structure-activity relationship analysis (SAR). In order to understand the interactions between ligand and the target molecule molecular docking study and homology modeling was conducted on compounds having higher activity against the fungus *Fusarium oxysporum f.sp. albedinis*.

J. N. Sangshetti and co-workers synthesized some linezolid-like Schiff bases and screened for their biofilm inhibition activity against *Pseudomonas aeruginosa* [44]. Out of these nine Schiff bases two of them are found to exhibiting high inhibition activity compared to standard linezolid. Also they are more potent than ciprofloxacin. Hence they are good antibacterial agents. Docking study of these highly active Schiff bases was also carried out against PqsD enzyme of *P. aeruginosa*. ADME analysis was also conducted and the results showed that they have capacity to develop as oral drug.

K. Gullapelli et al. synthesized oxadiazinanes and triazinane and conducted antibacterial analysis by means of well diffusion method against gram-positive and

gram-negative bacterial strains [45]. Results showed that they are good antibacterial agents. Molecular docking studies of the compounds were also done with the protein targets *DNA gyrase subunit b* and *topoisomerase II*. Results of docking study are in agreement with the antibacterial activity of the compounds.

Five 2-substituted 4-(2,5-dichlorothienyl)-1,3-thiazoles were synthesized, characterized and subjected to antibacterial and antifungal activity by B. K. Sarojini and co-workers [46]. The results showed that the thiazoles 4-(2,5-dichlorothien-3-yl)-2-amino-1,3-thiazole and 4-(2,5-dichlorothien-3-yl)-2-(8-quinolinyl)-1,3-thiazole are excellent antibacterial and antifungal inhibitors. Docking study was also carried out by taking L-glutamine: D-fructose-6-phosphate amidotransferase [GlcN-6-P] as target molecule. From the results it is clear that the 4-(2,5-dichlorothien-3-yl)-2-(8-quinolinyl)-1,3-thiazole has lower binding energy and good inhibition capacity of GlcN-6-P.

G. Gomathi and co-workers synthesized methyl 3-[(E)-(2-hydroxy-1-naphthyl)methylidene]carbazate by means of slow evaporation solution growth technique [47]. Proton NMR, powder XRD, FT-RAMAN, UV-VIS-DRS analysis, FT-IR and fluorescence studies were carried out. From UV-VIS-DRS and fluorescence studies it was clear that the compound has bluish green emission property. Antimicrobial activity of the compound was screened against pathogenic bacteria such as *Streptococcus faecalis*, *Shigella dysenteriae*, *Bacillus cereus*, *Vibrio Cholerae* and fungi such as *Candida glabrata*, *Candida krusei* and *Candida albicans*. Docking studies showed that the compound has good binding affinity towards human estrogen receptor.

Scope and aims of present investigations

In addition to significant roles in catalysis and organic synthesis Schiff base ligands and their metal complexes have a wide variety of applications in biological, industrial, analytical and clinical fields. Coordination chemistry of lanthanides and its

complexes have aroused much interest since, chemistry of lanthanides is a promising research area inspired by a wide variety of applications. On account of the excellent coordination nature of Schiff bases to the rare earth ions, the coordination chemistry of rare earth complexes of Schiff bases are interesting and their role in chemical, industrial and medical field are enough to recognize them as worthwhile for the synthesis of new complexes.

Therefore in the present course of investigation it is proposed to carry out analysis of antibacterial activity of the Schiff base ligands 3PHEP, 2PEHCT and 3TMAB and some of their lanthanide (III) complexes against six pathogens such as *S. aureus*, *E. faecalis*, *E. casseliflavus*, *E. coli*, *P. aeruginosa* and *E. hormaechei*. Ampicillin was taken as the standard antibiotic to compare the growth inhibitory power of the ligands and complexes. Molecular docking studies of all the ten Schiff base ligands were also proposed to conduct using AutoDock 4.2 in order to understand the mechanism by which the Schiff base molecules inhibit the growth of bacteria. Six target proteins from *S. aureus* and seven target proteins from *E. coli* were selected for this purpose. Drug ability of the Schiff bases is also to be preliminarily screened using Lipinski rule of five.

CHAPTER 10

MATERIALS AND METHODS

The methods and steps used for *in vitro* antibacterial and *in silico* molecular docking studies are discussed in this chapter. Details about the protein targets adopted for docking studies are also included.

***In vitro* antibacterial studies**

In vitro antibacterial analysis of the Schiff base compounds 2,2'-(5,5-dimethylcyclohexane-1,3-diylidene)bis(azanylylidene)diphenol (DMCHDP), N,N'-(5,5-dimethylcyclohexane-1,3-diylidene)dianiline (DMCHDA), 2,2'-(5,5-dimethyl cyclohexane-1,3-diylidene)bis(hydrazinecarboxamide) (DMCHHC), 2-((2-hydroxybenzylidene)amino)phenol (2HBAP), 2-(cyclohexylideneamino)phenol (2CHAP), 3-(1-(2-phenylhydrazono)ethyl)pyridine (3PHEP), 2-(1-(pyridine-3-yl)ethylidene)hydrazine carboxamide (2PEHC), 2-(1-(pyridine-3-yl)ethylidene) hydrazine carbothioamide (2PEHCT), 3-((thiophen-2-ylmethylene)amino)benzoic acid (3TMAB) and 2-(1-(2-phenylhydrazono)ethyl)pyridine (2PHEP) were conducted against *Staphylococcus aureus* and *Escherichia coli*. Three Schiff bases 2PEHC, 2PEHCT, 3TMAB and their La(III), Nd(III) and Sm(III) complexes were also subjected to antibacterial studies against the pathogens such as *Enterococcus faecalis*, *Enterococcus casseliflavus*, *Pseudomonas aeruginosa* and *Enterobacter hormaechei* apart from the former two bacteria. Disk diffusion method is employed for this purpose. Mueller- Hinton agar was used for preparing the medium. Ampicillin is the standard antibiotic used for comparison.

Disc diffusion method

Also called Kirby–Bauer test or agar diffusion test [48]. This method is used to determine efficient antibiotic against pathogenic microorganisms. First step is the preparation of agar plate followed by spreading bacteria on it [49]. Then added the discs containing sample and incubated at 37⁰C for 24 h. If the sample is effective against the bacteria, there will be a region around the bacteria where there is no bacterial growth. This region is called zone of inhibition. Diameter of the zone of inhibition was measured and compared with zones produced by reference compounds. Representation of disc diffusion method is shown in Fig. 10.1.

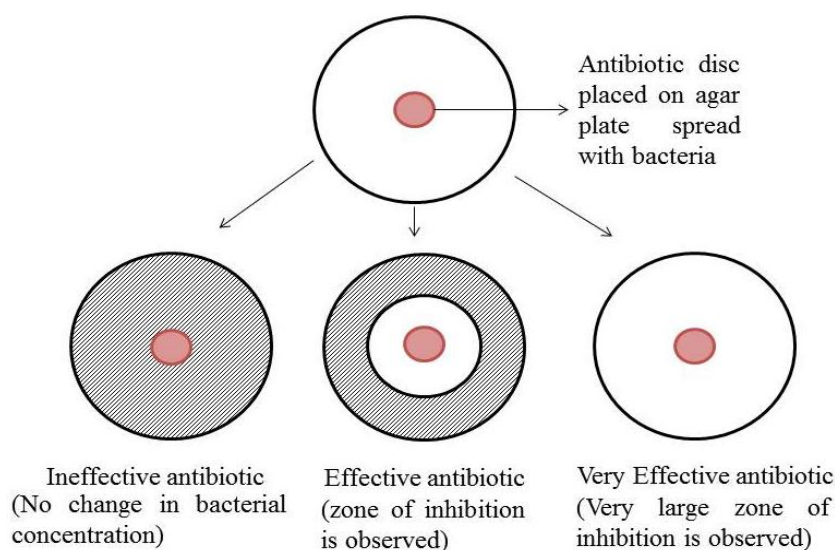


Fig. 10.1 Representation of disc diffusion method

Steps involved in the *in vitro* antibacterial studies

Steps involved in the *in vitro* antibacterial studies are described as follows

Mueller-Hinton agar (MHA) plate preparation: All the ingredients (Beef-300 g, Starch-1.5 g, Casein acid hydrolysate-17.5 g, agar-17 g, pH -7.3, Distilled water-1000 ml) were dissolved in distilled water and autoclaved after closing it with a sterilized cotton ball at 121⁰C for 15 minutes. Then cooled for half an hour and poured into a sterilized petri dish (diameter-90 mm and depth-4 mm) and placed in laminar flow hood

chamber. Allowed the plate to solidify and examined each set of plates for sterility by incubating at 30-35⁰C for 24 h.

Nutrient broth for inoculum preparation: All the ingredients (Peptone -5 g, NaCl-5 g, Beef extract-3 g, Yeast extract-3 g, Agar- 20 g, Distilled water-1000 ml, pH-7.4) were dissolved in distilled water by heating it and take 5-7 ml of the medium in separate test tubes. The test tubes were closed using cotton wool and autoclaved for 15 minutes at 121⁰C.

Inoculum preparation: For the preparation of inoculums growth method is used. From an agar plate culture, four to six isolated bacterial colonies having similar morphology was selected and then the growth is transferred to a tube consisting of nutrient broth (5 ml). Then incubation of the broth culture at 35⁰C was done until it gains the turbidity of 0.5 McFarland standards. Normally 2-6 hours will take to produce turbidity.

Disc preparation: Three Schiff base ligands, its La(III), Nd(III) and Sm(III) complexes and standard antibiotic ampicillin were dissolved in DMSO to prepare the stock solutions. It is then diluted to obtain various ranges of concentrations from 100-500 µgdisc⁻¹. Disc diffusion method was utilized to inoculate drug molecules. Using a micropipette samples were inoculated to the discs. Disc containing DMSO (control) was also tested. Discs are then incubated at 37⁰C for 24 h after placing it in a petri dish.

Test plate inoculation: A cotton swab is immersed into the inoculum suspension after controlling its turbidity using a sterile saline solution or broth. Rotate the cotton swab several times in suspension and strongly press it on the walls of the tube above the liquid level in order to remove excess inoculums. Then the inoculum was uniformly swabbed over the surface of Mueller-Hinton agar plate. This process was repeated by streaking and rotating the plate for uniformly distributing the inoculums and then dried for 20 minutes.

Allocation of disc containing samples on inoculated agar plates: Discs containing samples are allocated on the surface of the agar plate by means of forceps and then gently pressed down to attain uniform contact with agar plate. A minimum distance of 30 mm was preserved between the discs. Then the petri dishes were inverted and incubated in air ambience at 35⁰C for 24 h. If the sample (drug) is effective against the bacteria, there will be a region around the bacteria where there is no bacterial growth. This region is called zone of inhibition. Diameter of the zone is measured and compared with zones produced by reference compounds.

***In silico* molecular docking studies**

As a preliminary step Lipinski rule of five was evaluated in all Schiff base compounds to predict the drug like properties and then conducted docking studies. Molecular docking studies were conducted using AutoDock 4.2 program in order to establish the mechanism by which the Schiff base molecules inhibit the growth of bacteria. For this purpose 6 different targets (PDB ID: 1T2P, 3U2D, 2W9S, 1N67, 2ZCO and 4H8E) of one gram-positive bacteria (*S. aureus*) and 7 targets (PDB ID: 1HNJ, 1G2A, 2VF5, 2MBR, 2GT1, 2X5O and 2W6O) of one-gram negative bacteria (*E. coli*) were selected. Ten Schiff bases 2,2'-(5,5-dimethylcyclohexane-1,3-diylidene) bis(azanylylidene)diphenol (DMCHDP), N,N'-(5,5-dimethylcyclohexane-1,3-diylidene) dianiline (DMCHDA), 2,2'-(5,5-dimethylcyclohexane-1,3-diylidene)bis(hydrazine carboxamide) (DMCHHC), 2-((2-hydroxybenzylidene)amino)phenol (2HBAP), 2-(cyclohexylideneamino)phenol (2CHAP), 3-(1-(2-phenylhydrazono)ethyl)pyridine (3PHEP), 2-(1-(pyridine-3-yl)ethylidene)hydrazine carboxamide (2PEHC), 2-(1-(pyridine-3-yl)ethylidene)hydrazine carbothioamide (2PEHCT), 3-((thiophen-2-yl methylene)amino)benzoic acid (3TMAB) and 2-(1-(2-phenylhydrazono)ethyl)pyridine

(2PHEP) were docked with these 13 target proteins. Binding affinities of these molecules in the 4 binding sites of all bacteria (except in 4H8E) were also evaluated.

Lipinski rule of five

Also called Pfizer's rule of five or rule of five. The rule was developed in 1997 by Christopher A. Lipinski. It is a theoretical method to evaluate the drug ability of a chemical compound [50]. This rule is based on the view that an orally active drug will be small and slightly lipophilic. It depicts molecular properties and not predicts pharmacological activity. According to this rule a drug has good oral activity if it satisfies the following conditions

1. Molecular weight < 500
2. Octanol-water partition coefficient $\log P < 5$
3. Less than 5 hydrogen bond donors (total number of NH and OH bonds)
4. Less than 10 hydrogen bond acceptors (total number of N and O atoms)
5. Molar refractivity between 40 and 130

The origin of the name arises from the observation that all are multiples of five.

Softwares used for docking studies

Softwares such as Openbabel, Pymol, AutoDock Tools (MGL Tools), vina.exe and BIOVIA Discovery Studio were used to carry out the docking study.

The software Openbabel is used to interconvert different chemical file formats. Major features are chemical expert system, inter conversion of many chemical file formats, substructure search, based on simplified molecular-input line-entry system (SMILES), fingerprint calculation, 3D coordinate generation, wrappers for Python, Perl, Java, Ruby, C#.

Pymol software is used for chemical visualization and preparation of protein.pdb files for docking. MGL tools were used for preparation of protein.pdb files and

ligand.pdb files for docking. AutoDock [51] has applications in X-ray crystallography, structure-based drug design, lead optimization, virtual screening (HTS), combinatorial library design, protein-protein docking and chemical mechanism studies. Vina.exe is the docking software to execute docking analysis and give binding energy of ligand with protein. In order to derive active sites of protein and docking result analysis, the software Discovery Studio is employed.

Steps involved in docking process

The docking procedure involves the following steps.

Preparation of ligand: Structures of the ligands were drawn using ChemSketch software and saved in MOL format. This is then converted to PDB format using Open babel software. Ten Schiff base compounds were used for docking studies such as DMCHDP, DMCHDA, DMCHHC, 2HBAP, 2CHAP, 3PHEP, 2PEHC, 2PEHCT, 3TMAB and 2PHEP

Preparation of protein: Structures of the proteins were downloaded in PDB format from RCSB PDB web server. Then using Pymol software water molecules and ligands already present in the proteins were removed, hydrogen atoms were added and saved in PDB format. Six target proteins from *Staphylococcus aureus* and seven from *Escherichia coli* were utilized to check the interaction with synthesized ligands. Structures of the target proteins in *S. aureus* and *E. coli* are shown in Fig. 10.2 and 10.3 respectively.

Prediction of active site: Prediction of active sites is important in structure based drug design. Coordinates of binding sites of the proteins were identified using the software BIOVIA Discovery Studio.

Docking: Molecular docking calculations were carried out with the aid of the software AutoDock 4.2 and binding energy of the protein-ligand complexes was obtained.

Visualization of protein-ligand complexes: The protein-ligand complexes were

visualized using the software BIOVIA Discovery Studio. 3D and 2D interaction diagrams of the protein-ligand complexes were obtained. Hydrogen bond interactions such as conventional H bond and non-conventional H bonds, hydrophobic interactions such as amide pi-stacked, pi-pi stacked, pi-sigma, pi-pi T shaped, alkyl and pi-alkyl interactions, electrostatic interactions such as pi-anion and pi-cation interactions, Van der Waals interaction, unfavorable donor-donor and acceptor-acceptor interactions are commonly seen between protein and ligands. Binding affinity of the compound with the target protein is the resultant of all the interactions and binding energy existing between them.

Target proteins in Staphylococcus aureus

Sortase-A, DNA gyrase, dihydrofolate reductase, clumping factor A, dehydrosqualene synthase, undecaprenyl diphosphate synthase are the main target proteins in *Staphylococcus aureus*, which were selected for the present studies.

Staphylococcus aureus sortase-A: Sortases are extracellular transpeptidases of Gram-positive bacteria [52-53]. The function of the enzyme is sorting proteins into the cell wall compartment of gram-positive bacteria, hence named sortases. A C-terminal sorting signal with a conserved LPXTG motif (X denotes any amino acid) is involved in the sorting mechanism. Sortases are of two types, sortase A (SrtA) and sortase B (SrtB). Former one was first separated from *S. aureus* in 1999 and it is also called housekeeping sortases as they are substantial for surface protein sorting and visible in almost all gram-positive bacteria. Transpeptidase Sortase A, with cysteine as the active site will break the sorting signal between threonine and glycine of the LPXTG motif. Sortases have a great role in the cell wall envelope assembly and in bacterial pathogenicity. Thus they are good targets for therapeutic agents that may reduce infections in human because of gram-positive bacteria.

PDB ID	:	1T2P
Classification	:	Hydrolase
Expression System	:	<i>Escherichia coli</i>
Chains present	:	A, B and C
Sequence length	:	146
Ligands present	:	No ligands

DNA gyrase: Topoisomerase is an isomerase enzyme that provokes dramatic change in topology of DNA structure [54-55]. Topoisomerase are categorized as topoisomerase I and topoisomerase II, based on number of strands cut in one phase of action. New topoisomerases, type III and IV have also been discovered recently. DNA gyrase subclass of type II topoisomerase is responsible primarily on DNA replication. Presence of a metal ion and ATP is required for the functioning of topoisomerase II in all the stages. It is a tetrameric enzyme consisting of two Gyr A and two Gyr B subunits, which form an A₂B₂ complex in the active enzyme. Studies on DNA gyrase showed that it has catalytic activity and the shape is like a pair of scissors, with A subunits and B subunits as cutting blades (the breaking–resealing component) and handles (the ATP-driven energy transduction component) respectively. Gyrase cleaves the helix in both strands of closed circular DNA and passes another segment of DNA through the break and at last reseal the broken ends.

PDB ID	:	3U2D
Classification	:	Isomerase/Isomerase inhibitor
Expression System	:	<i>Escherichia coli</i> BL21 (DE3)
Chains present	:	A, B
Sequence length	:	198
Ligands present	:	4-bromo-5-methyl-N-[1-(3-nitropyridin-2-yl)]

piperidin-4-yl]-1H-pyrrole-2-carboxamide(08B),

Magnesium (ii) ion (MG)

Dihydrofolate reductase (DHFR): Dihydrofolate reductase (DHFR) is an enzyme that catalyses the formation of tetrahydrofolate (THF) by the reduction of dihydrofolate (DHF) in the presence of nicotinamide adenine dinucleotide phosphate (NADPH) [56-57]. Also it has a great role in the synthesis of thymidylate, purines, methionine and some other important metabolites. These enzymes are required for the cell proliferation. Thus inhibition of dihydrofolate reductase will results in destruction of intracellular tetrahydrofolate pool and hence prevents biosynthesis of RNA, DNA, thymidine and protein. Due to the wide range of cellular functions they are targets for anticancer and antimicrobial agents.

PDB ID	:	2W9S
Classification	:	Oxidoreductase
Expression System	:	<i>Escherichia coli</i> BL21 (DE3)
Chains present	:	A, B, C, D, E and F
Sequence length	:	161
Ligands present	:	Glycerol (GOL), Trimethoprim (TOP), NADPH, dihydro-nicotinamide- adenine-dinucleotide phosphate (NDP)

Clumping factor A (ClfA): In blood plasma there is a glycoprotein called fibrinogen (Fg) which is present at ~3 mg/ml concentration and had a significant role in coagulation and hemostasis. Six polypeptide chains are present in fibrinogen such as 2 Aa, 2 Bb and 2 γ -chains, that are dimeric and symmetrical. The γ -chain has C-terminal residues which are biologically important. In the process of fibrinogen-dependent platelet adherence and aggregation they interact with platelet integrin α IIb β 3. This C-terminal residue of γ -chain

is also targeted by the pathogenic bacterium *Staphylococcus aureus*, resulting in fibrinogen-dependent cell clumping and tissue adherence. Clumping factor A (ClfA) [58-59] was the first Fg γ -chain-binding *S. aureus* adhesin identified.

PDB ID	:	1N67
Classification	:	Cell adhesion
Expression System	:	<i>Escherichia coli</i>
Chains present	:	A
Sequence length	:	359
Ligands present	:	Magnesium (ii) ion (MG)

Dehydrosqualene synthase (CrtM): The golden carotenoid pigment staphyloxanthin is a virulence factor for *S. aureus*. Dehydrosqualene synthase [60-61] is involved in the synthesis of this pigment. In the synthesis pathway of the pigment two farnesyl diphosphate molecules undergo head to head condensation to synthesize the C30 hydrocarbon dehydrosqualene by the dehydrosqualene synthase (CrtM). Main responsibility of the pigment is that it preserves *S. aureus* against oxidative stress as a result of host immune defense by reactive oxygen species and neutrophils by acting as an antioxidant.

PDB ID	:	2ZCO
Classification	:	Trasferase
Expression System	:	<i>Escherichia coli</i>
Chains present	:	A
Sequence length	:	293
Ligands present	:	Nil

Undecaprenyl diphosphate synthase (UPPS): The role of undecaprenyl diphosphate synthase (UPPS) in the biosynthesis of cell wall of *Staphylococcus aureus* is very

significant [62-63]. There are many essential steps during cell wall biosynthesis. Some of them are formation of farnesyl diphosphate (FPP), reaction between two molecules of isopentyl diphosphate (IPP) and dimethylallyldiphosphate (DMAPP) in the presence of enzyme named farnesyl diphosphate synthase (FPPS), and after that eight isopentyl diphosphate molecules are added to generate undecaprenyl diphosphate (UPP). Undecaprenyl diphosphate synthase catalyse the formation of UPP. Then UPP is hydrolyzed to form monophosphate, it is then converted into lipid I and II resulting in the formation of the cell wall polymer peptidoglycan. Among the proteins mentioned above UPPS is important since it is vital for the formation of peptidoglycan. Also UPPS is not present in human and is an additional merit for the development of good antibacterial agents.

PDB ID	:	4H8E
Classification	:	Transferase/transferase inhibitor
Expression System	:	<i>Escherichia coli</i>
Chains present	:	A
Sequence length	:	256
Ligands present	:	Sulfate ion (SO ₄), Magnesium ion (MG), Farnesyl diphosphate (FPP)

Target proteins in Escherichia coli

The major target proteins in *Escherichia coli* include β -ketoacyl-acyl carrier protein synthase, peptide deformylase, L-glutamine: D-fructose-6-phosphate amidotransferase, murB, heptosyltransferase WaaC, murD and biotin carboxylase.

β -ketoacyl-acyl carrier protein synthase III (ecKAS III): In gram-negative bacteria, type II fatty acid (FAS II) has proved to be a good target. β -ketoacyl-acyl carrier protein synthase (KAS) is a type II fatty acid which is acting as an essential target in the field of

antibacterial drug discovery [64-65]. Three KAS enzymes such as KAS I, KAS II, and KAS III are present in bacteria. The KAS III initiate the starting steps of fatty acid biosynthesis and thus act as most appropriate target for antibacterial drug design.

PDB ID	:	1HNJ
Classification	:	Transferase
Expression System	:	<i>Escherichia coli</i>
Chains present	:	A
Sequence length	:	317
Ligands present	:	Phosphate ion (PO ₄), Malonyl-Coenzyme A (MLC)

Peptide deformylase (PDF): It is a prokaryotic metalloenzyme that is vital for the growth of bacteria [66-67]. This enzyme is not seen in mammalian cells and hence acts as a promising target for the development of potential antibacterial agents. The method of protein synthesis is similar in both mammalian and bacterial cells. The main difference is that *N*-formylmethionine initiates the protein synthesis in bacteria whereas in mammalian cells methionine takes the role of initiator. *N*-formylmethionine is formed through enzymatic transformylation of methionyl-tRNA in the presence of formylmethionine tRNA transferase. The methionine amino peptidase and peptide deformylase consequently remove *N*-formylmethionine of nascent bacterial proteins in successive steps. This cycle of formylation and deformylation is important for the growth of bacteria. Thus it will be a promising target for the development of chemotherapeutic agents.

PDB ID	:	1G2A
Classification	:	Hydrolase
Expression System	:	<i>Escherichia coli</i> BL21 (DE3)

Chains present	:	A, B, C
Sequence length	:	168
Ligands present	:	Actinonin (BB2), Nickel (II) ion (NI)

L-glutamine: D-fructose-6-phosphate amido-transferase: It is also named as glucosamine-6-phosphate synthase (GlcN-6-P synthase). The hexosamine metabolism involves conversion of fructose 6- phosphate into glucosamine 6-phosphate by utilizing glutamine [68-69]. This reaction catalyzed by glucosamine-6-phosphate synthase is irreversible, hence considered as an important step. The vital building unit of bacterial cell wall N-acetyl glucosamine is the final product formed in this pathway. Inactivation of GlcN-6-P synthase even for a short duration is harmful to bacterial cells.

PDB ID	:	2VF5
Classification	:	Transferase
Expression System	:	<i>Escherichia coli</i>
Chains present	:	X
Sequence length	:	608
Ligands present	:	Glucosamine-6-phosphate (GLP)

MurB: This enzyme is important for the survival of bacterial cells [70-71]. They are good targets for antibacterial agents. Enzymes involved in the biosynthesis of peptidoglycan are essential for the survival of bacterial cell wall. The osmotic integrity of the cell is maintained by the peptidoglycan and the lactyl ether connecting units link both peptide and glycan strands. UDP-N-acetylglucosamine is the starting component of peptidoglycan biosynthesis and proceeds through the formation of UDP-N-acetylmuramic acid, which is catalysed by the mur enzymes murA and murB. In the first step enolpyruvyl moiety present in the phosphoenolpyruvate is added to the 3' hydroxyl exist in UDP-N-acetylglucosamine with the help of murA enzyme. In the second step

enol ether is reduced to lactyl ether by using 1 equivalent of NADPH and a proton derived from solvent with the help of murB enzyme.

PDB ID	:	2MBR
Classification	:	Oxidoreductase
Expression System	:	-
Chains present	:	A
Sequence length	:	340
Ligands present	:	Uridine-diphosphate-2(N-acetylglucosaminy) butyric acid (EPU), Flavin-adenine dinucleotide (FAD)

Heptosyltransferase WaaC: The cell membrane prevents contact of cell with external environment. The outer leaflet of the membrane present in gram negative bacteria is created by lipopolysaccharides and hence essential for the growth of cells. The glycosyltransferase named heptosyltransferase WaaC is engaged in the synthesis of inner core region of lipopolysaccharides [72-73]. It catalyzes the addition of the first 1-glycero-d-manno-heptose molecule to one 3-deoxy-d-manno-oct-2-ulosonic acid (Kdo) residue of the Kdo₂-lipid A molecule. These heptose is an important component of the lipopolysaccharides core domain and its absence will cause truncated lipopolysaccharide associated with the deep-rough phenotype causing a greater susceptibility to antibiotic.

PDB ID	:	2GT1
Classification	:	Transferase
Expression System	:	<i>Escherichia coli</i>
Chains present	:	A, B
Sequence length	:	326
Ligands present	:	Nil

Mur D: Enzymes having great role in the peptidoglycan (a vital cell wall polymer of bacteria) biosynthesis are widely known targets for developing selective and efficient antibacterial agents. Cytoplasm is the place where the initial stage of peptidoglycan biosynthesis takes place and a monomeric building block is generated. This is then translocated through the cellular membrane to its outer part, and by glycosyl transfer and transpeptidation reactions incorporated into the growing peptidoglycan macromolecule. UDP-N-acetylmuramoyl-pentapeptide (UDP MurNAc-pentapeptide) is the building block of peptidoglycan, which is synthesized through four consecutive reactions catalysed by the cytoplasmic enzymes named mur ligases (murC, murD, murE and murF) [74-75]. Mur ligases catalyses the attachment of a pentapeptide chain to the terminal carboxyl group present in UDP-N-acetylmuramic acid (UDP-MurNAc). This is taking place through addition of L-Ala, D-Glu, meso-diaminopimelic acid or L-Lys, D-Ala- D-Ala dipeptide catalyzed by murC, murD, murE and murF respectively. Mechanism of operation of all Mur ligases is same. In order to activate the carboxyl group of UDP-N-acetylmuramic acid, one ATP molecule is required. An acyl phosphate intermediate is thus formed and the amino group present in the incoming dipeptide or aminoacid attacks this intermediate to produce a new peptide or aminoacid after eliminating the inorganic phosphate from the tetrahedral intermediate.

PDB ID	:	2X50
Classification	:	Ligase
Expression System	:	<i>Escherichia</i> DH5[alpha]
Chains present	:	A
Sequence length	:	439
Ligands present	:	Sulfate ion (SO ₄), Sulfite ion (SO ₃), Chloride ion (CL), Azide ion (AZI), N-

({3-[(4-(z)-(2,4-dioxo-1,3thiazolidin-5-ylidene)methyl]phenyl)amino)methyl]phenyl}carbonyl)-d-glutamic acid (VSV)

Biotin carboxylase (BC): In the field of drug discovery for antibacterial activity the biosynthetic pathway of type II fatty acid has considerable importance. The multifunctional enzyme acetyl-CoA carboxylase (ACCCase) is biotin-dependent and comprised of three proteins such as biotin carboxylase (BC), biotin carboxylase carrier protein (BCCP) and carboxyltransferase (CT). During the first half of the reaction a carboxyl group is transferred from bicarbonate to biotin of biotin carboxylase carrier protein in the presence of ATP molecule. This is catalyzed by BC. In the second half transfer of carboxyl group from carboxybiotinylated BCCP to acetyl-CoA will take place to form malonyl-CoA. Since biotin carboxylase catalyzes the most important initial step in fatty acid biosynthesis, it is a promising target for antibacterial agents [76-77].

PDB ID	:	2W6O
Classification	:	Ligase
Expression System	:	<i>Escherichia coli</i>
Chains present	:	A, C
Sequence length	:	449
Ligands present	:	4-amino-7,7-dimethyl-7,8-dihydroquinazolin-5(6H)-one (OA3), Chloride ion (CL)

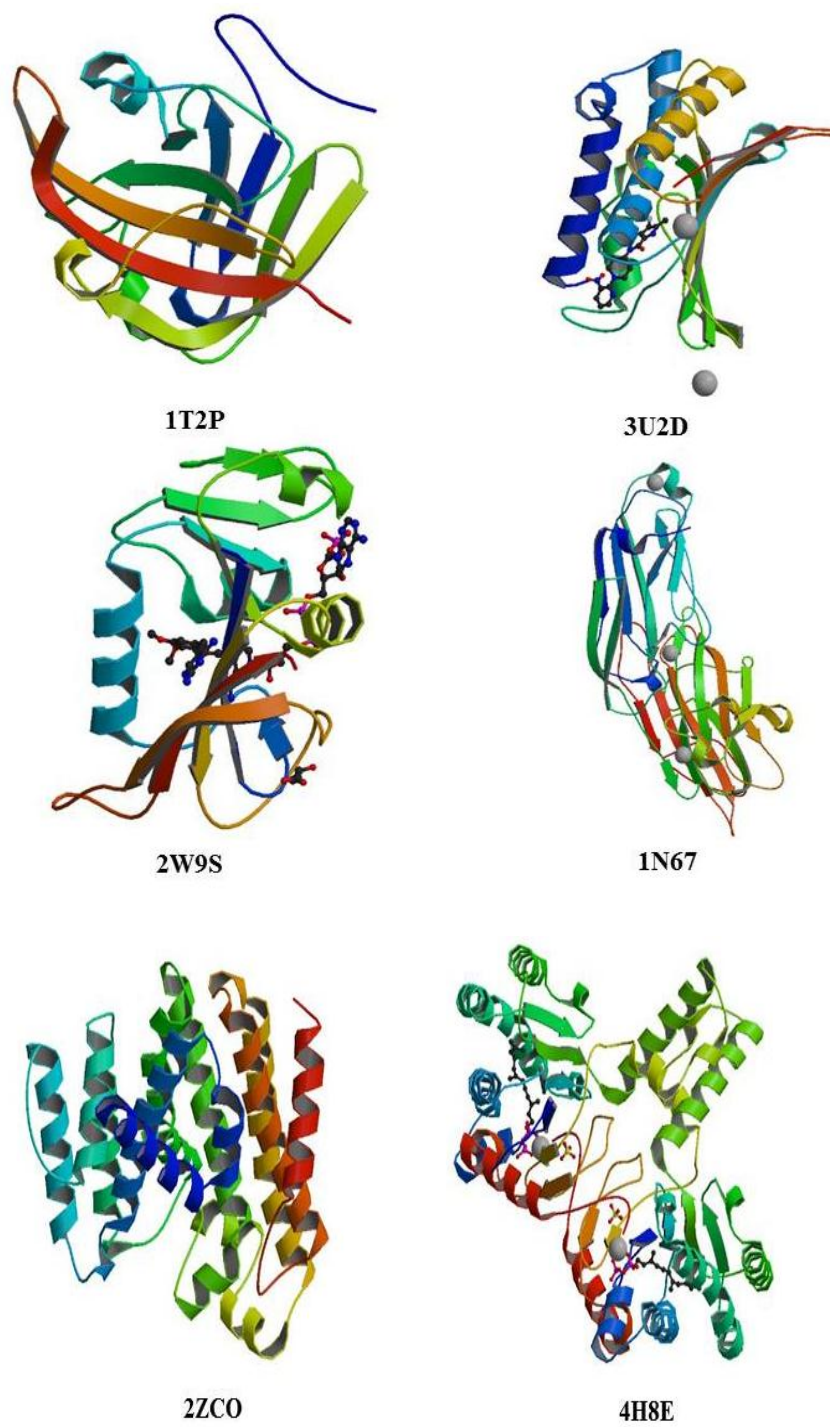


Fig. 10.2 Structures of the target proteins in *S.aureus*

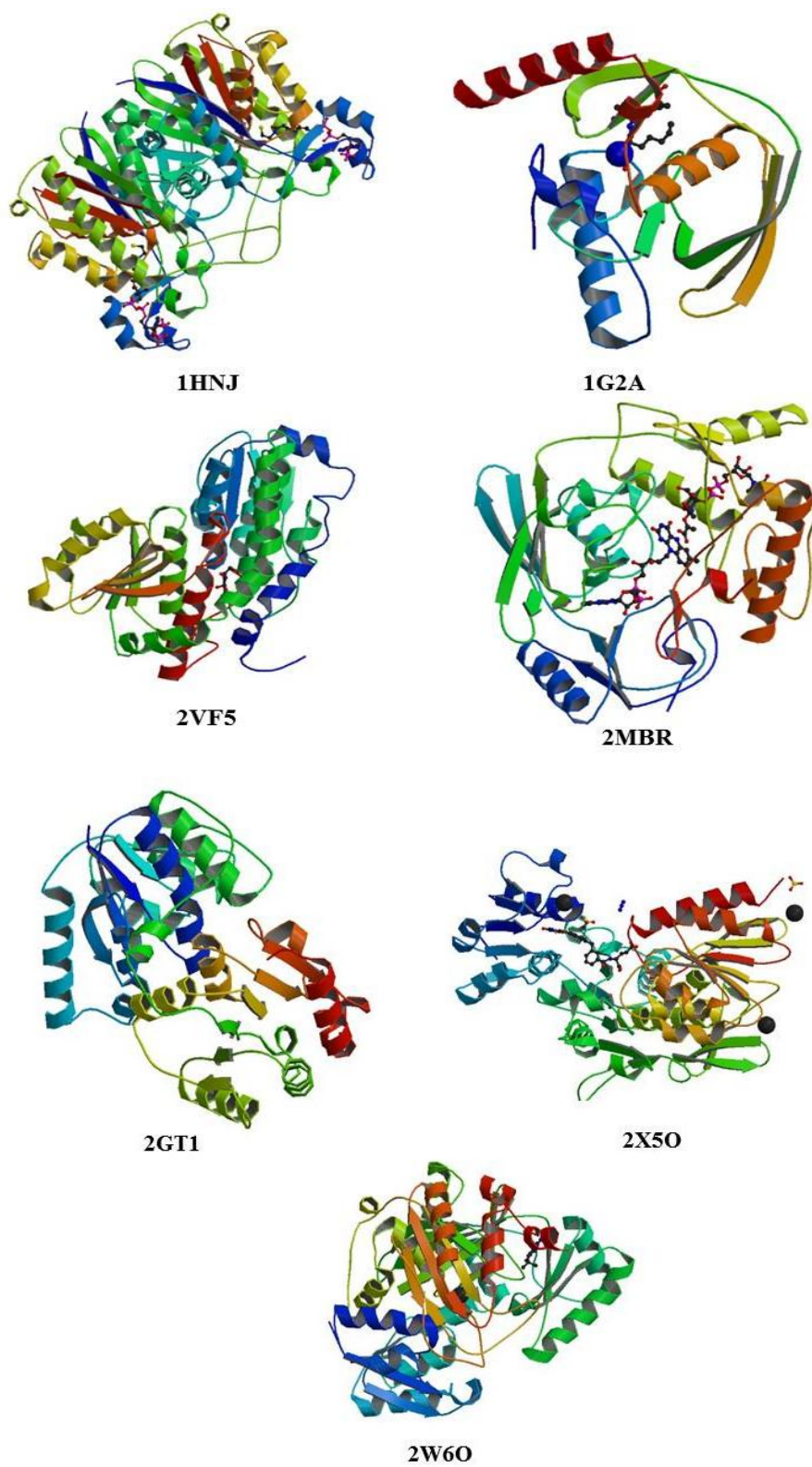


Fig. 10.3 Structures of the target proteins in *E. coli*

CHAPTER 11

***IN VITRO* ANTIBACTERIAL AND *IN SILICO* MOLECULAR DOCKING STUDIES ON SCHIFF BASES AND THEIR INNER TRANSITION METAL COMPLEXES**

This chapter deals with screening of growth inhibitory power of the Schiff bases 2,2'-(5,5-dimethylcyclohexane-1,3-diylidene)bis(azanylylidene)) diphenol (DMCHDP), N,N'-(5,5-dimethylcyclohexane-1,3-diylidene)dianiline (DMCHDA), 2,2'-(5,5-dimethylcyclohexane-1,3-diylidene)bis(hydrazinecarboxamide) (DMCHHC), 2-((2-hydroxybenzylidene)amino) phenol (2HBAP), 2-(cyclohexylideneamino) phenol (2CHAP), 3-(1-(2-phenylhydrazono)ethyl)pyridine (3PHEP), 2-(1-(pyridine-3-yl) ethylidene)hydrazine carboxamide (2PEHC), 2-(1-(pyridine-3-yl)ethylidene)hydrazine carbothioamide (2PEHCT), 3-((thiophen-2-ylmethylene)amino)benzoic acid (3TMAB) and 2-(1-(2-phenylhydrazono) ethyl)pyridine (2PHEP) against *Staphylococcus aureus* and *Escherichia coli*. The *in silico* molecular docking studies were also carried out to understand the mechanism by which the Schiff base compounds inhibit the growth of these two bacteria by selecting suitable targets present in them. Detailed procedures for the synthesis and characterization of Schiff bases such as DMCHDP, DMCHDA, DMCHHC, 2HBAP, 2CHAP, 3PHEP, 2PEHCT and 3TMAB are discussed in the chapters 3 and 8, and reported procedures were adopted for 2PEHC and 2PHEP [78-79]. The *in vitro* antibacterial analysis of the three Schiff base ligands 3PHEP, 2PEHCT, 3TMAB and their La(III), Nd(III) and Sm(III) complexes were also carried out against the pathogens such as *Enterococcus faecalis*, *Enterococcus casseliflavus*, *Pseudomonas aeruginosa* and *Enterobacter hormaechei* apart from the former two bacteria. Disc diffusion method was employed for the *in vitro* antibacterial analysis. Antibacterial

activity of all the ligands and complexes were compared with the activity of the standard drug ampicillin.

***In vitro* antibacterial studies of the Schiff bases**

In vitro antibacterial studies of the Schiff base compounds DMCHDP, DMCHDA, DMCHHC, 2HBAP, 2CHAP, 3PHEP, 2PEHC, 2PEHCT, 3TMAB and 2PHEP against *Staphylococcus aureus* and *Escherichia coli* were carried out at different concentrations such as 50, 100, 250 and 500 μgdisc^{-1} in DMSO. Ampicillin was used as standard antibiotic to compare the activity of synthesized ligands. Antibacterial activity of the Schiff base compounds are shown in Table 11.1.

Table 11.1 Antibacterial activity of the Schiff base compounds

Schiff base	Diameter of zone of inhibition (mm) at different concentrations (μgdisc^{-1})							
	<i>S. aureus</i>				<i>E. coli</i>			
	50	100	250	500	50	100	250	500
DMCHDP	12	16	22	26	12	15	19	22
DMCHDA	10	16	22	25	12	19	20	24
DMCHHC	10	16	20	25	10	19	21	22
2HBAP	9	17	21	22	8	10	14	16
2CHAP	11	15	19	25	9	9	12	15
3PHEP	10	17	20	25	8	12	13	16
2PEHC	7	10	14	17	2	3	10	13
2PEHCT	4	8	8	11	0	1	5	9
3TMAB	10	12	20	24	7	11	13	15
2PHEP	9	16	19	23	8	12	16	18
Ampicillin	15	21	28	30	12	19	21	25

Even though all Schiff bases have less activity than the standard antibiotic, all of them have appreciable growth inhibitory power. Diameter of zone of inhibition exhibited by ampicillin in *S. aureus* and *E. coli* are 30 and 25 mm respectively. Zone of inhibition was found to be increasing with concentration of the ligands. In *S. aureus* maximum zone of inhibition of about 26 mm was shown by DMCHDP and in *E. coli* maximum zone of inhibition of about 24 mm was shown by DMCHDA. Antibacterial activity against both *S. aureus* and *E. coli* was low for the ligands 2PEHC and 2PEHCT.

Fig. 11.1 represents the antibacterial activity of DMCHDP at different concentrations against *S. aureus*.

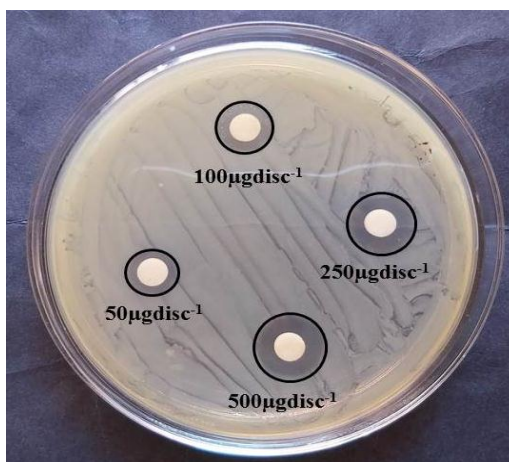


Fig. 11.1 Antibacterial activity of DMCHDP at different concentrations against *S. aureus*

***In silico* molecular docking studies**

In silico approach was used to predict the mechanism by which the Schiff base compounds inhibit bacterial growth. Compounds were first pre- filtered using Lipinski rule of five to check the drug like properties. Parameters such as mass, number of hydrogen bond donors, number of hydrogen bond acceptors, log P (octanol-water partition coefficient), molar refractivity of all compounds were evaluated by Lipinski rule of five and is given in Table 11.2. According to this rule an orally active drug will have fewer than two violations. Results showed that the ligands DMCHDP, DMCHDA, DMCHHC have only one violation and all other ligands have no violation of Lipinski rule. This suggests that these compounds have the potential of acting as an orally active drug.

In molecular docking studies the 3D structures of the compounds were docked with four active sites of the target proteins, PDB ID 1T2P, 3U2D, 2W9S, 1N67, 2ZCO and two active sites of the target proteins, PDB ID 4H8E of *Staphylococcus aureus* and with four active sites of the target proteins, PDB ID 1HNJ, 1G2A, 2VF5, 2MBR, 2GT1,

2X5O, 2W6O of *Escherichia coli* with the aid of AutoDock 4.2. Parameters such as binding energy, number of conventional hydrogen bond (HB) interactions and other interactions were used to determine the best binding mode.

Table 11.2 Lipinski rule of five

Parameters	Mass	Hydrogen bond donor	Hydrogen bond acceptor	log P	Molar Refractivity	
Limiting value for drug like property	<500	<5	<10	<5	40-130	
Schiff base	DMCHDP	322	2	4	5.15	98.03
	DMCHDA	290	0	2	5.74	94.7
	DMCHHC	254	6	8	0.24	67.94
	2HBAP	213	2	3	2.84	63.46
	2CHAP	189	1	2	3.42	58.28
	2PEHC	164	3	5	0.08	44.55
	3PHEP	211	1	3	2.91	66.51
	2PEHCT	180	3	4	0.24	51.75
	3TMAB	231	1	3	3.19	64.97
	2PHEP	211	1	3	2.91	66.51

Docking studies of Schiff base compounds with targets in Staphylococcus aureus

Binding affinity of the ten Schiff bases in the four sites (except in 4H8E, two sites) of 6 target proteins present in *Staphylococcus aureus* such as sortase-A (PDB ID: 1T2P), DNA gyrase (PDB ID: 3U2D), dihydrofolate reductase (DHFR) (PDB ID: 2W9S), clumping factor A (ClfA) (PDB ID: 1N67), dehydrosqualene synthase (CrtM) (PDB ID: 2ZCO), undecaprenyl diphosphate synthase (UPPS) (PDB ID: 4H8E) were studied. Stability of final protein-ligand complex was evaluated on the basis of two essential criteria: (1) the highest binding energy and (2) number of interactions of the ligand with the active site residues. Highest binding energy and number of interactions of the Schiff base compounds with protein models under study were enlisted in Table 11.3 and 11.4. A ligand can mainly undergo interactions such as Van der Waals, hydrogen bonding, hydrophobic and electrostatic while docking into the active site. From literature it is clear that binding energy has a great role than the number of interactions in predicting the best binding mode.

Table 11.3 Binding energy and number of interactions of Schiff bases, DMCHDP, DMCHDA, DMCHHC, 2HBAP and 2CHAP, docked with target proteins in *S.aureus*

Schiff base	Binding energy and interactions	Target proteins and active sites																					
		1T2P				3U2D				2W9S				1N67				2ZCO				4H8E	
		1	2	3	4	1	2	3	4	1	2	3	4	1	2	3	4	1	2	3	4	1	2
DMCHDP	-BE	7.6	7.5	6.3	6.2	6.7	6.8	6.8	6.9	9.3	9.9	10.3	7	9	9	9	9	8.3	7.8	7.6	8.4	7.8	6.2
	HB	2	2	1	1	1	1	1	0	1	2	1	1	2	2	1	2	2	2	1	3	3	3
	Other	7	5	5	10	8	5	3	6	8	8	14	5	9	7	11	7	6	6	6	6	8	4
DMCHDA	-BE	8	7.3	5.9	6.1	7.2	7.1	7.2	7.1	9.1	10.2	9.5	6.9	8.6	6.6	8.5	8.4	8	5.9	7.1	8.1	7.5	6.2
	HB	0	0	1	0	0	0	0	0	0	1	0	0	1	1	1	1	1	0	0	1	0	0
	Other	7	8	6	6	6	9	7	10	14	9	8	7	8	4	9	8	7	2	6	4	8	8
DMCHHC	-BE	7.1	6.6	5.4	6	6.2	7.2	6.2	7.2	7.8	8.5	7.8	6.2	8.1	8.1	8	8.1	7.5	7	6.2	7.5	7.8	6.2
	HB	4	5	2	3	7	5	7	6	1	3	4	3	5	5	3	5	6	7	2	4	6	2
	Other	7	3	4	7	3	3	3	3	6	6	4	6	8	6	6	8	2	5	4	2	5	9
2HBAP	-BE	7.4	7.4	5.2	5.3	5.8	6.7	7	6.7	7.8	7.7	7.7	7.7	7.3	7.3	7.3	7.2	7.6	6.5	6.5	7	7.8	7.2
	HB	2	2	1	1	0	2	1	0	0	0	0	1	3	2	4	2	2	1	0	1	0	1
	Other	6	7	5	6	2	5	4	4	5	5	5	6	8	3	4	3	7	3	5	5	9	9
2CHAP	-BE	6.8	6.8	5.1	5.7	6.4	6.8	7	6.9	7.4	7.4	7.4	6.5	7	6.9	6.9	6.9	7.7	5.8	7.8	6.5	8.2	8.2
	HB	1	1	1	3	1	1	0	0	0	1	1	1	2	2	1	1	1	3	1	2	1	0
	Other	4	4	3	5	3	6	6	5	6	6	5	5	6	4	4	7	6	4	7	2	7	5

BE- Binding energy in kcal/mol, HB- Conventional hydrogen bond, Other- Other interactions

Table 11.4 Binding energy and number of interactions of Schiff bases, 3PHEP, 2PEHC, 2PEHCT, 3TMAB and 2PHEP, docked with target proteins in *S.aureus*

Schiff base	Binding energy and interactions	Target proteins and active sites																					
		1T2P				3U2D				2W9S				1N67				2ZCO				4H8E	
		1	2	3	4	1	2	3	4	1	2	3	4	1	2	3	4	1	2	3	4	1	2
3PHEP	-BE	6.8	6.7	5.5	5.4	6.8	7	7.3	6.6	7.9	7.8	8	6.6	7.2	7.6	7.5	7.5	7.9	6.3	7.9	6.6	8.2	8.2
	HB	2	2	1	0	0	1	1	1	1	1	1	0	1	0	0	0	0	1	0	2	1	1
	Other	6	5	4	7	4	4	8	6	6	1	6	6	7	7	6	8	8	5	8	3	7	7
2PEHC	-BE	5.8	5.8	4.3	4.8	5.1	5.5	6.1	5.1	6.1	6.3	6.1	6.1	6.3	6.9	6.2	6.9	6.1	5.6	5.7	6.1	6.2	6.3
	HB	6	5	2	3	4	5	2	4	1	3	1	4	4	5	4	5	2	4	1	2	0	0
	Other	4	5	4	4	2	2	1	3	4	2	7	2	3	2	3	2	9	0	4	9	6	5
2PEHCT	-BE	5.1	5	4.2	4.1	4.7	4.9	5.2	5	6.5	6.3	6.4	5.8	5.6	5.6	5.5	5.6	5.7	5	5.3	5.9	6.1	6.1
	HB	3	4	3	2	3	2	2	3	3	3	3	2	3	3	3	3	3	3	1	3	2	2
	Other	3	5	8	8	2	4	5	4	7	7	7	2	4	5	5	7	5	4	5	5	5	4
3TMAB	-BE	6.3	6	4.8	5	5.8	6.1	6.1	6.1	6.7	6.8	7	5.7	7	7	7	7	7.3	5.5	6.6	6.7	6.8	7
	HB	1	0	2	1	3	3	4	2	0	1	2	1	2	3	2	2	1	3	0	2	2	0
	Other	6	3	3	6	4	1	2	4	7	7	8	4	4	7	5	4	6	2	7	4	7	8
2PHEP	-BE	6.8	6.7	5.2	5.3	5.9	7	7.1	7	7.7	7.5	7.9	6.9	7.1	7	6.9	7.1	7.6	6.6	7.5	6.8	7.9	7.8
	HB	2	0	2	1	1	0	0	0	2	1	1	1	1	0	1	1	0	0	0	2	0	0
	Other	4	4	4	5	2	3	6	4	5	6	7	4	7	5	5	6	5	3	9	4	6	7

BE- Binding energy in kcal/mol, HB- Conventional hydrogen bond, Other- Other interactions

Among the interactions conventional hydrogen bond (HB) (more prominent) and hydrophobic interactions are more effective than the others [80-81]. Coordinate values of the four binding sites selected for docking are shown in Table 11.5. Considering the binding energy and number of interactions, the compounds DMCHDP, DMCHDA, 2PEHCT and 2PHEP have high binding affinity towards the target dihydrofolate reductase (DHFR) (PDB ID: 2W9S). Binding affinity of DMCHHC, 2PEHC and 3TMAB was high towards the target clumping factor A (ClfA) (PDB ID: 1N67) whereas 2CHAP and 3PHEP have high affinity towards the target undecaprenyl diphosphate synthase (UPPS) (PDB ID: 4H8E). Dehydrosqualene synthase (CrtM) (PDB ID: 2ZCO) was found to be active target for 2HBAP. Details of binding energy and interactions of the site having highest binding affinity between ligand and target are mainly considered for discussion.

Table 11.5 Coordinate values of active sites in target proteins of *S.aureus*

Active site and coordinates	PDB ID of target proteins of <i>S.aureus</i>						
	1T2P	3U2D	2W9S	1N67	2ZCO	4H8E	
1	x	-17.38	17.99	-0.48	27.16	59.12	27.46
	y	-9.54	-2.66	5.99	42.54	11.62	3.94
	z	-7.59	11.95	33.4	71.29	52.34	8.95
2	x	-10.63	5.99	23.51	17.91	66.37	38.21
	y	-19.54	8.83	-22.25	52.54	-2.12	5.94
	z	-12.59	20.45	30.20	61.04	47.09	4.70
3	x	-13.63	28.99	2.769	25.91	51.62	-
	y	-20.54	-9.16	-23.50	55.54	27.62	-
	z	9.40	9.45	22.45	76.79	62.09	-
4	x	0.37	9.99	-26.23	20.41	59.62	-
	y	-6.04	16.58	9.24	33.29	1.12	-
	z	-28.84	27.20	68.20	70.79	41.34	-

Docking studies of DMCHDP with dihydrofolate reductase (DHFR): From Table 11.3 it is clear that the ligand is more effective in sites 2 and 3 of the target 2W9S with a maximum binding energy of -9.9 and -10.3 kcal/mol respectively. Interaction pattern showed that DMCHDP interacted with the target 2W9S through 2 hydrogen bonds in

active site 2 (LEU20, SER49 residues) and 1 hydrogen bond in active site 3 (ALA7 residue). In the active site 2, first hydrogen bond is formed between nitrogen atom of the Schiff base (-C=N-) and H of LEU20. Second was originated from phenolic H to the N of SER49. In site 3 the hydrogen bond is formed between phenolic oxygen of the ligand and H atom of ALA7 (2.24 Å). Other interactions present in site 2 were carbon H bond (GLN19), alkyl interaction (LEU20, ILE50), pi-alkyl interaction (LYS29) and unfavourable acceptor-acceptor interaction (ILE14). In site 3, apart from conventional H bond non classical H bond, Van der Waals and hydrophobic interactions were also observed. PHE92 and ILE5 residues present in the site 3 of 2W9S interacted by means of pi-pi T shaped and amide-pi stacked interactions respectively. Amino acid residues LEU20 and ILE50 formed two alkyl interactions each and the residues ALA7, ILE31, ILE5 and PHE92 forms pi-alkyl interactions. Considering binding energy and interactions we assume that DMCHDP has more binding affinity towards the site 3 of the target protein 2W9S. Thus the inhibition mechanism of S.aureus by DMCHDP may involve deactivation of the function of dihydrofolate reductase enzyme.

Docking studies of DMCHDA with dihydrofolate reductase (DHFR): DMCHDA is also more effective in sites 2 and 3 of the target 2W9S with a maximum binding energy of -10.5 and -9.5 kcal/mol respectively. In site 2 there is a conventional hydrogen bond interaction with SER49 residue (imine N with H of SER49, 2.06 Å), whereas in site 3 hydrogen bond interaction was absent. In both sites there are three alkyl interactions (ILE50, LEU20), three pi-alkyl interactions (ILE14, ALA7, ILE5) and a pi-sigma interaction (ILE31). The Van der Waals interaction is with ILE14 and PHE92 residue in site 2 and 3 respectively. In addition to these interactions there is an amide pi-stacked interaction with ASN18 in site 2. Considering binding energy and interactions we assume that DMCHDA has more binding affinity towards the site 2 of the target 2W9S.

Thus DMCHDA also deactivate dihydrofolate reductase enzyme preferentially than the other five enzymes.

Docking studies of DMCHHC with clumping factor A (ClfA): In the case of DMCHHC high binding energy of about -8.5 kcal/mol is observed in the active site 2 of 2W9S and -8.1 kcal/mol in the active sites 1, 2 and 4 of 1N67. In the target 2W9S it forms three conventional H bond between H of terminal NH₂ with ASN18 (2.29 Å) and carbonyl oxygen with TYR98 (2.87 Å) and GLN95 (2.35 Å). In addition to this 2 Van der Waals and 4 hydrophobic interactions are also present. In the target 1N67 it makes 5 conventional hydrogen bond interactions with VAL450, HIS252, PRO25, ASP385 residues of site 1, 2 and 4. The H bond is formed between the N atom of imine group with H of HIS252 (2.74 Å), H atom of terminal NH₂ group with carbonyl O of carboxyl group in PRO251 (2.74 Å) and ASP385 (2.43 Å), H atom of terminal NH₂ group with carbonyl O in VAL450 (2.28 Å), H atom of NH group with carbonyl O of carboxyl group in ASP385 (2.08 Å). Number of interactions other than H bond was eight (five alkyl and 3 Van der Waals) for sites 1 and 4 while it is six for second site. The binding affinity was comparable in 2W9S and 1N67. Considering all the factors DMCHHC is slightly more effective against the enzyme Clumping factor A (1N67).

Docking studies of 2HBAP with dehydrosqualene synthase (CrtM): Considering the three factors to select the good binding site, site 1 of 2ZCO may be active for 2HBAP. Binding energy of -7.6 kcal/mol, two H bond between phenolic H of the ligand with carbonyl O in VAL133 (2.94 Å) and GLN165 (2.83 Å), three Van der Waals, six hydrophobic and one electrostatic interaction were observed. Binding affinity in site 4 of 2W9S is also comparable with a binding energy of -7.7 kcal/mol. But only one hydrogen bond interaction and six other interactions are present. Hence 2HBAP is more powerful to deactivate dehydrosqualene synthase (2ZCO).

Docking studies of 2CHAP and 3PHEP with undecaprenyl diphosphate synthase (UPPS): Schiff bases such as 2CHAP and 3PHEP are very effective against the enzyme undecaprenyl diphosphate synthase. Observed binding energy for site 1 of 2CHAP is -8.2 kcal/mol and forms an H bond with ILE92. In addition to this there are 7 other interactions. 3PHEP molecule also has same binding energy value and number of interactions in both sites of 4H8E. In the case of 2CHAP the H bond interaction is between phenolic H with carbonyl O in ILE92 (2.72 Å) whereas in the case of 3PHEP it is between H atom of NH group present in ligand with carbonyl O in ILE92 (2.96 Å). The number of hydrophobic interactions present in 2CHAP and 3PHEP are 5 and 6 respectively. A pi-sulfur interaction is observed between pyridine ring of ligand with S atom of MET32 residue in the case of 3PHEP.

Docking studies of 2PEHC with clumping factor A (ClfA): Highest binding energy of -6.9 kcal/mol was observed in site 2 and 4 of 1N67 upon docking of 3PEHC with this target protein. There are five H bond interactions. H atom of terminal NH₂ group forms three H bond interactions. 1) With O atom of carbonyl group in TYR448 (2.10 Å), 2) with O atom of carbonyl group in SER447 (2.77 Å), 3) with O atom of OH group in TYR399 (2.25 Å). Carbonyl oxygen forms H bond interaction with TYR399 (2.75 Å). N atom in the pyridine moiety forms an H bond with ARG395 (2.76 Å). Also present two pi-alkyl interactions in site 2 and 4 of 1N67.

Docking studies of 2PEHCT with dihydrofolate reductase (DHFR): When 2PEHCT is docked with target protein it is found that the first three sites of 2W9S have highest binding energy of -6.5, -6.3 and -6.4 kcal/mol respectively. Thus it deactivates dihydrofolate reductase. There are 3 conventional H bond and 7 other interactions in all cases. Considering the interactions along with binding energy site 1 is found to be slightly more active than other two sites. The H bond interaction is between pyridine N

with H in ALA7 (2.83 Å), NH hydrogen with phenolic oxygen in TYR98 (2.51 Å) and NH hydrogen with carbonyl oxygen in PHE92 (2.05 Å). All hydrophobic interactions are between pyridine ring of 2PEHCT and amino acid residues of 2W9S. The S atom of the ligand interacts with phenyl ring in TYR98.

Docking studies of 3TMAB with clumping factor A (ClfA): The best binding mode of 2TMAB was observed in site 2 of 1N67 with a binding energy -7 kcal/mol. Three conventional H bond interactions with TYR399, PRO251, ASP385 (between N atom of imine group with H of TYR399 (2.71 Å), H of COOH group with carbonyl O in PRO25 (2.41 Å) and ASP385 (2.68 Å)) and seven other interactions were observed in this site. On comparing with site 2 of 1N67, the binding energy of site 1 of 2ZCO (-7.3 kcal/mol) and site 3 of 2W9S (-7 kcal/mol) is comparable but less interactions.

Docking studies of 2PHEP with dihydrofolate reductase (DHFR): Same binding energy value of about -7.9 kcal/mol is observed in site 3 of 2W9S and site 1 of 4H8E when 2PHEP is docked with different sites of various target protein in *S. aureus*. Also slightly comparable affinity in site 1 of 2W9S with a binding energy -7.7 kcal/mol is observed. More probability of best binding is in 2W9S due to the presence of conventional hydrogen bond interaction between NH hydrogen with carbonyl O in PHE92 (1.90 Å) and 8 other interactions such as Van der Waals, non-conventional H bond, pi-sigma, pi-alkyl and pi-pi T shaped interaction.

In brief out of 6 target protein the Schiff base compounds are active against 2W9S, 1N67, 4H8E, 2ZCO than IT2P and 3U2D. Maximum binding energy of the ligands varies between -6.5 to -10.3 kcal/mol. Maximum binding energy of -10.3 kcal/mol is observed when DMCHDP was docked with 2W9S. It is observed that DMCHDP and DMCHDA have high binding energy compared to the other Schiff bases. This is attributed to the fact that in the active pockets of the target having large size the

bulky ligands will bind strongly. The ligands 2PEHC and 2PEHCT have lowest binding energy compared to other ligands. This is supported by *in vitro* antibacterial analysis of the ligand molecules. Diameter of zone of inhibition exhibited by DMCHDP and DMCHDA are 26 mm and 25 mm respectively at $500 \mu\text{gdisc}^{-1}$. In the case of 2PEHC and 2PEHCT it is only 17 mm and 11 mm respectively at $500 \mu\text{gdisc}^{-1}$. Total number of interactions is high in the case of DMCHHC and is supportive to the results of Lipinski rule of five. In the case of ligands having high molecular mass the effect of hydrophobic interactions will slightly predominate than conventional hydrogen bond [79]. Table 11.6 and 11.7 indicate the amino acid residues interacted with Schiff base compounds. 3D and 2D interaction diagrams of Schiff bases are shown in Fig. 11.2(a-j) and Fig. 11.3(a-j) respectively. Schiff base compounds derived from 5,5-dimethylcyclohexanone such as DMCHDP, DMCHDA and DMCHHC are found to be active against the target 2W9S. The ligands DMCHDP and 2PHEP are found to occupy in the same active pocket of the target protein 2W9S whereas 2CHAP and 3PHEP will occupy in the same active pocket of the target 4H8E.

Docking studies of Schiff base compounds with targets in Escherichia coli

The binding affinity of the ten Schiff bases in the four sites of 7 targets in *Escherichia coli* such as β -ketoacyl-acyl carrier protein synthase III (ecKAS III) (PDB ID: 1HNJ), Peptide deformylase (PDF) (PDB ID: 1G2A), L-glutamine: D-fructose-6-phosphate amido-transferase (PDB ID: 2VF5), murB (PDB ID: 2MBR), heptosyltransferase WaaC (PDB ID: 2GT1), mur D (PDB ID: 2X5O) and biotin carboxylase (BC) (PDB ID: 2W6O) were studied. Highest binding energies and number of interactions of all Schiff base compounds with protein models under study are enlisted in Table 11.8 and 11.9. Here also the active site and efficiency are predicted on

Table 11.6 Interactions of Schiff bases, DMCHDP, DMCHDA, DMCHHC, 2HBAP and 2CHAP, with amino acid residues present in the binding pockets of various target proteins of *S.aureus*

Schiff base	Active target	Active site	Binding energy (kcal/mol)	Interactions	Amino acid residue
DMCHDP	2W9S	3	-10.3	Van der Waals Hydrogen bond Hydrophobic	ILE14, GLY15, VAL6, LYS45 ALA7 (HB-2.24 Å), THR46 (NCHB-3.28 Å) PHE92 (π -T-5.02 Å), ILE5 (amide- π stack -3.92 Å), LEU20 (R- 4.36 Å), LEU20(R-4.31 Å), ILE50 (R-4.43 Å), ILE50 (R- 4.51 Å), ALA7 (π -R-5.17 Å), ILE31(π -R -5.18 Å), ILE5 (π -R- 4.95 Å), PHE92 (π -R- 4.27 Å)
DMCHDA	2W9S	2	-10.2	Van der Waals Hydrogen bond Hydrophobic	ILE14 SER49 (HB - 2.06 Å) ASN18 (amide- π stack - 4.09 Å), LEU20 (R- 4.43 Å), LEU20 (R-4.48 Å), ILE50 (R- 4.57 Å), ILE31(π - σ -3.99 Å), ILE5 (π -R - 4.93 Å), ALA7 (π -R - 4.63 Å), PHE92 (π -R - 4.56 Å)
DMCHHC	1N67	1	-8.1	Van der Waals Hydrogen bond Hydrophobic	ILE339, PHE449, ARG395 VAL450 (HB - 2.28 Å), HIS252(HB - 2.74 Å), ASP385(HB - 2.08 Å), ASP385(HB - 2.43 Å), PRO251(HB - 2.74 Å) PRO341(R- 4.43 Å), PRO341(R- 4.68 Å), VAL288(R- 3.43 Å), VAL288(R- 4.08 Å), VAL288(R- 5.13 Å)
2HBAP	2ZCO	1	-7.6	Van der Waals Hydrogen bond Hydrophobic Electrostatic	ASN168, ASP48, TYR41 VAL133(HB - 2.94 Å), GLN165 (HB - 2.83 Å) PHE22 (π -T - 4.90 Å), LEU164 (π - σ - 3.98 Å), VAL137 (π - σ - 3.81 Å), ALA134 (π -R - 5.31 Å), CYS44 (π -R - 5.39 Å), val137 (π -R - 4.80 Å) ARG45(π + - 4.42 Å)
2CHAP	4H8E	1	-8.2	Van der Waals Hydrogen bond Hydrophobic	HIS50, MET32 ILE92(HB - 2.72 Å) ALA76(R- 4.95 Å), PRO96 (R- 4.06 Å), PHE148(π -R - 4.42 Å), PHE99(π -R - 5.29 Å), ILE92(π -R - 5.15 Å)

HB - Conventional hydrogen bond, NCHB – Non-conventional hydrogen bond, π -T - π - π T shaped, amide- π stack- amide- π stacking, R – alkyl, π -R- pi-alkyl, π - σ - pi-sigma, π + - pi-cation, π -stack – pi-pi stacking, π -S – pi-sulfur

Table 11.7 Interactions of Schiff bases, 3PHEP, 2PEHC, 2PEHCT, 3TMAB and 2PHEP, with amino acid residues present in the binding pockets of various target proteins of *S.aureus*

Schiff base	Active target	Active site	Binding energy (kcal/mol)	Interactions	Amino acid residue
3PHEP	4H8E	1	-8.2	Hydrogen bond	ILE92(HB - 2.96 Å)
				Hydrophobic	HIS50(π -stack - 4.83 Å), PHE99(π -T - 5.56 Å), LEU95(amide- π stack - 4.59 Å), PRO96(π -R - 3.86 Å), ALA76(π -R - 4.95 Å), ILE92(π -R - 4.98 Å)
				Pi-sulfur	MET32(π -S - 5.35 Å)
2PEHC	1N67	2	-6.9	Hydrogen bond	ARG395 (HB - 2.76 Å), TYR399 (HB - 2.75 Å), TYR399 (HB - 2.25 Å), TYR448 (HB - 2.10 Å), SER447(HB - 2.77 Å)
				Hydrophobic	VAL288(π -R - 3.71 Å), PRO341(π -R - 5 Å)
2PEHCT	2W9S	1	-6.5	Van der Waals	VAL6
				Hydrogen bond	ALA7(HB - 2.83 Å), TYR98(HB - 2.51 Å), PHE92(HB - 2.05 Å)
				Hydrophobic	PHE92(π -T - 4.95 Å), ILE5(amide- π stack - 4.39 Å), ILE31(π - σ - 3.78 Å), ALA7(π -R - 5.20 Å), ILE5(π -R - 5.21 Å)
3TMAB	1N67	2	-7.0	Pi-sulfur	TYR98(π -S - 5.40 Å)
				Van der Waals	SER447, TYR369, VAL288
				Hydrogen bond	PRO251(HB - 2.41 Å), ASP385(HB - 2.68 Å), TYR399(HB - 2.71 Å)
2PHEP	2W9S	3	-7.9	Hydrophobic	HIS252(π -T - 4.74 Å), PRO341(π -R - 4.25 Å), PRO341(π -R - 4.49 Å)
				Electrostatic	HIS252(π^+ - 3.79 Å)
				Van der Waals	THR46
2PHEP	2W9S	3	-7.9	Hydrogen bond	PHE92(HB - 1.90 Å), ASP27(NCHB - 3.64 Å)
				Hydrophobic	PHE92(π -T - 4.88 Å), LEU20(π - σ - 3.86 Å), ILE31(π - σ - 3.59 Å), ILE14(π -R - 4.90 Å), ILE5(π -R - 5.32 Å), ALA7(π -R - 5.25 Å)

HB - Conventional hydrogen bond, NCHB – Non-conventional hydrogen bond, π -T - π - π T shaped, amide- π stack- amide- π stacking, R – alkyl, π -R- pi-alkyl, π - σ - pi-sigma, π^+ - pi-cation, π -stack – pi-pi stacking, π -S – pi-sulfur

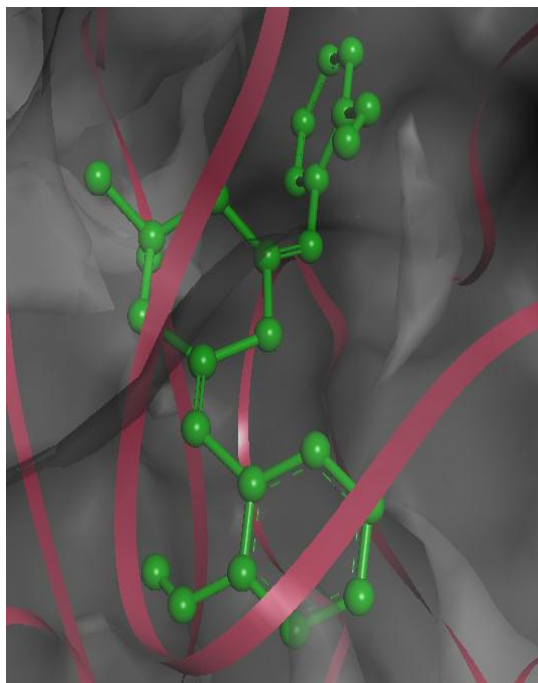


Fig. 11.2a 3D interaction diagram of DMCHDP with active site 3 of 2W9S

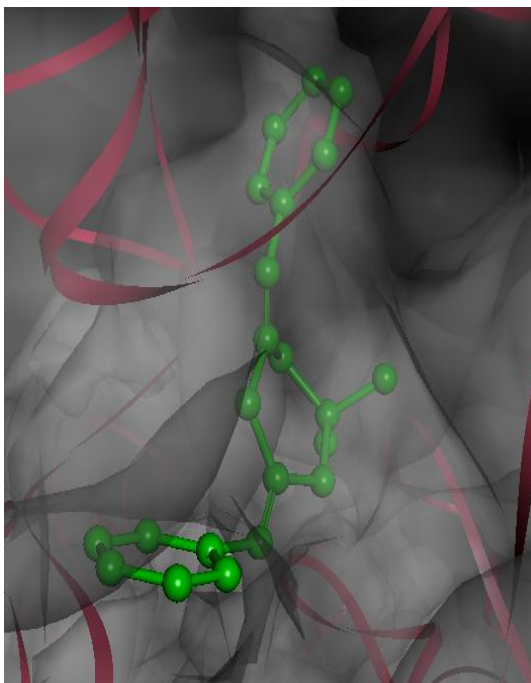


Fig. 11.2b 3D interaction diagram of DMCHDA with active site 2 of 2W9S

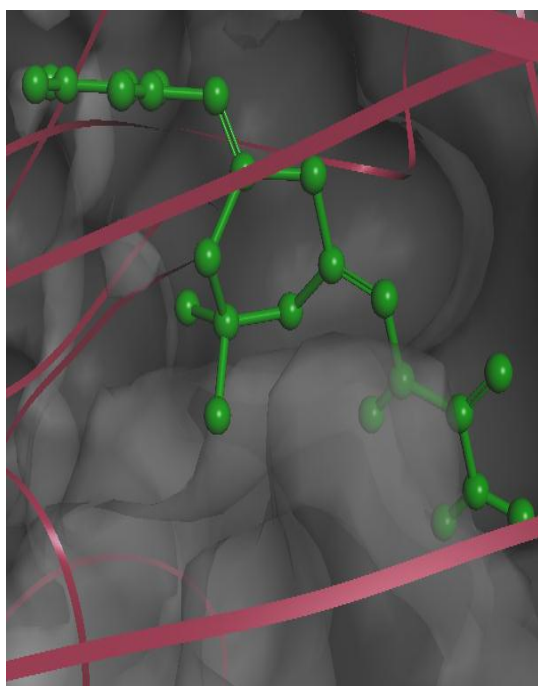


Fig. 11.2c 3D interaction diagram of DMCHHC with active site 1 of 1N67

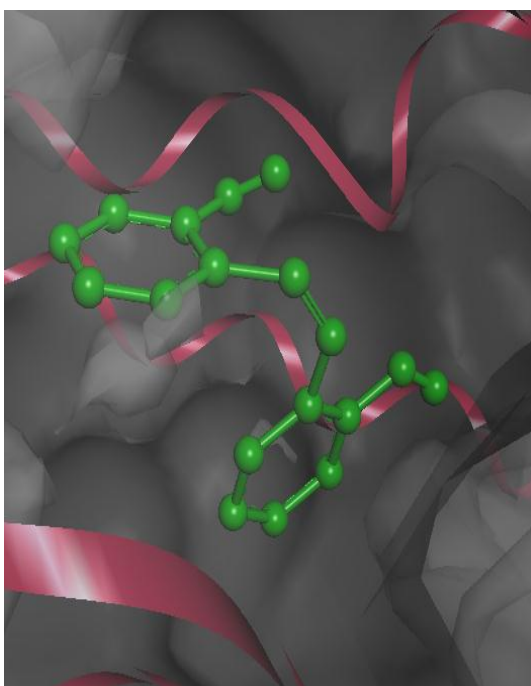


Fig. 11.2d 3D interaction diagram of 2HBAP with active site 1 of 2ZCO

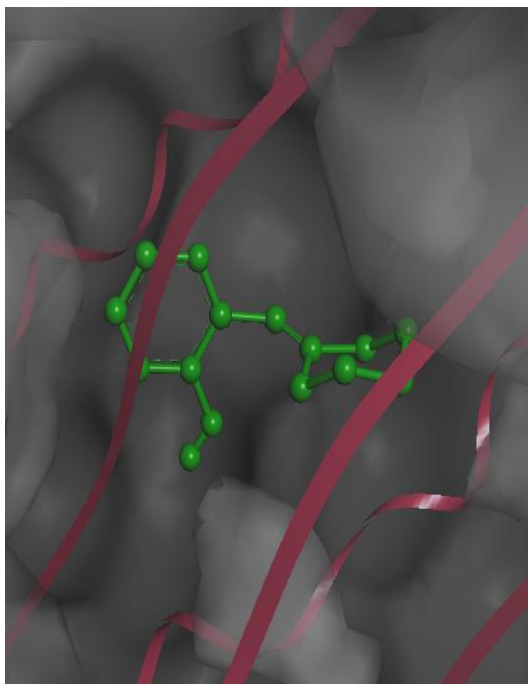


Fig. 11.2e 3D interaction diagram of 2CHAP with active site 1 of 4H8E

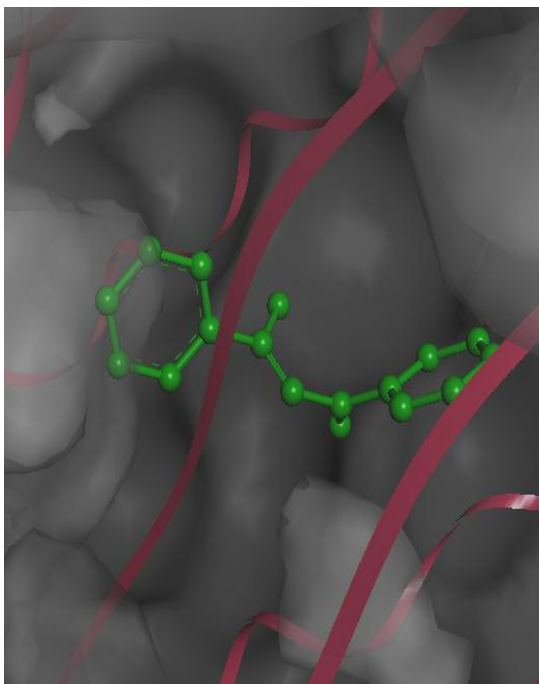


Fig. 11.2f 3D interaction diagram of 3PHEP with active site 1 of 4H8E

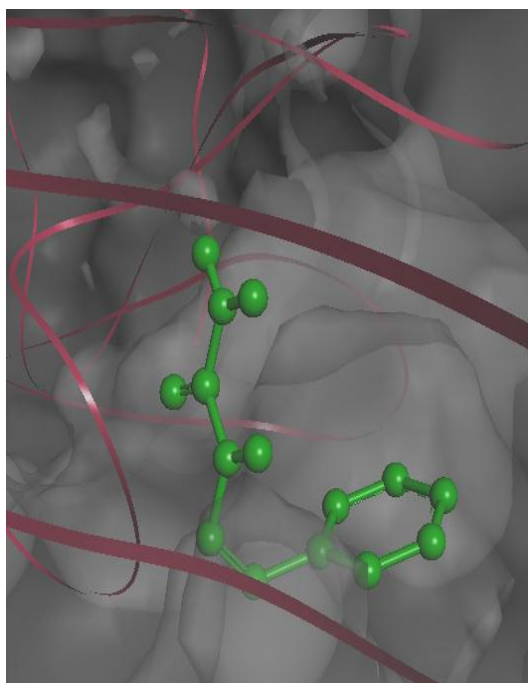


Fig. 11.2g 3D interaction diagram of 2PEHC with active site 2 of 1N67

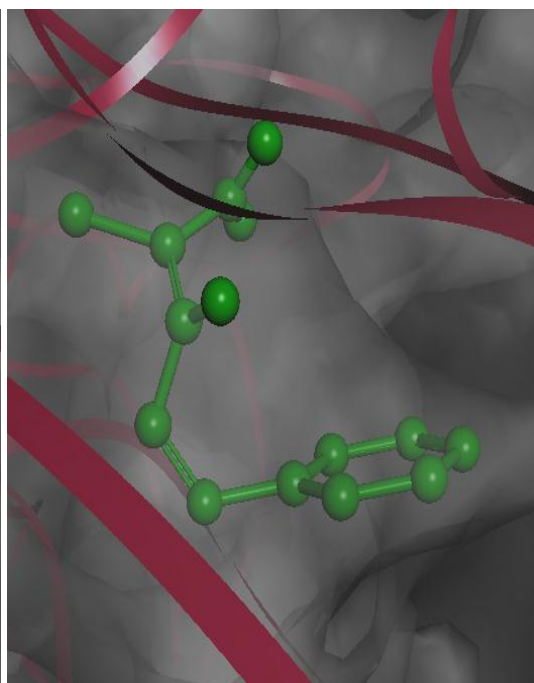


Fig. 11.2h 3D interaction diagram of 2PEHCT with active site 1 of 2W9S

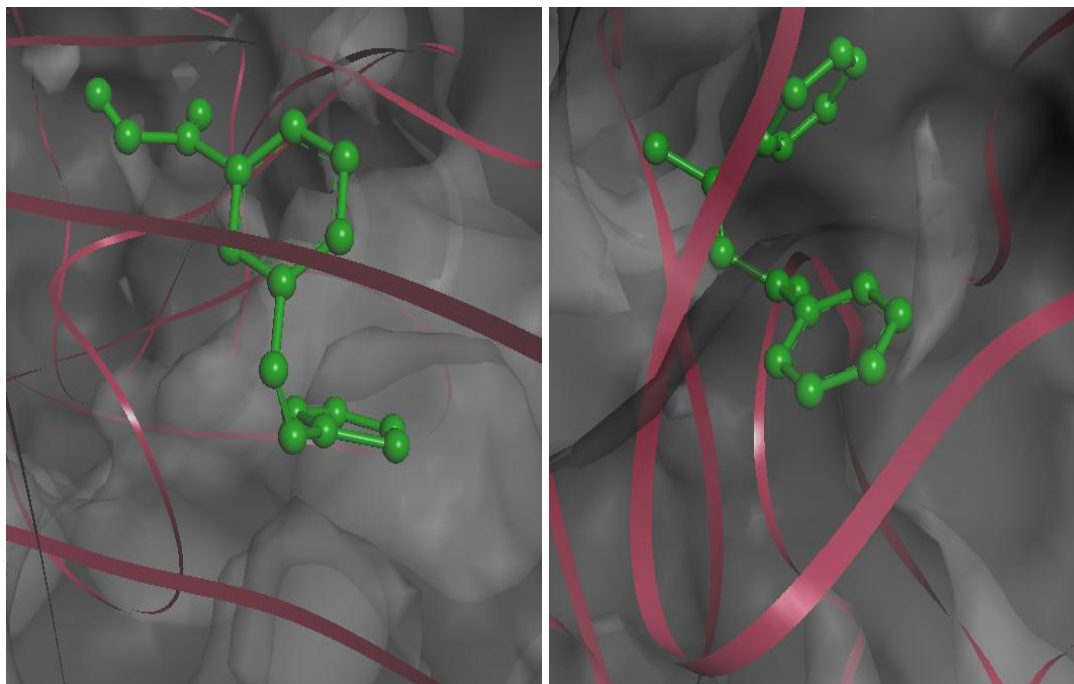


Fig. 11.2i 3D interaction diagram of 3TMAB with active site 2 of 1N67

Fig. 11.2j 3D interaction diagram of 2PHEP with active site 3 of 2W9S

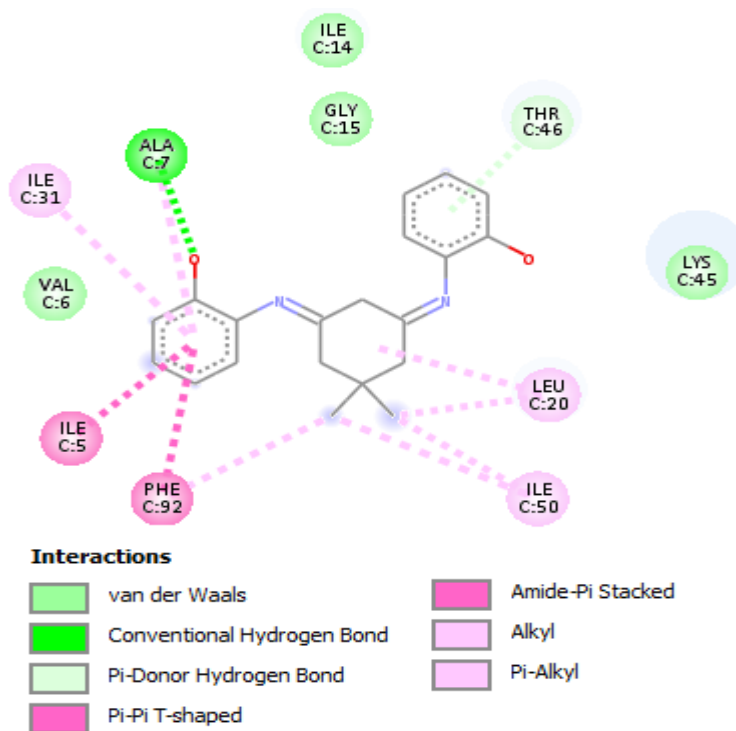


Fig. 11.3a 2D interaction diagram of DMCHDP with active site 3 of 2W9S

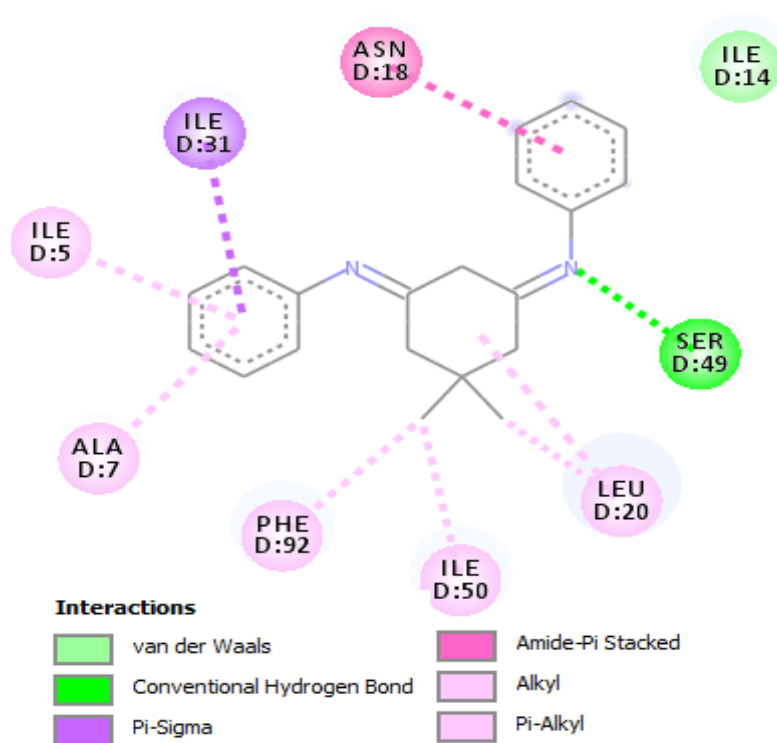


Fig. 11.3b 2D interaction diagram of DMCHDA with active site 2 of 2W9S

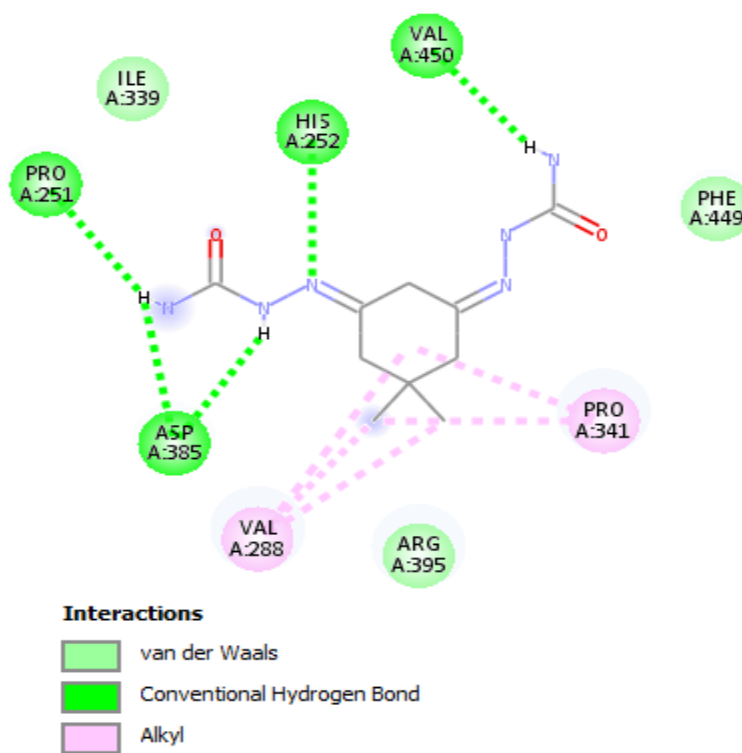


Fig. 11.3c 2D interaction diagram of DMCHHC with active site 1 of 1N67

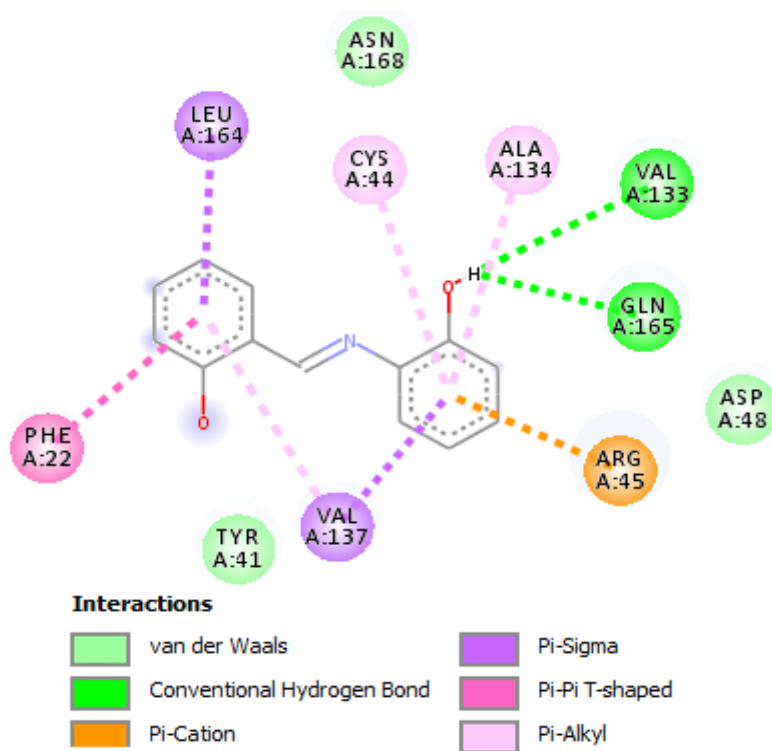


Fig. 11.3d 2D interaction diagram of 2HBAP with active site 1 of 2ZCO

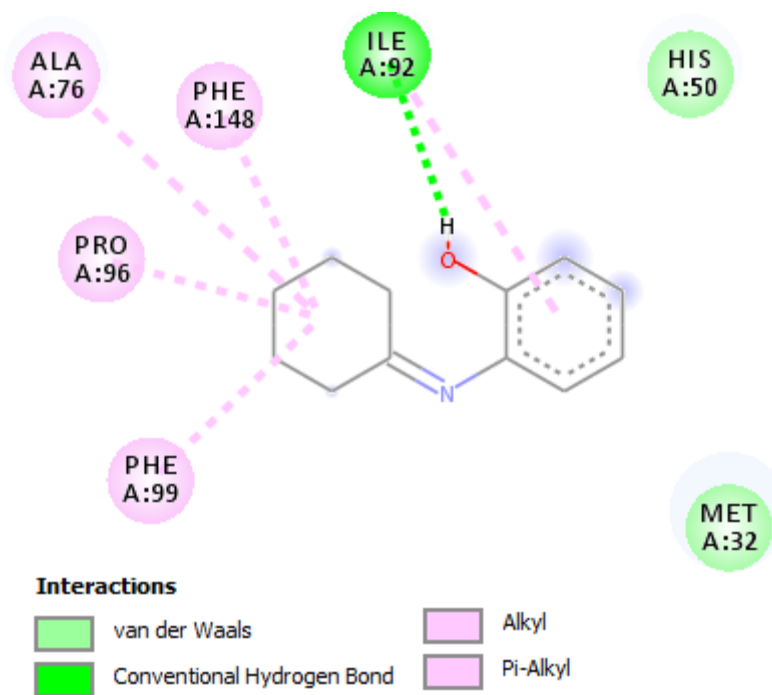


Fig. 11.3e 2D interaction diagram of 2CHAP with active site 1 of 4H8E

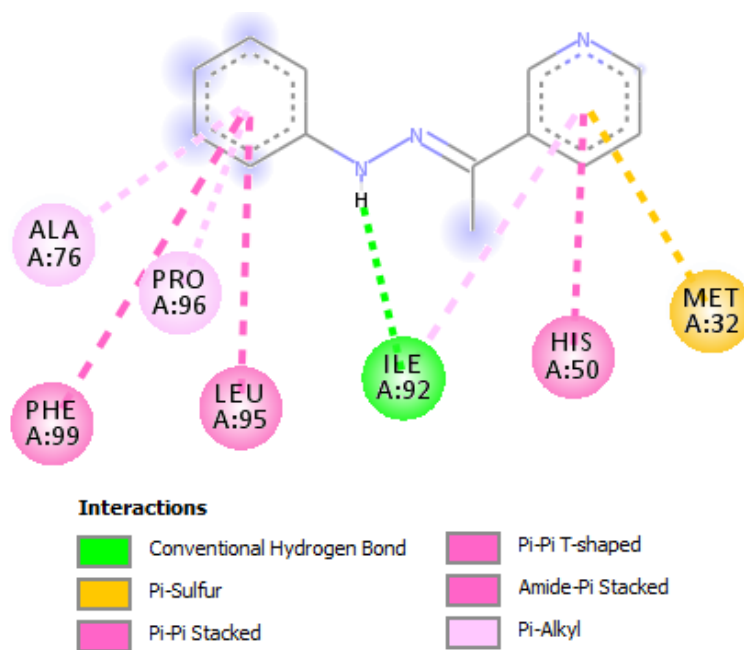


Fig. 11.3f 2D interaction diagram of 3PHEP with active site 1 of 4H8E

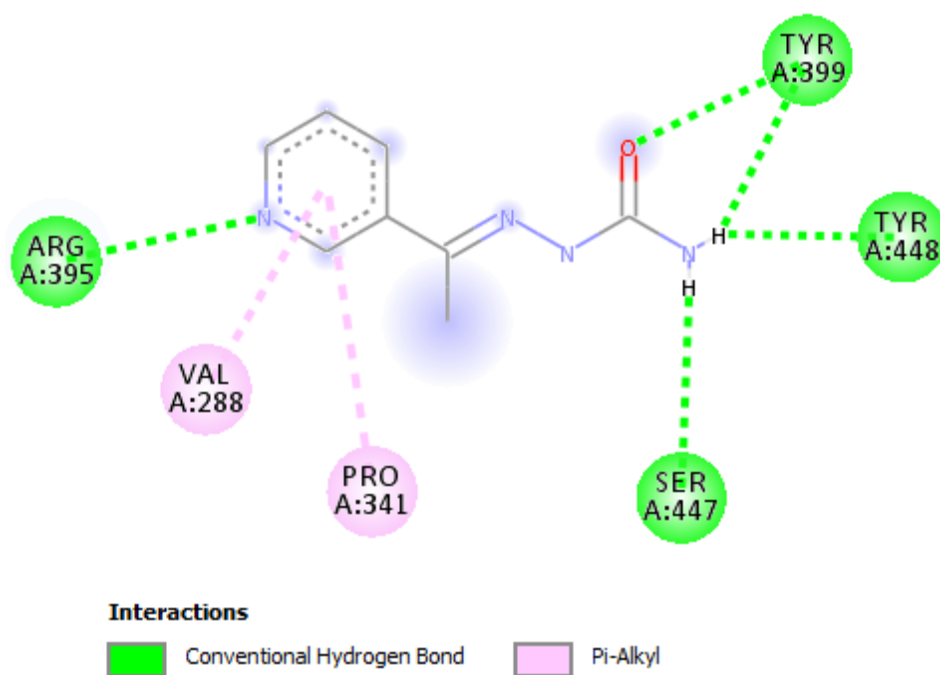


Fig. 11.3g 2D interaction diagram of 2PEHC with active site 2 of 1N67

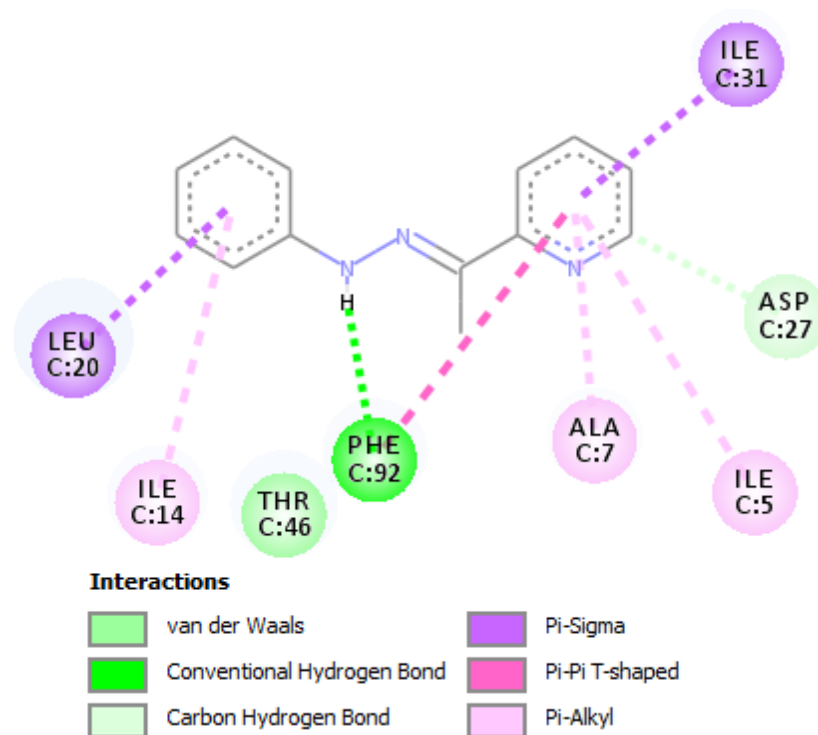


Fig. 11.3h 2D interaction diagram of 2PEHCT with active site 1 of 2W9S

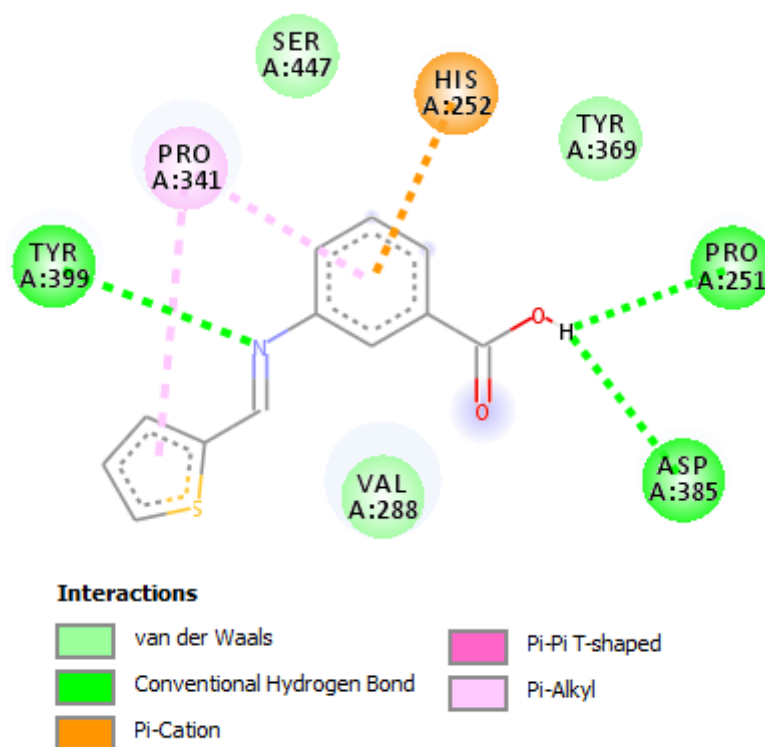


Fig. 11.3i 2D interaction diagram of 3TMAB with active site 2 of 1N67

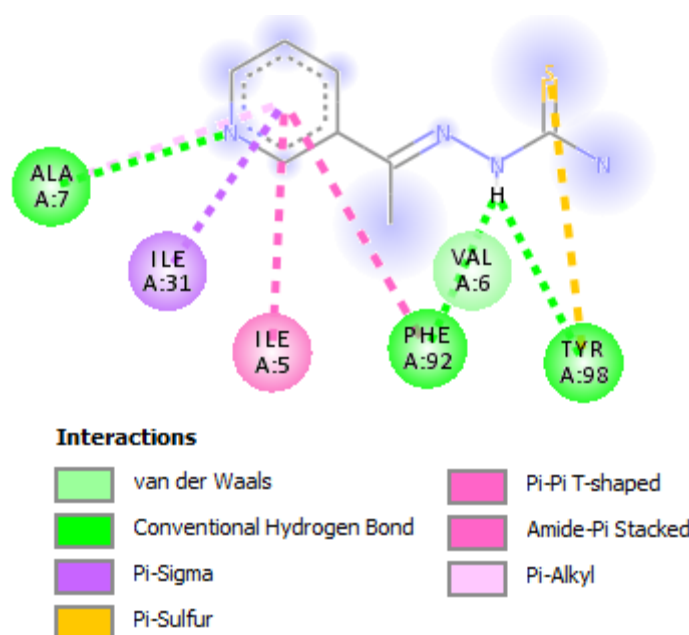


Fig. 11.3j 2D interaction diagram of 2PHEP with active site 3 of 2W9S

the basis of binding energy and interactions. The coordinate values of the four binding sites selected for docking are shown in Table 11.10.

Docking studies of DMCHDP with biotin carboxylase (BC): Highest binding energy of -8.8 and -8.9 kcal/mol is observed in the site 2 and 4 of 2W6O respectively for the ligand DMCHDP. In site 2 there are 2 H bond interactions between N of imine with H of GLY364 (3.08 Å) and phenolic O with GLY364 (2.74 Å) whereas in site 4 only one H bond between phenolic H with ASN340 (1.86 Å). In addition to this 13 other interactions are present in site 2. Hydrophobic interactions such as pi-sigma and pi-alkyl, Van der Waals, pi-donor H bond and unfavourable acceptor-acceptor interaction are present. In site 4 there is only 8 other interactions. So DMCHDP is slightly more active in site 2 than site 4 of 2W6O and deactivate the function of biotin carboxylase.

Table 11.8 Binding energy and number of interactions of Schiff bases, DMCHDP, DMCHDA, DMCHHC, 2HBAP and 2CHAP, docked with target proteins in *E.coli*

Schiff base	Binding energy and interactions	Target proteins and active sites																											
		1HNJ				1G2A				2VF5				2MBR				2GT1				2X50				2W60			
		1	2	3	4	1	2	3	4	1	2	3	4	1	2	3	4	1	2	3	4	1	2	3	4	1	2	3	4
DMCHDP	-BE	8.1	8	6.5	5.8	8.3	7.8	6.8	8	7.8	6.2	7.4	6.8	8.7	8.3	7.3	6.6	7.8	7.6	7.1	7.4	7.5	7.5	7.5	6.9	7.2	8.8	8.7	8.9
	HB	1	3	1	2	0	1	1	4	3	1	0	2	1	1	2	0	1	1	1	2	2	2	2	1	1	2	1	1
	Other	5	9	5	8	5	8	8	5	6	2	6	5	6	7	2	4	6	8	4	9	4	7	4	6	7	13	5	8
DMCHDA	-BE	7.6	7.4	6.5	5.3	8	7.1	6.5	7.1	7.1	6.1	7.1	6.5	9.1	7.8	6.9	6.3	7	7.3	7.3	7.3	7	7	7	6.7	6.7	8.1	8.3	8.3
	HB	1	1	0	0	0	0	0	0	1	1	0	1	1	0	0	0	0	0	1	1	0	0	0	0	0	0	0	0
	Other	4	10	8	7	5	6	6	7	9	5	6	7	7	8	3	4	7	5	5	7	4	4	5	6	4	9	5	5
DMCHHC	-BE	6.7	6.7	6.1	5.7	7.3	7.8	7.8	8	7.7	7.2	6.7	7.8	8.2	7.6	6.4	6.1	7.7	7.1	6.6	5.9	7.2	6.7	6.5	6.4	6.6	8.7	7.1	7.1
	HB	2	3	5	6	7	6	5	8	4	4	3	5	4	2	3	5	5	3	4	6	6	4	5	4	2	3	3	2
	Other	6	3	5	3	6	5	8	6	4	2	6	5	5	5	4	2	5	6	2	2	1	1	4	1	6	9	1	1
2HBAP	-BE	6.9	6	5.6	5.1	6.4	7.1	7.1	6.2	7.2	7.2	6	7.2	7.2	7.2	5.8	6	6.7	5.8	5.8	5.5	6.4	5.9	6	5.9	6.2	7.1	6.2	6.1
	HB	1	2	0	3	1	2	3	1	3	4	1	2	2	2	4	1	1	1	2	1	2	1	1	2	3	0	3	2
	Other	4	7	4	5	8	6	5	6	4	2	4	4	1	2	0	6	5	4	1	7	3	6	7	3	5	3	1	2
2CHAP	-BE	6.7	6.1	5.1	4.9	6.8	6.4	6.4	6.9	6	6	5.8	6	7.5	7.1	5.5	5.8	6.1	6	5.7	5.1	5.7	5	5.5	5.7	5.7	7	6.5	6.5
	HB	2	0	0	0	0	0	1	1	2	1	0	1	1	1	0	0	0	2	0	1	2	0	2	1	0	0	1	1
	Other	3	4	3	2	6	6	4	6	3	2	3	3	5	3	1	6	4	3	3	5	1	3	6	5	3	4	3	4

BE- Binding energy in kcal/mol, HB- Conventional hydrogen bond, Other- Other interactions

Table 11.9 Binding energy and number of interactions of Schiff bases, 3PHEP, 2PEHC, 2PEHCT, 3TMAB and 2PHEP, docked with target proteins in *E.coli*

Schiff base	Binding energy and interactions	Target proteins and active sites																											
		1HNJ				1G2A				2VF5				2MBR				2GT1				2X50				2W6O			
		1	2	3	4	1	2	3	4	1	2	3	4	1	2	3	4	1	2	3	4	1	2	3	4	1	2	3	4
3PHEP	-BE	6.8	6.3	5.4	5	6.6	6.8	6.8	6.8	6.6	6.6	6.3	6.6	7.9	7	6.1	5.7	6.1	6.6	5.7	5.8	6.8	5.9	6	6.2	6.4	7.2	3	6.8
	HB	0	1	0	2	1	1	1	1	2	2	1	2	1	1	3	1	2	0	1	1	3	1	1	0	0	1	1	1
	Other	6	4	8	4	7	4	3	6	4	4	3	5	9	7	2	4	7	4	6	4	4	3	3	8	4	2	5	5
2PEHC	-BE	5.9	5.4	5.1	4.5	6.8	6.6	6.7	6.7	6.5	6.6	5.8	6.5	6.4	5.9	4.8	5	5.7	5.7	5.3	5	5.9	6.1	5.5	5.5	5.3	6.6	6.1	6.1
	HB	3	3	0	1	4	3	4	5	4	3	4	4	3	3	1	1	2	2	4	2	3	4	4	4	1	5	3	4
	Other	6	4	2	2	3	5	5	7	3	1	5	3	1	2	1	4	3	4	1	3	1	4	3	1	4	2	4	3
2PEHCT	-BE	5.3	5	4.8	4.3	5.6	5.7	5.7	5.7	5.8	5.6	5.2	5.8	6	5.6	4.8	5	5.4	4.9	4.8	4.8	5.9	5.1	5.2	4.9	5.2	5.8	5.7	5.6
	HB	1	3	2	2	4	4	4	2	3	5	3	4	4	3	5	1	1	2	3	2	2	2	2	2	3	2	3	3
	Other	6	2	2	4	5	6	6	3	2	0	5	1	1	1	2	4	5	3	2	2	0	4	4	2	2	2	4	3
3TMAB	-BE	5.9	6.1	5.5	5.1	6.5	6.1	6.5	6.4	6.7	6.5	6	6.7	7.2	6.6	5.5	5.6	6.1	6.1	5.4	5.4	6	5.4	6.1	5.4	6.3	6.8	6.2	6.3
	HB	1	2	2	1	1	1	2	2	3	3	2	2	3	1	3	0	2	2	2	1	5	1	2	1	3	2	0	0
	Other	6	4	3	3	9	8	7	7	3	1	5	1	5	6	2	4	5	2	3	2	1	7	3	4	5	3	2	1
2PHEP	-BE	6.7	6.5	5.7	5.2	7.1	6.8	6.8	7.1	6.4	6.4	6.4	6.2	7.6	5.9	5.3	6	6.3	6.4	5.7	5.8	6.6	5.7	5.7	6.2	6.3	6.9	6.8	6.8
	HB	0	1	0	2	2	2	2	2	1	2	1	0	1	1	1	0	0	0	1	1	1	1	1	0	0	1	0	1
	Other	5	7	4	4	7	7	8	7	3	4	5	3	10	4	2	5	8	4	6	7	1	3	7	5	3	4	5	5

BE- Binding energy in kcal/mol, HB- Conventional hydrogen bond, Other- Other interactions

Table 11.10 Coordinate values of active sites in target proteins of *E. coli*

Active site and coordinates	PDB ID of target proteins of <i>E. coli</i>							
	1HNJ	1G2A	2VF5	2MBR	2GT1	2X5O	2W6O	
1	x	26.31	11.47	29.58	2.24	20.56	-3.93	11.86
	y	15.79	-9.03	17.24	11.38	33.89	23.60	1.57
	z	31.30	10.24	-0.64	15.58	56.00	16.79	5.54
2	x	44.56	-9.53	39.08	-7.26	37.81	-20.68	-8.13
	y	21.29	-6.78	6.74	23.63	43.14	23.85	9.32
	z	26.05	33.74	4.35	6.58	60.50	16.79	20.29
3	x	22.06	-2.28	10.83	15.24	-2.43	-19.18	-35.13
	y	31.79	-15.03	29.24	-5.12	50.14	34.85	16.82
	z	17.30	27.24	11.60	15.33	42.50	16.79	37.29
4	x	31.06	45.72	23.58	-6.76	-17.43	-18.68	-20.63
	y	34.54	4.713	15.74	-13.12	41.89	18.35	8.07
	z	4.05	14.74	9.10	20.33	35.25	5.29	38.79

Docking studies of DMCHDA with murB: DMCHDA may inhibit the growth of *E. coli* by deactivating murB enzyme (2MBR). Binding energy, number of conventional hydrogen bond interactions, number of hydrophobic interactions are respectively -9.1 kcal/mol, 1 (N of imine with H of ARG214 (2.67 Å) and 7. Out of seven other interactions, four are alkyl interactions and three are pi-alkyl interactions. Alkyl interaction is between cyclohexanone part of the ligand and the amino acid residues PRO111, ILE110, ILE122 whereas pi-alkyl interaction is between phenyl ring and amino acid residues PRO221, LEU218 and PRO111.

Docking studies of DMCHHC with biotin carboxylase (BC): DMCHHC is more active in site 2 of 2W6O with a binding energy of -8.7 kcal/mol. Three H bond is formed between H atom of terminal NH₂ group with VAL365 (2.74Å) and carbonyl O with ARG33 (2.87Å) and GLY364 (2.11Å). Six hydrophobic interactions arise from the cyclohexanone part of the ligand and also there are three Van der Waals interactions. Thus it deactivates the enzyme biotin carboxylase.

Docking studies of 2HBAP with L-glutamine: D-fructose-6-phosphate amido-transferase: Even though the binding energy of sites 1 and 2 of both 2VF5 and

2MBR are same (-7.2 kcal/mol) when 2HBAP is docked with these target proteins the activity is high against 2VF5 due to large number of interactions. In site 2 of 2VF5 there are 4 H bond interactions (phenolic O with THR302 (2.63 Å), N of imine with SER401 (2.74 Å), phenolic H with ALA602 (2.27 Å) and LYS603 (2.46 Å) and 2 other interactions. Thus it deactivates the function of L-glutamine: D-fructose-6-phosphate amido-transferase in preference to murB enzyme.

Docking studies of 2CHAP and 3PHEP with murB: The ligands 2CHAP and 3PHEP are active in site 1 of 2MBR with a binding energy of -7.5 and -7.9 kcal/mol respectively. Number of H bond interactions is same in both cases whereas other interactions are 5 and 9 respectively for 2CHAP and 3PHEP. H bond is formed with same amino acid residue SER116 by imine N of 2CHAP (2.29 Å) and N in pyridine moiety of 3PHEP (2.26 Å). Both the ligands thus deactivate the function of the enzyme murB.

Docking studies of 2PEHC with peptide deformylase (PDF): Binding energies of -6.6, -6.7 and -6.8 kcal/mol were observed in different sites of the target protein 1G2A when 2PEHC is docked into it. But considering the interactions and applying hypothetical equation it is found that 2PEHC is more active in site 4 of 1G2A where binding energy is -6.7 kcal/mol. Here 5 H bonds are formed between O atom of carbonyl group with LEU91 (1.89 Å) and GLN50 (2.55 Å), NH hydrogen with O of COO group in GLU133 (2.28 Å) and H atoms of terminal NH₂ with same O atom of COO group in GLU133 (1.96 Å) and with O atom of carbonyl group in GLN50 (2.31 Å). In addition there are 7 other interactions present in this site. Here the pi-pi stacking interaction is between pyridine ring and imidazole ring in HIS132 residue. So the deactivating ability of 2PEHC is more prominent against peptide deformylase.

Docking studies of 2PEHCT with peptide deformylase (PDF): It is found that 2PEHCT has comparable activity against both 1G2A and 2VF5. The sites 2 and 3 of 1G2A are found to be equally active with a binding energy of -5.7 kcal/mol and same number of interactions. In 2VF5 sites 1 and 4 are more active. Considering the three factors to select the active site, 2PEHCT has more binding affinity in sites 2 and 3 of 1G2A. In site 2 there are 4 conventional hydrogen bond interactions (H atom of NH group with carbonyl oxygen of GLY89 (2.12 Å), H atom of terminal NH₂ group with carbonyl oxygen of GLY45 (2.30 Å), S atom with H of LEU9 (2.69 Å) and HIS132 (2.98 Å)) and 6 other interaction. As in the case of 2PEHC the pi-pi stacking interaction is between pyridine ring and imidazole ring in HIS132 residue. The sulphur atom present in the ligand undergoes pi-sulfur interaction with imidazole ring in HIS136 residue.

Docking studies of 3TMAB and 2PHEP with murB: Both 3TMAB and 2PHEP are found to be active in site 1 of 2MBR with a binding energy of -7.2 and 7.6 kcal/mol. When 3TMAB is docked into site 1 of 2MBR three H bond interaction were observed between carbonyl oxygen of COOH group and H of GLY47 (1.87 Å), GLY49 (2.01 Å), and GLU48 (2.68 Å), whereas only one H bond (N of pyridine moiety with ASP169(2.29 Å)) is observed in the case of 2PHEP. Number of interaction other than H bond is 5 and 10 respectively for 3TMAB and 2PHEP. Thus they deactivate murB enzyme.

In brief out of 7 target proteins the Schiff bases are more active against the targets 2MBR, 2W6O, 2VF5 and 1G2A than 1HNJ, 2GT1 and 2X5O. Majority of the compounds are more active against murB enzyme (2MBR) and site 1 of the enzyme is most active. Maximum binding energy of the compounds varies between -5.7 to -9.1 kcal/mol. Highest binding energy is observed for DMAN

(-9.1 kcal/mol). The binding energy of DMCHDP, DMCHDA and DMCHHC are high compared to the other Schiff bases. This is also attributed to the high molecular mass. Here also 2PEHC and 2PEHCT have the lowest activity against target proteins compared to other ligands which is supported by experimental data. The diameter of zone of inhibition exhibited by DMCHDP, DMCHDA and DMCHHC are 22 mm, 24 mm and 22 mm respectively at 500 μgdisc^{-1} . But in the case of 2PEHC and 2PEHCT it is only 13 mm and 9 mm respectively at 500 μgdisc^{-1} . The Table 11.11 and 11.12 indicates the amino acid residues interacted with ligands. The 3D and 2D interaction diagram of ligands are shown in Fig. 11.4(a-j) and Fig. 11.5(a-j) respectively. It is observed that the Schiff bases DMCHDA, 2CHAP, 3PHEP, 3TMBA and 2PHEP occupy in the same active pocket of the target 2MBR.

In general, the stability of a protein-ligand complex is proportional to the binding energy. But some complexes which display moderate binding score may have increased number of H bond interactions and hydrophobic interactions. In order to consider the overall affinity of a ligand towards a protein receptor, factors like binding energy, H bond and other interactions have to be taken into account. By analysing the docking result we suggest a hypothetical equation $80\%X+15\%Y+5\%Z$ for predicting the overall affinity of a ligand towards a receptor. Here X=binding energy, Y= number of conventional hydrogen bond interactions and Z= number of interactions other than conventional hydrogen bond.

Table 11.11 Interactions of Schiff bases, DMCHDP, DMCHDA, DMCHHC, 2HBAP and 2CHAP, with amino acid residues present in the binding pockets of various target proteins of *E.coli*

Schiff base	Active target	Active site	Binding energy (kcal/mol)	Interactions	Amino acid residue
DMCHDP	2W6O	2	-8.8	Van der Waals	PHE363, ARG331, TYR391
				Hydrogen bond	GLY364(HB - 2.74 Å), GYY364(HB - 3.08 Å), TYR391(HB - 2.78 Å)
				Hydrophobic	MET302(π - σ - 3.67 Å), ARG366(π -R - 4.71 Å), ARG331(π -R - 5.44 Å), TYR391(π -R - 4.74 Å), PHE363(π -R - 5.14 Å), PHE363(π -R - 4.10 Å), PHE363(π -R - 4.80 Å), TYR391(π -R - 4.63 Å)
				Unfavourable acceptor-acceptor	MET302(2.89 Å)
DMCHDA	2MBR	1	-9.1	Hydrogen bond	ARG214(HB - 2.67 Å)
				Hydrophobic	ILE110(R - 4.54 Å), PRO111(R - 5.35 Å), ILE110(R - 3.70 Å), ILE122(R - 4.74 Å), PRO221(π -R - 5.49 Å), LEU218(π -R - 5.22 Å), PRO111(π -R - 3.82 Å)
DMCHHC	2W6O	2	-8.7	Van der Waals	VAL365, MET302, PHE363
				Hydrogen bond	VAL365 (HB - 2.74 Å), GLY364(HB - 2.11 Å), ARG331(HB - 2.87 Å)
				Hydrophobic	MET302 (R - 5.40 Å), MET302 (R - 4.28 Å), TYR391(π -R - 4.69 Å), PHE363(π -R - 5.03 Å), TYR391(π -R - 5.21 Å), PHE363(π -R - 5.07 Å)
2HBAP	2VF5	2	-7.2	Hydrogen bond	THR302(HB - 2.63 Å), SER401(HB - 2.74 Å), ALA602(HB - 2.27 Å), LYS603(HB - 2.46 Å)
				Electrostatic	GLU488(π - - 4.35 Å)
				Unfavourable donor-donor	SER303(1.26 Å)
2CHAP	2MBR	1	-7.5	Van der Waals	ASN51
				Hydrogen bond	SER116(HB - 2.29 Å)
				Hydrophobic	ILE119 (R - 5.26 Å), ILE45(π - σ - 3.99 Å), ILE173(π -R - 5.18 Å), ILE119(π -R - 5.24 Å)

HB - Conventional hydrogen bond, NCHB – Non-conventional hydrogen bond, π -T - π - π T shaped, amide- π stack- amide- π stacking, R – alkyl, π -R- pi-alkyl, π - σ - pi-sigma, π + - pi-cation, π -stack – pi-pi stacking, π -S – pi-sulfur

Table 11.12 Interactions of Schiff bases, 3PHEP, 2PEHC, 2PEHCT, 3TMAB and 2PHEP, with amino acid residues present in the binding pockets of various target proteins of *E.coli*

Schiff base	Active target	Active site	Binding energy (kcal/mol)	Interactions	Amino acid residue
3PHEP	2MBR	1	-7.9	Van der Waals Hydrogen bond Hydrophobic Electrostatic	GLY115, GLU334 SER116 (HB - 2.26 Å), ILE45(NCHB - 3.42 Å) ILE45(π - σ - 3.81 Å), LEU44 (π -R - 5.33 Å), ARG327(π -R - 4.81 Å), ILE173(π -R - 5.40 Å) ARG327(π + -4.06 Å), ARG327(π + -3.88 Å)
2PEHC	1G2A	4	-6.2	Van der Waals Hydrogen bond Hydrophobic Electrostatic	GLY89, GLY45 LEU91(HB - 1.89 Å), GLN50(HB - 2.55 Å), GLY50(HB - 2.31 Å), GLU133(HB - 1.96 Å), GLU133(HB - 2.28 Å), GLU133(NC - 3.49 Å) HIS132(π -stack - 4.03 Å), ILE44(π -R - 4.87 Å), CYS129(π -R - 4.71 Å) HIS132(π + - 4.33 Å)
2PEHCT	1G2A	2	-5.7	Hydrogen bond Hydrophobic Electrostatic Pi-sulfur Unfavourable donor- donor	GLY45(HB - 2.30 Å), LUE91(HB - 2.69 Å), HIS132(HB - 2.98 Å), GLU89(HB - 2.12 Å) HIS132(π -stack - 4.34 Å), CYS129(π -R - 4.87 Å), ILE44(π -R - 5.45 Å) HIS132(π + - 4.83 Å) HIS136(π -S - 5.69 Å) GLY45(1.92 Å)
3TMAB	2MBR	1	-7.2	Van der Waals Hydrogen bond Hydrophobic Electrostatic	ASN51 GLY47(HB - 1.87 Å), GLU48(HB - 2.68 Å), GLY49 (HB - 2.01 Å) LEU44(π - σ - 3.85 Å), ILE119(π -R - 4.89 Å), ARG327(π -R - 4.67 Å) ARG327(π + - 4.25 Å)
2PHEP	2MBR	1	-7.6	Van der Waals Hydrogen bond Hydrophobic Electrostatic	ILE45, ILE73 ASP169 (HB - 2.29 Å), PHE163(NCHB - 3.59 Å), TYR167(NCHB - 3.56 Å), GLN168(NCHB - 3.55 Å) ILE119(π -R - 5.22 Å), LEU44(π -R - 5.47 Å), ARG327(π -R - 4.63 Å) ARG327(π + - 3.89 Å), ARG327(π + - 3.73 Å)

HB - Conventional hydrogen bond, NCHB – Non-conventional hydrogen bond, π -T - π - π T shaped, amide- π stack- amide- π stacking, R – alkyl, π -R- pi-alkyl, π - σ - pi-sigma, π + - pi-cation, π -stack – pi-pi stacking, π -S – pi-sulfur

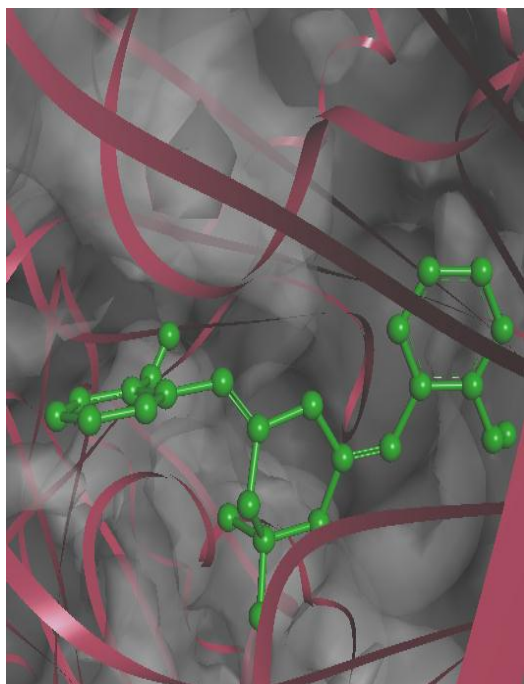


Fig. 11.4a 3D interaction diagram of DMCHDP with active site 2 of 2W6O

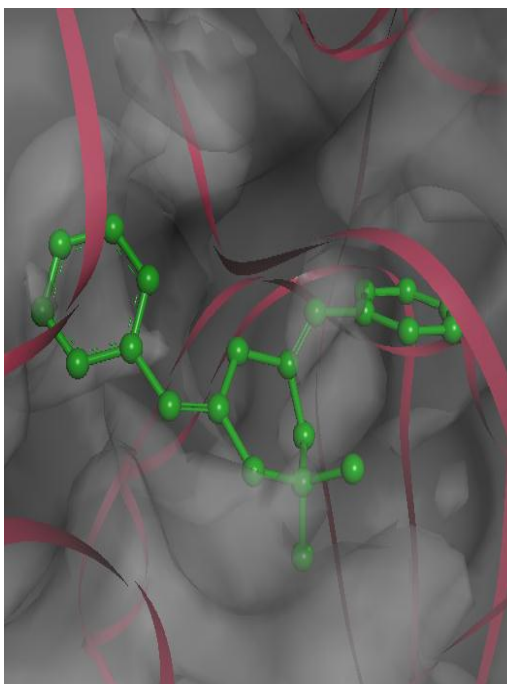


Fig. 11.4b 3D interaction diagram of DMCHDA with active site 1 of 2MBF

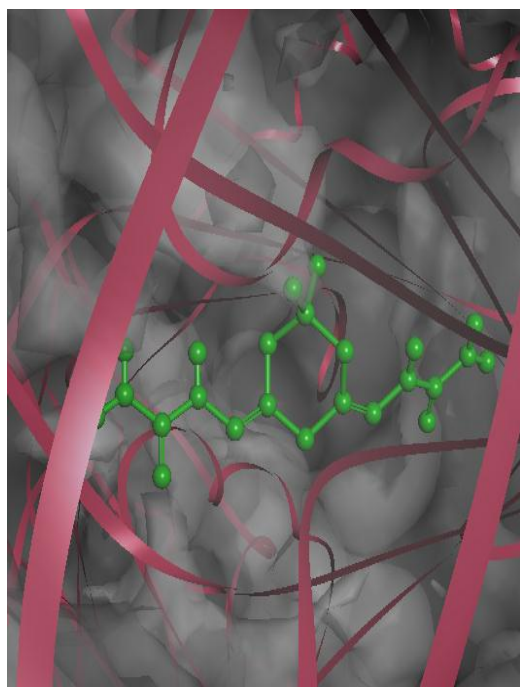


Fig. 11.4c 3D interaction diagram of DMCHHC with active site 2 of 2W6O

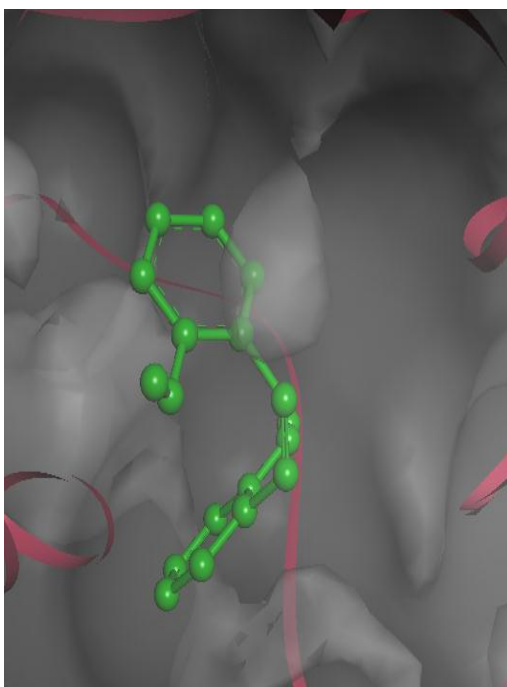


Fig. 11.4d 3D interaction diagram of 2HBAP with active site 2 of 2VF5

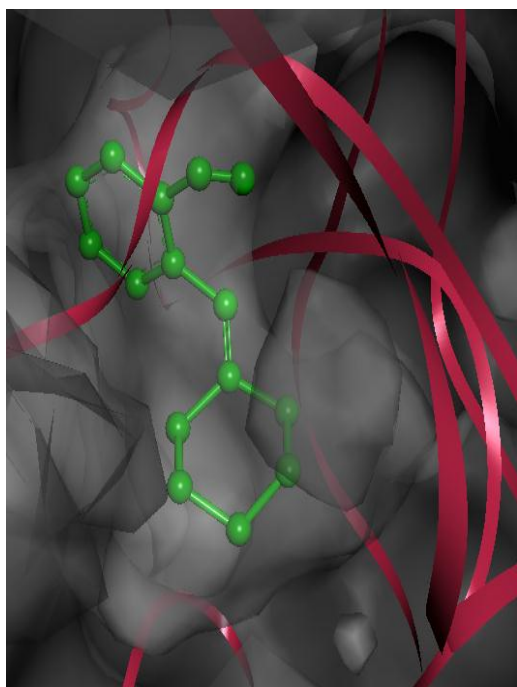


Fig. 11.4e 3D interaction diagram of 2CHAP with active site 1 of 2MBR

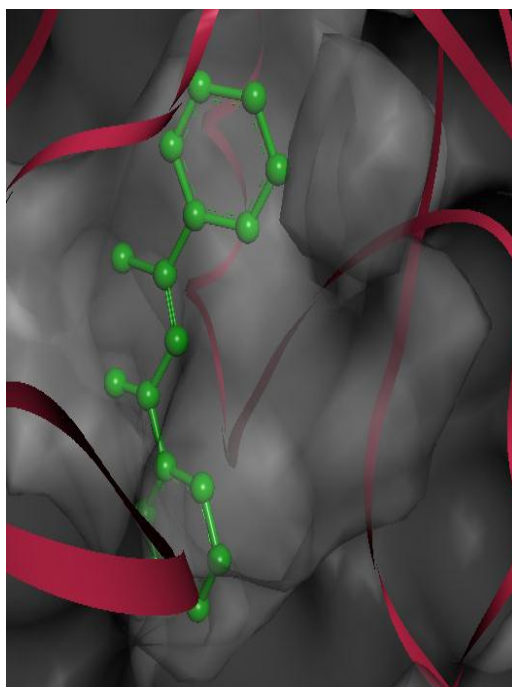


Fig. 11.4f 3D interaction diagram of 3PEHP with active site 1 of 2MBR

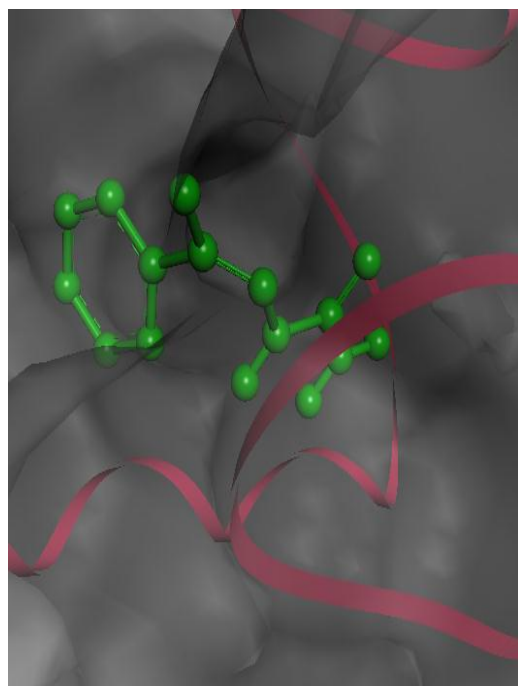


Fig. 11.4g 3D interaction diagram of 2PEHC with active site 4 of 1G2A

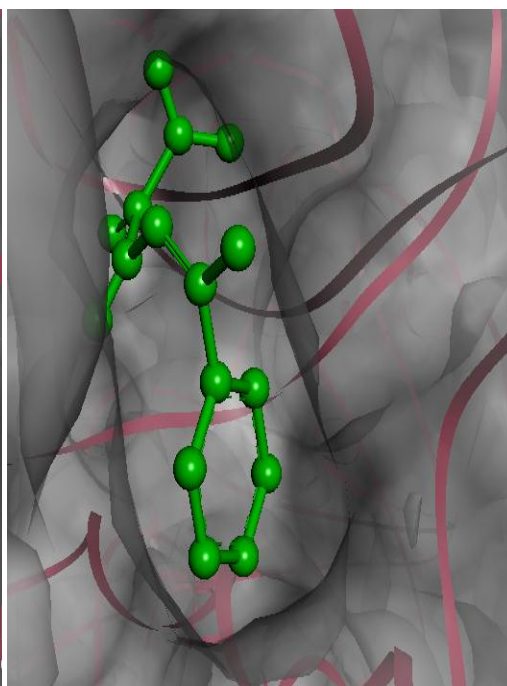


Fig. 11.4h 3D interaction diagram of 2PEHCT with active site 2 of 1G2A

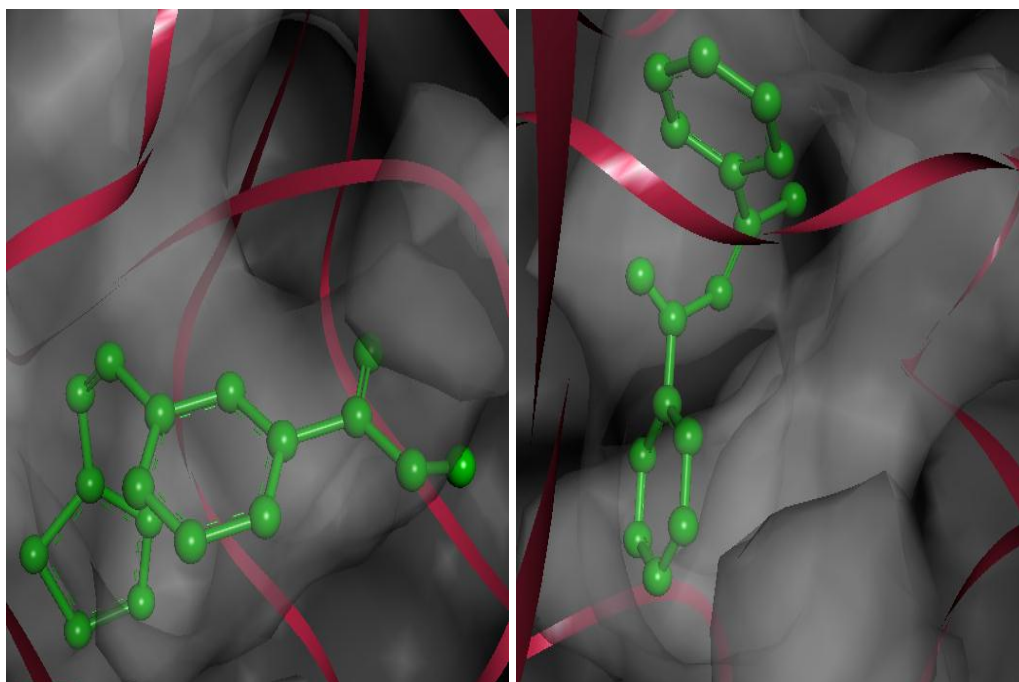


Fig. 11.4i 3D interaction diagram of 3TMAB with active site 1 of 2MBR

Fig. 11.4j 3D interaction diagram of 2PHEP with active site 1 of 2MBR

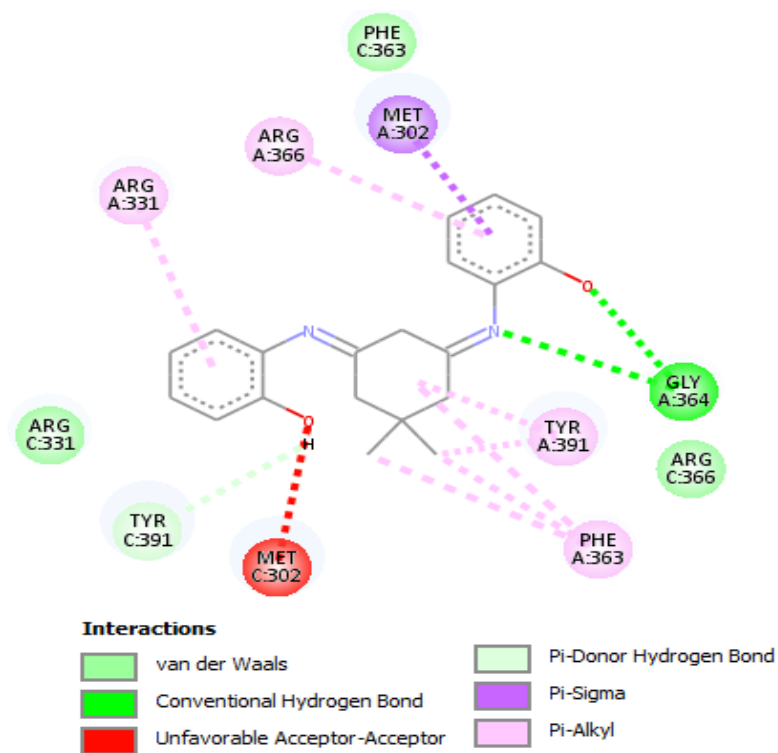


Fig. 11.5a 2D interaction diagram of DMCHDP with active site 2 of 2W6O

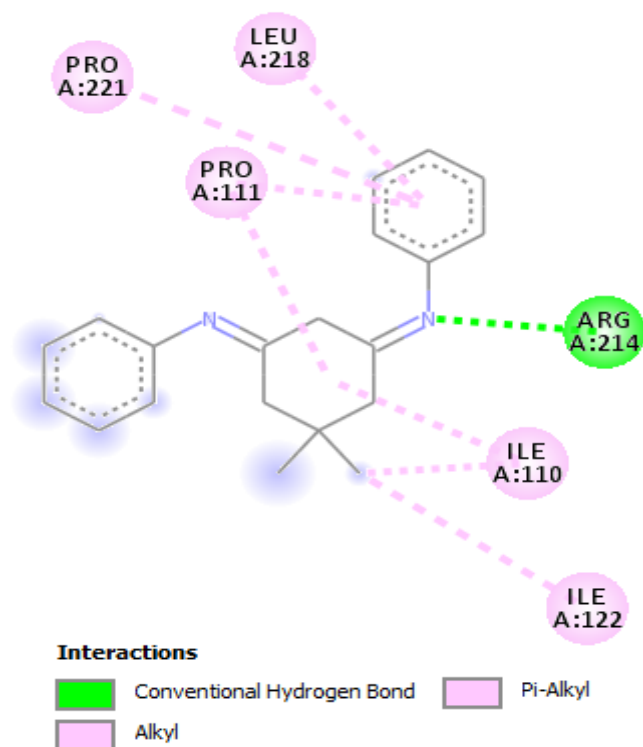


Fig. 11.5b 2D interaction diagram of DMCHDA with active site 1 of 2MBR

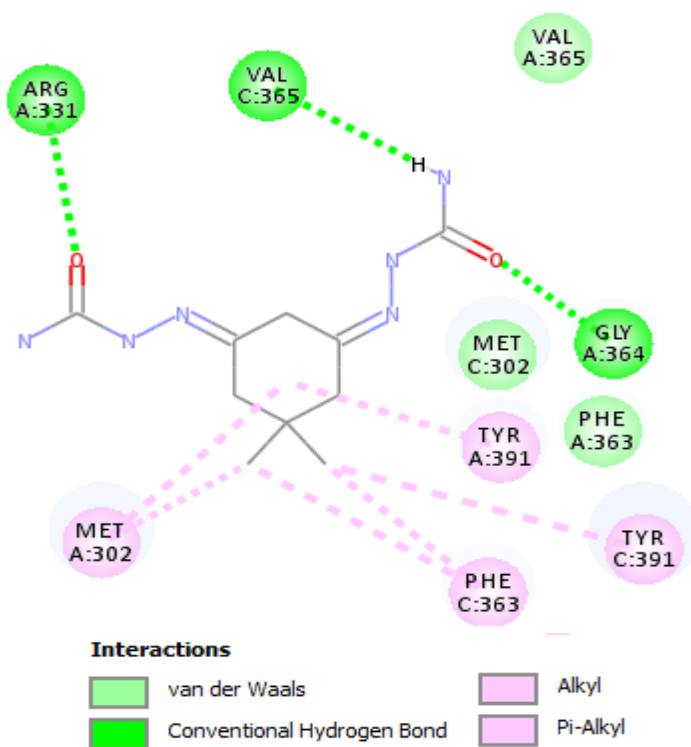


Fig. 11.5c 2D interaction diagram of DMCHHC with active site 2 of 2W6O

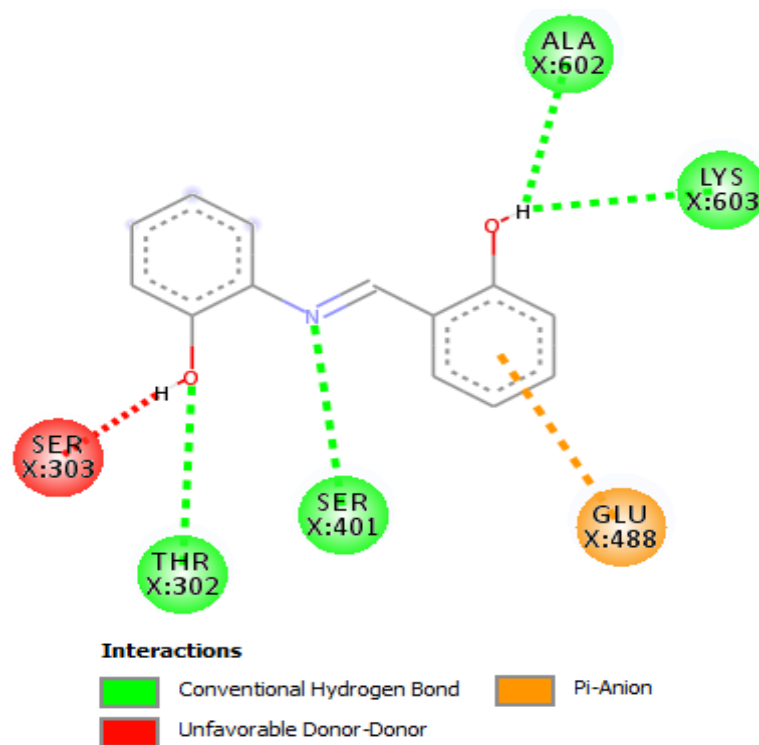


Fig. 11.5d 2D interaction diagram of 2HBAP with active site 2 of 2VF5

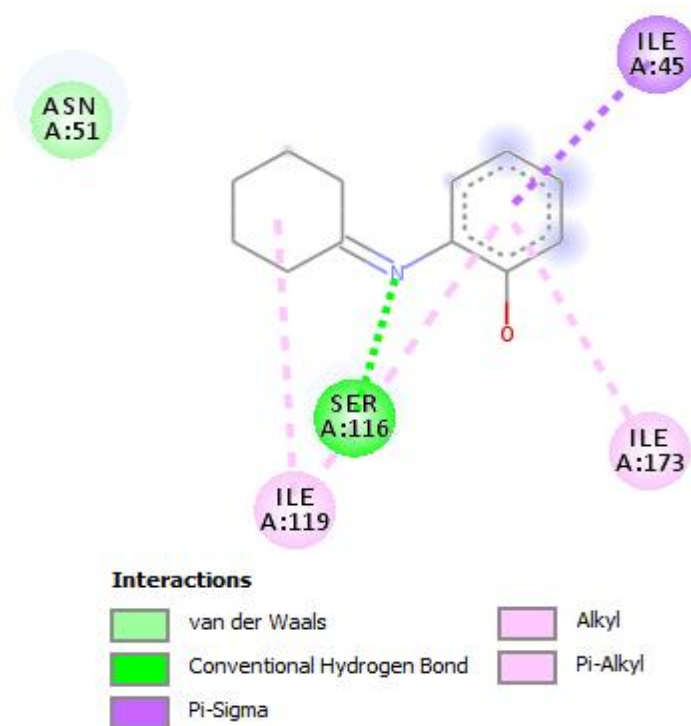


Fig. 11.5e 2D interaction diagram of 2CHAP with active site 1 of 2MBR

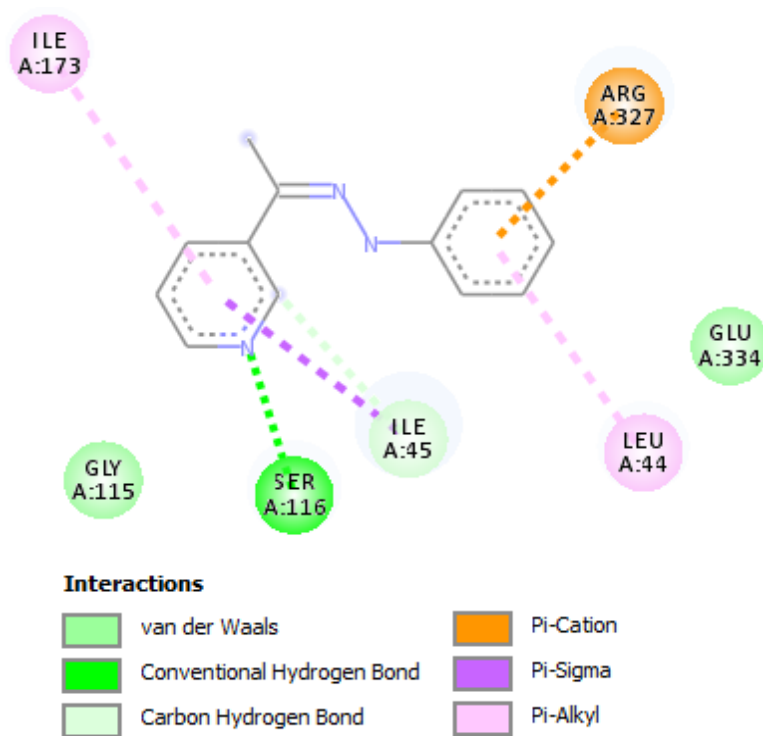


Fig. 11.5f 2D interaction diagram of 3PHEP with active site 1 of 2MBR

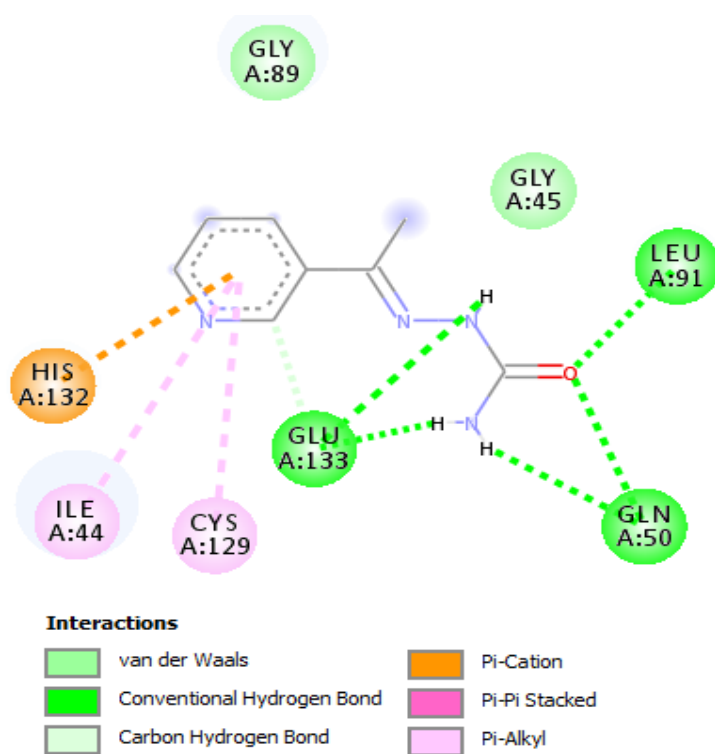


Fig. 11.5g 2D interaction diagram of 2PEHC with active site 4 of 1G2A

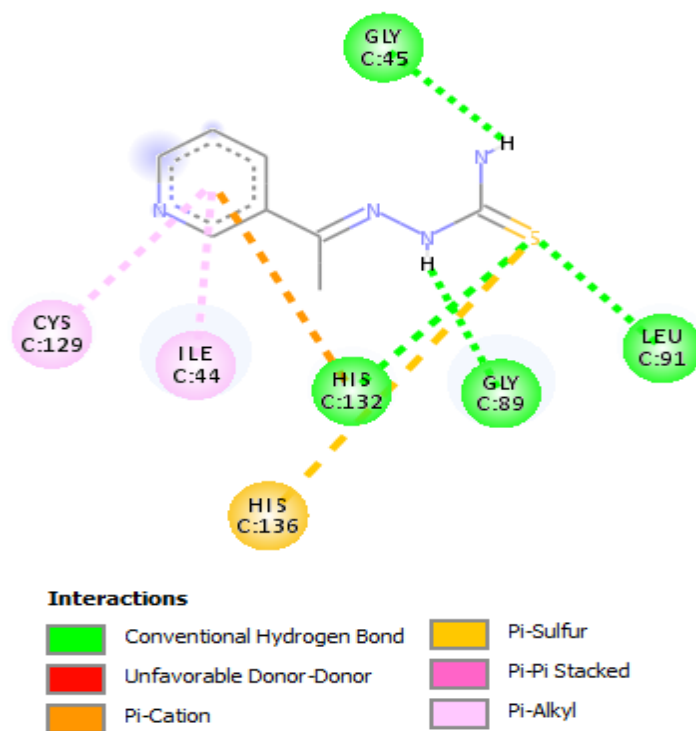


Fig. 11.5h 2D interaction diagram of 2PEHCT with active site 2 of 1G2A

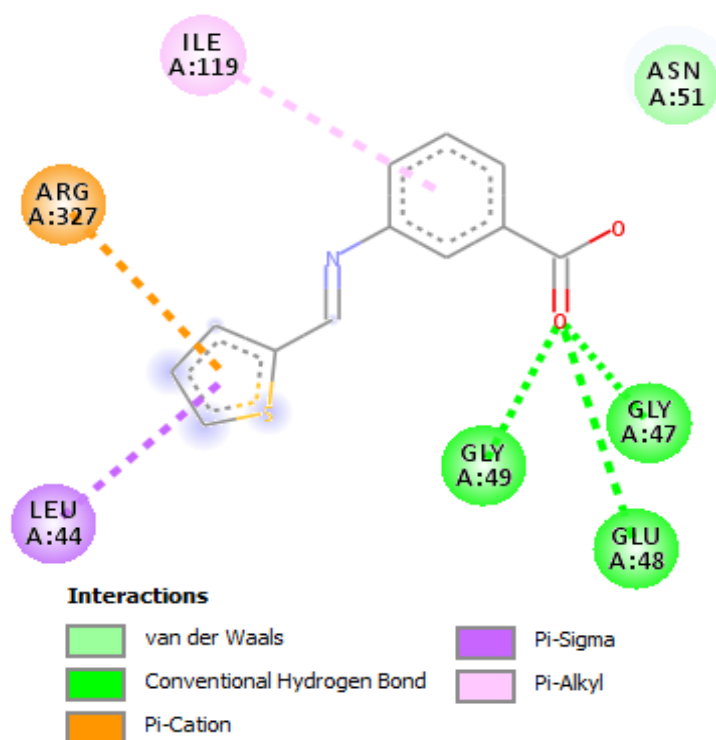


Fig. 11.5i 2D interaction diagram of 3TMAB with active site 1 of 2MBR

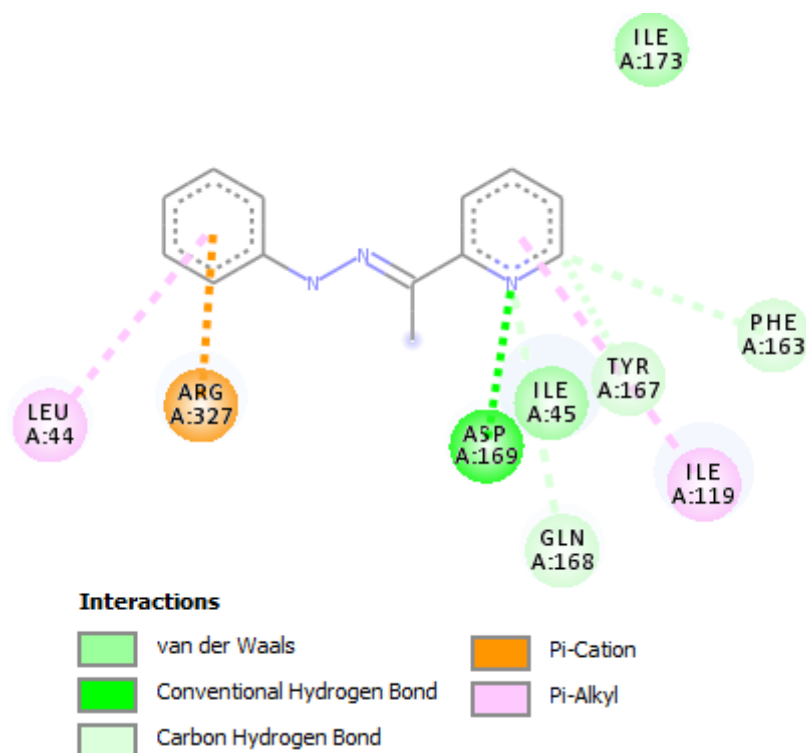


Fig. 11.5j 2D interaction diagram of 2PHEP with active site 1 of 2MBR

***In vitro* antibacterial studies of the heterocyclic Schiff bases and their inner transition metal complexes**

Schiff bases ligands 3-(1-(2-phenylhydrazono)ethyl)pyridine (3PHEP), 2-(1-pyridine-3-yl)ethylidene)hydrazinecarbothioamide (2PEHCT), 3-((thiophen-2-ylmethylene)amino)benzoic acid (3TMAB) and their inner transition metal complexes of La(III), Nd(III) and Sm(III) were subjected to antibacterial studies against three gram-positive and three gram-negative bacterial strains using disc diffusion method. *Staphylococcus aureus*, *Enterococcus faecalis*, *Enterococcus casseliflavus*, *Escherichia coli*, *Pseudomonas aeruginosa* and *Enterobacter hormaechei* are the bacterial strains used for the screening. In order to conduct the antibacterial studies the compounds were dissolved in the solvent DMSO to prepare solutions having concentrations $50 \mu\text{gdisc}^{-1}$, $100 \mu\text{gdisc}^{-1}$, $250 \mu\text{gdisc}^{-1}$ and $500 \mu\text{gdisc}^{-1}$. Ampicillin was used as the standard

antibiotic to compare the antibacterial activity of the compounds. The solvent DMSO was also subjected to antibacterial screening.

Schiff base 3PHEP and its inner transition metal complexes

Antibacterial activity of the Schiff bases and their inner transition metal complexes are given in Table 11.13. Schiff base ligand 3PHEP and its La(III), Nd(III) and Sm(III) complexes were found to be less active than the standard antibiotic. 3PHEP is more active against the bacterial strains *P. aeruginosa* and *E. hormaechei* and less active against *E. casseflavis*. Standard antibiotic ampicillin exhibited appreciable activity against all the bacterial strains. La(III), Nd(III) and Sm(III) complexes also exhibits high activity against *P. aeruginosa* and *E. hormaechei*, but less active than the ligand 3PHEP. La(III), Nd(III) complexes are more active than Sm(III) against *E. faecalis* and *E. coli* whereas Sm(III) complex is more active than La(III), Nd(III) complex in *S. aureus* and *E. casseflavis*. Also at high concentration of about 500 μgdisc^{-1} the activity of La(III) and Nd(III) complexes are slightly greater than that of the ligand. Same activity is observed for 3PHEP and its complexes against *E. hormaechei*. The solvent DMSO was found to be inactive towards all bacterial strains under study.

Schiff base 2PEHCT and its inner transition metal complexes

In the case of 2PEHCT and its complexes the activity is high against the bacterial strains *P. aeruginosa* and *E. hormaechei*. Activity of the standard antibiotic is higher than the ligand and complexes. 2PEHCT exhibited low activity against *E. coli*. Nd(III) and Sm(III) complexes are more active than ligand against *E. faecalis* and *P. aeruginosa*. Diameter of zone of inhibition of Nd(III) and Sm(III) complexes are 15 mm and 11 mm respectively at 500 μgdisc^{-1} . The enhancement of growth inhibitory power of Schiff base ligands upon coordination can be explained on the basis of Tweedy's chelation theory [82].

Table 11.13 Diameter of zone of inhibition (mm) at different concentration (μgdisc^{-1}) of the Schiff bases and their inner transition metal complexes

Bacteria	Conc. (μgdisc^{-1})	3PHEP (L)				2PEHCT (L'H)				3TMBA (L''H)				Ampicillin
		L	La	Nd	Sm	L'	La	Nd	Sm	L''	La	Nd	Sm	
<i>S. aureus</i>	50	10	6	6	7	4	6	5	6	10	6	5	8	15
	100	17	7	7	8	8	8	6	7	12	8	6	10	21
	250	20	8	9	10	8	9	9	8	20	9	9	12	28
	500	25	10	10	12	11	10	10	10	24	10	10	15	30
<i>E. casseflavis</i>	50	3	5	5	7	4	5	7	3	4	5	4	2	9
	100	5	7	7	9	7	6	7	5	6	6	6	4	14
	250	7	8	9	11	8	7	9	6	9	9	8	6	16
	500	10	10	10	12	10	10	10	8	10	10	10	8	20
<i>E. faecalis</i>	50	8	6	7	1	5	5	8	7	5	5	6	3	10
	100	8	9	9	2	6	7	10	8	5	7	7	4	15
	250	10	10	11	4	8	8	12	10	7	8	9	6	18
	500	11	12	13	6	10	10	15	11	10	10	10	8	20
<i>E. coli</i>	50	8	10	9	5	0	6	9	3	7	7	6	5	12
	100	12	11	10	5	1	7	10	5	11	9	7	7	19
	250	13	13	11	8	5	9	13	7	13	11	9	8	21
	500	16	15	12	10	9	10	15	10	15	12	10	11	25
<i>P. aeruginosa</i>	50	19	12	11	10	14	14	18	14	16	13	16	9	20
	100	21	13	13	15	18	18	21	19	21	15	18	12	26
	250	23	17	16	18	21	20	23	21	23	17	20	16	28
	500	25	20	20	20	24	22	25	25	25	20	25	20	30
<i>E. hormaechei</i>	50	7	4	6	5	4	7	7	6	5	5	4	5	7
	100	7	6	7	5	5	9	7	8	5	6	5	8	9
	250	9	8	9	8	8	10	8	9	6	7	8	9	11
	500	10	10	10	10	10	12	10	10	10	10	10	10	15

When coordinate with metal, ligand will reduce the positive charge on the metal by partial sharing of delocalized electrons. As a result metal polarity gets reduced and lipophilicity of the molecule increases compared to the free ligand. This enables the

complexes to cross the lipid membrane and to enter into the cytoplasm of the cell. As a result the cytotoxicity of the metal chelates will enhance. In the bacterial strain *E. hormaechei* all the complexes are slightly more active than the ligand. Compared to other two complexes and ligand, Nd(III) complex is more active against *E. coli* and exhibits a zone of inhibition of about 15 mm at $500 \mu\text{gdisc}^{-1}$. Antibacterial activity of 2PEHCT, Nd(III)-2PEHCT and Sm(III)-2PEHCT at $500 \mu\text{gdisc}^{-1}$ against *E. faecalis* is shown in Fig. 11.6.

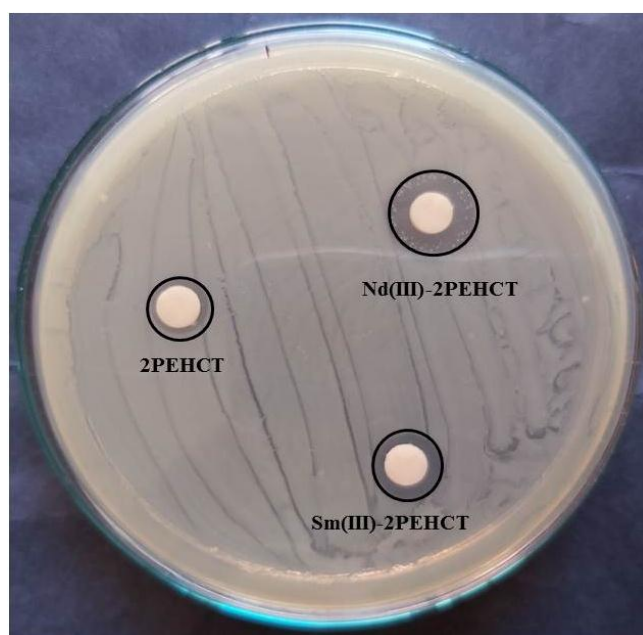


Fig. 11.6 Antibacterial activity of 2PEHCT, Nd(III)-2PEHCT and Sm(III)-2PEHCT at $500 \mu\text{gdisc}^{-1}$ against *E. faecalis*

Schiff base 3TMBA and its inner transition metal complexes

The activity is also high in the case of 3TMBA and its complexes against the bacterial strains *P. aeruginosa* and *E. hormaechei*, but less than that of standard antibiotic. Maximum zone of inhibition of about 25 mm is shown by the Nd(III) complex and ligand in *P. aeruginosa*. In the case of *E. hormaechei* the activity of ligand and complexes are almost same and the diameter of zone of inhibition exhibited at a maximum concentration of $500 \mu\text{gdisc}^{-1}$ is 10 mm. La(III) and Nd(III) complexes exhibits slightly higher activity than 3TMBA against *E. faecalis*

SUMMARY

In vitro antibacterial studies of the Schiff bases, 2,2'-(5,5-dimethylcyclohexane-1,3-diylidene)bis(azanylylidene)diphenol (DMCHDP), N,N'-(5,5-dimethylcyclohexane-1,3-diylidene)dianiline (DMCHDA), 2,2'-(5,5-dimethylcyclohexane-1,3-diylidene)bis(hydrazinecarboxamide) (DMCHHC), 2-((2-hydroxybenzylidene)amino)phenol (2HBAP), 2-(cyclohexylideneamino)phenol (2CHAP), 3-(1-(2-phenylhydrazono)ethyl)pyridine (3PHEP), 2-(1-(pyridine-3-yl)ethylidene)hydrazine carboxamide (2PEHC), 2-(1-(pyridine-3-yl)ethylidene) hydrazine carbothioamide (2PEHCT), 3-((thiophen-2-ylmethylene)amino)benzoic acid (3TMAB) and 2-(1-(2-phenylhydrazono) ethyl)pyridine (2PHEP) were determined using disc diffusion method. *Staphylococcus aureus* and *Escherichia coli* are the pathogens taken for antibacterial screening. Different concentration of the compounds in DMSO such as 50, 100, 250 and 500 μgdisc^{-1} were employed for antibacterial investigations. Ampicillin was taken as the standard antibiotic to compare the activity of the Schiff base compounds.

Even though all Schiff bases have less activity than the standard antibiotic, all of them have appreciable growth inhibitory power against *Staphylococcus aureus* and *Escherichia coli*. The zone of inhibition was found to be increased with concentration of Schiff bases. Maximum inhibition was exhibited by DMCHDP and DMCHDA in *S. aureus* and *E. coli* respectively. The compounds 2PEHC and 2PEHCT have less activity in both strains.

In order to understand the mechanism by which the Schiff base compounds inhibit the growth of these two bacteria, *in silico* molecular docking studies were also carried out by selecting suitable targets present in them. All Schiff bases obey Lipinski rule of five and hence possess drug like properties. Molecular docking studies were

conducted to evaluate the binding affinity of the compounds with target proteins present in *S. aureus* and *E. coli*. The compounds were docked with four active sites of the targets such as Sortase-A (PDB ID: 1T2P), DNA gyrase (PDB ID: 3U2D), dihydrofolate reductase (DHFR) (PDB ID: 2W9S), clumping factor A (ClfA) (PDB ID: 1N67), dehydrosqualene synthase (CrtM) (PDB ID: 2ZCO) and two sites of the target undecaprenyl diphosphate synthase (UPPS) (PDB ID: 4H8E) of *S. aureus* and with four active sites of the targets such as β -ketoacyl-acyl carrier protein synthase III (ecKAS III) (PDB ID: 1HNJ), peptide deformylase (PDF) (PDB ID: 1G2A), L-glutamine: D-fructose-6-phosphate amido-transferase (PDB ID: 2VF5), murB (PDB ID: 2MBR), heptosyltransferase WaaC (PDB ID: 2GT1), mur D (PDB ID: 2X5O) and biotin carboxylase (BC) (PDB ID: 2W6O) of *E. coli* by using the software AutoDock 4.2.

In *S. aureus* the Schiff base compounds are found to be more active against the targets 2W9S, 1N67, 4H8E and 2ZCO whereas in *E. coli* the activity was high against the targets 2MBR, 2W60, 2VF5 and 1G2A. Thus the compounds inhibit the growth of these pathogens by deactivating their target proteins. The binding energy of DMCHDP and DMCHDA are high compared to other Schiff bases when docked with target proteins of both pathogens. This can be due to high molecular mass. Maximum binding energy of the compounds varies between -6.5 to -10.3 kcal/mol and -5.7 to -9.1 kcal/mol in *S. aureus* and *E. coli* respectively. In *S. aureus* maximum binding energy of -10.3 kcal/mol was observed when DMCHDP was docked with 2W9S whereas in *E. coli* maximum binding energy of -9.1 kcal/mol was observed when DMCHDA was docked with 2MBR. The Schiff bases 2PEHC and 2PEHCT exhibits low binding affinity to all target proteins and is supported by the results of *in vitro* antibacterial screening. In *S. aureus* the Schiff bases DMCHDP and 2PHEP occupy the active site 3 of the target 2W9S whereas 2CHAP and 3PHEP occupy site 1 of the target 4H8E. In *E. coli* site 1 of

target 2MBR was found to be the most active pocket for the compounds. The ligands DMCHDP, 2CHAP, 3PHEP, 3TMBA and 2PHEP were found to occupy in this active pocket.

Screening of *in vitro* antibacterial activity of the three heterocyclic Schiff bases 3PHEP, 2PEHCT, 3TMBA and their La(III), Nd(III) and Sm(III) complexes were also conducted against three gram positive bacteria such as *Staphylococcus aureus*, *Enterococcus faecalis* and *Enterococcus casseliflavus* and three gram negative bacteria such as *Escherichia coli*, *Pseudomonas aeruginosa* and *Enterobacter hormaechei* using disc diffusion method. Ampicillin was taken as the standard antibiotic and 50-500 μgdisc^{-1} in DMSO was the concentration range employed for the study.

Standard antibiotic ampicillin exhibits appreciable activity in all bacterial strains. The activity of all the ligands and complexes are found to be less than the standard antibiotic. All the ligands and complexes are more active against the bacterial strains *P. aeruginosa* and *E. hormaechei*. The Nd(III) and Sm(III) complexes of 2PEHCT are more active than the ligand against *E. faecalis* and *P. aeruginosa*. In *E. hormaechei* all the complexes of 2PEHCT are slightly more active than the ligand whereas the ligands 3PHEP, 3TMBA and their complexes have same activity. The La(III) and Nd(III) complexes of 3PHEP are more active than its Sm(III) complex against *E. coli* and *E. faecalis* whereas Sm(III) complex of 3PHEP is more active against *S. aureus* and *E. casseliflavus* than its La(III) and Nd(III) complexes.

REFERENCES

1. A. Takeuchi, H. Sprinz, E. H. LaBrec and S. B. Formal, *Am. J. Pathol.* 47, 1011-1044 (1965).
2. D. Mel, E. J. Gangarosa, M. L. Radovanović, B. L. Arsić and S. Litvinjenko, *Bull. World Health Organ.* 45, 457-464 (1971).
3. S. Kaur, N. H. Modi, D. Panda and N. Roy, *Eur. J. Med. Chem.* 45, 4209-4214 (2010).
4. N. Campbell, “*Biology*”, Addison Wesley Longman Inc., Menlo Park, CA, 5th edition (1999).
5. R. J. Curran, Ph. D thesis “*Silver(I) complexes as antimicrobial and anticancer drugs*”, National University of Ireland (2009).
6. A. Ogston, *Rev. Infect. Dis.* 6, 122-128 (1984).
7. J. Kluytmans, A. van Belkum and V. Herbrugh, *Clin. Microbiol. Rev.* 10, 505-520 (1997).
8. A. M. Cole, S. Tahk, A. Oren, D. Yoshioka, Y. H. Kim, A. Park and T. Ganz, *Clin. Diagn. Lab. Immunol.* 8, 1064-1069 (2001).
9. D. V. Tyne, M. J. Martin and M. S. Gilmore, *Toxins.* 5, 895-911 (2013).
10. A. C. Anderson, D. Jonas, I. Huber, L. Karygianni, J. Wölber, E. Hellwig, N. Arweiler, K. Vach, A. Wittmer and A. Al-Ahmad, *Front. Microbiol.* 6, 1-14 (2016).
11. C. Iaria, G. Stassi, G. B. Costa, R. D. Leo, A. Toscano and A. Cascio, *BMC Infect. Dis.* 5, 1-3 (2005).
12. R. Bentley and R. Meganathan, *Microbiol. Rev.* 46, 241-280 (2004).
13. G. Reid, J. Howard and B. S. Gan, *Trends Microbiol.* 9, 424-428 (2001).

14. G. P. Bodey, R. Bolivar, V. Fainstein and L. Jadeja, *Clin. Infect. Dis.* 5, 279-313 (1983).
15. E. B. M. Breidenstein, C. sar de la Fuente-Nunez and R. E. W. Hancock, *Trends Microbiol.* 19, 419-426 (2011).
16. C. M. Ohara, A. G. Steigerwalt, B. C. Hill, J. J. Farmer III, G. R. Fanning, and D. J. Brenner, *J. Clin. Microbiol.* 27, 2046-2049 (1989).
17. H. C. Gram, *Fortschr. Med.* 2, 185-189 (1884).
18. K. Gould, *J. Antimicrob. Chemother.* 71, 572-575 (2016).
19. G. Schneider and H. -J. Bohm, *Drug Discov. Today.* 7, 64-70 (2002).
20. L. G. Ferreira, R. N. dos Santos, G. Oliva and A. D. Andricopulo, *Molecules.* 20, 13384-13421 (2015).
21. D. Hecht and G. B. Fogel, *J. Chem. Inf. Model.* 49, 1105-1121 (2009).
22. X. -Y. Meng, H. -X. Zhang, M. Mezei and M. Cui, *Curr. Comput-Aid Drug.* 7, 146-157 (2011).
23. S. A. Patil, S. N. Unki, A. D. Kulkarni, V. H. Naik and P. S. Badami, *Spectrochim. Acta A.* 79, 1128-1136 (2011).
24. B. K. Singh, A. Prakash, H. K. Rajour, N. Bhojak and D. Adhikari, *Spectrochim. Acta A.* 76, 376-383 (2010).
25. N. Raman, A. Kulandaisamy and K. Jeyasubramanian, *Synth. React. Inorg. Met. - Org. Chem.* 31, 1249-1270 (2001).
26. V. B. Badwaik, R. D. Deshmukh and A. S. Aswar, *J. Coord. Chem.* 62, 2037-2047 (2009).
27. Z. H. Chohan, M. Praveen and A. Ghaffaf, *Synth. React. Inorg. Met. -Org. Chem.* 28, 1673-1687 (1998).

-
28. A. Prakash, B. K. Singh, N. Bhojak and D. Adhikari, *Spectrochim. Acta A.* 76, 356-362 (2010).
 29. B. K. Singh, P. Mishra, A. Prakash and N. Bhojak, *Arab. J. Chem.* 10, S472-S483 (2017).
 30. A. Saxena and R. Saxena, *Orient. J. Chem.* 29, 589-595 (2013).
 31. L. Lekha, K. K. Raja, G. Rajagopal and D. Easwaramoorthy, *J. Mol. Struct.* 1056–1057, 307-313 (2014).
 32. W. M. Al Momani, Z. A. Taha, A. M. Ajlouni, Q. M. Abu Shaqra and M. Al Zouby, *Asian Pac. J. Trop. Biomed.* 3, 367-370 (2013).
 33. S. Alghool, M. Sh. Zoromba, H. F. Abd El-Halim, *J. Rare Earths.* 31, 715-721 (2013).
 34. K. Mohanan, R. Aswathy, L. P. Nitha, N. E. Mathews and B. S. Kumari, *J. Rare Earths.* 32, 379-388 (2014).
 35. Z. A. Taha, A. M. Ajlouni, K. A. Al-Hassan, A. K. Hijazi and A. B. Faiq, *Spectrochim. Acta A.* 81, 317- 323 (2011).
 36. V. Mutalik and M. A. Phaniband, *J. Chem. Pharm. Res.* 3, 313-330 (2011).
 37. A. S. Ramasubramanian, B. R. Bhat and R. Dileep, *Synth. React. Inorg. Met.-Org. Nano-Metal Chem.* 42, 548-553 (2012).
 38. S. Alghool, H. F. Abd El-Halim, M. S. Abd El-sadek, I. S. Yahia and L. A. Wahab, *J. Therm. Anal. Calorim.* 112, 671-681 (2013).
 39. V. S. Dofe, A. P. Sarkate, D. K. Lokwani, S. H. Kathwate and C. H. Gill, *Res. Chem. Intermed.* 43, 15-28 (2017).
 40. A. Bharathi, S. M. Roopan, C. S. Vasavi, P. Munusami, G. A. Gayathri and M. Gayathri, *Biomed. Res. Int.* 2014, 1-10 (2014).
 41. G. Sabbagh and N. Berakdar, *J. Mol. Graph. Model.* 61, 214-223 (2015).
-


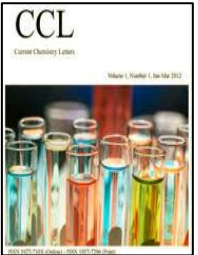
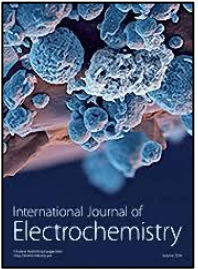
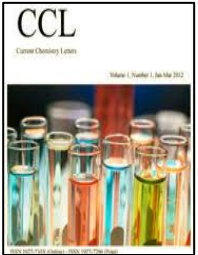
42. M. I. Abdullah, A. Mahmood, M. Madni, S. Masood and M. Kashif, *Bioorg. Chem.* 54, 31-37 (2014).
43. F. Abridach, Y. Rokni, A. Takfaouia, M. Khoutoul, H. Doucet, A. Asehrou and R. Touzani, *Biomed. Pharmacother.* 103, 653-661 (2018).
44. J. N. Sangshetti, F. A. Kalam Khan, R. H. Patil, S. D. Marathe, W. N. Gade and D. B. Shinde, *Bioorg. Med. Chem. Lett.* 25, 874-880 (2015).
45. K. Gullapelli, G. Brahmeshwari, M. Ravichander and Uma Kusuma, *Egypt. J. Basic Appl. Sci.* 4, 303-309 (2017).
46. B. K. Sarojini, B. G. Krishna, C. G. Darshanraj, B. R. Bharath and H. Manjunatha, *Eur. J. Med. Chem.* 45, 3490-3496 (2010).
47. G. Gomathi, K. Srinivasan, D. Velmurugan and R. Gopalakrishnan, *RSC. Adv.* 5, 44742-44748 (2015).
48. A. L. Bauer, W. M. M. Kirby, J. C. Sherris and M. Turck, *Am. J. Clin. Pathol.* 45, 493-496 (1966).
49. J. H. Mueller and J. Hinton, *Proc. Soc. Exp. Biol. Med.* 48, 3330-3333 (1941).
50. C. A. Lipinski, F. Lombardo, B. W. Dominy and P. J. Feeney, *Adv. Drug Deliv. Rev.* 46, 3-26 (2001).
51. S. Forli, R. Huey, M. E. Pique, M. F. Sanner, D. S. Goodsell and A. J. Olson, *Nat. Protoc.* 11, 905-919 (2016).
52. Y. Zong, T. W. Bice, H. Ton-That, O. Schneewind and S. V. L. Narayana, *J. Biol. Chem.* 279, 31383-31389 (2004).
53. N. Raman, S. Sobha and Liviu Mitu, *Monatsh. Chem.* 143, 1019-1030 (2012).
54. A. E. Eakin, O. Green, N. Hales, G. K. Walkup, S. Bist, A. Singh, G. Mullen, J. Bryant, K. Embrey, N. Gao, A. Breeze, D. Timms, B. Andrews, M. Uria-Nickelsen, J. Demeritt, J. T. Loch III, K. Hull, A. Blodgett, R. N. Illingworth, B.

-
- Prince, P. A. Boriack-Sjodin, S. Hauck, L. J. MacPherson, H. Ni, and B. Sherer, *Antimicrob. Agents Chemother.* 56, 1240-1246 (2011).
55. G. Gomathi and R. Gopalakrishnan, *Mater. Sci. Eng. C.* 64, 133-138 (2016).
56. H. Heaslet, M. Harris, K. Fahnoe, R. Sarver, H. Putz, J. Chang, C. Subramanyam, G. Barreiro and J. R. Miller, *Proteins.* 76, 706-717 (2009).
57. M. Dinari, F. Gharahi and Parvin Asadi, *J. Mol. Struct.* 1156, 43-50 (2018).
58. C. C. S. Deivanayagam, E. R. Wann, W. Chen, M. Carson, K. R. Rajashankar, M. Hook and S. V. L. Narayana, *EMBO J.* 21, 6660-6672 (2002).
59. R. M. Wadapurkar, M. D. Shilpa, A. K. S. Katti and M. B. Sulochana, *Inform. Med. Unlocked.* 10, 58-70 (2018).
60. C. -I. Liu, G. Y. Liu, Y. Song, F. Yin, M. E. Hensler, W. -Y. Jeng, V. Nizet, A. H. -J. Wang and E. Oldfield, *Science.* 319, 1391-1394 (2008).
61. A. K. Kahlon, S. Roy and A. Sharma, *J. Biomol. Struct. Dyn.* 28, 201-210 (2013).
62. W. Zhu, Y. Zhang, W. Sinko, M. E. Hensler, J. Olson, K. J. Molohon, S. Lindert, R. Cao, K. Li, K. Wang, Y. Wang, Y. -L. Liu, A. Sankovsky, C. A. F. de Oliveirac, D. A. Mitchell, V. Nizete, J. A. McCammonc and E. Oldfield, *Proc. Natl. Acad. Sci.* 110, 123-128 (2013).
63. P. Anitha, P. Lavanya, A. Anbarasu and S. Ramaiah, *J. Comput. Biol.* 3, 3-9 (2014).
64. X. Qiu, C. A. Janson, W. W. Smith, M. Head, J. Lonsdale and A. K. Konstantinidis, *J. Mol. Biol.* 307, 341-356 (2001).
65. K. Cheng, Q. -Z. Zheng, Y. Qian, L. Shi, J. Zhao and H. -L. Zhu, *Bioorg. Med. Chem.* 17, 7861-7871 (2009).
66. J. M. Clements, R. P. Beckett, A. Brown, G. Catlin, M. Lobell, S. Palan, W. Thomas, M. Whittaker, S. Wood, S. Salama, P. J. Baker, H. F. Rodgers, V.
-

- Barynin, D. W. Rice, and M. G. Hunter, *Antimicrob. Agents Chemother.* 45, 563-570 (2001).
67. F. A. K. Khan, K. S. Jadhav, R. H. Patil, D. B. Shinde, R. B. Arote and J. N. Sangshetti, *Biomed. Pharmacother.* 83, 1146-1153 (2016).
68. S. Mouilleron, M. –A. Badet-Denisot and B. Golinelli-Pimpaneau, *J. Mol. Biol.* 377, 1174-1185 (2008).
69. A. M. Vijesh, A. M. Isloor, S. Telkar, T. Arulmoli and H. –K. Fun, *Arab. J. Chem.* 6, 197-204 (2013).
70. T. E. Benson, C. T. Walsh and J. M. Hogle, *Biochemistry.* 36, 806-811 (1997).
71. B. M. Sapkal and Dhananjay H. More, *Der Pharma Chem.* 5, 164-172 (2013).
72. S. Grizot, M. Salem, V. Vongsouthi, L. Durand, F. Moreau, H. Dohi, S. Vincent, S. Escaich and A. Ducruix, *J. Mol. Biol.* 363, 383-394 (2006).
73. R. Sivakumar, R. V. Pradeepchandran, Korlakunta and N. Jayaveera, *Inter. J. Pharm. Res. Innov.* 4, 1-5 (2001).
74. N. Zidar, T. Tomasic, R. Sink, V. Rupnik, A. Kovac, S. Turk, D. Patin, D. Blanot, C. C. Martel, A. Dessen, M. M. Premru, A. Zega, S. Gobec, L. P. Masic and D. Kikelj, *J. Med. Chem.* 53, 6584-6594 (2010).
75. N. Zidar, T. Tomasic, R. Sink, A. Kovac, D. Patin, D. Blanot, C. C. Martel, A. Dessen, M. M. Premru, A. Zega, S. Gobec, L. P. Masic and D. Kikelj, *Eur. J. Med. Chem.* 46, 5512-5523 (2011).
76. I. Mochalkin, J. R. Miller, L. Narasimhan, V. Thanabal, P. Erdman, P. B. Cox, J. V. N. Vara Prasad, S. Lightle, M. D. Huband, and C. K. Stover, *ACS Chem. Biol.* 4, 473-483 (2009).
77. Y. Ma, D. Ren, J. Zhang, J. Liu, J. Zhao, L. Wang and F. Zhang, *Tetrahedron Lett.* 56, 4076-4079 (2015).

78. M. Paulson Binsi, Thomas K. Joby, K. Ragi, Varghese C. Sinia and J. Reeja, *Curr. Chem. Lett.* 8, 1-11 (2019).
79. N. Kuriakose, “*Physicochemical, thermoanalytical, electrochemical, and antitumour studies of transition metal complexes of Schiff bases derived from heterocyclic carbonyl compounds*”, Ph. D. Thesis. 1-264 (2015).
80. E. Nittinger, T. Inhester, S. Bietz, A. Meyder, K. T. Schomburg, G. Lange, Robert Klein and M. Rarey, *J. Med. Chem.* 60, 4245-4257 (2017).
81. R. F. de Freitas and M. Schapira, *Med. Chem. Commun.* 8, 1970-1981 (2017).
82. B. G. Tweedy, *Phytopatology.* 55, 910-918 (1964).

LIST OF PUBLICATIONS

1. **Ragi. K**, Joby Thomas Kakkassery, Vinod P. Raphael, Reeja Johnson, Vidhya Thomas K, “*In vitro* antibacterial and *in silico* docking studies of two Schiff bases on *Staphylococcus aureus* and its target proteins”, *Future Journal of Pharmaceutical Sciences*, vol 7, 1-9, 2021, doi.org/10.1186/s43094-021-00225-3 
2. **Ragi K**, Joby Thomas Kakkassery, Vinod P. Raphael, Binsi M. Paulson, Reeja Johnson, “Corrosion inhibition of mild steel by N,N’-(5,5-dimethylcyclohexane-1,3-diyldene)dianiline in acid media: Gravimetric and electrochemical evaluations”, *Current Chemistry Letters*, vol. 9, 1-14, 2020, doi: 10.5267/j.ccl.2020.8.001 
3. **Ragi K**, Joby Thomas Kakkassery, Vinod P Raphael, Sini Varghese C, Binsi. M. Paulson, “Synthesis, cyclic voltammetric, electrochemical and gravimetric corrosion inhibition investigations of Schiff base derived from 5-5-dimethyl cyclohexanone and 2-aminophenol on mild steel in 1 M HCl and 0.5 M H₂SO₄”, *International Journal of Electrochemistry*, vol 2019, 1-13, 2019, doi.org/10.1155/2019/1094148 
4. M. Paulson Binsi, Thomas K. Joby, **K. Ragi**, Varghese C. Sini and Johnson Reeja. “Interaction of two heterocyclic Schiff bases derived from 2-acetyl pyridine on mild steel in hydrochloric acid: physicochemical and corrosion inhibition investigations”, *Current Chemistry Letters*, vol. 9, 19-30, 2019, doi: 10.5267/j.ccl.2019.6.005 

5. Vidhya Thomas K, Joby Thomas Kakkassery, Vinod P. Raphael, **K. Ragi** and Reeja Johnson, “Ixora coccinea extract as an efficient eco-friendly corrosion inhibitor in acidic media: Experimental and theoretical approach”, *Current Chemistry Letters*, vol.9, 1-12, 2021, doi:10.5267/j.ccl.2020.12.001



6. Reeja Johnson, Joby Thomas Kakkassery, Vinod Raphael Palayoor, **Ragi Kooliyat** and Vidhya Thomas Kannanaikkal, “Experimental and theoretical investigations on the corrosion inhibition action of thiadiazole derivatives on carbon steel in 1M HCl medium”, *Oriental Journal of Chemistry*, vol. 36, 1179-1188, 2020, doi:10.13005/ojc/360624



7. Binsi M. Paulson, K. Joby Thomas, Vinod P. Raphael, K. S. Shaju, **K. Ragi**, “Mitigation of concrete reinforced steel corrosion by penta sodium triphosphate: physicochemical and electrochemical investigations”, *SN Applied Sciences*, vol. 2020, 1-11, 2020 doi: 10.1007/s42452-020-03586-1



8. Sini Varghese Cheruvathur, Joby Thomas Kakkassery, Vinod Raphael Palayoor, Binsi M. Paulson and **Ragi Kooliyat**, “Electrochemically synthesized poly(2-aminobenzenesulphonic acid) – an efficient protection for carbon steel corrosion”, *Oriental Journal of Chemistry*, vol. 35, 678-683, 2019, doi: 10.13005/ojc/350223



LIST OF CONFERENCE PAPERS

1. **K. Ragi**, K. Joby Thomas, Vinod. P. Rapheal, C. Sini Varghese, Binsi. M. Paulson, “Gravimetric and electrochemical investigations on corrosion inhibition of N,N’-(5,5-dimethylcyclohexane-1, 3-diylidene)dianiline on mild steel surface

- in 1M HCl”, *International Conference on Chemistry and Physics of Materials*, St. Thomas College, Thrissur, 2018
2. Vinod P Raphael, Joby Thomas K, **Ragi K**, Shaju K S, “Spectral, electrochemical and biological studies on a heterocyclic semicarbazone and its copper and cadmium chelates”, *UGC Sponsored National seminar on Recent Advances in Chemistry*, Vimala college, Thrissur, 2017
 3. Vinod P. Raphael, Joby Thomas K, **Ragi. K**, Shaju K S, “Interaction of two heterocyclic semicarbazones on carbon steel surface in sulphuric acid”, *National Seminar on Current Trends in Chemistry*, Cochin University of Science and Technology, 2018
 4. Nimmy Kuriakose, Joby Thomas K, **Ragi K**, Binsi M Paulson, Sini Varghese C, “Evaluation of antitumor activity of Cu(II) complexes derived from heterocyclic Schiff base ligands”, *International conference on Materials for the millennium (MATCON 2019)*, Cochin University of Science and Technology, 2019
 5. Binsi. M. Paulson, Joby Thomas K, **Ragi. K**, Sini Varghese C, Reeja Johnson, “Corrosion inhibition efficacy of 2-acetylpyridine phenylhydrazone on mild steel in acid media- physicochemical and electrochemical investigations”, *International conference on Materials for the millennium (MATCON 2019)*, Cochin University of Science and Technology, 2019
 6. Sini Varghese C, Joby Thomas K, **Ragi. K**, Binsi. M. Paulson, “Corrosion inhibition investigations of 3-formylindole phenylhydrazone on copper in nitric acid medium”, *International Conference on Chemistry and Physics of Materials*, St. Thomas College, Thrissur, 2018
 7. Vidhya Thomas K, Joby Thomas K, **Ragi. K**, Reeja Johnson, “Excellent eco-friendly corrosion inhibition behaviour of croton persimilis extract (CPE) for mild

- steel in acidic media: physicochemical, electrochemical and surface morphological studies”, *National seminar on Current Trends in Chemistry (CTriC 2020)*, Cochin University of Science and Technology, 2020
8. Binsi. M. Paulson, Joby Thomas K, Vinod P Raphael, **Ragi. K**, Sini Varghese C, “Efficacy of sodium citrate-zinc acetate mixture to inhibit steel reinforcement corrosion in concrete block contaminated with NaCl”, *International Conference on Chemistry and Physics of Materials*, St. Thomas College, Thrissur, 2018
 9. Sini Varghese C, Joby Thomas K, Binsi M Paulson, **Ragi. K** “Corrosion inhibition investigations on 2-pyridinecarbaldehyde-2-aminophenol on carbon steel in 1M HCl”, *KSCSTE Sponsored National Seminar on Recent Trends in Computational Chemistry and Drug Design*, St Joseph’s College (Autonomous), Irinjalakuda, 2019.

**PAPERS ACCEPTED/COMMUNICATED/
TO BE COMMUNICATED**

1. Vidhya Thomas K, Joby Thomas K, Vinod Raphael, **Ragi. K**, Reeja Johnson and Ramesh Babu, “Green corrosion inhibition properties of Croton Persimilis extract on mild steel in acid media”, Accepted in *Journal of Bio- and Tribo-Corrosion*
2. **Ragi K**, Joby Thomas Kakkassery, Vinod P Raphael, Vidhya Thomas K, Reeja Johnson, “Synthesis, characterization and antibacterial activity of lanthanide (III) complexes of 2-(1-(pyridine-3-yl)ethylidene)hydrazinecarbothioamide”, Communicated to *Vietnam Journal of Chemistry*
3. Evaluation of corrosion inhibition efficiency of 2,2’-(5,5-dimethylcyclohexane-1,3-diylidene)bis(hydrazinecarboxamide) on mild steel in 1.0 M HCl (to be communicated)